Sensitivity of ocean circulation and marine biogeochemical processes to variations in surface wind stress and diapycnal mixing in the surface ocean

Author:
Ridder, Nina Nadine

Publication Date:
2014

DOI:
https://doi.org/10.26190/unsworks/16989

Sensitivity of ocean circulation and marine biogeochemical processes to variations in surface wind stress and diapycnal mixing in the surface ocean

Nina Nadine Ridder

Supervisor: Professor Matthew H. England

School of Biological, Earth and Environmental Sciences

University of New South Wales

Sydney Australia

A thesis submitted for the degree of Doctor of Philosophy at the University of New South Wales.

January 2014

PLEASE TYPE

THE UNIVERSITY OF NEW SOUTH WALES
Thesis/Dissertation Sheet

Surname or Family name: RIDDER

First name: NINA Other name/s: NADINE

Abbreviation for degree as given in the University calendar: PhD

School: BIOLOGICAL, EARTH AND ENVIRONMENTAL SCIENCES Faculty: SCIENCE

Title:
Sensitivity of ocean circulation and marine biogeochemical processes to variations in surface wind stress and diapycnal mixing in the surface ocean

Abstract

This thesis investigates the sensitivity of the biogeochemical cycling of dissolved inorganic carbon and oxygen to variations in global ocean circulation and transport in response to perturbations in (i) the prevailing surface wind stress conditions in a global climate model, and (ii) the diapycnal mixing background parameterization scheme in the upper 1000 m of a numerical ocean model. The global climate model is a fully coupled earth system model of intermediate complexity (UVic ESCM) using a relatively coarse resolution to facilitate the assessment of equilibrated climate conditions. The global ocean model is a one-degree ocean general circulation model (MOM4p1) coupled to a biogeochemical model of intermediate complexity (TOPAZ2). Special attention is given to the comparison between the impacts of low- and mid-latitude perturbations and the identification of low-latitude mechanisms with possible implications for the global climate. The three main findings of this thesis are: (i) low-latitude surface wind stress changes can significantly affect the biogeochemical cycling of oxygen and carbon and could thus have an important contribution to the overall control of the global climate. (ii) The commonly accepted Drake Passage Effect does not dominate the link between Southern Hemisphere westerly wind stress and the formation of North Atlantic Deep Water or the Atlantic outflow if the impact of wind-driven changes on Antarctic sea-ice is considered. (iii) Variations in thermocline thickness and biogeochemical processes, in particular remineralization, can offset and even reverse the influence of alterations in equatorial ocean stratification and vertical mixing on ocean oxygenation and the extent of low-oxygen regions. This will be shown in the discussion of two cases, in which ocean stratification is increased (decreased) due to variations in low-latitude surface wind stress and diapycnal mixing, while ocean oxygenation increases (decreases) and low-oxygen regions contract (extend). Additionally, this study identifies a dominance of Southern Hemisphere westerly wind stress compared to tropical winds in the determination of the global overturning circulation. Changes in the nutrient supply to one of the key marine ecosystems in the south east Pacific due to tropical and mid-latitude wind stress variations are also examined.

FOR OFFICE USE ONLY Date of completion of requirements for Award:

THIS SHEET IS TO BE GLUED TO THE INSIDE FRONT COVER OF THE THESIS

ORIGINALITY STATEMENT

'I hereby declare that this submission is my own work and to the best of my knowledge it contains no materials previously published or written by another person, or substantial proportions of material which have been accepted for the award of any other degree or diploma at UNSW or any other educational institution, except where due acknowledgement is made in the thesis. Any contribution made to the research by others, with whom I have worked at UNSW or elsewhere, is explicitly acknowledged in the thesis. I also declare that the intellectual content of this thesis is the product of my own work, except to the extent that assistance from others in the project's design and conception or in style, presentation and linguistic expression is acknowledged.'

Signed .....

Date .....

AUTHENTICITY STATEMENT

'I certify that the Library deposit digital copy is a direct equivalent of the final officially approved version of my thesis. No emendation of content has occurred and if there are any minor variations in formatting, they are the result of the conversion to digital format.'

Acknowledgements

I would like to express my deepest appreciation to all those who have guided and supported me academically, administratively and personally throughout the past three and a half years. In particular, I thank Prof. Matthew England for his supervision, guidance and encouragement in course of this project. Without him sacrificing his time and sharing his vast knowledge in oceanography and climatology this thesis would not have been possible. I am also deeply grateful to my co-supervisors, Prof. Katrin Meissner, for her support and valuable help especially in the first stages of this project, and Dr. Willem Sijp, for his guidance during my first steps using Matlab. I additionally extend my gratitude to Prof. Jorge Sarmiento, Dr. Keith Rodgers, Dr. John Dunne and Dr. Matthew Harrison for hosting me at AOS and NOAA/GFDL and for their valuable contributions to Part V of this thesis. In course of our collaboration I was able to vastly improve my skills in modelling oceanic as well as biogeochemical processes. For this I would like to express my deepest appreciation. Further I would like to thank Prof. Niki Gruber for his input during my stay at the ETH in Zurich which led to the improvement of the study presented in Part II of this thesis.

This project was funded primarily through the International Postgraduate Research Scholarship (IPRS) scheme of the Australian Government Department of Industry, Innovation, Science, Research and Tertiary Education. I also acknowledge the financial support of the CCRC, the ARC CoE for Climate System Science and the University of New South Wales.

Special thanks are due to all my friends, both near and far, who helped me endure the sometime seemingly impossible tasks that I had to face in course of this PhD program. My deepest appreciation to Graham Simpkins, Penny Maher, Maike Voss, Aart Suri and

Mercedes Hannelore Rittmann Frank for their endless support and encouragement. I would have been lost without you! I am also deeply indebted to my family, who have always shown me unconditional love, motivation and encouragement in everything I have done.

Finally, my deepest thanks to Andrew Rickards, without whom the completion of this thesis would not have been possible. His emotional support during the past stages of this PhD has been invaluable and I am feeling incredibly lucky to have him in my life.

Supporting Publications

Ridder, N. N., K. J. Meissner, and M. H. England, Sensitivity of the oceanic carbon reservoir to tropical surface wind stress variations, *Geophys. Res. Lett.*, **40**, doi:10.1002/grl.50498, 2013.

Ridder, N. N. and M. H. England, Sensitivity of ocean oxygenation to variations in tropical zonal wind stress magnitude, *Global Biogeochem. Cycles*, conditionally accepted.

Ridder, N. N. and M. H. England, Sea-ice feedbacks reverse the link between Southern Ocean winds and North Atlantic Deep Water formation, *Nature Geosciences*, under review.

Ridder, N. N., K. Rodgers, J. Dunne, M. Harrison and J. Sarmiento, Impact of diapycnal diffusivity parameterisation schemes on dissolved oxygen concentrations in a global ocean model, *Biogeosciences*, to be submitted.

Ridder, N. N. and M. H. England, On the impact of high- and low-latitude wind stress changes on oceanic properties, *J. Phys. Oceanogr.* or *J. Climate*, in prep.

Abstract

This thesis investigates the sensitivity of the biogeochemical cycling of dissolved inorganic carbon and oxygen to variations in global ocean circulation and transport in response to perturbations in (i) the prevailing surface wind stress conditions in a global climate model, and (ii) the diapycnal mixing background parameterization scheme in the upper 1000 m of a numerical ocean model. The global climate model is a fully coupled earth system model of intermediate complexity (UVic ESCM) using a relatively coarse resolution to facilitate the assessment of equilibrated climate conditions. The global ocean model is a one-degree ocean general circulation model (MOM4p1) coupled to a biogeochemical model of intermediate complexity (TOPAZ2). Special attention is given to the comparison between the impacts of low- and mid-latitude perturbations and the identification of low-latitude mechanisms with possible implications for the global climate. The three main findings of this thesis are: (i) low-latitude surface wind stress changes can significantly affect the biogeochemical cycling of oxygen and carbon and could thus have an important contribution to the overall control of the global climate. (ii) The commonly accepted Drake Passage Effect does not dominate the link between Southern Hemisphere westerly wind stress and the formation of North Atlantic Deep Water or the Atlantic outflow if the impact of wind-driven changes on Antarctic sea-ice is considered. (iii) Variations in thermocline thickness and biogeochemical processes, in particular remineralization, can offset and even reverse the influence of alterations in equatorial ocean stratification and vertical mixing on ocean oxygenation and the extent of low-oxygen regions. This will be shown in the discussion of two cases, in which ocean stratification is increased (decreased) due to variations in low-latitude surface wind stress and diapycnal mixing, while ocean oxygenation increases (decreases) and low-oxygen regions contract (extend). Additionally, this study identifies a dominance of Southern Hemisphere westerly wind stress compared to tropical winds in the determination of the global overturning

circulation. Changes in the nutrient supply to one of the key marine ecosystems in the south east Pacific due to tropical and mid-latitude wind stress variations are also examined.

Contents

List of Figures

List of Tables

Preface

The focus of this study is the sensitivity of oceanic circulation, carbon and oxygen to tropical and mid-latitude wind-driven changes and to diapycnal mixing in the upper 1000 m of the global ocean. The cycling of carbon dioxide (CO_2) between atmosphere and ocean is a key mechanism in the determination of the composition of the atmosphere and thus has the potential to affect the climate on a global scale. Within the Earth system the ocean is the biggest carbon reservoir containing approximately 93% of all exchangeable carbon (Siegenthaler and Sarmiento, 1993; Solomon et al., 2007). It is believed to have driven major climate shifts in the past, such as the glacial-interglacial cycle, by changing the atmospheric carbon load and thus altering the acting radiative forcing (e.g. Broecker, 1982; Sigman et al., 2010). In today's climate the ocean has been identified as the only true net sink for anthropogenic CO_2 between 1800 and 1994 (Sabine et al., 2004). Oceanic carbon sequestration is highly influenced by dissolved oxygen (O_2) concentrations, as these are crucial in the control of biogeochemical processes within the ocean. While O_2 itself is produced and dissolved in biogeochemical reactions, namely photosynthesis and remineralization, respectively, O_2 concentrations have a significant influence on biological activity. When sufficiently abundant, O_2 enables marine ecosystems to thrive and facilitates the export of dissolved inorganic carbon (DIC) from the surface to the deep ocean allowing the additional oceanic uptake of atmospheric carbon. In contrast, low O_2 concentrations are a potential stressor for marine life and limit the biological removal of carbon from the surface ocean. Ocean oxygenation is thus an important indicator for the response of marine biology to changing conditions and gives indications about the performance of the biological carbon pump.

Observations spanning the past few decades suggest a negative trend in ocean oxygenation (e.g. Stramma et al., 2008, 2010) while the oceanic carbon load has increased since

the onset of anthropogenic carbon emissions (Sabine et al., 2004). The response of both tracers to anthropogenic climate change is the result of a variety of different, partly counteracting, mechanisms. For instance, the anthropogenic increase of the atmospheric carbon load, in separation of all other changes, shifts the partial pressure difference between atmosphere and ocean towards an increase in oceanic carbon uptake. In contrast, rising ocean temperatures decreases carbon solubility and thus counteracts the effect of an increased atmospheric carbon pressure. The interplay of these and other mechanisms makes a prediction of the future evolution of the climate system in regards to these two biogeochemical properties challenging. In the case of carbon for instance, increased atmospheric CO_2 concentrations in isolation of any other changes should lead to higher oceanic carbon uptake. However, observations in the Southern Ocean, which accounts for up to 40% of the total carbon uptake by the global ocean (Sabine et al., 2004), suggest a significant weakening of the carbon sink in this region (Le Quéré et al., 2007; Lovenduski et al., 2008). It has been suggested that changes in the Southern mid- to high-latitude wind fields are causing this weakening by counteracting the increased air-sea carbon flux due to higher atmospheric CO_2 concentrations. To understand the observed evolution of oceanic carbon and oxygen concentrations and to better constrain future climate predictions in response to anthropogenic greenhouse gas emissions it is essential to understand the impact of all factors determining ocean oxygenation and the cycling of carbon between the atmosphere and ocean. This thesis contributes to this by isolating the systems sensitivity to a choice of changing conditions and analysing the governing mechanisms in detail.

The overall controlling, physical mechanism directly and indirectly determining DIC and dissolved O_2 concentrations are transport processes within the ocean. Amongst the most important factors determining oceanic transport are (i) the exchange of momentum between atmosphere and ocean via wind stress at the ocean's surface and (ii) the buoyancy differences between the surface and deep ocean due to temperature and/or salinity variations. These forcings determine the location of the formation and re-surfacing of deep waters and thus play an important role in the movement of water through the global ocean. Additionally to directly altering O_2 and DIC concentrations via tracer advection, ocean circulation changes affect biogeochemical tracers indirectly via the circulation's

influence on the distribution of nutrients and heat between low- and high-latitudes as well as between the surface and deep ocean.

Another important mechanism contributing to the determination of ocean transport is the kinetic energy provided by small scale mixing caused by the interaction and breaking of internal waves. Another area of interest in this project is the parameterised vertical mixing of tracers such as temperature, salinity and biogeochemical tracers, e.g. O_2, DIC and nutrients. While orders of magnitudes smaller than its horizontal counterpart, vertical diffusivity has the potential to alter tracer transport sufficiently to notably change physical and biogeochemical parameters and with this the concentration of O_2 and DIC. The representation of these mechanisms is thus likely to be sensitive to the choice of parameterization scheme representing diapycnal mixing in a numerical ocean model. Possible causes for this include mixing-induced changes in the stratification within the ocean and the resulting variations in ocean overturning and circulation between different mixing schemes.

An understanding of the key mechanisms determining the global overturning circulation, their impact on marine biogeochemistry and their response to changing climate conditions is imperative to facilitate an accurate representation of the Earth's climate system and reliable predictions about its past and future evolution. The aim of this project is to contribute to this understanding through the analysis of the sensitivity of ocean circulation, and thus oceanic carbon and dissolved oxygen concentrations, to variations in (i) surface wind stress conditions at different latitudes and (ii) the vertical background diffusivity within the upper ocean. For this several model studies have been performed to analyse the response of the most important mechanisms governing O_2 and DIC concentrations to those varying conditions. Special attention was given to alterations in (i) ocean transport, (ii) physical parameters determining tracer saturation concentrations, and (iii) biogeochemical processes directly affecting O_2 and DIC concentrations.

This thesis is divided into five independent but interrelated parts. Each part, with the exception of Part IV, was prepared for submission to a scientific journal and includes an abstract, an introduction, details about the applied method and conclusions specific to each part. The content of Part IV is presently being refined for a new paper submission

to *J. Phys. Oceanogr.* or *J. Climate*. The order of the parts is in some ways arbitrary as each part is self-contained; comprising an independent piece of scientific research. The first four parts do however contain a common theme; namely, analyzing the oceans sensitivity to changes in equatorial / mid-latitude surface wind stress using an Earth system model of intermediate complexity (UVic ESCM; Weaver et al., 2001). The last part of the thesis analyses the effect of alterations in vertical mixing in the upper 1000 m on biogeochemistry in a one-degree resolution ocean model (MOM4p1; Griffies et al., 2009) coupled to a biogeochemistry model of intermediate complexity (TOPAZ2; Dunne et al., 2013). The referenced figures and tables within each part can be found at the end of the respective part with references between parts using the nomenclature Figure (number of Part).(number of Figure) (e.g. Figure I.3 - Figure 3, Part I; Figure II.4 - Figure 4, Part II). References to scientific literature are listed in a combined list of all parts at the end of the thesis and adopt the style of the Journal *Biogeosciences*. As each part contains a specific discussion and conclusion section, the chapter "Concluding Remarks" is limited to a brief summary of this thesis and contains recommendations for future research.

Part I consists of a full assessment of the sensitivity of marine DIC concentrations to low-latitude surface wind stress changes. Special attention was given to the analysis of variations in ocean temperature, salinity as well as ocean transport and marine biology, all vital for the marine carbon cycle. The study isolates physical and biological mechanisms to identify their specific impact on oceanic carbon and analyses their complex interplay to determine the overall response of the system. The aim of Part I is to identify the potential contribution of changes in low-latitude mechanisms in the ocean to past and future changes in the carbon cycle. This work was published in *Geophysical Research Letters*.

Part II continues the analysis of the impact of low-latitude surface wind stress changes but focuses on their effect on marine biology. The efficiency of the biological carbon pump, which has been identified to be highly sensitive to equatorial wind changes in Part I, is assessed in more detail. This is done through a detailed investigation of the response in ocean oxygenation, which facilitates the focus on changes in the gas exchange and marine biology by simplifying the involved chemistry. The aim of Part II is to shed light on the response of marine biology important to the carbon cycle to changes at the

ocean surface at low latitudes. This work is currently under review for publication in *Global Biogeochemical Cycles*.

Part III contains an analysis of the impact of variations in the strength of Southern Hemisphere westerly winds on the global overturning circulation. It challenges the importance of the "Drake Passage Effect" in the control of Southern Hemisphere westerly winds over the Atlantic overturning circulation described in Toggweiler and Samuels (1995). The aim of Part III is to present and establish a new mechanism, in which wind-driven Antarctic sea-ice changes lead to deep-ocean buoyancy changes reversing the impact of the link of the Southern Hemispheric westerlies on Atlantic meridional overturning circulation as described by Toggweiler and Samuels (1995). This work is currently under review for publication in *Nature Geosciences*.

Part IV can be seen as an extension of Part I, II and III in that it compares the impact of low-latitude surface wind stress changes on ocean parameters important for the evolution of biogeochemical tracers to those imposed by changes in SH mid-latitude winds. The aim of this part is to highlight the importance of both regions in the determination of the physical processes that govern ocean oxygenation and oceanic carbon sequestration. As mentioned before, Part IV was not prepared as a scientific paper. Therefore it does not follow the structure of the other parts of this thesis. In its function as a comparison of the results of Part I to III, Part IV does not contain a separate abstract or a detailed method section. Instead the reader is referred to the previous parts for details of the applied model and the performed experiments. A subset of the results presented in this part is currently under preparation for submission to *J. Phys. Oceanogr.* or *J. Climate*.

Part V assesses the impact of different diapycnal background diffusivity parameterizations on marine biology. As in Part IV, this part uses ocean oxygenation as a proxy for the response of processes involved in the biological carbon pump. The aim of Part V is to analyse the impact of global mean and latitudinal variations in the strength of vertical mixing on marine biology. This work is about to be submitted for publication in *Biogeosciences*.

In summary, the overall aim of this project is to contribute to a better understanding

of the past and possible future evolution of ocean oxygenation and carbon content by analysing the response of key mechanisms driving the production and depletion of these two tracers to changes in the physical forcing in the surface ocean and at the air/sea interface. It applies two state-of-the-art numerical models of different resolutions and analyses the modelled response of ocean temperature, salinity as well as ocean transport, ventilation and marine biology in a set of sensitivity experiments. This enables the here presented project to identify processes involved in the complex interplay of mechanisms determining the air-sea carbon exchange, ocean oxygenation as well as marine biology, and enables a prediction of the overall impact of possible past and future climate conditions on the global ocean.

Part I: Carbon and low-latitude surface wind stress

Abstract

The impact of variations of the Walker cell on the ocean carbon cycle is assessed using a coupled climate model. Idealized wind perturbations are investigated, with the trade winds increased/decreased by 10, 20, and 30%. A global-mean reduction in oceanic carbon storage is found for increased equatorial easterlies, while moderately decreased trade winds give increased uptake. There is a non-linear response to weakened tropical winds due to Pacific Ocean biological pump changes; with reduced nutrient upwelling resulting in decreased biological activity and remineralization in the deep ocean. This partially offsets the increased carbon uptake due to weaker trade winds. The overall change in net carbon storage reaches -26.2 PgC (12 ppm) in the 30% increase case and 4.2 PgC (-2 ppm) in the 20% decrease cases. Regional DIC changes reach -3.3 mmol m^{-3} (2.1 mmol m^{-3}) in the 10% decrease (increase) case. Gradually increasing wind perturbations give a similar pattern of DIC response to the full equilibrated solution.

I.1 Introduction

The ocean is the major sink for anthropogenic carbon while also being the biggest carbon reservoir; holding approximately 93% of all exchangeable carbon in the Earth system (Solomon et al., 2007). The properties that govern the ocean's ability to take up carbon at the atmosphere-ocean interface comprise (1) the partial pressure difference of CO_2 between atmosphere and ocean (ΔpCO_2), (2) the solubility of CO_2 in sea water and (3) the gas transfer coefficient, or gas piston velocity. These parameters are influenced by various processes, the most important being (i) the surface wind stress that directly affects the gas transfer coefficient, (ii) sea surface temperature (SST) which determines the solubility of carbon in sea water, (iii) biogeochemical processes, for instance net primary productivity (NPP), that acts to remove carbon from the surface ocean and thus determine ΔpCO_2 and (iv) ocean circulation processes, which can act to remove or add carbon-rich waters from/to the surface ocean. Subduction and deep convection for instance can remove carbon from the surface ocean and transport it into the deep ocean, thus facilitating further uptake of atmospheric carbon in today's climate. Upwelling of deep carbon-rich waters to the ocean surface in contrast can lead to CO_2 outgassing acting to counter the net oceanic uptake of anthropogenic CO_2. Furthermore, vertical transport within the ocean

determines the nutrient supply to marine ecosystems, which plays an important role in the removal of carbon from the atmosphere and the surface ocean via the biological pump.

All of the aforementioned processes are predicted to be modified in some way under the influence of global climate change (e.g. reviewed in Houghton et al., 2001; Solomon et al., 2007). The partial pressure difference for instance is changing due to anthropogenic emissions while the seawater solubility of CO_2 is being altered due to changes in SST, with solubility varying inversely with temperature (Watson et al., 1995). Ocean circulation as well as the gas transfer coefficient are also likely to change due to projected changes in the strength and position of wind fields in a warming climate, and changes to surface buoyancy fields (e.g. Russell et al., 2006; Vecchi and Soden, 2007; Collins et al., 2010; Tokinaga and Xie, 2011; Tokinaga et al., 2012). The Walker circulation for instance has been estimated to have decreased over the past six decades under the observed global temperature increase as a result of a reduction in the mean sea level pressure gradient across the Pacific (Collins et al., 2010; Tokinaga et al., 2012). Model studies predict this negative trend to persist into the future (Vecchi and Soden, 2007; Collins et al., 2010). They further predict a decrease in the equatorial trade winds and therefore zonal surface wind stress in warmer climates (e.g. Vecchi and Soden, 2007) by 0.003 N m^{-2} $°C^{-1}$ (Collins et al., 2010). This decrease in the easterly trade winds is not limited to the Pacific region (Tokinaga and Xie, 2011); the equatorial easterlies in the Atlantic have also been estimated to have decreased over the past six decades and model studies predict a further weakening (Vecchi and Soden, 2007). The reduction in surface wind stress is expected to lead to significant changes in SST, a weakening of ocean surface westward currents and equatorial upwelling, as well as a shoaling of the mean thermocline depth (e.g. Philander, 1981; McPhaden, 1993; Clarke and Lebedev, 1996; Vecchi and Soden, 2007). It is therefore likely that such a modification of the trade winds will affect the ocean carbon cycle via ocean circulation changes, wind speed changes, SST changes and the resultant biogeochemical response.

Paleoclimate records of Pacific Ocean SST suggest that such a change in zonal trade winds already occurred in the Pliocene (3.3 Ma - 3.0 Ma) (Haywood et al., 2005; Ravelo et al., 2006; Shukla et al., 2009). Analysis of paired $\delta^{18}O$ and magnesium-to-calcium ratio measurements from the tropical Pacific show that the east Pacific thermocline was deeper

during the Pliocene and the east-to-west SST gradient across the Pacific was significantly weaker than during modern, non-ENSO conditions (Wara et al., 2005). It is now believed that the modern-day SST gradient in the equatorial Pacific developed during the cooling at the end of the Pliocene (e.g. Ravelo et al., 2006). The timing of the shoaling of the thermocline and the increase in the east-west temperature gradient during the mid-Pleistocene transition suggests that sustained long-term shifts in the tropics could play an important role in the evolution of the global climate on longer time scales (Ravelo et al., 2006). Even though it is commonly accepted that oceanic high latitude processes are the main drivers of major climate shifts through fluctuations in atmospheric CO_2 (e.g. Sigman et al., 2010), these findings could hint to a more active role of the tropical Pacific in the control of the global climate state and atmospheric CO_2. With this, and keeping in mind the integral role of the low-latitude Pacific Ocean in the atmosphere's heat balance (Cane, 1998), low-latitude processes have to be considered when investigating the drivers of global climate transitions.

Given the possibility of past and future modifications of the Walker cell, we undertake here a sensitivity study to examine the response of the ocean carbon cycle to changes in the strength of the zonal equatorial surface wind stress by factors of $\pm 10\%$, $\pm 20\%$ and $\pm 30\%$ between 30°N and 30°S in the Pacific, the Atlantic and the Indian Ocean. The focus here is on the long-term equilibrated carbon cycle response.

I.2 Model and experimental design

The study employs the University of Victoria Earth System Climate Model (UVic ESCM, Version 2.9) (Weaver et al., 2001). The model consists of the ocean global circulation model (OGCM) MOM2.2, with a zonal resolution of 3.6° and a meridional resolution of 1.8° (Pacanowski, 1995). Ocean circulation is forced by monthly mean reanalysis winds from the National Centers for Environmental Prediction (NCEP) (Kalnay et al., 1996). The OGCM is coupled to a two-dimensional energy-moisture balance model of the atmosphere, a thermodynamic/dynamic sea-ice model (Semtner, 1976; Hibler, 1979; Hunke and Dukowicz, 1997), a land surface scheme, a vegetation model (TRIFFID) (Meissner et al., 2003) and a sediment model (Archer, 1996). The UVic ESCM includes representations for both, biological (Schmittner et al., 2008) and solubility cycling of carbon

(Ewen et al., 2004). The UVic ESCM has been assessed against observational data and proven to be able to represent ocean properties, such as ocean circulation, temperature and salinity as well as biological processes, reasonably well (e.g. Meissner et al., 2003; Schmittner et al., 2008; Meissner et al., 2012).

For this study we integrate one control (CTRL) and six sensitivity simulations. CTRL is forced with NCEP reanalysis wind fields while the other scenarios are forced with either an increase (hereafter $\tau_{+10\%}$, $\tau_{+20\%}$ and $\tau_{+30\%}$) or a decrease (hereafter $\tau_{-10\%}$, $\tau_{-20\%}$ and $\tau_{-30\%}$) in the easterly components of the zonal surface wind stress (τ_x) by 10%, 20% or 30% between 30°N and 30°S. The westerly wind component of the zonal surface wind stress field remains unchanged.

All model scenarios are integrated with constant forcing until an equilibrium is reached. Atmospheric CO_2 concentrations are fixed to the year 2000 value of 369 ppm in all experiments. To investigate the changes in the oceanic carbon budget, oceanic carbon can be split into different components: saturation carbon (C^{sat}), disequilibrium carbon (ΔC), soft tissue (C^{soft}) and hard tissue carbon (C^{hard}) following a method summarised by Williams and Follows (2011). Here we analyse changes in total dissolved inorganic carbon (DIC) as well as changes in C^{sat} and the circulation-driven component of ΔC only. This is achieved by switching the marine ecosystem model on or off for all simulations (including the control experiments). Via this method we can isolate changes due to the solubility pump, affecting C^{sat} and the circulation-driven part of ΔC, from those due to the biological pump, affecting C^{soft} and C^{hard}. Note that the exclusion of marine biology leads to a reduced carbon content in the ocean throughout all experiments compared to the equivalent experiments including a biological model.

I.3 Vertical distribution of DIC changes

The equatorial overturning cells show a clear weakening in response to the reduction in surface wind stress and a strengthening in the increased τ_x case; with changes varying between - 13.6 Sv and 12.4 Sv (Figure I.1a and I.1b). The overturning in density coordinates shows equivalent results with maximum changes in the equatorial cells of -15.1 Sv and 13.5 Sv for experiments $\tau_{+30\%}$ and $\tau_{-30\%}$, respectively (Figure I.2). The changes in

the other major overturning cells, such as the North Atlantic Deep Water and Antarctic Bottom Water overturning cells, do not exceed 2 Sv (Figure I.3). In the experiments with smaller wind perturbations, the overturning response exhibits similar patterns but with reduced magnitudes (Figure I.4).

The changes in zonal mean DIC at the surface and at depth at high latitudes are mostly of the same sign, except for over a region between the surface and ∼200 m depth at the Equator (Figure I.1c and I.1d). The main driver for this change is the solubility pump; in particular changes in surface ocean temperatures, caused by a combination of decreased upwelling, reduced Ekman transport away from the equator and a reduction of the western boundary currents (compare Figure I.1c and Figure I.1e). The resulting SST differences at high latitudes (cooling for decreased τ_x and vice versa for increased τ_x) alter the solubility of CO_2 in waters at regions of high ventilation depth (Figure I.5) and thereby affect the strength of the solubility pump as shown in panels I.1(e) and I.1(f). Note that the global oceanic carbon budget for CTRL without biology is much smaller than for the full model. Accordingly changes are smaller than in comparison to the full model too.

The deep ocean between ∼20°S and ∼60°N and depths below ∼600 m in $\tau_{-30\%}$ (∼800 m in $\tau_{+30\%}$) exhibits changes of the opposite sign compared to the rest of the global ocean (Figure I.1c and I.1d) which are due to marine biology. This can be seen by the lack of the DIC response differences in the deep ocean when the biological pump is suppressed compared to the experiments with biology (compare Figure I.1c and I.1d with Figure I.1e and I.1f). This is confirmed by an assessment of the nutrient to DIC upwelling ratio into the surface layer between 30°S and 30°N at the eastern boundary of each basin (Figure I.6), which shows that the relative changes in nutrient upwelling exceed the relative changes DIC upwelling. Equivalent patterns of change, only less pronounced, can be found in the experiments with wind perturbations of ±10% and ±20% (Figure I.7).

I.4 Global DIC inventory response

In experiments with the biological pump switched off, the global carbon content scales with the changes in surface wind stress (grey bars in Figure I.8a). This leads to an

almost linear increase in net global DIC for decreased surface wind stress. A linear trend is also noted for the increased wind cases ($\tau_{+10\%}$, $\tau_{+20\%}$ and $\tau_{+30\%}$) in these pure solubility-pump experiments. Hence, overall, the net DIC in the solubility pump experiments varies inversely and linearly with tropical zonal wind stress strength. The model suggests maximum changes of up to 20 PgC ($\tau_{-30\%}$) and -24 PgC ($\tau_{+30\%}$) respectively. This response is in part due to changes in high-latitude SST, especially in regions of deep and intermediate water formation (Figure I.5), resulting in variations in carbon solubility and thus the physical carbon pump.

When biology is turned on, an increase in equatorial wind stress still leads to a reduction in global DIC in all experiments, which scales with the change in the wind stress and is slightly higher than the changes obtained when excluding biological impacts (compare blue to grey bars in Figure I.8a). The response to a zonal wind stress decrease however is more complex and non-linear. These changes indicate that the biological pump offsets the solubility pump under decreased τ_x conditions (Figure I.8a).

The non-linear behaviour described above derives exclusively from changes in the biological pump of the Pacific Ocean (black bars in Figures I.8b and I.8c), which exhibit total DIC changes of the opposite sign compared to all other ocean basins (Figure I.8b). Furthermore, the total DIC change in the Pacific is twice as high for a decrease in τ_x compared to the equivalent increase in τ_x in the $\tau_{-30\%}$ and $\tau_{+30\%}$ experiments.

I.5 Response in the biological pump

Overall the changes in DIC averaged over the upper 1000m correspond well to changes in apparent oxygen utilization (AOU; also averaged over the upper 1000 m; Figure I.9). Focusing on the decreased surface wind stress experiments, the difference plots reveal an overall increase in the DIC concentration in all ocean basins. However, the Pacific basin shows a clear decrease in the upper 1000 m at the eastern boundary of the basin. At the same time DIC increases at the western boundary of the North Pacific. This pattern is also seen at the depth of the 20-degree isotherm, which can be taken as a proxy for the depth of the pycnocline (Figure I.10). A similar pattern evolves when the experiments are reconfigured to run as a transient perturbation, starting at zero and ramping up to

maximum wind anomalies of ±10%, ±20%, ±30% after 50 years (Figure I.11). Similar patterns of change but of lower amplitude can be found in the Atlantic and the Indian Ocean, respectively. The experiments using an increased τ_x show the same pattern but with opposite sign (Figure I.9; right column).

The corresponding pattern of DIC and AOU changes gives a clear indication that the DIC changes are at least partly caused by changes in marine biological activity. As the DIC changes at the eastern boundary of each ocean basin are not present in the solubility pump experiments (Figure I.12), solubility changes are not the cause of this feature of the DIC response to trade wind changes. In contrast, at the western boundary of the North Pacific and North Atlantic the solubility experiments do exhibit a similar increase in DIC, which suggests that the changes in these regions are caused by an interplay of both physical and biological processes.

The changes in the eastern tropical ocean regions are caused by changes in upwelling of nutrients into the euphotic zone. Specifically a decrease in τ_x leads to a decrease in upwelling, nutrient availability, NPP and remineralization (Figure I.13) and therefore in DIC at depth, explaining the DIC changes seen in the intermediate and deep ocean at low latitudes (Figures I.1c and I.1d). This signal is consistent for all ocean basins and across all six wind perturbation experiments.

The Humboldt Current Large Marine Ecosystem shows the response with highest magnitude, resulting in the higher sensitivity of Pacific Ocean carbon storage to changes in τ_x (Figure I.8b). Overall, net upwelling across the 200 m interface in the equatorial Pacific Ocean varies between 34.6 Sv in $\tau_{+30\%}$ and 21.3 Sv in $\tau_{-30\%}$ compared to 27.6 Sv in CTRL. The Atlantic and Indian Oceans do include similar upwelling systems with net values at 200 m of 12.1 Sv and 13.7 Sv in CTRL, respectively. Here, however, the response of the total basin is dominated by the DIC changes outside of these upwelling regions due to the lower biological activity in these regions. This reverses the positive correlation between total DIC and τ_x seen in the Pacific into a negative correlation in the other ocean basins (Figure I.8b). Net upwelling at 200 m in the Atlantic and the Indian ocean reaches maximum values of 10.4 Sv (14.4 Sv) in the Atlantic and 12.2 Sv (15.7 Sv) in the Indian Ocean in $\tau_{-30\%}$ ($\tau_{+30\%}$), respectively.

The upwelling in the east Pacific is strongly influenced by the equatorial undercurrent

(EUC) (Rodgers et al., 2008). Changes in the depth of isopycnal surfaces compared to the EUC can therefore alter the nutrient supply to this region. In a previous model study investigating the effect of changes in low latitude surface wind stress, Rodgers et al. (2008) described a decoupling between the pycnocline and the ferrocline in the equatorial Pacific. Here we find a similar decoupling. While the pycnocline in the equatorial Pacific changes in all sensitivity experiments (shoaling for increased and deepening for decreased wind stress conditions; Figures I.14 and I.15), the mean depth of the nutricline remains almost unchanged (Figure I.15). This alters the supply of nutrients to the east Pacific and contributes to the change in biological activity described above.

I.6 Summary and Conclusions

This study assesses the impact of changes in tropical surface wind stress on the marine carbon cycle in a series of sensitivity experiments designed to assess the model response to idealized tropical wind perturbations. While an increase in low latitude surface wind stress leads to an almost linear decrease in total DIC, the changes induced by a decreased trade wind system show a non-linear response. This should have implications for the future carbon cycle in response to ongoing warming and weakening of the Walker circulation (Collins et al., 2010; Tokinaga et al., 2012).

Isolating the two carbon pumps reveals that the solubility pump forces each ocean basin in the same way and thereby leads to an approximate linear dependence of global DIC on equatorial zonal wind stress. The changes in the solubility pump are due to changes in global ocean SST and circulation; in particular a warming of high-latitude surface waters for strengthened τ_x conditions leading to decreased carbon solubility and vice versa for weaker equatorial trade winds.

In the full carbon cycle experiments the non-linearity in the response to decreased τ_x conditions is caused by changes in Pacific Ocean productivity near the eastern boundaries. Weaker nutrient upwelling in $\tau_{-10\%}$, $\tau_{-20\%}$ and $\tau_{-30\%}$ leads to a decrease in NPP which causes a decrease in the export of organic material to the deep ocean, resulting in decreased DIC formation through remineralization at depths at low- and mid-latitudes that offsets the solubility driven increases in carbon. The same interplay of the two com-

peting pumps determines the total DIC change in the increased τ_x experiments. However the changes in ocean productivity in the increased τ_x experiments are less pronounced, and are unable to offset the linear changes driven by the alteration of carbon solubility.

Overall the processes determining the response of ocean carbon to changes in low latitude winds can be summarised as follows: The main driver behind all changes in both carbon pumps are modifications in ocean circulation, most importantly (a) the poleward transport of surface waters and (b) equatorial upwelling. Modifications in the poleward transport affect mid- and high-latitude SST, which respond with the same sign as the perturbation (i.e. increased winds, increased mid- to high-latitude SST). This cooling (warming) for decreased (increased) equatorial winds leads to changes in carbon solubility in seawater. This affects the solubility pump directly and is of the same sign in all ocean basins. On the other hand, modifications in equatorial upwelling lead to changes in the nutrient availability and with this net primary productivity, export production and remineralization, i.e. the biological carbon pump. This results in changes in DIC at depths. This mechanism dominates the response of the Pacific Ocean in the reduced wind experiments. In all other ocean basins and under increased tropical wind conditions the effect of this mechanism is small compared to changes in carbon solubility due to SST changes.

In respect to past climate regimes, this study provides an estimate of the potential impact of low-latitude wind changes on the global carbon cycle. In this study the focus was on the equilibrium response of the coupled climate system; a closer investigation of possible impacts due to potential changes in the Redfield ratio and atmospheric CO_2 feedbacks is left for future studies.

In conclusion this study sheds light on the carbon cycle response to altered tropical trade winds, showing that oceanic carbon uptake behaves in two competing ways to determine the net DIC response. This leads to an almost linearly decreasing total carbon content for increasing τ_x conditions but a non-linear response for equivalent wind stress reductions (Figure I.8). With progressing climate change, and if ongoing trends in the tropical trade wind strength continue, this has implications for the uptake, storage and distribution of DIC in the respective ocean basins. However, the sign of the response; namely increased ocean carbon storage for decreased winds, implies a negative or self-limiting feedback.

This suggests that the global atmospheric CO_2 response to tropical wind changes will be small, despite significant regional implications.

I.7 Acknowledgements

This study was funded by the Australian Research Council (FL100100214 and FT10010043) and supported by an award under the Merit Allocation Scheme on the NCI National Facility at the Australian National University. N. Ridder was funded under the IPRS scheme of the Australian Government Department of Industry, Innovation, Science, Research and Tertiary Education. The authors thank Michael Eby for his engagement during the review progress, Rüdiger Gerdes for his helpful comments during final stages of this manuscript and Willem Sijp for assistance in configuring the model experiments used in this study. The authors also thank two anonymous reviewers for their helpful comments.

I.8 Figures

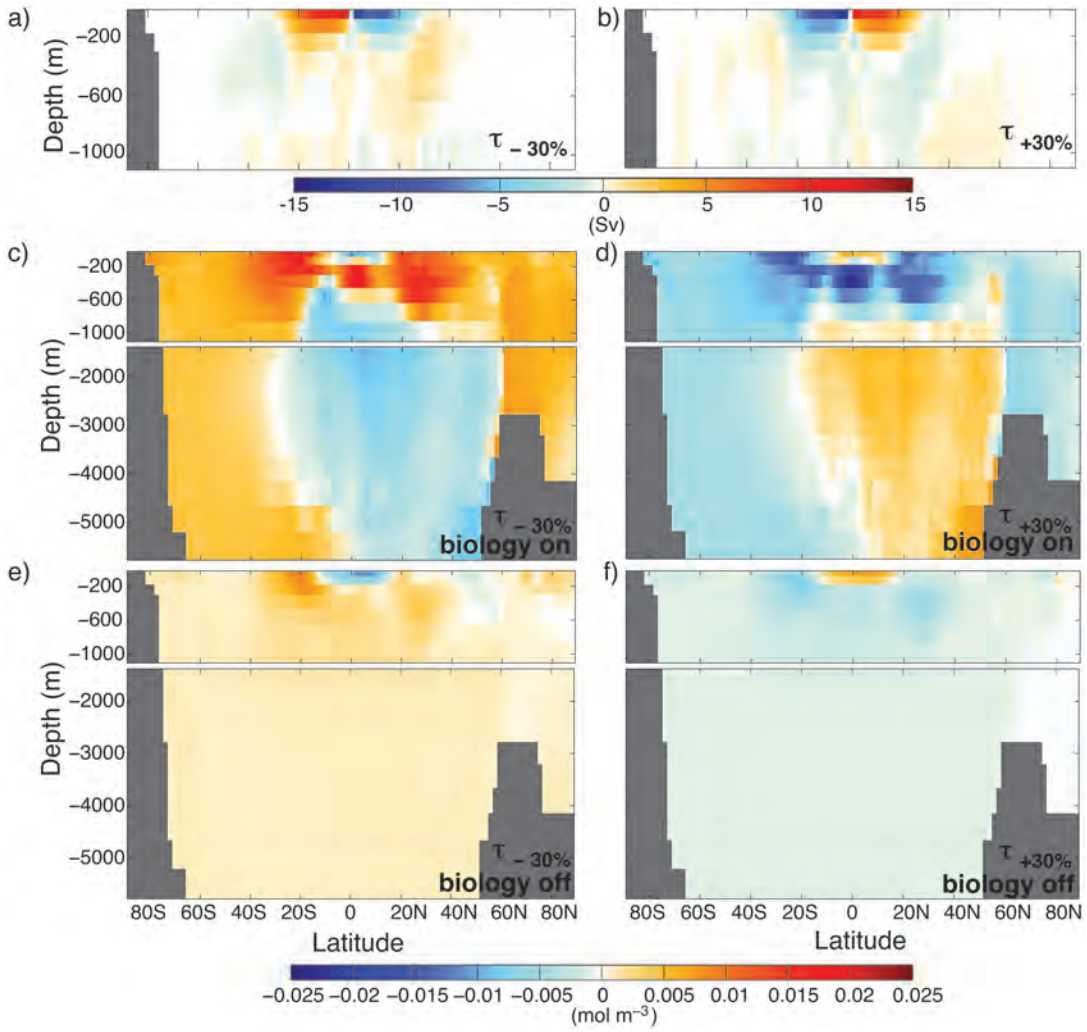

Figure I.1: (a) Difference in annual mean MOC (Sv) in the upper 1000 m between $\tau_{-30\%}$ and CTRL; (c) annual mean zonal DIC changes (mol m^{-3}) between $\tau_{-30\%}$ and CTRL; (e) as (c) but for experiments without marine biology; (b),(d) and (f) as in (a), (c) and (e) respectively, only for $\tau_{+30\%}$ minus CTRL.

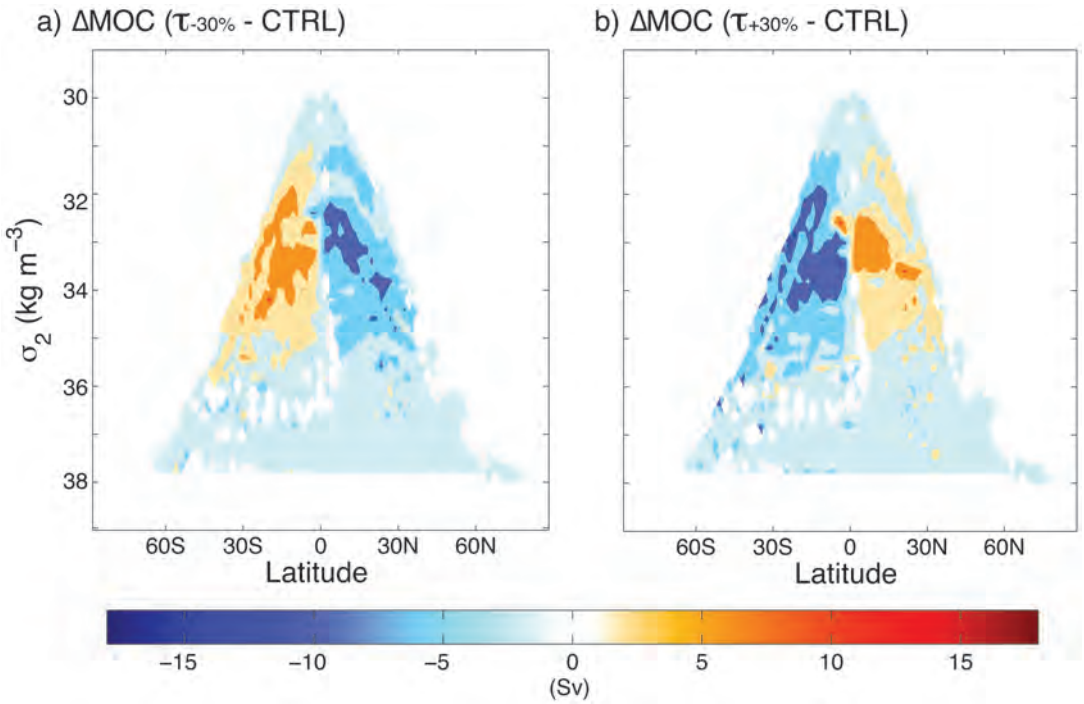

Figure I.2: (a) Changes in annual mean MOC (Sv) in density space between the 30% reduced low-latitude wind stress experiment and unperturbed conditions ($\tau_{-30\%}$ minus CTRL). (b) as (a) but for $\tau_{+30\%}$ minus CTRL.

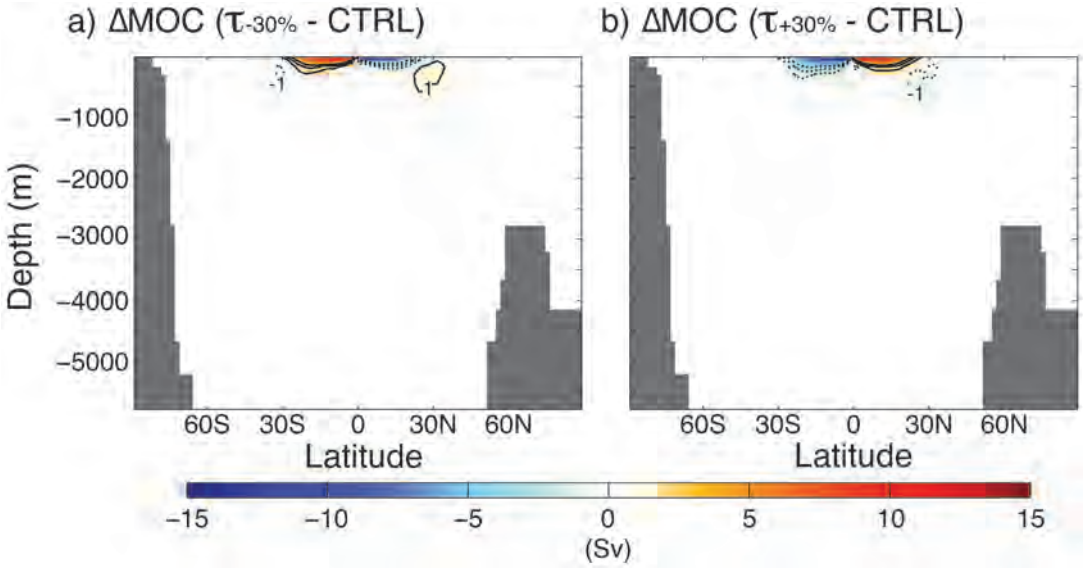

Figure I.3: (a) Difference in annual mean MOC (Sv) in depth space at all depths between $\tau_{-30\%}$ and CTRL. Contour intervals are 1 Sv starting at ±1 Sv. Solid contours indicate changes with positive sign while dotted contours mark changes of negative sign. (b) as (a) but for $\tau_{+30\%}$ minus CTRL.

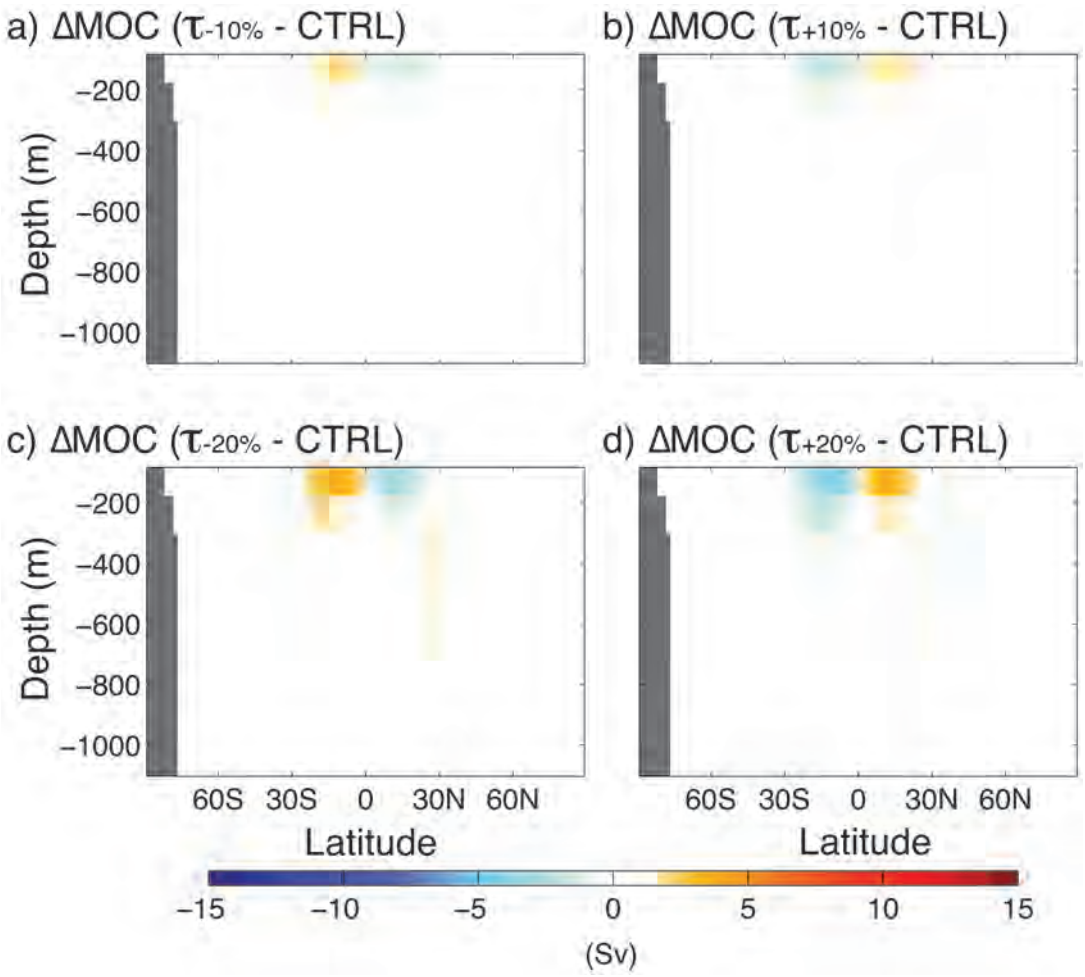

Figure I.4: Changes in annual mean MOC (Sv) in the upper 1000 m (as Figure I.1) for (a) $\tau_{-10\%}$ minus CTRL, (b) $\tau_{+10\%}$ minus CTRL, (c) $\tau_{-20\%}$ minus CTRL and (d) $\tau_{+20\%}$ minus CTRL.

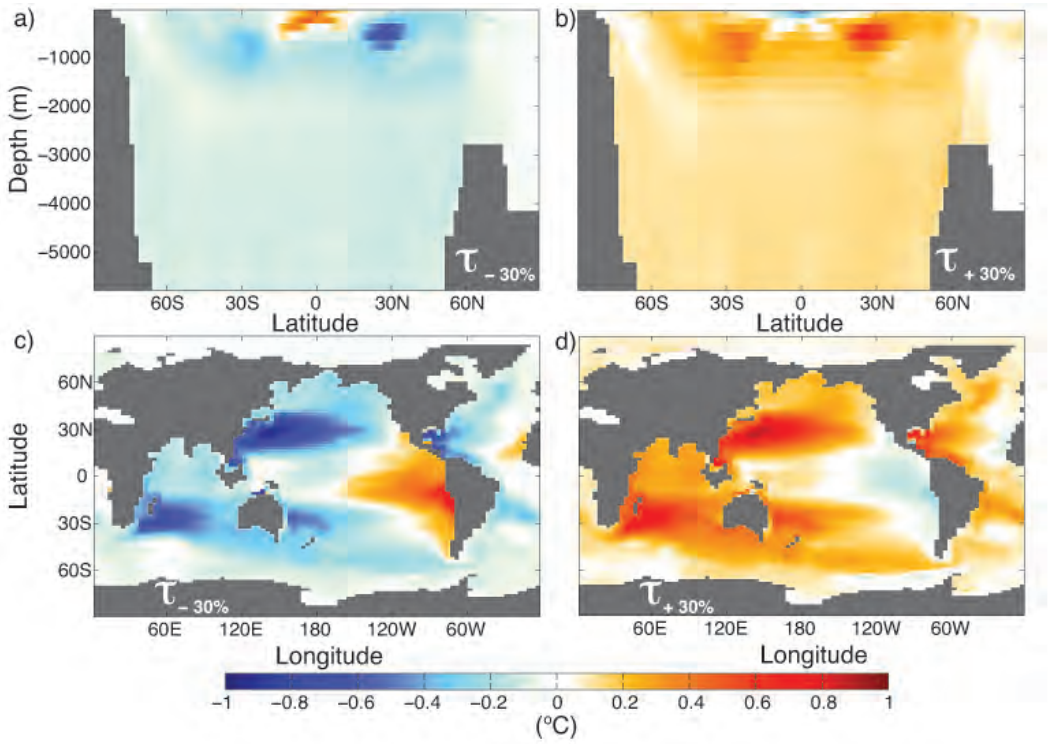

Figure I.5: (a) Annual mean zonal temperature difference (°C; $\tau_{-30\%}$ minus CTRL); (b) as (a) but for $\tau_{+30\%}$ minus CTRL. (c) Annual mean upper ocean temperature differences (averaged between surface and 1000 m) for $\tau_{-30\%}$ minus CTRL; (d) as (c) but for $\tau_{+30\%}$ minus CTRL.

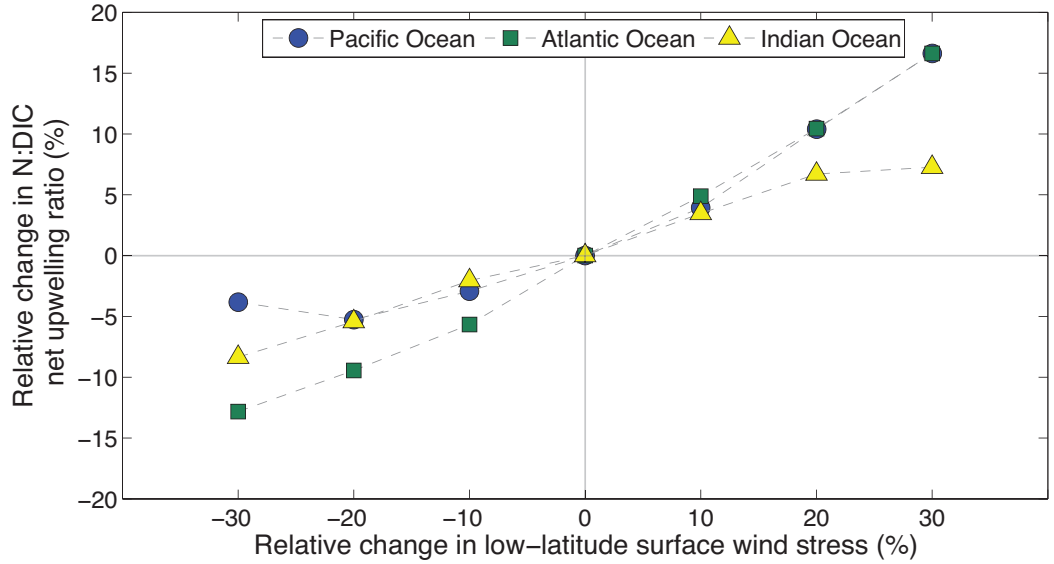

Figure I.6: Relative change in the ratio of nutrients to DIC in the net integrated upwelling at the eastern boundaries of the Pacific Ocean (blue circles), Atlantic Ocean (green squares) and the Indian Ocean (yellow triangles) in all experiments compared to CTRL. The upwelling was calculated at 50 m depth between 30°S and 30°N off the coast of the respective basins. The longitudinal extent was limited to 22 degrees in all cases.

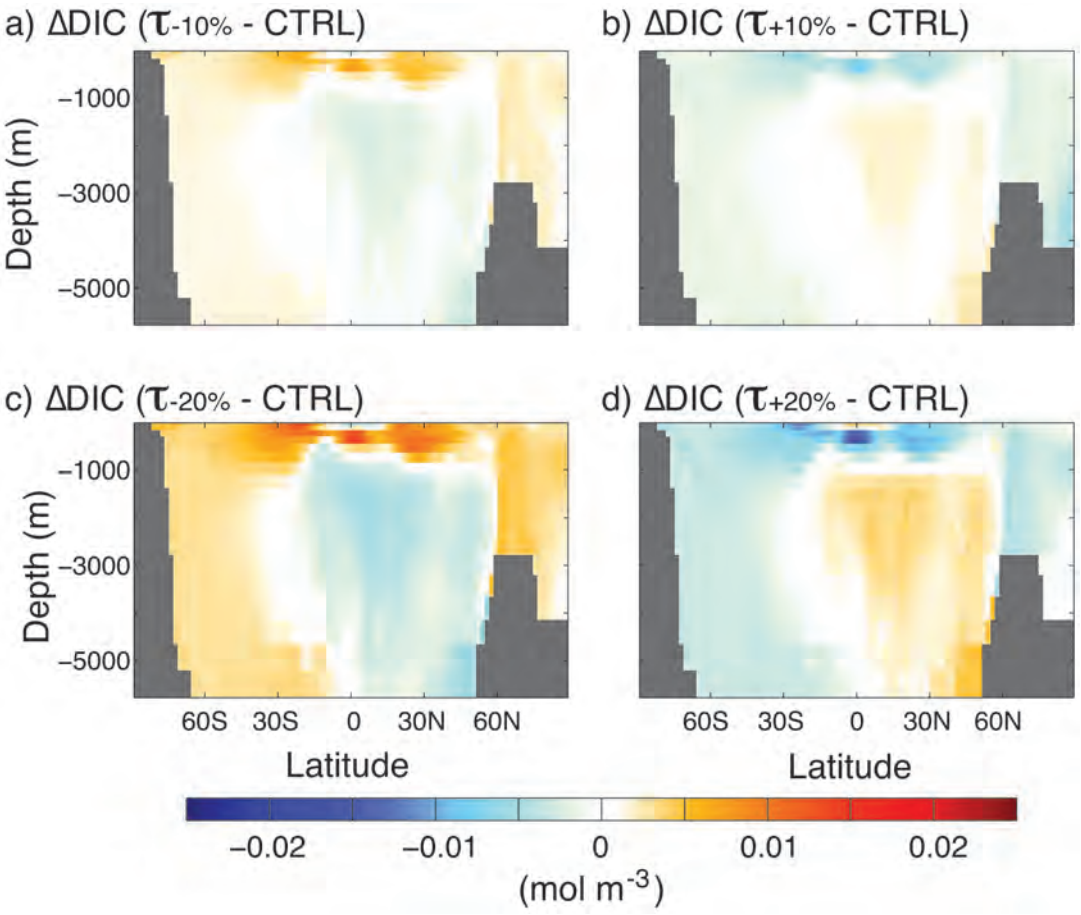

Figure I.7: (a) Annual mean zonal DIC changes (ΔDIC; mol m^{-3}) between $\tau_{-10\%}$ and CTRL. (b), (c), (d) as (a) but for $\tau_{+10\%}$, $\tau_{-20\%}$ and $\tau_{+20\%}$, respectively.

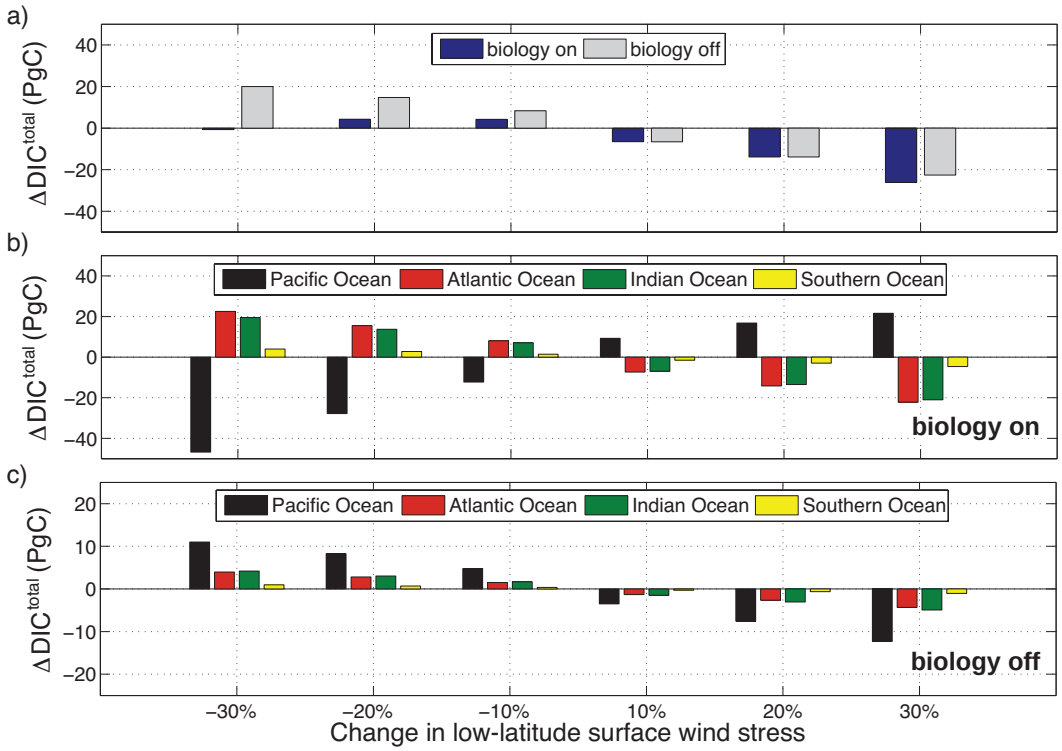

Figure I.8: (a) Difference in annual mean global DIC (PgC) between the respective wind stress experiments and CTRL. Blue bars show changes in annual mean global total DIC using the full carbon cycle while grey bars represent annual mean changes for the respective experiment with marine biology model switched off. (b) Difference in annual mean total DIC content (PgC) in the different ocean basins between wind stress experiments and CTRL using the full carbon cycle; black (Pacific Ocean), red (Atlantic Ocean), green (Indian Ocean) and yellow (Southern Ocean); (c) same as (b) with biology model switched off. Note that the range of the y-axis in panel (c) is smaller compared to the range in (a) and (b) to highlight changes; this is necessary due to the reduced carbon content in all experiments that exclude the biological carbon pump.

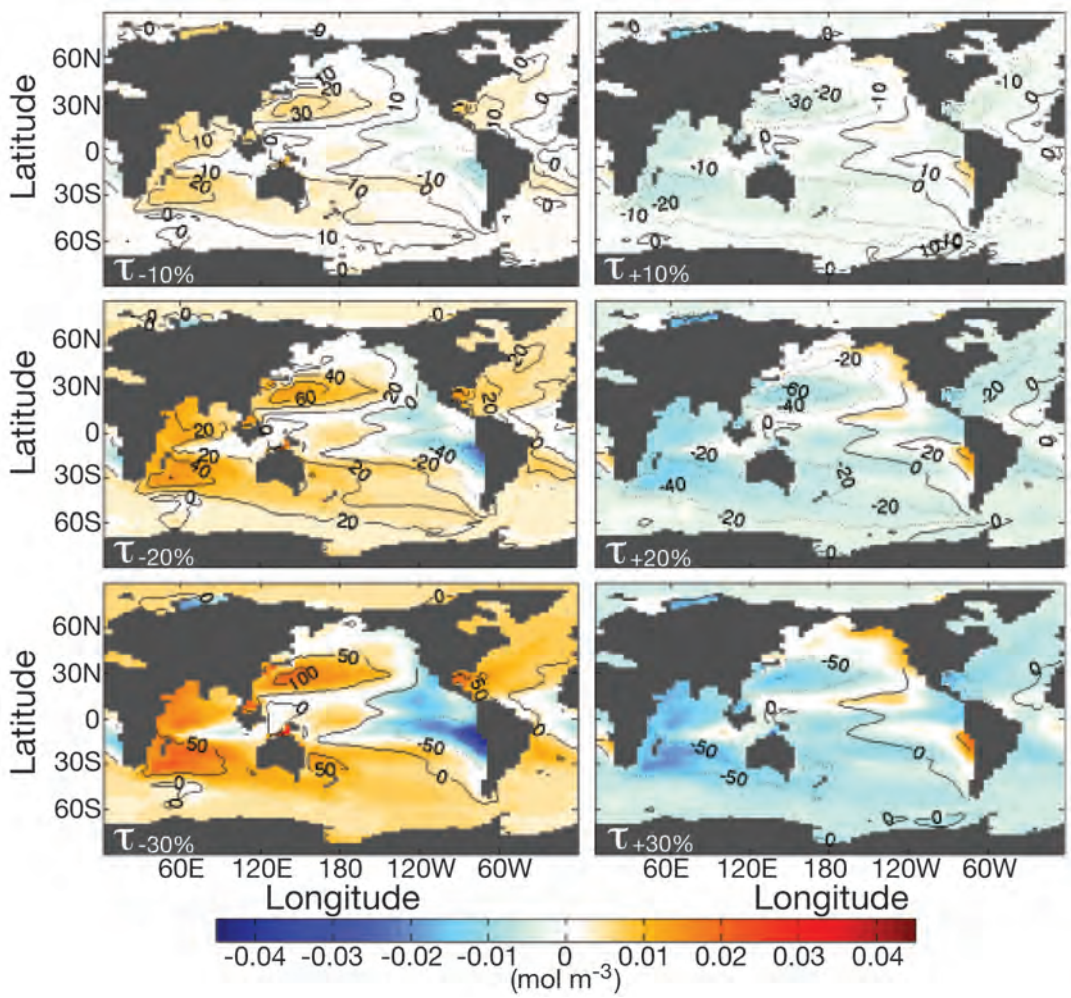

Figure I.9: Changes in annual mean upper ocean DIC (averaged between surface and 1000 m; colour shading) and changes in annual mean upper ocean AOU (μM; contours). Left column: decreased surface wind stress experiments minus CTRL. Right column: increased surface wind stress experiments minus CTRL. Contour intervals are 2 μM (top row), 5 μM (middle row) and 10 μM (bottom row), where 1 μM is 1 μmol l^{-1}.

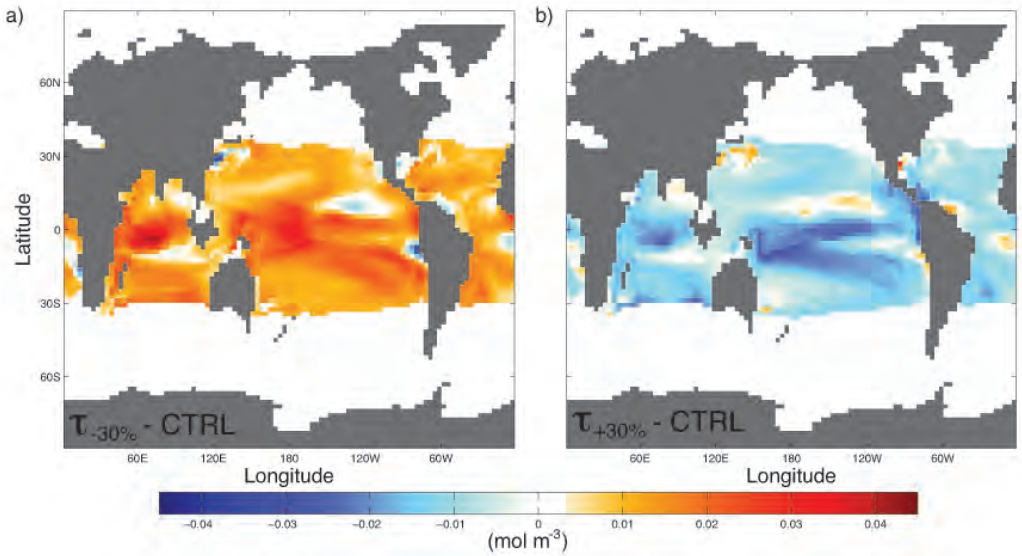

Figure I.10: Change in annual mean DIC concentration (mol m-3) on the 20-degree isotherm (D_{20}), which is used as proxy for the depth of the pycnocline, for (a) $\tau_{-30\%}$ minus CTRL and (b) $\tau_{+30\%}$ minus CTRL.

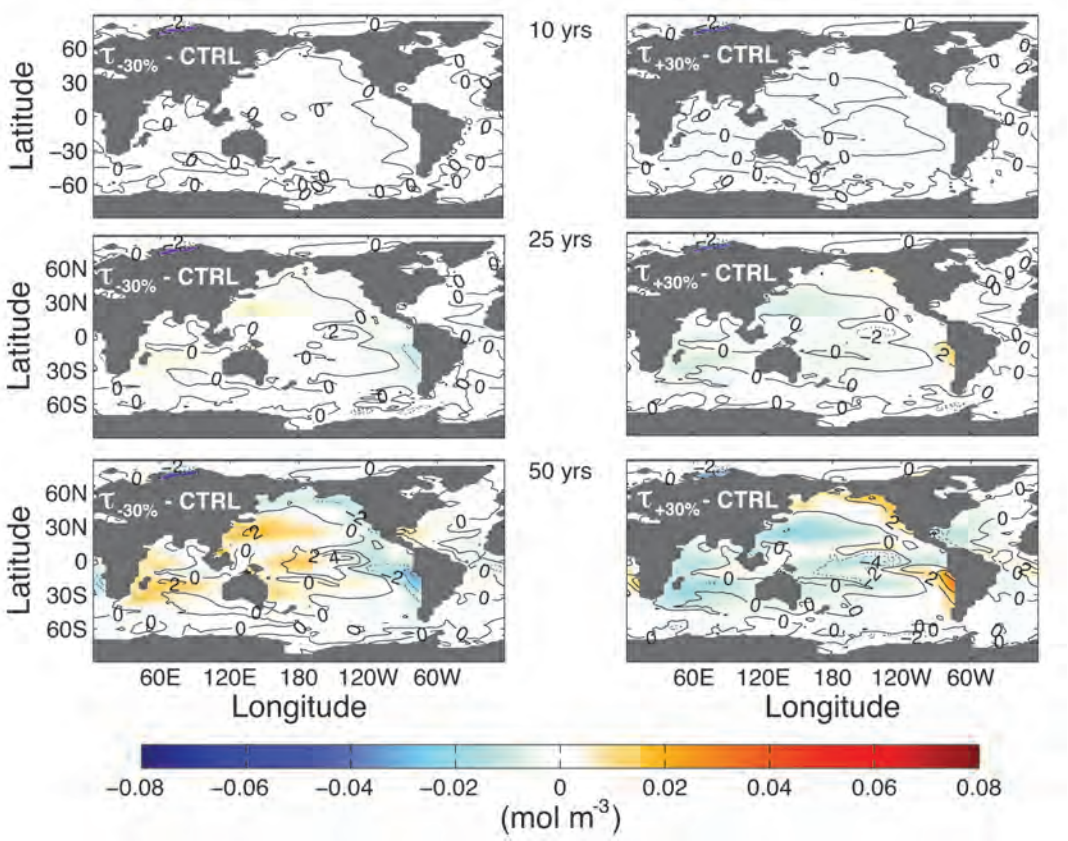

Figure I.11: Annual mean changes in upper ocean DIC (averaged between surface and 1000 m; mol m^{-3}) and AOU (averaged between surface and 1000 m; μM) in response to transient surface wind stress perturbations. In these experiments wind stress changes were introduced slowly, increasing from zero over a period of 50 years to reach maximum amplitudes equivalent to those used in the equilibrium experiments described in the main article. Left column: decreasing surface wind stress ($\tau_{-30\%}$) experiment minus CTRL. Right column: increasing surface wind stress ($\tau_{+30\%}$) experiments minus CTRL. Contour intervals are 2 μM with dotted lines indicating a decrease in AOU and solid contours marking an increase in AOU.

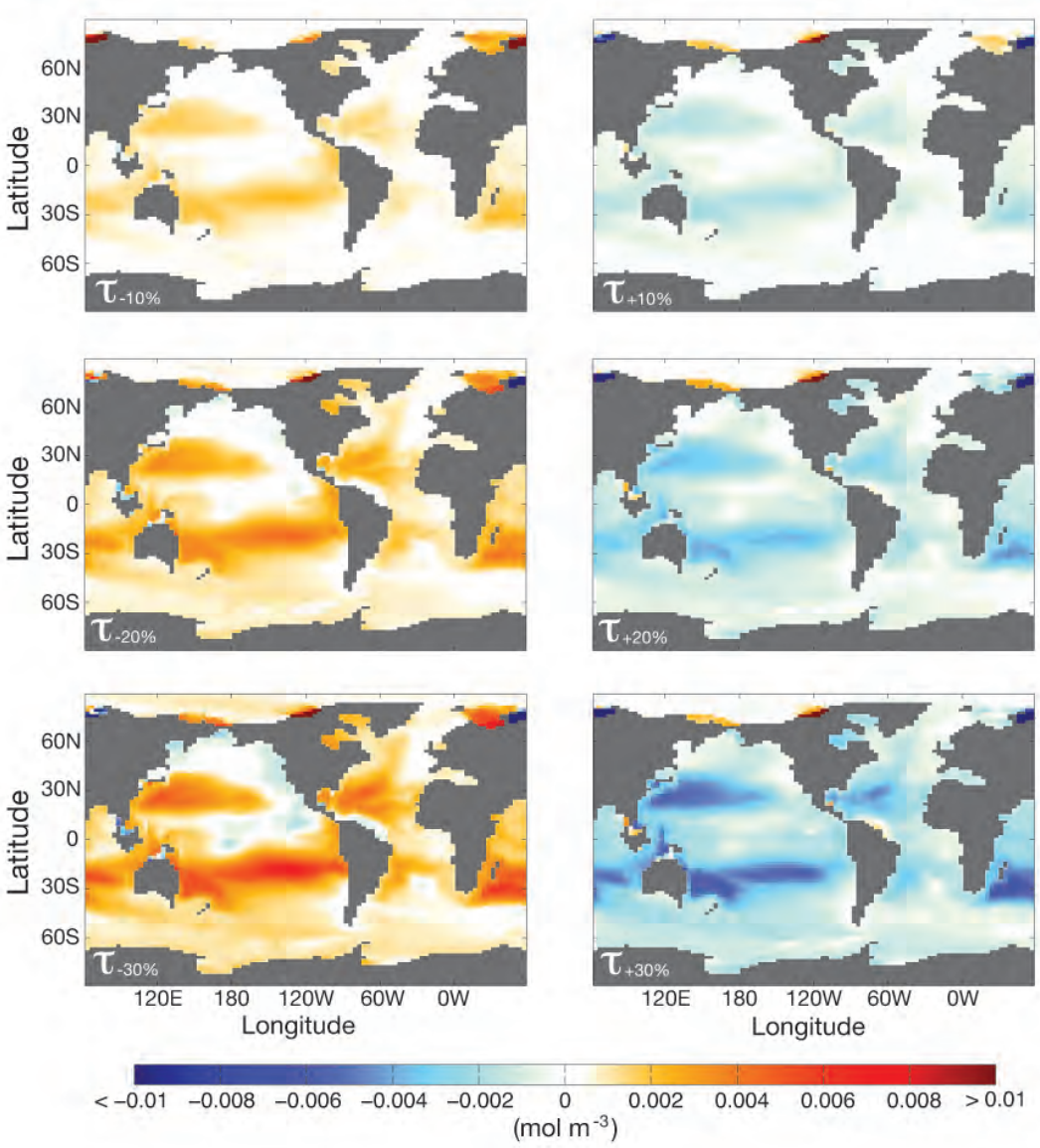

Figure I.12: Annual mean changes in mean upper ocean DIC (averaged between surface and 1000 m; mol m^{-3}) in solubility experiments (marine biogeochemistry model switched off). Left column: decreased surface wind stress experiments minus CTRL; Right column: increased surface wind stress experiments minus CTRL. Note that the colour scale used here is different to Figure I.9 to highlight the sign of changes in the solubility experiments; specifically changes are of a much reduced amplitude compared to the full carbon cycle experiments shown in Figure I.9.

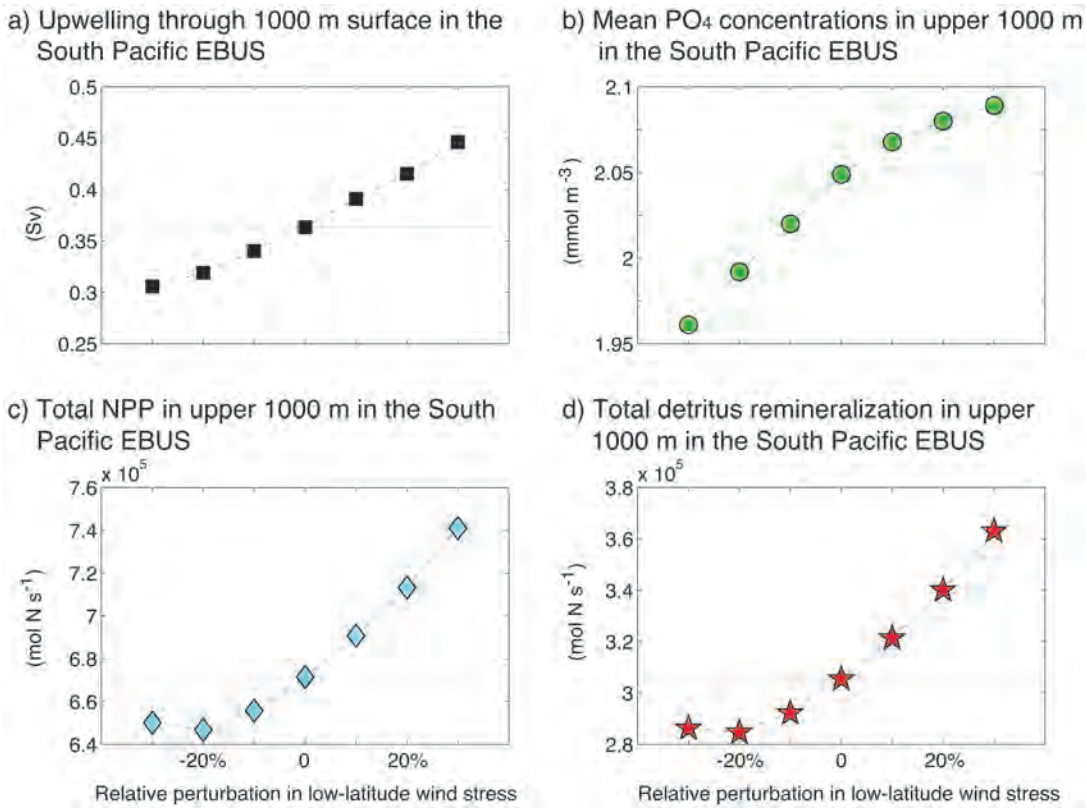

Figure I.13: (a) Annual mean upwelling (Sv) through the 1000 m depth surface in the Eastern Boundary Upwelling System (EBUS) in the South Pacific (between 100°W - 65°W and 30°S - 0°) as a function of the applied relative low-latitude wind stress perturbation. (b) ,(c) and (d) as (a) but for annual mean concentrations of PO_4 (mmol m−3), the annual mean volume-integrated net primary productivity (NPP; mol N s^{-1}) and detritus remineralization (mol N s^{-1}) in the upper 1000 m of the South Pacific EBUS.

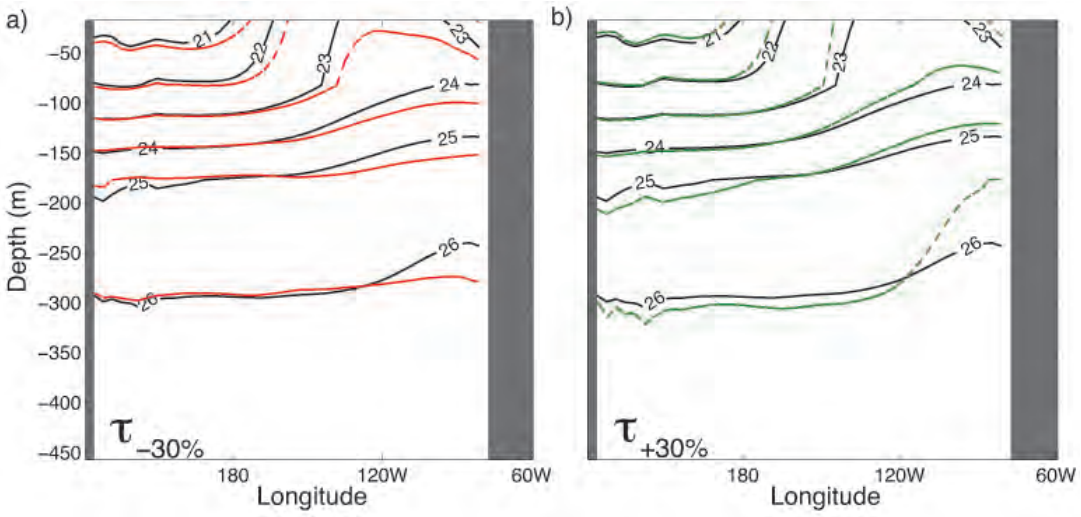

Figure I.14: Annual mean depth of density surfaces along the equatorial Pacific at 0.9°S. Contours show annual mean potential density (minus 1000) in units of kg m^{-3}; (a) $\tau_{-30\%}$ (red contours) vs. CTRL (black contours), (b) $\tau_{+30\%}$ (green contours) vs. CTRL (black contours).

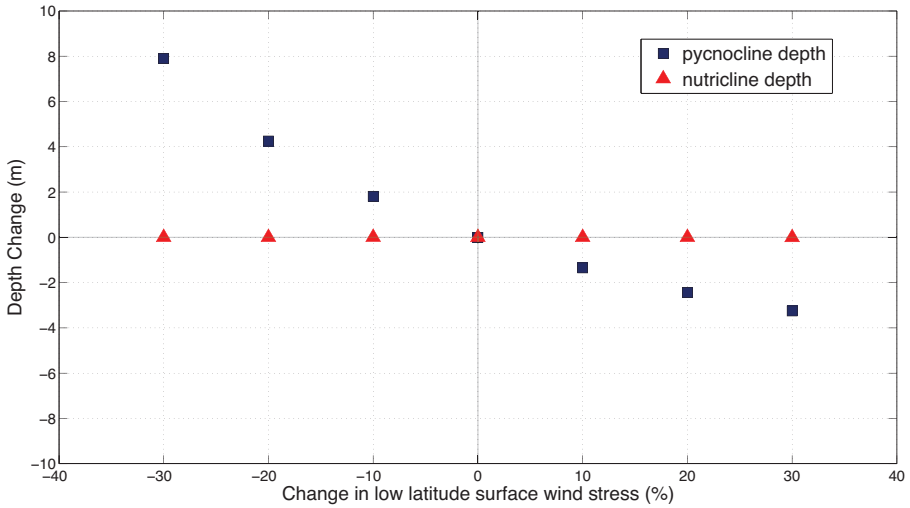

Figure I.15: Annual mean zonal depth change (m) of the 20-degree isotherm (blue squares) and the nutricline (red triangles) in the Pacific Ocean at 0.9°S versus wind stress perturbations. The 20-degree isotherm (D_{20}) is used as a proxy for the pycnocline depth; the nutricline depth is taken to be the depth of the strongest gradient in the vertical profile of the NO_3 concentration at 0.9°S in the Pacific Ocean.

Part II: Ocean Oxygenation and low-latitude surface wind stress

Abstract

Ocean oxygenation has been observed to have changed over the past few decades and is projected to change further under global climate change due to an interplay of several mechanisms. In this study we isolate the effect of modified tropical surface wind stress conditions on the evolution of ocean oxygenation in a numerical climate model. We find that ocean oxygenation varies inversely with low-latitude surface wind stress. Approximately one third of this response is driven by SST anomalies; the remaining two thirds result from changes in ocean circulation and marine biology. Global mean O_2 concentration changes reach maximum values of +4 μM and -3.6 μM in the two most extreme perturbation cases of -30% and +30% wind change, respectively. Localised changes lie between +92 μM under 30% reduced winds and -56 μM for 30% increased winds. Overall we find that the extent of the global low-oxygen volume varies with the same sign as the wind perturbation; namely weaker winds reduce the low oxygen volume on the global scale and vice versa for increased trade winds. We identify two regions, one in the Pacific Ocean off Chile, the other in the Indian Ocean off Somalia, that are of particular importance for the evolution of oxygen minimum zones in the global ocean.

II.1 Introduction

Marine life and biogeochemical processes are highly dependent on the oxygen (O_2) content of the ocean. Concentrations of O_2 below certain thresholds can disturb whole ecosystems and have a high impact on the cycling of important oceanic tracers, such as carbon and nitrogen. Three different concentration limits are of particular interest when studying the effect of dissolved O_2 on marine biogeochemistry; (i) hypoxia, (ii) suboxia and (iii) anoxia. Hypoxic conditions are those under which certain species suffer from an insufficient amount of O_2 for respiration, thus making these regions uninhabitable for that particular species. The minimum O_2 concentration which marks the border to hypoxic conditions varies depending on species. For the purpose of this paper we follow the definition of Gnanadesikan et al. (2012) who define the threshold for hypoxia to be at 88 μM. In suboxic waters nitrogen is involved in remineralization (denitrification) instead of O_2, reducing the availability of nitrogen as a nutrient for other biogeochemical processes, i.e. photosynthesis (e.g. Codispoti et al., 2001; Oschlies et al., 2008). Most species are unable

to survive under suboxic conditions (Oschlies et al., 2008) hence regions with these low oxygen concentrations are often referred to as "Dead Zones" or Oxygen Minimum Zones (OMZ) (Cline and Richards, 1972). We again follow Gnanadesikan et al. (2012) and refer to water masses with O_2 concentrations below 8.8 μM as suboxic. Anoxic conditions describe waters that contain O_2 concentrations below 0.1 μM (Oguz et al., 2000). At this threshold sulphate-reduction occurs and starts to replace NO_3-respiration (Paulmier and Ruiz-Pino, 2009).

Low-oxygen conditions can be found in eastern boundary shadow zones and are caused by a combination of high biologic activity (e.g. Helly and Levin, 2004) and minimal lateral renewal of surface waters (Reid Jr, 1965). The strongest OMZs are located in the Pacific Ocean and contain O_2 concentrations below 0.1 μM. The Atlantic and Indian Ocean contain similar low oxygen zones however do not reach anoxic conditions (Paulmier and Ruiz-Pino, 2009; Stramma et al., 2010). A change in the oxygenation of the ocean, and with this in the volume of low-oxygen waters, will potentially significantly affect the carbon and nitrogen cycles as well as the removal of other greenhouse gases from the atmosphere. This can lead to an amplifying feedback on global climate change as reduced biological productivity implies reduced ocean carbon uptake. Observations show a negative trend in the ocean oxygenation and suggest that low-oxygen regions have been expanding in volume over the past few decades (e.g. Stramma et al., 2008, 2010, 2012).

Model studies have so far yielded contradicting results regarding the future fate of low-oxygen regions under global climate change. Several studies suggest an expansion of suboxic conditions (e.g. Shaffer et al., 2009; Frölicher et al., 2009b) due to an increase in stratification causing a reduction in ocean ventilation (Matear et al., 2000; Bopp et al., 2002). Other studies contradict these projections; for example Duteil and Oschlies (2011) show that the choice of the background diapycnal mixing can dampen the effect of global climate change on OMZs. Matear and Hirst (2003) find that due to a reduction in export production in the low-oxygen regions, O_2 concentrations in the tropical thermocline can increase in global warming simulations. Gnanadesikan et al. (2012) also find increased O_2 concentrations in one of the strongest OMZ's in the Southeast Pacific off Chile. In their

study a shift in surface winds to a more along-shore orientation of wind stress due to changes in atmospheric circulation, in particular the strengthening of the subtropical high over this region, leads to higher oxygenation of waters off Chile at the core of the OMZ. This result is of particular interest as the Walker circulation and with this equatorial winds have been observed to have changed over the past few decades (e.g. Harrison, 1989; Trenberth and Hurrell, 1994; Clarke and Lebedev, 1996; Vecchi and Soden, 2007; L'Heureux et al., 2013). Several model and observational studies further suggest that low-latitude winds are likely to change further under global warming due to changes in the strength of the atmospheric equatorial zonal circulation (e.g. Vecchi et al., 2006; Vecchi and Soden, 2007; Collins et al., 2010; Tokinaga and Xie, 2011; Tokinaga et al., 2012). However, as yet there is no consensus on whether this circulation will strengthen or weaken. A change in zonal atmospheric circulation at low latitudes would likely affect the future evolution of low-oxygen zones in significant ways, for example via potential changes in circulation, upwelling, interior advection of oxygen and nutrient fluxes, which have been shown to induce changes in ocean biogeochemistry (Ridder et al., 2013). To elaborate the sensitivity of ocean oxygenation to low latitude surface winds we assess the impact of different tropical zonal easterly surface wind stress fields (hereafter τ_x) on global mean O_2 concentrations as well as on low-oxygen regions using a coupled climate model of intermediate complexity.

II.2 Model and Experimental Setup

This study uses the University of Victoria Earth System Climate Model (UVic ESCM v2.9), which consists of a full ocean global circulation model (OGCM) based on the GFDL Modular Ocean Model in Version 2.2 (Pacanowski, 1995) coupled to a two-dimensional energy-moisture balance model of the atmosphere, a thermodynamic/dynamic sea-ice model (Semtner, 1976; Hibler, 1979; Hunke and Dukowicz, 1997), a land surface scheme, a vegetation model (TRIFFID) (Meissner et al., 2003) and a sediment model (Archer, 1996). The OGCM has a zonal resolution of 3.6°, and a meridional resolution of 1.8° with 19 vertical levels. Ocean circulation is forced by a monthly-cycle wind climatology which for this study is predescribed by reanalysis winds from the National Center for Environmental Prediction (NCEP; Kalnay et al., 1996).

An NPZD model, which is nested within the OGCM, accounts for processes related to marine biology (Schmittner et al., 2008). Organic parameters are incorporated in the form of zooplankton and detritus and different classes of phytoplankton; nitrogen fixing diazotrophs and other phytoplankton. Oxygen concentrations are determined using a constant stoichiometry in relation to availability of nutrients, namely NO_3 and PO_4. The source term of oxygen includes the air-sea flux of O_2 and is inversely proportional to the sink term of PO_4 and therefore phytoplankton growth. The model thus represents photosynthesis as a reduction in PO_4 in combination with a production of O_2 at the same rate. Conversely, respiration consumes oxygen; in the model this occurs at a rate equal to the remineralization of PO_4. The marine biological model accounts for a decrease in remineralization rate in low oxygen environments ($[O_2] < 10$ μM). Following OCMIP recommendations it limits O_2 consumption below concentrations of 5 μmol kg^{-1} and includes denitrification as a nutrient sink in these regions. In its current version the model slightly overestimates the production of oxygen due to (i) nitrogen fixation, as it assumes the same stochiometry here as for primary production, and (ii) the continuation of remineralization under truly anoxic and nitrate-depleted conditions. However, while this results in an increase in the modelled global mean surface oxygen flux by about 0.05 mol O_2 m^{-2} yr^{-1}, the effect on relative changes in the air-sea O_2 exchange between the different experiments and CTRL are insignificant. The impact on modelled global mean O_2 concentrations, denitrification, remineralization and the extent of low-oxygen volumes in general are also negligible. A detailed description of the marine biological model can be found in Schmittner et al. (2008).

The UVic ESCM has been verified against observational data and proven to be able to represent ocean properties, including ocean circulation, temperature, salinity as well as biological processes reasonably well (e.g. Weaver et al., 2001; Schmittner et al., 2008). Despite a small warm bias in sea surface temperatures (SST) of roughly 0.39°C over observed low oxygen regions, indicating shortcomings in the representation of the Eastern Boundary Upwelling System, the model is able to reproduce the oceanic oxygen inventory within 3% of the value provided by the World Ocean Atlas (Oschlies et al., 2008) and reaches a correlation coefficient of 0.9 (Cocco et al., 2013). Like most OGCMs, the UVic

ESCM overestimates the extent and strength of low-oxygen regions slightly, nevertheless the model captures their broad observed patterns reasonably well (Oschlies et al., 2008; Cocco et al., 2013). For further assessment of the performance of the UVic ESCM in regards to key biogeochemical parameters the reader is referred to Cocco et al. (2013).

In this study the UVic ESCM is used to perform seven model experiments to assess the impact of changed low latitude wind conditions on ocean oxygenation. A similar study has been undertaken exploring identical wind stress anomalies and their impact on dissolved inorganic carbon (Ridder et al., 2013). Here we assess the same wind stress changes and their impact on dissolved oxygen. The reference scenario (hereafter CTRL) uses monthly average NCEP reanalysis wind fields. The six additional experiments use NCEP data with changed conditions in the latitudes between 30° N and 30° S. These changes consist of decreases in the easterly zonal wind stress component by factors of 10%, 20% and 30% (hereafter $\tau_{-10\%}$, $\tau_{-20\%}$, $\tau_{-30\%}$, respectively) and equivalent increases in the easterly components (hereafter $\tau_{+10\%}$, $\tau_{+20\%}$, $\tau_{+30\%}$). The westerly component of the zonal surface wind stress as well as the wind speed, and with this the gas piston velocity, remains unchanged, both inside the tropics and globally. This idealised approach of systematically changing easterly wind stress is used to simplify the identification of the wind-driven mechanisms determining ocean oxygenation. Under more realistic conditions any variation in the Walker Circulation is expected to result in more complex wind stress changes, with regionally varying conditions of strengthened or weakened winds. This should be kept in mind when interpreting the results of this study, which aims to assess the sensitivity of ocean oxygenation to large-scale wind stress changes and the associated ocean dynamics and biogeochemical mechanisms, with implications for predictions of the future evolution of dissolved oxygen.

All model experiments commence from an equilibrated simulation, which used contemporary forcing fields and was integrated for 8,000 years. The model experiments then run until an equilibrium under the new wind conditions is reached. Additionally, a set of transient perturbation experiments has been performed, in which the perturbation starts at time t=0 and is ramped up from zero to maximum wind anomalies of ±10%, ±20% and ±30% over half a century. Observed multi-decadal variability in the Pacific

zonal wind stress, which has recently been demonstrated to have varied between around ±10-20% during the past century, with peaks of over ±30% (England et al., 2014), leaves the chosen perturbation anomalies well within the observed range of variability. Furthermore, future trends in tropical zonal winds and the Walker Circulation could also span this range (see, e.g. Collins et al., 2010). The atmospheric CO_2 concentration was fixed at 369 ppm in all wind field scenarios.

A passive dye tracer is introduced into the OGCM to track changes in Subantarctic Mode Water (SAMW). The dye tracer follows the model's transport equation for tracers such as temperature and salinity but is restored to one at the surface between 58.5°S - 45.9°S and 70.2°E - 70.2°W at every time step. Everywhere else the dye tracer is initiated with a concentration of zero and it then evolves freely according to the modelled ocean transport. To additionally allow the determination of ventilation time changes due to the applied wind stress perturbations, a second tracer, a passive age tracer, has also been implemented in the model (as per England, 1995). This age tracer also follows the model's transport equation for tracers and is also set to zero everywhere at the beginning of the model integration. However, the age tracer is then increased everywhere and at every time step by a constant value equal to the length of the ocean model time step, except in the surface layer, where the tracer is set to retain a constant value of zero throughout the run. To facilitate an accurate analysis of water mass age changes, the age tracer was introduced into the equilibrated experiments under the chosen wind stress field and was integrated until the age tracer reaches an equilibrium with age changes of less than six months per century of integration (as in England, 1995). The age changes yielded by this new tracer are in broad agreement with the age changes derived from radiocarbon concentration ($\Delta^{14}C$ anomaly) changes (not shown).

II.3 Transient experiments

II.3.1 Changes in the Oxygen Minimum Zones (OMZs)

In the first decades after the onset of a transient introduction of the wind stress perturbations the hypoxic and suboxic volumes, both respond with the opposite sign compared to the applied perturbation, i.e. low-oxygen volumes expand for weakening winds and con-

tract for strengthening winds (Figure II.1). This behaviour is caused by the wind-induced changes in the supply of oxygen-rich subsurface waters from the equatorial western to the eastern boundary of each basin, which is one of the major sources of the ventilation for low-oxygen regions, particularly in the equatorial Pacific (Stramma et al., 2008). The easterward equatorial subsurface transport (at 170°W, between 15°S - 15°N and 50 m - 600 m depth) within the Pacific Ocean for instance decreases almost linearly from 16.5 Sv in CTRL to 9.1 Sv in equilibrium following the decline in wind stress of up to 30%, while increased winds lead to stronger eastward subsurface currents (23.6 Sv in experiment $\tau_{+30\%}$ in equilibrium).

The evolution of the hypoxic volume experiences a change in sign after approximately 20 to 30 years of transient wind stress change. The suboxic volume experiences a similar sign reversal later in the model integration (not shown). In both cases the reversal of sign is caused by a combination of changes in (i) the atmosphere-ocean O_2 flux due to modified dissolved oxygen concentrations, (ii) denitrification as a result of the variations in the suboxic volume and (iii) nitrogen fixation caused by changes in the number of diazotrophs due to altered nutrient upwelling. In the case of weakening trade wind conditions the expansion of the suboxic volume forces an increase in anaerobic remineralization, which acts as a source of O_2. The simultaneous reduction in nitrogen fixation, which removes O_2 to form NO_3, and in the outgassing of O_2 due to initially lower oxygen concentrations, then lead to a net gain in O_2. In combination with increases in the ventilation of the South Pacific shadow zone and the supply of oxygen-rich waters from high latitudes, which can be seen in the increase in SAMW formation off Peru/Chile (Figure II.2; discussed in detail below), the modifications in the nitrogen cycle eventually reverse the sign of change in the global hypoxic volume (Figure II.3). The same mechanisms but of opposite sign are at play under strengthening wind conditions.

II.3.2 Global Oxygen Changes

A transient introduction of the wind perturbations ramped up over 50 years initially shows global mean oxygen concentration changes of the same sign as the perturbation, i.e. decreasing global mean O_2 for weakened winds and vice versa for strengthened winds following the evolution of the oceanic low-oxygen volume as decribed above (Figures II.4a

and II.4b). The maximum signature of change in this early phase of the wind perturbations is reached between 10 and 15 years into the integration and scales approximately with the perturbation. After around 20 years of integration the net global ocean oxygenation begins to reverse in its tendency, with decreasing concentrations for increasing winds, and vice versa for reduced magnitude winds. Thereafter oxygen changes are almost linear in time in all experiments (Figure II.4a).

One third of the changes in global mean O_2 can be accounted for by the transient response of the oxygen saturation concentration (O_2^{sat}; Weiss 1970; Figures II.4c and II.4d). These are caused by temperature changes and are of the opposite sign compared to the wind perturbation throughout the whole integration, i.e. negative for strengthened winds and vice versa for weakened winds.

The response of apparent oxygen utilization (AOU; Figures II.4e and II.4f) dominates the response of global mean O_2 in all experiments, and is the reason for the change of sign in the response of global mean O_2 within the first two decades after the introduction of the wind perturbations. The transient changes in AOU in the first decades after the onset of the perturbation are driven by the initial response of the OMZs to modifications in the lateral ventilation of eastern boundary shadow zones and the resulting changes in the nitrogen cycle affecting oxygen consumption, as discussed above. The sign reversal is caused by a combination of the changes in (i) atmosphere-ocean O2 flux due to varied dissolved oxygen concentrations, (ii) denitrification as a result of the volume changes of the suboxic regions and (iii) nitrogen fixation caused by a variation in the number of nitrogen fixing diazotrophs due to the changed rate of upwelling of nutrients (see above).

Changes in ocean transport from the southern to low-latitudes start to contribute to the response of global mean O_2 concentrations to wind perturbations about 20 years after the onset of the transient perturbation. At this time water that had been ventilated at high latitudes during the onset of the perturbation is now returning nutrients and oxygen-rich waters (via SAMW) to the equatorial region (Figure II.2b). At the same time the wind-driven slow down of the South Pacific subtropical gyre leads to a more ventilated south Pacific shadow zone, with more SAMW entering the Pacific OMZ, thus

increasing O_2 concentrations in this region and offsetting the reduction in biological O_2 production at low latitudes (Figure II.2). An increased O_2 concentration in SAMW due to the reduction in the global mean remineralization of organic material amplifies this oxygenating effect in the South Pacific Ocean despite a moderate weakening of the SAMW transport reaching the equatorial region (Figure II.5). This change in O_2 transport compensates for the reduced inflow of oxygen-rich waters into the equatorial south-east Pacific and, together with the changes in marine biology, finally reverses the change in global ocean oxygenation over time (Figures II.4a and II.4b). The same mechanisms but of opposite sign are at play under strengthened wind stress conditions. Here an initial increase in the inflow of oxygen to the eastern boundary low-oxygen volumes in the first decades of the perturbation is replaced by an overall decrease in global mean O_2 due to (i) an increased loss of oxygen to the atmosphere and in the nitrogen cycle, (ii) an expansion of the South Pacific shadow zone and (iii) decreased O_2 concentrations in SAMW compared to normal wind conditions.

II.4 Equilibrium response

II.4.1 Changes in OMZs

In equilibrium the volumes of water masses within the global ocean with hypoxic and suboxic conditions expand under increased tropical easterly wind stress, and contract under decreased winds (Figure II.6), generally continuing the trend of the transient experiments. The global equilibrium response of the low-oxygen volumes is dominated by the Pacific Ocean, which exhibits a high sensitivity to the applied perturbations (Figure II.6). The Indian Ocean shows changes of the opposite sign compared to the Pacific and the Atlantic Ocean. Both the Pacific and the Indian Oceans exhibit a pattern of increased O_2 in the east and decreased O_2 in the west of the basin for weaker wind stress and vice versa for stronger winds (Figures II.7a, II.7b, II.8a and II.8c). In the Pacific Ocean the eastern boundary off Chile (at 32°S - 8°S, 272°E - 290°E and at 240-550 m depth; Figures II.7c, II.7d, II.8a and II.8c) develops changes of higher amplitude compared to the changes at the western boundary. In fact the changes in O_2 at the eastern boundary dominate the response of the whole Pacific basin and reduce the extent of the Pacific OMZ.

The Indian Ocean reacts in the opposite sense, with higher changes at the western boundary off Somalia and Kenya (at 9°S - 9°S, 42°E - 82°E and at 240-500 m depth; Figures II.7a, II.7b, II.8a and II.8c) determining the overall response of the Indian Ocean low-oxygen volume. This leads to contracting low-oxygen volumes in the Pacific basin and expanding low-oxygen water masses in the Indian Ocean for weakened surface wind stress (vice versa for strengthened winds). The difference between the two ocean basins is caused by their different geometry: the Pacific Ocean has an enclosed eastern boundary with a strong upwelling region, which sets the response in O_2 via changes in the nutrient supply from greater depths and hence local biological activity and remineralization in addition to the meridional inflow of oxygen-rich waters. The eastern boundary of the Indian Ocean, in contrast, is influenced not only by local upwelling and meridional supply of dissolved oxygen, but also by the supply of oxygen-rich waters from the Pacific Ocean, via variations in the Indonesian Throughflow, which weakens for a decline in surface wind stress and vice versa for strengthened winds. The Indonesian Throughflow partially compensates the upwelling fluxes along the eastern boundary of the Indian Ocean, so that the western boundary region exhibits the strongest net response to wind variations within the Indian basin.

In the low oxygen waters off Chile the decreased τ_x experiments cause an increased meridional and vertical supply of oxygen to the low-oxygen region (Figures II.9c and II.9d). One of the major mechanisms behind this change is a decrease in the strength of the Equatorial Undercurrent (EUC) System and the South Equatorial Current (SEC) (Figure II.8b), which in combination with a stronger proportional component in the along-shore winds results in an increased inflow of oxygen rich waters from the south where colder temperatures facilitate increased oxygen concentrations (Figures II.10e and II.9c). Additionally, the region experiences an increase in net upwelling (Figure II.9d), which supplies more oxygen from greater depths, where decreased remineralization (Figure II.11) leads to higher O_2 concentrations. This decrease in remineralization, and with this the reduction in oxygen depletion, results from a decreased import of organic material from shallower layers above 240 m, where reduced upwelling results in lower biological activity and thus export production (Figure II.9). The changes in net upwelling are caused by a slower

Ekman transport away from the Equator. This reduces the downwelling of water in the descending branch of the equatorial overturning cells, which completely compensates for the reduced upwelling at the eastern boundary of the basin. Experiment $\tau_{+30\%}$ shows similar results but of the opposite sign (Figures II.9e and II.9f). Experiments incorporating smaller perturbations exhibit similar patterns of response and mechanisms, although of reduced amplitude (not shown). It may be noted, however, that the relative coarse resolution of the UVic ESCM limits the accuracy in representing near coast winds, which are essential for the dynamics of the Eastern Boundary Upwelling systems. Therefore, the modelled change in the coastal upwelling regions may be biased by the model's coarse resolution.

The region off Somalia responds with a weakening of the southern subtropical gyre (Figure II.8b), which leads to a decreased inflow of water from the south (Figure II.12c). This results in a loss of O_2 in this region, expanding the OMZ in $\tau_{-30\%}$ compared to CTRL. At the same time the zonal transport of oxygen-rich waters from the east (north of 10°S) into the OMZ is increased. However this cannot compensate for the decreased supply of O_2 due to the decreased inflow caused by the weakened gyre (Figures II.12c and II.12d). Also, a decrease in remineralization, which derives from reduced import of organic material from shallower layers above 240 m with lower NPP (Figure II.12), cannot fully compensate for the decreased supply of oxygen from the south. Increasing the surface wind stress in the tropics causes a similar pattern of response, but of the opposite sign, leading to an overall increase in O_2 in the Indian Ocean OMZ (Figures II.12e and II.12f).

II.4.2 Global Oxygen Changes

In equilibrium the overall response in global mean concentration of O_2 is consistent with the transient experiments, leading to a more oxygenated ocean under weakened wind stress and vice versa for increased wind conditions, scaling almost linearly with the magnitude of perturbation (Figure II.13a). In agreement with the results described in the transient perturbations, roughly one third of the O_2 change can be accounted for by changes in temperature, i.e. oxygen saturation concentrations (O_2^{sat}; Figure II.13b). This derives from changes in sea surface temperature (SST), which, in case of a τ_x decrease,

show a warm anomaly limited to the equatorial Pacific and Atlantic Ocean stretching westward from the eastern boundary of the basin (Figure II.10). The remaining surface ocean at mid- and high-latitudes experience a decrease in SST increasing O_2^{sat} in areas where intermediate and deep waters are formed. The changes in the air-sea O_2 flux confirms that SST changes overall lead to a decreased release of O_2 from the ocean into the atmosphere under decreased trade wind conditions (Figures II.11 and II.14). Strengthened wind conditions cause a similar response but of opposite sign. The anomalies scale with the applied wind perturbation, with $\tau_{-30\%}$ and $\tau_{+30\%}$ showing the highest net integrated O_2 changes.

Alterations in AOU account for the main part of the response in global mean O_2 (compare Figures II.13a and II.4a to Figures II.13c and II.4c, respectively). The AOU changes are in turn driven by changes in the lateral transport of water masses supplying oxygen-rich waters to low-oxygen regions and by changes in the upwelling of deep, nutrient-rich waters affecting net primary productivity (NPP), as demonstrated below.

Changes in O_2 with the oxygen saturation effect removed (Figures II.7a and II.7b; color), mostly coincide with changes in water age (Figures II.7a and II.7b; contoured) with younger waters exhibiting higher concentrations. The zero line of both property anomalies coincide in many regions, which shows that as the age and ventilation rate change, so does the oxygen content. This is consistent with Gnanadesikan et al. (2012) who found similar results in the Pacific Ocean for their experiments using the SRES A2 increasing CO_2 emissions scenario.

This correlation between O_2 and water age can also be seen in the relationship between changes in O_2 concentration and those in age of the corresponding waters for experiments $\tau_{-30\%}$ and $\tau_{+30\%}$ (Figures II.7c and II.7d). Both experiments exhibit the expected response of O_2 concentrations to ventilation and thus water age changes, i.e. higher O_2 concentrations in more rapidly ventilated younger waters and vice versa for older waters. However, both experiments also contain waters that contradict the negative correlation between O_2 anomalies and age changes. This is especially obvious when looking at the global mean changes in O_2 versus age depending on model layer depth (Figure II.15). In

experiment $\tau_{+30\%}$ (triangles) increased winds lead to a more rapid ventilation resulting in younger waters compared to CTRL, especially at greater depth (colors). However the mean O_2 concentration changes in all depth layers indicates a decrease despite the increase in ventilation. Experiment $\tau_{-30\%}$ (circles) shows equivalent results but of opposite sign. This behavior of O_2 concentrations in both experiments is counter intuitive to the assumption of increasing oxygenation for increasing ventilation. This indicates that changes in the biological cycling of oxygen, in particular in the remineralization of organic matter, must play a role in the projected changes in O_2. These changes are caused by modifications in the net upwelling of nutrients and O_2 into the upper ocean (Figure II.11). The net upwelling through the 1377.5 m surface for instance changes with the same sign as the applied perturbation (see black diamonds in Figure II.11). Consequently experiments $\tau_{-10\%}$, $\tau_{-20\%}$ and $\tau_{-30\%}$ exhibit a reduction in the upwelling of nutrients while the trade wind increase experiments show enhanced upwelling. Accordingly mean NPP and with this mean export production (not shown) and remineralization rate (R) decrease with weaker equatorial winds and increase when the winds are strengthened (blue squares and red stars in Figure II.11, respectively). At greater depths the reduction in O_2 due to decreased NPP under weaker τ_x is completely compensated for by the decreased use of O_2 for remineralization due to a reduced presence of organic matter (see red stars in Figure II.11), which in turn results in a higher upwelling of O_2 from greater depth, completely compensating the reduced O_2 production (see yellow triangles in Figure II.11). This is consistent with findings of Matear et al. (2000) who also found increased O_2 concentrations in their model experiments with lower NPP. Under strengthened τ_x conditions, higher NPP provide more organic matter that is in turn remineralized at depth, leading to lower oxygen concentrations in these experiments. However, the amount of change caused by increased winds is smaller than in the equivalent decreased winds experiment (compare e.g. Figures II.5a and II.5b; II.7a and II.7b). This higher sensitivity to decreased winds is caused by differences in both (i) the northward transport into the southeast Pacific (i.e. ocean transport/ventilation) and (ii) the upwelling of PO_4 across intermediate depths resulting from biological processes (Figure II.16). For weakened winds the surface northward transport in the upper 1000 m across 45°S between 150°W and 70°W (which catches the eastern limb of the subtropical gyre) decreases (Figure II.16a) due to the wind-driven weakening of the subtropical gyre and the equatorial

overturning cells (Ridder et al., 2013). The same mechanism would cause an equivalent increase for stronger winds, if the applied wind perturbations were acting in isolation of interior buoyancy changes. However, a decline in the density gradient between high and low latitudes under increased wind conditions dampens the acceleration of the northward transport. This ultimately leads to a non-linear response in the ventilation of the Pacific Ocean despite the linear increase in forcing of the applied wind perturbations (Figure II.16a). The stronger sensitivity in the upwelling of PO_4 to weakened winds is caused by variations in wind-driven upwelling in combination with changed deep ocean remineralization. As described above, reduced biological activity for weakened winds decreases remineralization (Figure II.11) and thus the formation of PO_4 in the deep ocean. Consequently the PO_4 concentration in the upwelled water, whose amount is already reduced due to the weakened equatorial upwelling cells, is reduced. This affects the growth and productivity of phytoplankton, in particular diazotrophs, which are not limited by other nutrients, and thus ultimately the availability of organic material for remineralization. This feedback is limited for strengthened τ_x through the model's application of a maximum growth rate for diazotrophs. This results in a higher decrease of PO_4 upwelling in experiments with weakened winds compared to the equivalent changes in experiments with strengthened winds (Figure II.16c).

II.5 Summary and Conclusions

This study demonstrates that the net volume-integrated global ocean oxygen content is inversely proportional to changes in low-latitude surface wind stress. One third of the changes in the global mean O_2 concentration is driven by changes in SST and thus O_2^{sat}. The remaining two thirds are caused by changes in ocean circulation/ventilation in combination with changes in biological activity. Considering that some waters are more gradually ventilated under decreased wind conditions yet show higher O_2 concentrations compared to CTRL (and vice versa for increased τ_x conditions), changes in marine biological cycling must fundamentally control the response in O_2 in addition to ventilation/circulation in these waters. In particular, biological activity responds to the wind-driven changes in upwelling of nutrients, causing a decrease (increase) in NPP for decreased (increased) winds, which then leads to changes in export production and

remineralization of the same sign. Put simply, reduced equatorial trade winds lead to decreased biological activity and eventually, over time, to decreased O_2 consumption, resulting in increased O_2 concentrations in the absence of other changes. This also affects the global low-oxygen volumes which become more oxygenated in experiments with weaker τ_x and vice versa for strengthened τ_x conditions. The global response is dominated by changes in the Pacific Ocean, which is more sensitive to a decrease than to an increase in τ_x, showing higher absolute anomalies in experiments $\tau_{-10\%}$, $\tau_{-20\%}$ and $\tau_{-30\%}$ than in the experiments with equivalent τ_x increases.

The OMZ in the Pacific Ocean off Peru-Chile (at 32°S - 8°S, 272°E - 290°E and 240-550 m depth) experiences the highest change in O_2. For weakened τ_x conditions this area increases its O_2 content due to an increase in ventilation from the south (caused by a weakening of the EUC and SUC), and an increased transport of O_2 from greater depths in combination with lower remineralization between 240 m and 550 m. The same processes but of opposite sign cause a decrease in O_2 concentrations in this region under strengthened τ_x conditions. The driving mechanism behind these changes are more along-coast wind conditions in experiments with surface wind stress smaller than CTRL, similar to the findings in Gnanadesikan et al. (2012), and more off-shore wind conditions in experiments with higher surface wind stress.

A similar mechanism is at play in the tropical Indian Ocean along the eastern boundary, however the impact on O_2 is mostly compensated by changes in the Indonesian Throughflow of Pacific Ocean waters with their altered O_2 signature. Along the western boundary, low-oxygen regions in the Indian Ocean become more depleted of O_2 due to a decreased subtropical gyre and thus a decreased ventilation of waters off Somalia from the south. The driving mechanism in this area is a change in wind conditions, similar to the driving mechanism in the Pacific but of opposite sign, i.e. anomalous off-shore conditions in experiments with reduced surface wind stress and higher onshore conditions for increased surface winds.

In conclusion, this study shows that in isolation of other changes, the tropical zonal wind fields alter circulation, SST and biological cycling in such a way to increase net ocean

oxygenation of sea water and to contract the global low-oxygen volume under decreased trade winds, and vice versa for increased τ_x. Under reduced wind stress, as is projected to occur during the 21^{st} Century (e.g. Collins et al., 2010), the weakened equatorial overturning cells would cause a deceleration of the Ekman transport and thus a reduction in poleward heat transport away from the Equator. The resulting colder SST in the subtropics and at mid- and high-latitudes would then lead to higher oxygen concentrations in waters that are subsequently transported into the ocean interior, ultimately increasing global mean dissolved oxygen. At the same time the supply of nutrients to the photic zone would be decreased due to a weakening in the upwelling branch of the overturning, resulting in overall reduced NPP and with this oxygen depletion via remineralization. Increased trade winds would lead to the opposite effect of increased nutrient supply to the photic zone, and thus higher NPP and remineralization.

II.6 Acknowledgments

This study was funded by the ARC and supported by an award under the Merit Allocation Scheme on the NCI National Facility at the ANU. We acknowledge the help of Willem Sijp during the set up of the model on the NCI system. The authors thank Niki Gruber for his input at the early stages of this project and Andreas Oschlies for his valuable support and input during the review process, along with an anonymous reviewer, which helped to improved this study considerably.

II.7 Figures

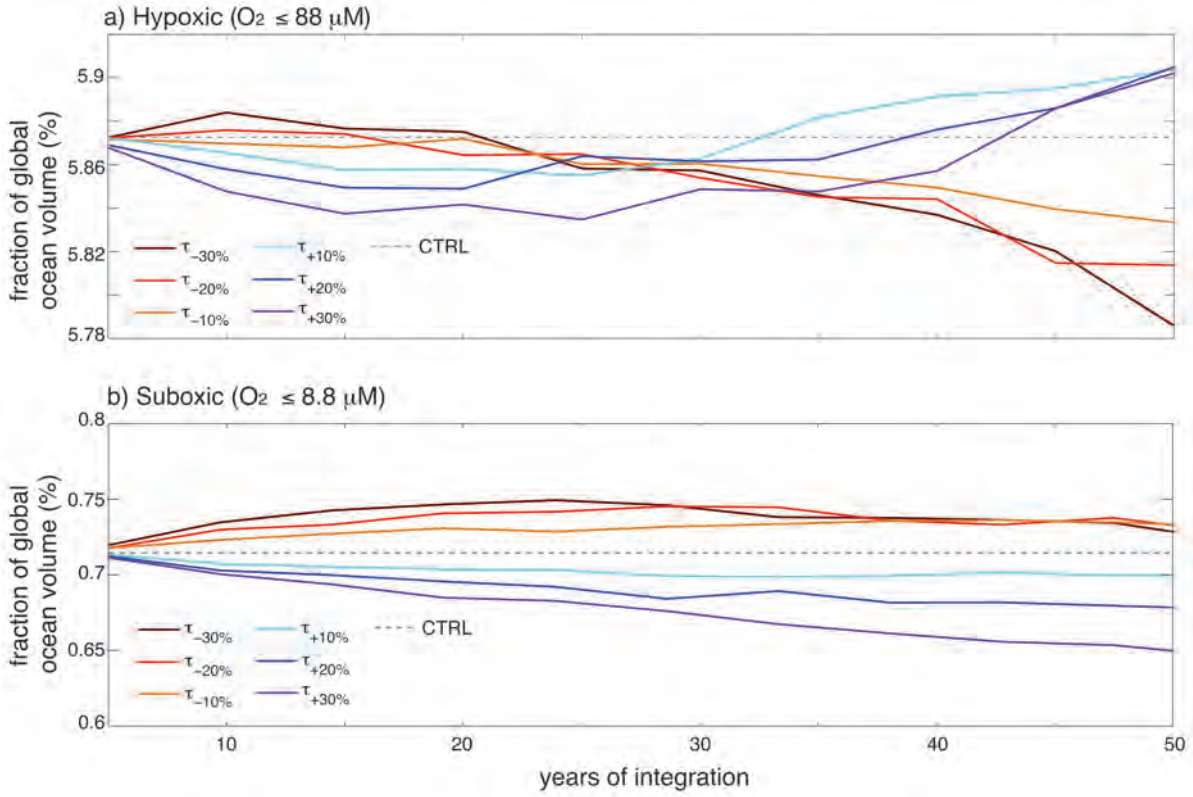

Figure II.1: Evolution of the fraction of the (a) hypoxic ($[O_2] \in [0.0\ \mu M;\ 88.0\ \mu M]$) and (b) suboxic ($[O_2] \in [0.0\ \mu M;\ 8.8\ \mu M]$) water mass volume under transient wind changes. Note the different y-axis scales in panels (a) and (b).

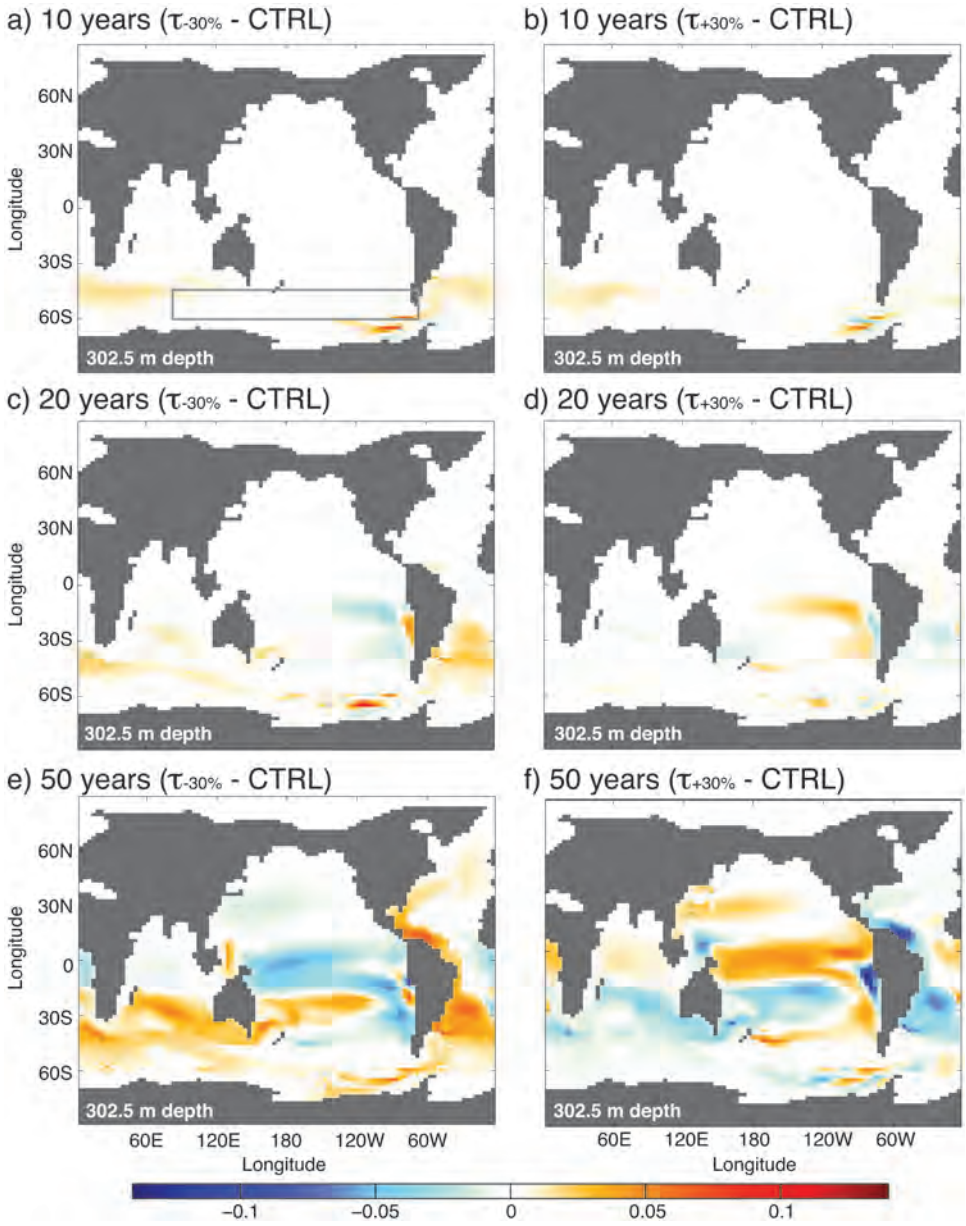

Figure II.2: Changes in SAMW transport under a transient introduction of wind stress perturbations. Colorshading shows the difference in dye tracer (dimensionless) at 302.5 m depth between $\tau_{-30\%}$ minus CTRL (left column) and $\tau_{+30\%}$ minus CTRL (right column) 10 years (a, b), 20 years (c, d) and 50 years (e, f) after the onset of the perturbation. Grey box in (a) marks surface area where dye tracer was released.

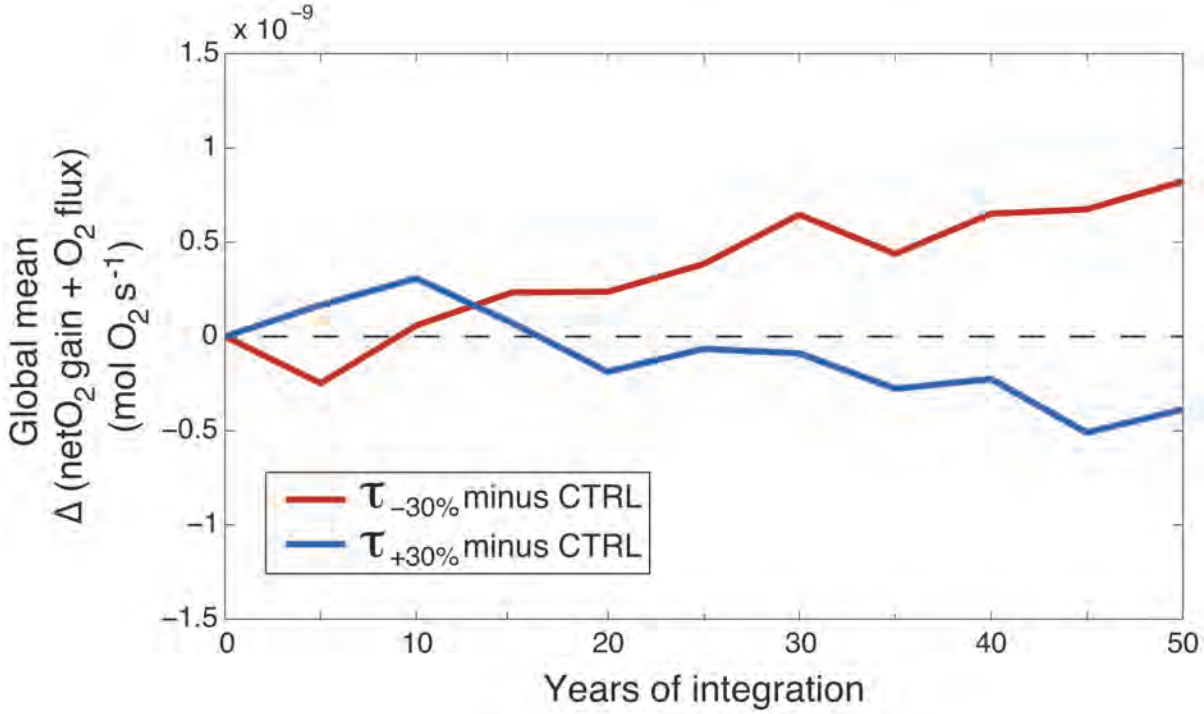

Figure II.3: Evolution of global mean net O_2 gain (through denitrification and nitrogen fixation) and oxygen release to the atmosphere under transient wind stress changes compared to CTRL. For clarity only the response to the transient introduction of 30% stronger (minus CTRL, blue) and weaker (minus CTRL, red) winds are shown.

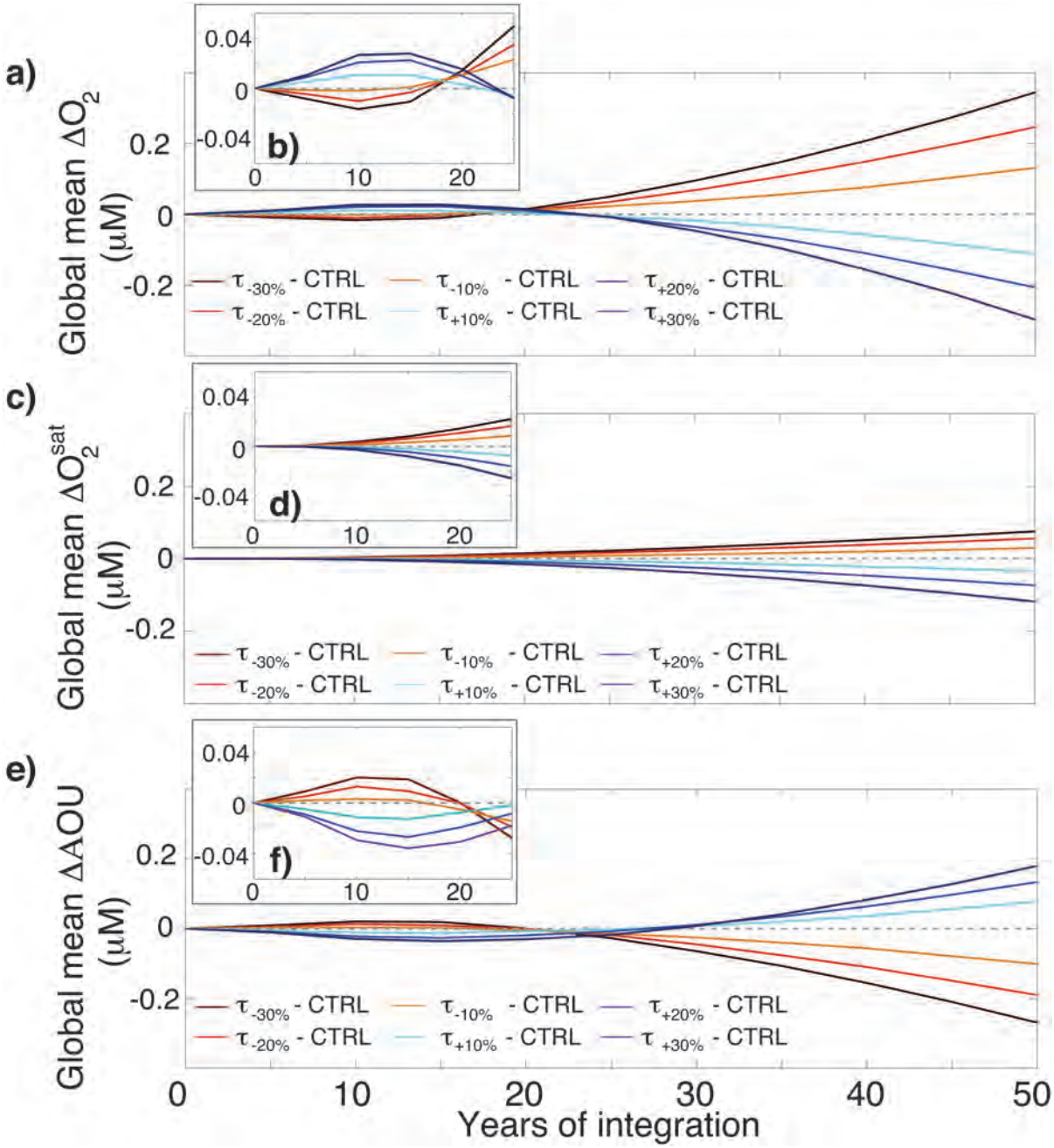

Figure II.4: Evolution of global mean (a, b) oxygen concentration, (c, d) oxygen saturation concentration (O_2^{sat}) and (e, f) apparent oxygen utilisation (AOU) all in μM under transient implementation of low-latitude wind perturbations.

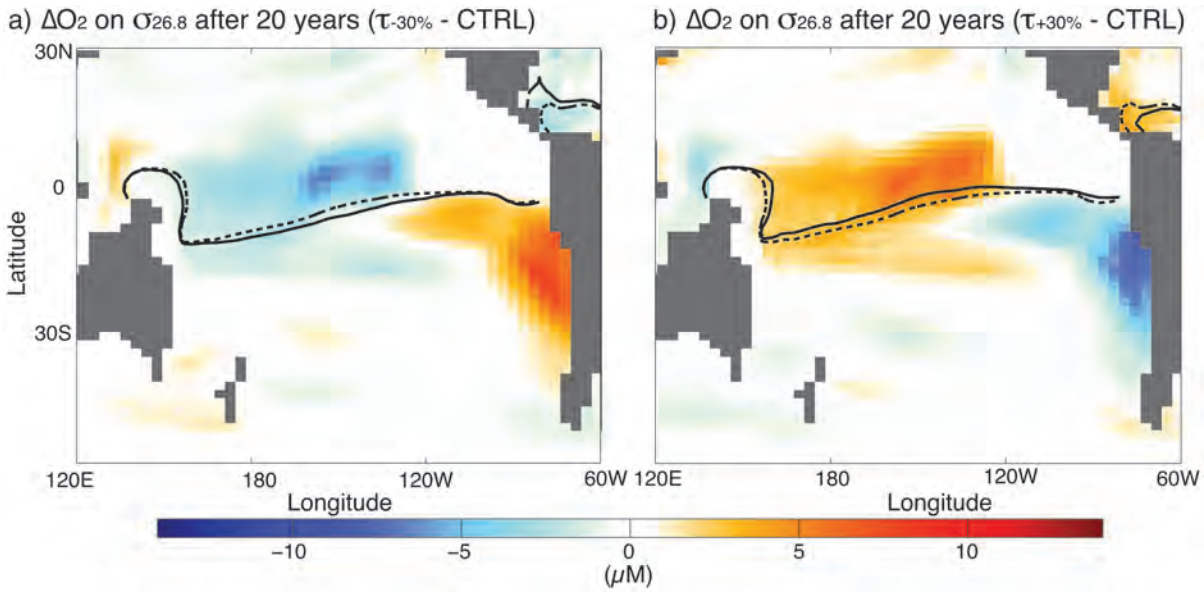

Figure II.5: a) Pacific oxygen concentration change (μM) in SAMW (here taken to be on the $\sigma_{26.8}$-isopycnal) 20 years after the onset of a transient wind perturbation; $\tau_{-30\%}$ minus CTRL. Contour lines indicate the extent of SAMW dye with [dye]<0.001 north of contours and [dye]>0.001 south of contours; solid line represents dye in $\tau_{-30\%}$, dotted line shows dye in CTRL. (b) as (a) but for $\tau_{+30\%}$ minus CTRL and $\tau_{+30\%}$ for solid contour lines.

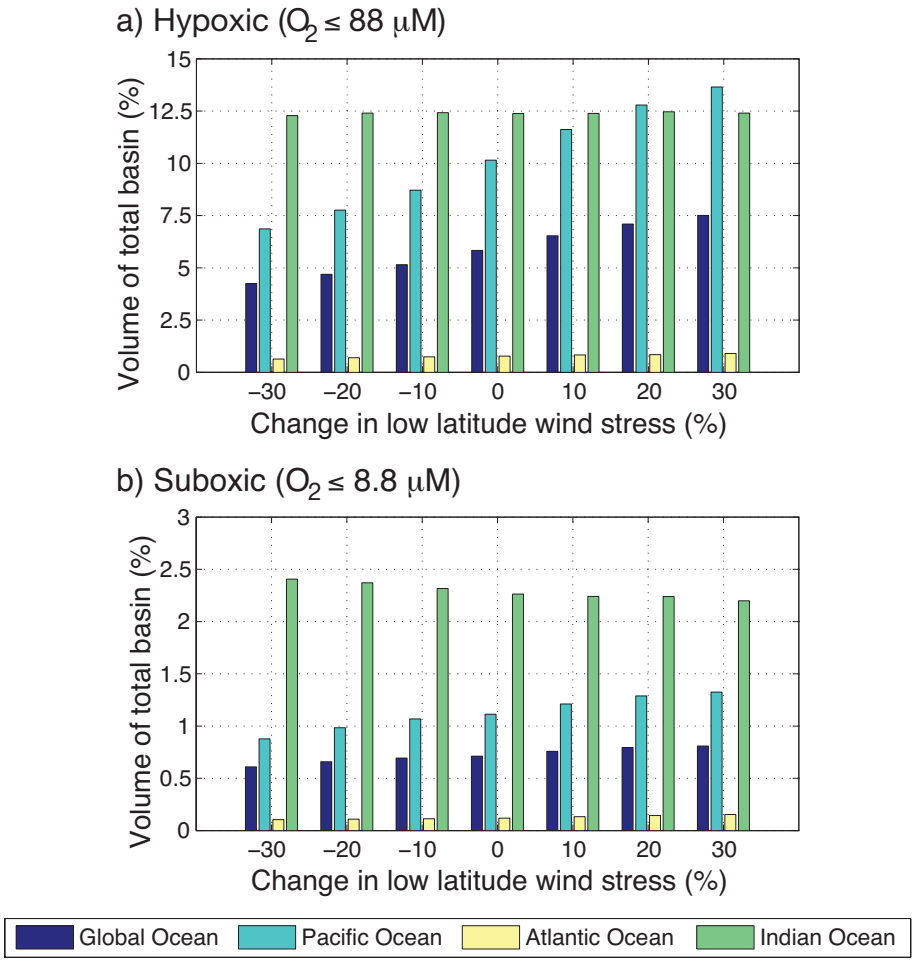

Figure II.6: Fraction of the (a) hypoxic ($[O_2] \in [0.0\ \mu M;\ 88.0\ \mu M]$) and (b) suboxic ($[O_2] \in [0.0\ \mu M;\ 8.8\ \mu M]$) water mass volume in the global (navy), Pacific (blue), Atlantic (yellow) and the Indian Ocean (green) in equilibrium with the perturbed low-latitude surface wind stress conditions (%). Note the different y-axis scales in panels (a) and (b).

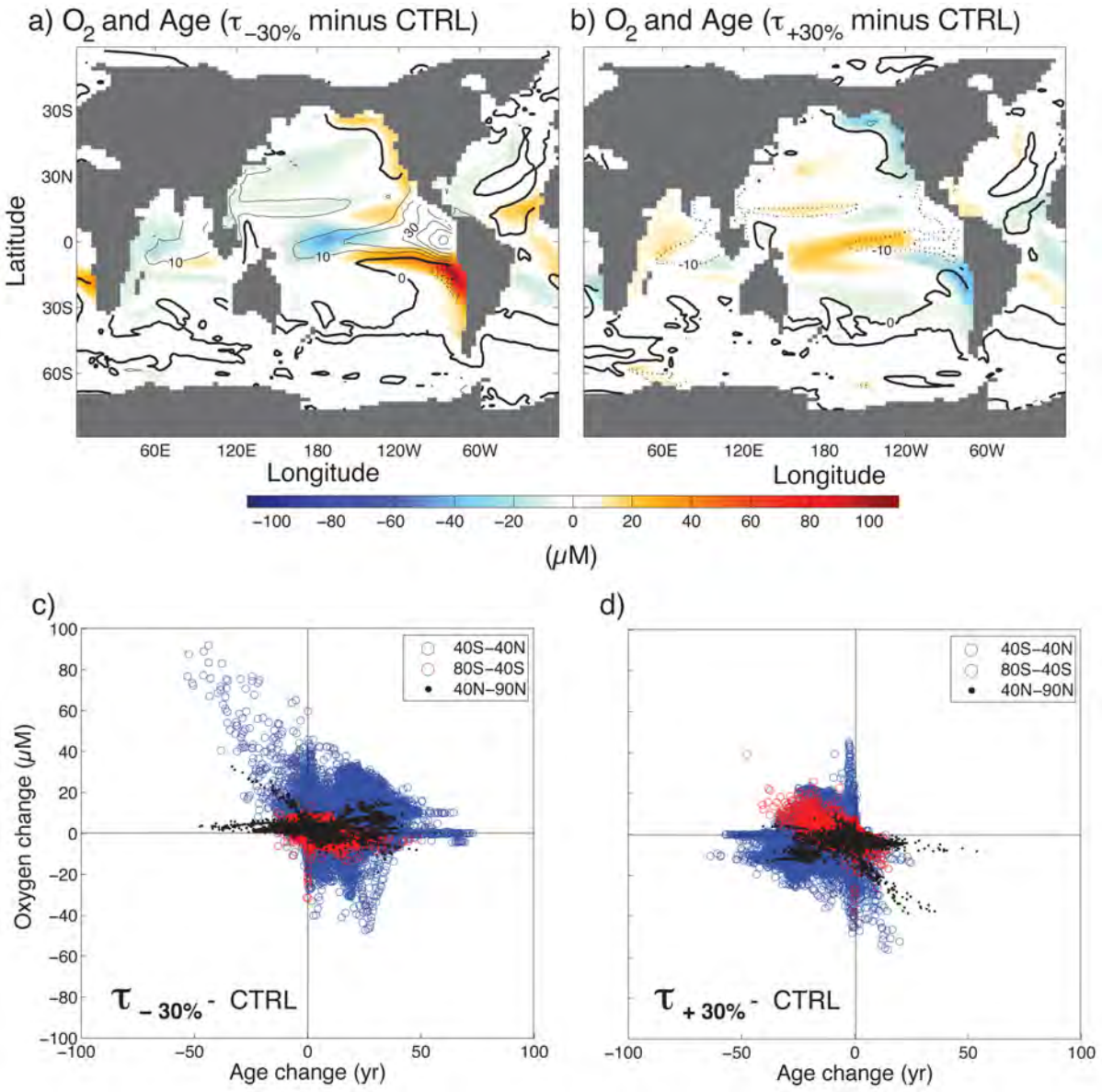

Figure II.7: (a) Oxygen changes (oxygen saturation effects removed; shading) in μM and age changes (yr; contours) at 302.5 m depth in equilibrium with perturbations in experiment $\tau_{-30\%}$ relative to CTRL. The thin solid lines mark regions with older water, dotted lines indicate younger water and zero contour is solid bold. Contour interval is 10 years. (b) As (a) but for experiment $\tau_{+30\%}$ minus CTRL. (c) Scatter plot of O_2 changes (μM) and age changes (yr) in different latitude bands in experiment $\tau_{-30\%}$ relative to CTRL. (d) As (c) but for experiment $\tau_{+30\%}$ minus CTRL.

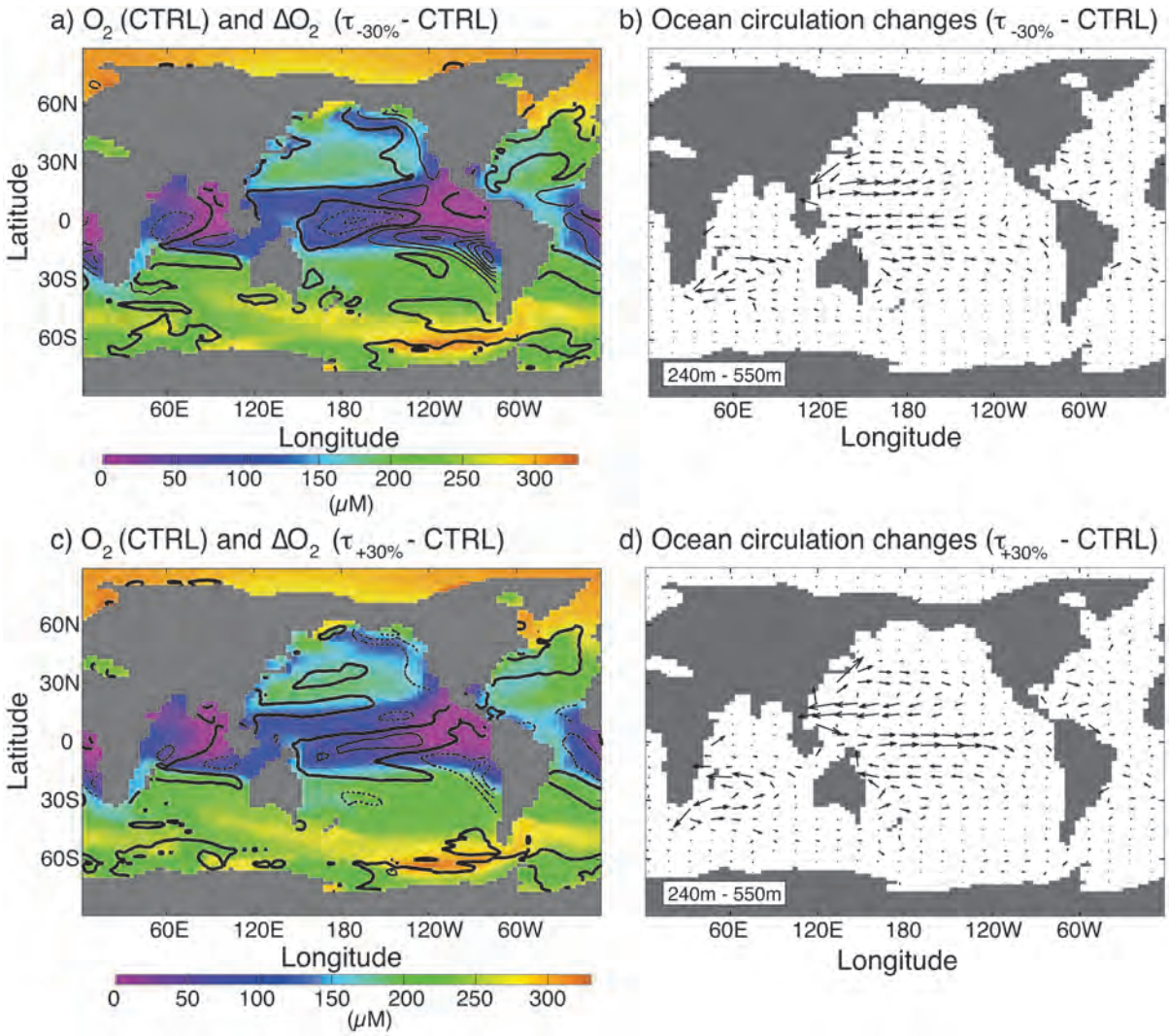

Figure II.8: (a) Oxygen concentration (μM) averaged over 240 m to 550 m in CTRL (colour shading). Contours show the difference in oxygen concentration averaged over the same depth range ($\tau_{-30\%}$ minus CTRL). Dashed lines indicate a decrease in equilibrated O_2 in $\tau_{-30\%}$ compared to CTRL, solid lines represent an increase in equilibrated O_2 ($\tau_{-30\%}$ minus CTRL). The zero contour is solid bold; contour intervals are 10 μM; (b) Changes in ocean circulation averaged over 240 m to 550 m depth ($\tau_{-30\%}$ minus CTRL); (c) and (d) as (a) and (b), respectively, only for $\tau_{+30\%}$ minus CTRL.

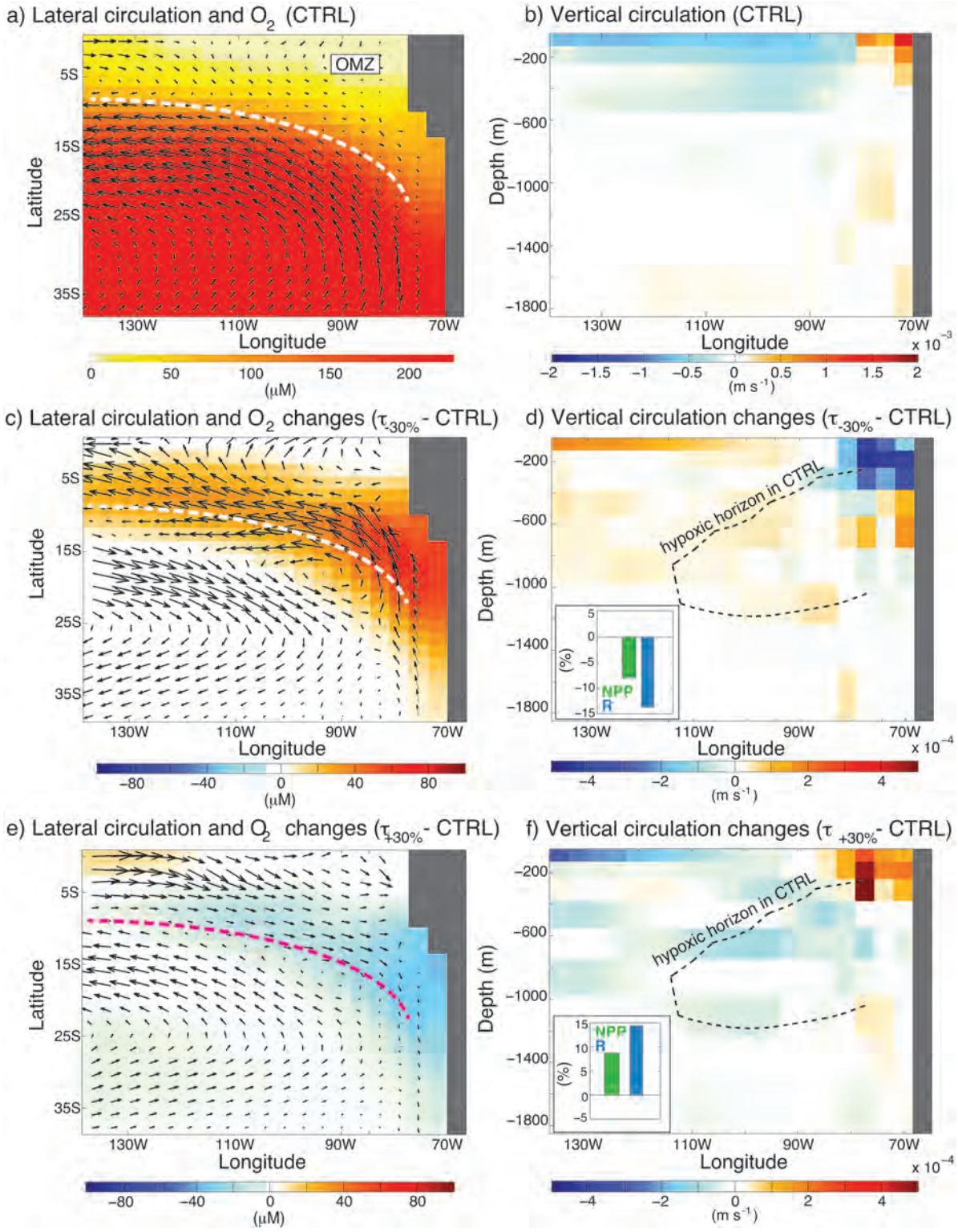

Figure II.9: (a) Equilibrium oxygen concentration (μM; colour shading) and horizontal circulation (m s^{-1}; vectors) off Chile in CTRL, both averaged over 240 m to 550 m depth. The dashed line refers to the transition between the westward flowing South Equatorial Current (SEC) and the eastward flowing Equatorial Undercurrent (EUC) System in CTRL; (b) Vertical velocity (m s^{-1}) averaged over 0° to 32°S in the Pacific Ocean; (c) as (a) but for $\tau_{-30\%}$ minus CTRL; (d) as (b) but for $\tau_{-30\%}$ minus CTRL, dashed contour indicates the horizon of the hypoxic volume at 13.5°S in CTRL, which marks the latitude of highest O_2 change in this region between $\tau_{-30\%}$ and CTRL. The bar diagram embedded in the figure shows the relative change in net primary productivity (NPP; green bars) and remineralization (R; blue bars) integrated in the water column between 0° and 32°S; 130°W and 70°W ($\tau_{-30\%}$ minus CTRL); (e) and (f) as (a, c) and (b, d),

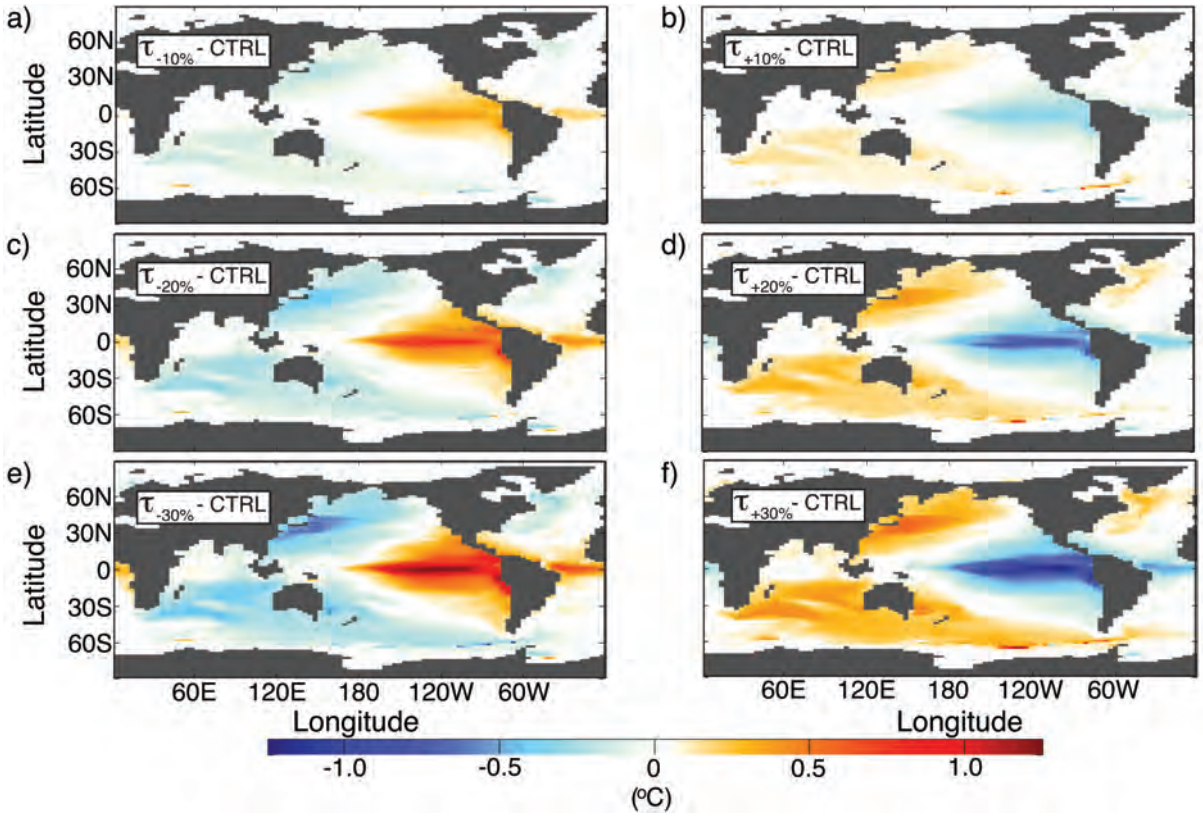

Figure II.10: Sea surface temperature changes (°C) in all equilibrated perturbation experiments shown relative to CTRL.

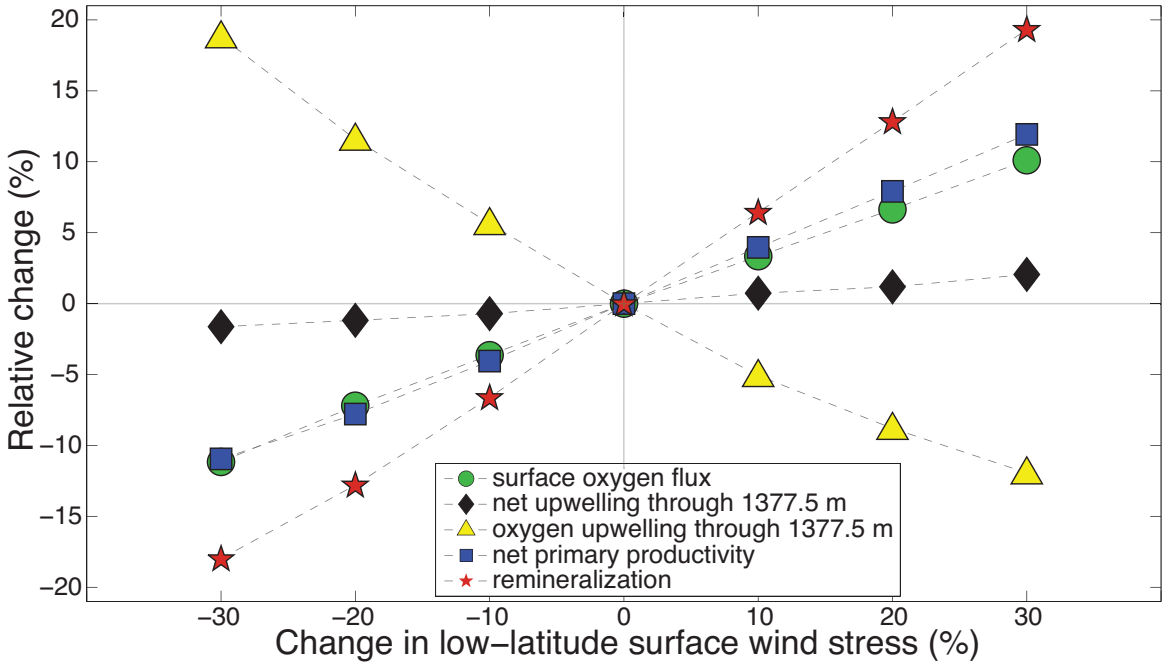

Figure II.11: Relative changes in various properties area-averaged over the Pacific Ocean between 40°S and 40°N, for all wind perturbation experiments relative to control. Shown are the air-sea oxygen flux at the surface (green circles), net upwelling through 1377.5 m (black diamonds; integral of vertical velocity over the 1377.5 m-surface), oxygen upwelling through 1377.5 m (yellow triangles; integral of the product between vertical velocity and oxygen concentrations over the 1377.5 m-surface), net primary productivity (blue squares) and remineralization (red stars).

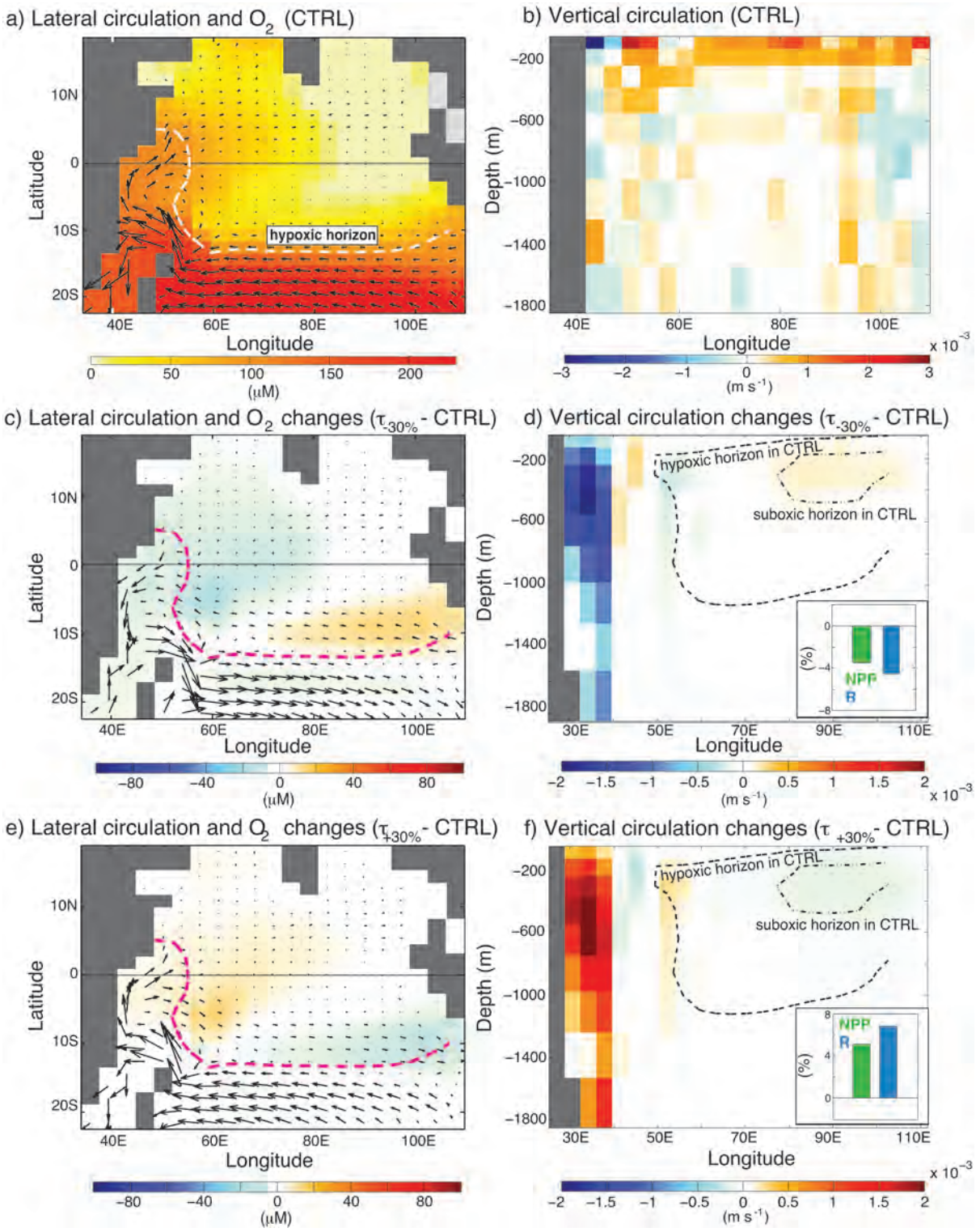

Figure II.12: (a) Equilibrium oxygen concentration (μM; colour shading) and horizontal circulation (m s^{-1}; vectors) off Somalia in CTRL, both averaged over 240 m to 550 m depth; (b) Vertical velocity (m s^{-1}) averaged over 9.9°N to 9.9°S in the Indian Ocean; (c) as (a) but for $\tau_{-30\%}$ minus CTRL. Dashed line represents the 88 μM isoline of O_2 averaged between 240 m to 550 m depth in CTRL; (d) as (b) but for $\tau_{-30\%}$ minus CTRL, dashed (dashed-dotted) contour indicates the horizon of the hypoxic (suboxic) volume at 4.5°S in CTRL, which marks the latitude of highest O_2 change in this region between $\tau_{-30\%}$ and CTRL. The bar diagram embedded in the figure shows the relative change in net primary productivity (NPP; green bars) and remineralization (R; blue bars) integrated in the water column between 9.9°N and 9.9°S; 40°E and 110°E ($\tau_{-30\%}$ minus CTRL); (e) and (f) as (a, c) and (b, d), respectively but for $\tau_{+30\%}$ minus CTRL.

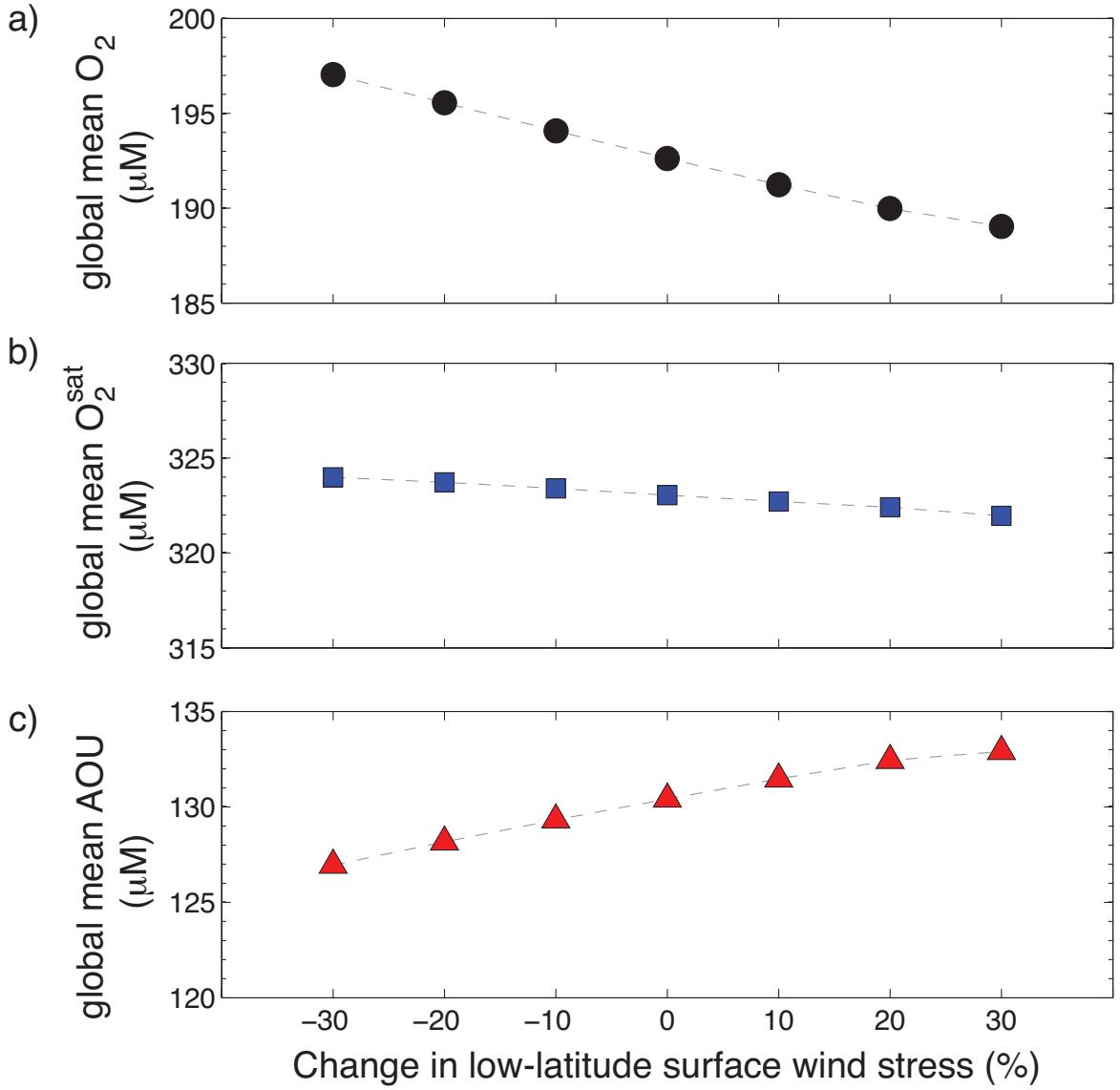

Figure II.13: Global mean equilibrated (a) oxygen concentration, (b) oxygen saturation concentration (O_2^{sat}) and (c) apparent oxygen utilization (AOU) (μM) as a function of low-latitude easterly surface wind stress change (%). The y-axis scales are offset but each of uniform range.

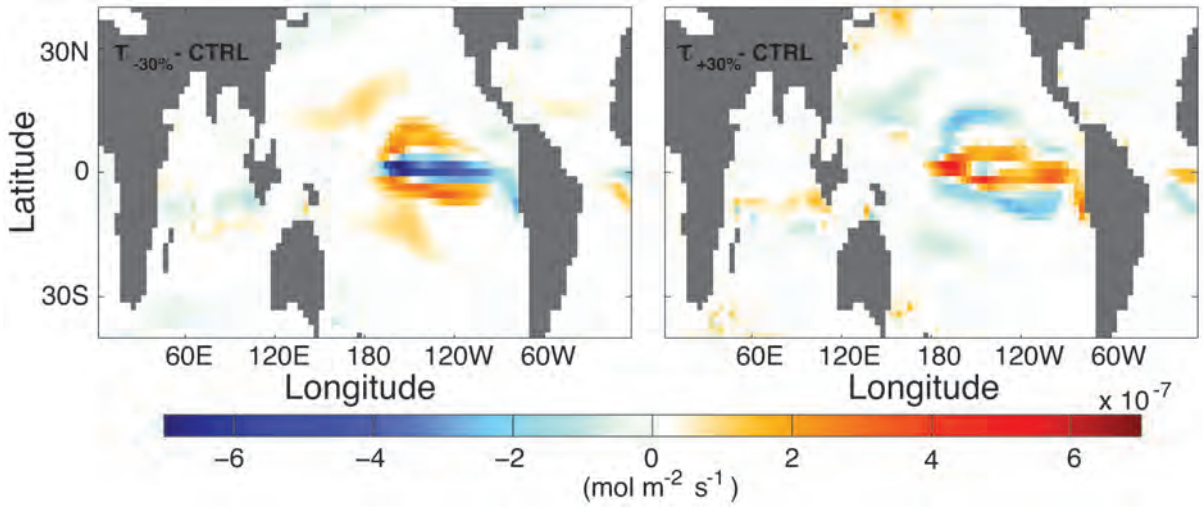

Figure II.14: Changes in tropical downward air-sea oxygen flux (10^{-7} mol m^{-2} s^{-1}) in the equilibrated perturbation experiments $\tau_{-30\%}$ minus CTRL (left) and $\tau_{+30\%}$ minus CTRL (right). All experiments in this figure use the corrected stoichiometry ratio between nitrogen and oxygen.

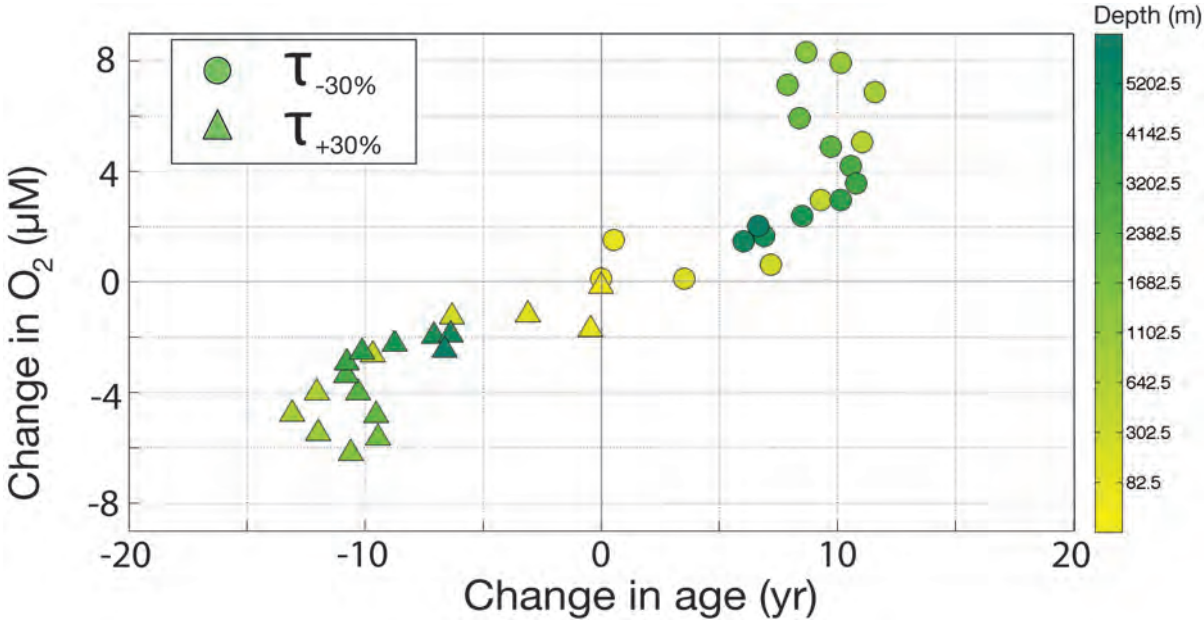

Figure II.15: Scatter plot of equilibrated mean O_2 change (μM) and age change (yr) at different model layers. Dots mark changes in $\tau_{-30\%}$; triangles mark changes in $\tau_{+30\%}$. Colours indicate the model layer; from yellow (shallow) to green (deep). Note the uneven depth scale of the model layers.

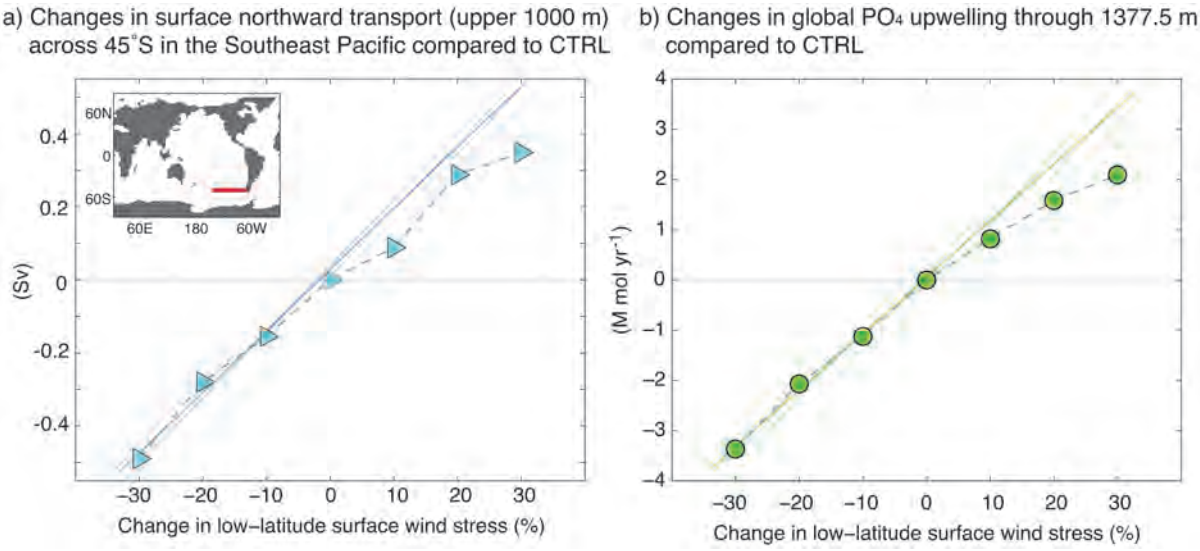

Figure II.16: (a) Changes in surface northward transport (upper 1000 m) across 45°S in the eastern South Pacific Ocean between 153°W - 70°W (red line) compared to CTRL. Surface northward transport in CTRL is 0.094 Sv. Blue line is the linear fit to the changes in the three reduced wind stress experiments. (b) Changes in global upwelling of PO_4 across 1377.5 m depth compared to CTRL (70.44 M mol PO_4 yr^{-}1). Green line is the linear fit to the changes in the three reduced wind stress experiments.

Part III: Impact of Southern Hemispheric westerly wind stress on North Atlantic Deep Water Formation

III.1 Main article

Previous model studies of the impact of Southern Hemisphere westerly winds on ocean circulation have proposed a link between the strength of these winds and the North Atlantic overturning circulation (Toggweiler and Samuels, 1993, 1995; Cai and Baines, 1996; McDermott, 1996; Rahmstorf and England, 1997; Toggweiler and Samuels, 1998; Gnanadesikan and Hallberg, 2000; Brix and Gerdes, 2003). Through the so-called Drake Passage Effect (Toggweiler and Samuels, 1993, 1995), the northward Ekman transport at the tip of South America is thought to control the rate of production and outflow of North Atlantic Deep Water (NADW), with the formation of NADW directly related to the zonally-integrated strength of Southern Ocean wind stress. Here we show that this relationship breaks down and in fact weakly reverses in a coupled climate model that includes atmospheric and thermodynamic sea-ice feedbacks. In particular we find that an increase in the Southern Hemisphere westerly winds decreases sea-ice coverage in the formation regions of Antarctic Bottom Water (AABW), thus enhancing ocean heat loss to the atmosphere, leaving colder and denser AABW. This alters the interhemispheric buoyancy balance between NADW and AABW, leading to a reduction in Atlantic overturning for stronger winds. The reverse occurs under weaker wind conditions, with enhanced sea-ice coverage insulating the ocean, leaving AABW warmer and less dense, thereby allowing a more vigorous overturn of NADW. As such we find that changes in the Southern Ocean westerlies drive changes in the strength of NADW overturn in the opposite sense to that previously assumed. This could have important implications for paleoclimatic records, as well as for the present day climate wherein a recent multi-decadal increase in Southern Hemisphere westerlies (Thompson et al., 2011) has coincided with enhanced Antarctic sea-ice (Simpkins et al., 2013).

The link between NADW formation and the wind-driven northward Ekman-transport in the circumpolar belt of the Southern Ocean was originally proposed using results from a numerical sensitivity study using an ocean-only model (Toggweiler and Samuels, 1993, 1995). The study isolated the impact of mechanical forcing due to Southern Hemisphere

westerly winds from other processes that have the potential to influence ocean circulation; for example, suppressing air-sea thermal feedbacks by restoring sea surface temperature (SST) to observations, and neglecting sea-ice processes at high-latitudes. The models sea surface salinity (SSS) was also restored to observations and thus along with SST did not evolve in response to the applied wind perturbation.

Other model studies have also obtained a positive correlation between Southern Ocean westerly wind strength and NADW formation rates, applying similar model configurations omitting either atmosphere or sea-ice feedbacks and their influence on sea surface temperature, sea surface salinity or both (Cai and Baines, 1996; McDermott, 1996; Rahmstorf and England, 1997; Toggweiler and Samuels, 1998; Gnanadesikan and Hallberg, 2000). One study extended previous investigations by including a sea-ice model (Brix and Gerdes, 2003), however while the sea-ice and ocean model exchange information about net heat and fresh water fluxes, there is a restoring term included for salinity and prescribed atmospheric temperatures used to calculate the air-sea heat fluxes. This approach omits important feedbacks between the atmosphere, the ocean and sea-ice, via for example variations in wintertime sea-ice formation and brine rejection, and therefore Antarctic surface water densities. These feedbacks are potentially crucial for determining the response of the Atlantic thermohaline circulation to shifts in the Southern Hemisphere westerly winds via the interplay between NADW and AABW (Crowley, 1992; Broecker, 1998; Sijp and England, 2009).

Sea-ice influences the atmosphere-ocean-ice exchange of (i) momentum, due to the control of sea-ice over the oceans exposure to surface wind stress, (ii) heat, based in part on the insulating effect of sea-ice, and (iii) freshwater via changes in sea-ice formation (e.g. brine rejection) and sea-ice melt. Air-sea and ice-sea heat and freshwater fluxes in turn determine ocean surface temperature and salinity, and thus also surface density, and along with the surface wind stress the interior ocean stratification. Southern Ocean surface density and interior stratification has been shown to significantly influence the overturning in the Atlantic Ocean via the so-called bipolar seesaw effect (Crowley, 1992; Broecker, 1998; Kamenkovich and Radko, 2011). With Antarctic sea-ice and thereby Antarctic Bottom Water (AABW) both sensitive to the strength and position of the

Southern Hemisphere westerlies (Hall and Visbeck, 2002; Oke and England, 2004; Saenko et al., 2012; Spence et al., 2013), it is possible that the omission of a sea-ice module in past ocean-only studies has misrepresented the climate feedbacks operating via the Drake Passage Effect. Here we re-examine the link between Southern Ocean winds and NADW overturn using a model that incorporates dynamic-thermodynamic sea-ice physics within a coupled climate model setting. Apart from re-examining the Drake Passage Effect in a more realistic setting, this study has potential implications for present-day and future climate change, with a recently observed poleward intensification of Southern Hemisphere winds (Thompson et al., 2011) and robust projections of ongoing change this century (Swart and Fyfe, 2012; Eyring et al., 2013). These wind changes have the potential to significantly alter Southern Ocean water-masses, abyssal ocean density, and thus the Atlantic meridional overturning circulation.

To examine the climate and sea-ice feedbacks operating within the Drake Passage Effect, we extend on previous studies by examining a coupled climate model with a simplified atmosphere that allows the ocean to be forced by prescribed winds (see section III.2). Thus while atmospheric heat and moisture is fully coupled to the other model components including the sea-ice module, the wind fields are prescribed, which has the advantage of allowing us to quantify the impact of Southern Ocean wind changes on Antarctic sea-ice, interior water masses, and the North Atlantic overturning circulation.

Changes in the Southern Hemisphere westerly wind stress (Figure III.1a-c) induce changes in the modelled Ekman divergence around Antarctica. This alters the removal of surface waters at the latitude of the tip of South America and the Deacon Cell strength (Figure III.1d-f), decreasing for weakened Southern Hemispheric westerlies and increasing for stronger winds. North Atlantic overturning is also significantly affected by the Southern Ocean wind strength changes, but opposite to the sense obtained in past ocean-only studies: in particular, stronger Southern Ocean winds reduce NADW formation while weaker winds strengthen North Atlantic overturn. Given the results of past ocean-only studies, particularly those resolving air-sea thermal feedbacks (Rahmstorf and England, 1997), this finding of an inverse dependence of NADW formation on Southern Ocean winds is most likely due to dynamic/thermodynamic sea-ice feedbacks operating in the

coupled climate model.

To investigate this, the response of Antarctic sea-ice thickness and sea-ice advection to changes in Southern Ocean wind stress are examined in Figure III.2a and III.2b. Stronger westerly winds drive an increased northward Ekman advection of sea-ice around Antarctica (Figure III.2b), with more ice transported equatorward and an increase in meltwater at the northern edge of the Antarctic sea-ice margin. To the south, nearer the Antarctic continental margin, the enhanced northward ice advection leads to a reduction in sea-ice thickness, especially in the Ross and Weddell Seas (Figure III.2b). This increases the exposure of the surface ocean to cold atmospheric temperatures at these locations, leading to enhanced ocean heat loss and a resulting cooling of SST adjacent to Antarctica. The decreased SST triggers an increase in surface ocean densities (Figure III.2d), thus enhancing the production of Antarctic Bottom Water (Figure III.3c). These sea-ice coverage and water-mass changes predominantly take place in the Weddell and Ross Seas, regions of high importance for the formation of AABW (Rintoul, 1998; Orsi et al., 1999). The net result is a decrease in AABW temperatures (Figure III.2d), and an increase in AABW density (Figure III.2d) and ventilation (Figure III.3c) for stronger winds compared to the unperturbed conditions. Most importantly, this enhances the bipolar contrast in ocean densities between AABW and NADW, leading to a weaker overturn and ventilation of NADW despite stronger Southern Ocean winds (Figure III.3c).

Weaker westerly winds have the opposite effect over the Antarctic sea-ice expanse: namely, reducing northward advection of sea-ice, and increasing polar sea-ice coverage and sea-ice thickness, particularly in the Weddell and Ross Seas (Figure III.2a). This reduces ocean heat loss to the atmosphere, which in turn leads to warmer and thus less dense AABW (Figure III.2c). In both the strengthened and weakened wind experiments, this sea-ice / thermal feedback mechanism occurs from the onset of the wind perturbation until a new equilibrium is reached (see the transient T-S-density analysis shown in Figures III.2c and III.2d).

The changed density of AABW caused by variations in wind-driven sea-ice cover affects the interhemispheric contrast in buoyancy forcing of the global ocean. This is mainly

driven by changes in the temperature of AABW (Figure III.2c,d), which eventually also affects NADW temperature-salinity via overturning changes induced by the bipolar seesaw. For example, in the control unperturbed climate AABW is denser than NADW (Figure III.2c,d), just as occurs in the observed ocean. However when the wind forcing anomalies are applied, the AABW temperatures and density is impacted almost immediately. For stronger Southern Ocean winds the density difference between AABW and NADW is increased (Figure III.2d), primarily driven by temperature changes in AABW; while the density of NADW remains virtually unchanged from the control unperturbed conditions (Figure III.2d). In contrast, AABW becomes colder and denser, with bottom water ventilation from the south also increased markedly (Figure III.1 e,f). As a result the Atlantic overturning cell shallows and NADW formation is weakened under increased wind conditions, despite the mechanical wind forcing of increased northward surface mass transport in the Southern Ocean.

Weakened westerly winds reduce the density difference between AABW and NADW (Figure III.2c). This is initially due to increased sea-ice coverage, which insulates the surface ocean from cold Antarctic air temperatures, warming oceanic SST and leaving AABW less dense than in the unperturbed experiment. Eventually the North Atlantic climate responds as well, with a significant freshening of NADW once a new equilibrium is reached (Figure III.2c). Because NADW production increases in this experiment, which is normally associated with warmer and saltier waters in the region, the freshening of the North Atlantic (Figure III.2c) can be traced to the model importing lower salinity waters from the south due to an increase in precipitation off the North American coast. Wetter conditions over the Labrador, Greenland and Norwegian Seas further contribute to the freshening of NADW. To summarise, a decrease in Southern Hemisphere westerlies leads to an increase in Antarctic sea-ice cover and insulation of the surface ocean. This leads to warmer surface waters and thus reduced AABW formation, and via the bipolar seesaw a deepening and strengthening of the North Atlantic overturning cell, which dominates over the mechanical effect of the wind-driven weakening of Ekman transport at the latitudes of the Drake Passage (Figures III.1g, III.3a and III.4). Localised precipitation changes lead to a fresher North Atlantic than would otherwise be the case under more vigorous NADW conditions.

We have shown here that surface buoyancy changes around the Antarctic continental margin due to wind-driven variations in sea-ice coverage dominate the mechanical forcing of North Atlantic Deep Water production invoked by the famous Drake Passage Effect (Figures III.3 and III.4). As such, the widely assumed relation between NADW production and Southern Hemisphere westerly wind stress does not necessarily hold when sea-ice feedbacks are resolved. In regards to the importance of the Southern Ocean westerly winds to ocean circulation and the removal of anthropogenic carbon from the atmosphere (Le Quéré et al., 2007; Lovenduski et al., 2008), this finding could have important implications for the prediction of the future evolution of the climate system where a recent multi-decadal increase in Southern Hemisphere westerlies (Thompson et al., 2011) has coincided with enhanced Antarctic sea-ice (Simpkins et al., 2013), and with potential impacts on NADW production (Bryden et al., 2005; Pérez et al., 2013). The results are also pertinent to paleoclimate studies, which suggest that Southern Hemisphere warming during deglaciation events, which preceded Greenland warming by several millennia (Sowers and Bender, 1995; Petit et al., 1999), could have triggered the resumption of North Atlantic Deep Water overturning despite an increase in freshwater flux into the Atlantic Ocean (Knorr and Lohmann, 2003).

III.2 Methods

Earth System Model of Intermediate Complexity.

The model used in this study is the University of Victoria (UVic) intermediate complexity Earth System Climate Model (ESCM; Weaver et al., 2001). The model includes a multi-level ocean general circulation model (MOM2.2) with horizontal resolution of 3.6° longitude by 1.8° latitude (Pacanowski, 1995), a dynamic/thermodynamic sea-ice model (Semtner, 1976; Hibler, 1979; Hunke and Dukowicz, 1997), a land surface scheme, and models to represent vegetation (Meissner et al., 2003), sedimentation (Archer, 1996) and marine biology (Schmittner et al., 2008). The UVic ESCM represents atmosphere-ocean interactions by coupling the ocean model to a simple energy-moisture balance model of the atmosphere. As such the surface boundary conditions of the ocean vary depending on the state of the atmosphere as well as via heat and freshwater exchange with the model

sea-ice. For the purposes of this study the surface wind stress at the atmosphere-ocean interface is taken to be the monthly mean wind climatology from the National Center for Environmental Prediction (NCEP; Kalnay et al., 1996). In addition to forcing the circulation in the ocean model, the prescribed surface wind stress also influences the evolution of sea-ice, which resolves thermodynamic and dynamic processes (Semtner, 1976; Hibler, 1979; Hunke and Dukowicz, 1997).

The models coarse resolution does not resolve mesoscale oceanic eddies; instead a parameterization is included of the effect of eddies on the mean ocean flow via the Gent-McWilliams thickness diffusion scheme (Gent and McWilliams, 1990). Importantly, inclusion of the full physics of ocean eddies within the model is not expected to alter the findings of this study, as the Drake Passage Effect is artificially strong in models without ocean eddies (Morrison and McC. Hogg, 2013). This is because eddies act to partially compensate northward Ekman transport via a poleward mass flux (Morrison and McC. Hogg, 2013; Rintoul et al., 2001; Marshall and Radko, 2003; Saenko, 2007; Farneti et al., 2010; Farneti and Gent, 2011). As such, if resolving eddies, the model would likely only see a greater control of the Atlantic meridional overturning by the bipolar seesaw, at the expense of the wind-driven Drake Passage Effect.

Experimental set up

For this study the model was integrated for one control and two wind perturbation simulations. The control experiment is forced using seasonally-varying NCEP reanalysis winds (Kalnay et al., 1996). The wind fields of the two perturbation experiments are the same as in control, but include a 30% reduction and a 30% increase, respectively, in the westerly component of the zonal wind stress south of 30°S (Figure III.1). The two perturbation experiments are initiated from the equilibrated control model experiment. The wind perturbation experiments are then run until a new equilibrium is reached under the perturbed wind conditions. The wind-stress perturbations are applied to the momentum fluxes in both the ocean and the sea-ice models. While the forcing of temperature and salinity depends on the evolution of air-sea heat and freshwater fluxes throughout the integration of the experiments, the applied wind stress field includes monthly variations but no variability on interannual time-scales.

Water-mass analysis

To allow an assessment of changes in ocean transport and the rate of interior ocean ventilation, several tracers are introduced into the equilibrated experiments. One set of tracers are water-mass dye tracers that obey the same equation as the models dynamic tracers (temperature and salinity), but are strategically configured to track the ventilation of a given water mass into the ocean interior. Two such tracers were released to track, respectively, changes in Antarctic Bottom Water (AABW) and North Atlantic Deep Water (NADW). For the first (AABW), the tracer concentration is restored to a constant value of 1 within the volume of water deeper than 3660 m and south of 60°S. For the second (NADW), the tracer concentration is restored to a constant value of 1 in the region in the North Atlantic spanned by 110°W - 0° and 42°N - 73°N below 1100 m. Tracer concentrations in the layers above the two areas of tracer release are set to zero throughout the model integration to avoid contamination of the tracer spreading fields by water not exiting at depth.

A second passive tracer, an age tracer (England, 1995), also obeys the models tracer equation, only it is configured in such a way to trace the volume-weighted time-scale for water to ventilate the ocean interior from the sea surface. To achieve this the tracer is set to zero everywhere at the beginning of the model integration, and then increased every time step by a constant value equal to the length of the model time step everywhere except within the surface-most layer, where the tracer is set to retain a constant value of zero throughout the integration. To facilitate an accurate analysis of water mass age changes, all experiments were integrated until the age tracer reached full equilibrium (England, 1995).

The different water masses within each model experiment can also be tracked using the large-scale patterns of dissolved oxygen concentrations (O_2, Figure III.3; Marshall and Speer, 2012). The UVic ESCM has been shown to represent ocean oxygenation and the broad observed pattern of dissolved oxygen concentrations reasonably well (e.g. Duteil and Oschlies, 2011; Cocco et al., 2013). The model calculates dissolved oxygen concentrations using a nutrient, phytoplankton, zooplankton and detritus (NPZD) model nested within the global ocean model. The model accounts for the air-sea flux of O_2 as

well as its biological production/depletion by inversely coupling O_2 concentrations to the sink term of PO_4 via a fixed stoichiometric ratio (Schmittner et al., 2008; Ridder et al., 2013). The model thus links photosynthesis to a reduction in PO_4 and the utilization of O_2 for remineralization to an equivalent increase in PO_4. The overall signature of O_2 concentrations is in good agreement with modelled water-mass age. By displaying O_2 in Figure III.3 rather than water-mass age the significance of ventilation changes to biogeochemical tracers and related processes is highlighted.

III.3 Acknowledgements

This study was funded by the Australian Research Council (ARC) including the ARC Centre of Excellence in Climate System Sciences and supported by an award under the Merit Allocation Scheme on the NCI National Facility at the Australian National University. NNR is funded under the International Postgraduate Research Scholarship scheme of the Australian Government Department of Industry, Innovation, Science, Research and Tertiary Education. MHE is funded under the ARC Laureate Fellowship program (FL100100214).

III.4 Figures

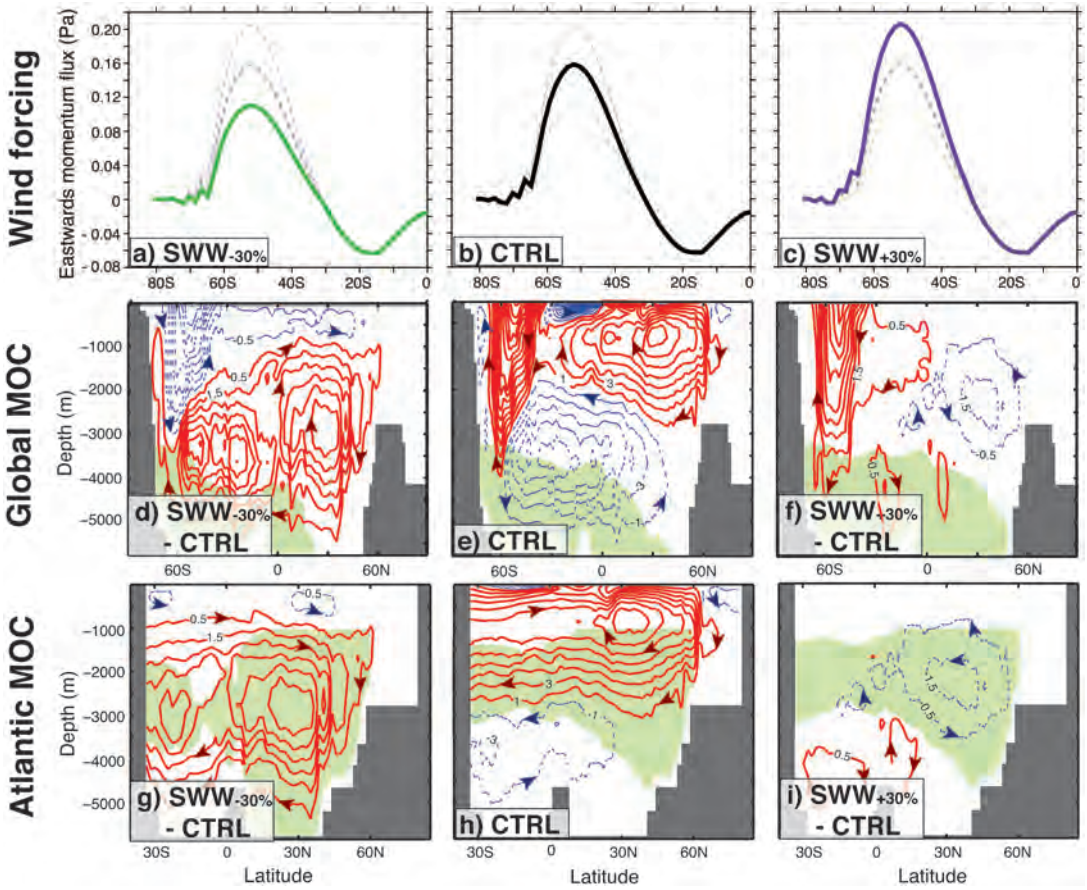

Figure III.1: Changes in Southern Ocean surface wind forcing and the meridional overturning circulation. Applied Southern Ocean zonal mean eastward momentum flux (Pa) in the experiments with (a) decreased winds ($SWW_{-30\%}$; solid, green), (b) control winds (CTRL), and (c) increased winds ($SWW_{+30\%}$; dashed, purple). In panels (a)-(c) all experiments are indicated for easy reference. (d) Changes in global meridional overturning circulation (MOC; Sv) in $SWW_{-30\%}$ - CTRL. Green shading indicates regions where the zonal mean AABW tracer concentration exceeds 0.1 in the $SWW_{-30\%}$ experiment 600 years after the start of tracer release; (e, f) as in (d) but showing MOC for CTRL and $SWW_{+30\%}$ minus CTRL, and the regions where AABW tracer concentration exceeds 0.1 for CTRL and $SWW_{+30\%}$, respectively. (g) Change in Atlantic MOC (Sv) in $SWW_{-30\%}$ relative to CTRL. Green shading indicates regions where the zonal mean NADW tracer concentration is larger than 0.1 in experiment $SWW_{-30\%}$ 200 years after tracer release; (h, i) as in (g) but showing MOC for CTRL and $SWW_{+30\%}$ minus CTRL, and the regions where NADW tracer concentration exceeds 0.1 for CTRL and $SWW_{+30\%}$, respectively. Contour intervals in the CTRL MOC panels (e,h) are 2 Sv starting from 1 Sv; and 1.0 Sv starting from 0.5 Sv in the MOC difference panels (d,f,g,i). Dashed blue contours indicate negative values, solid red contours represent positive values.

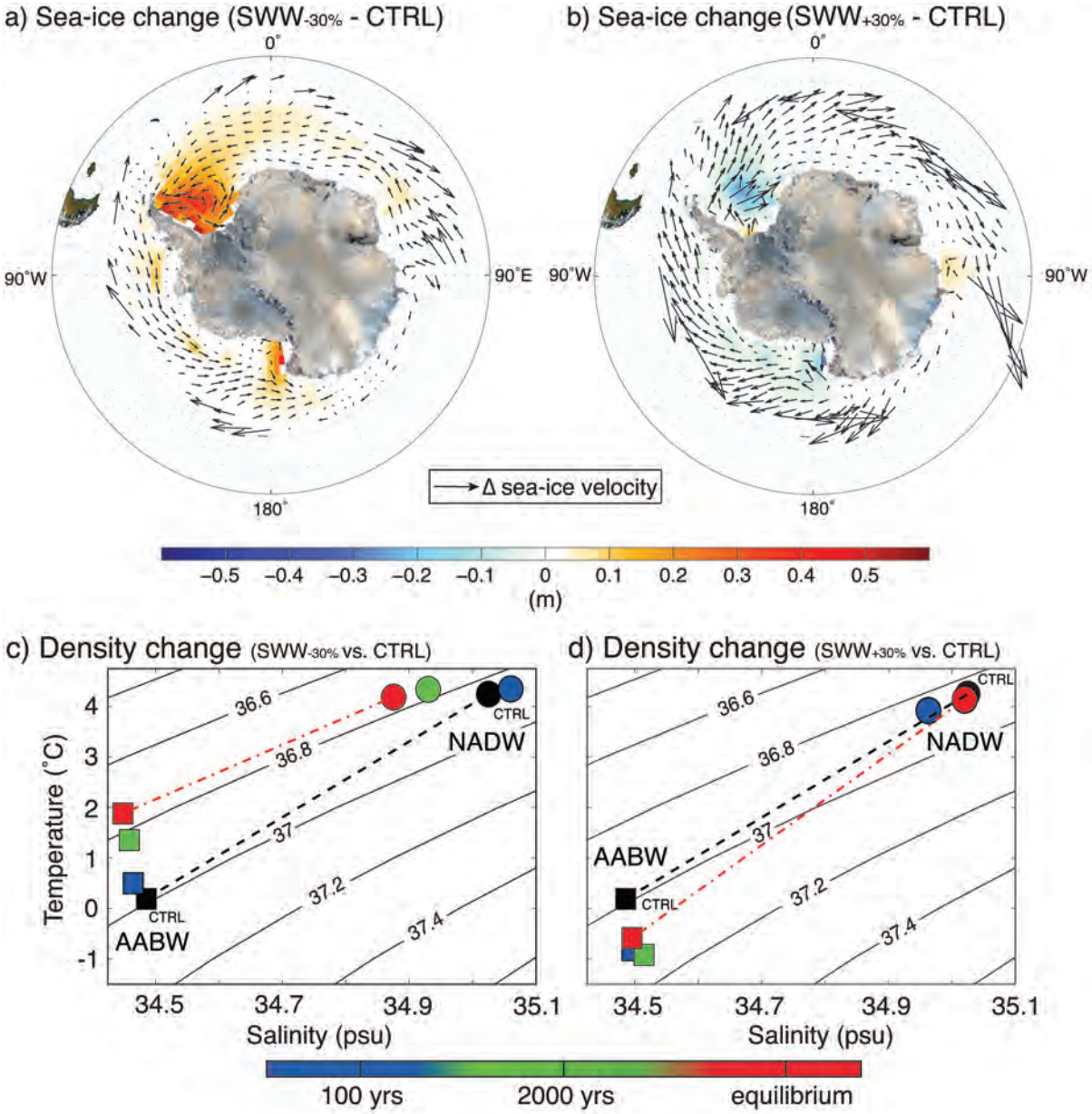

Figure III.2: Response of sea-ice coverage and water mass T-S and density to Southern Ocean wind perturbations. (a) Changes in sea-ice thickness (m) between the wind-reduced case ($SWW_{-30\%}$) and CTRL. Vectors indicate changes in sea-ice velocity; (b) as (a) but for the 30% wind-increased case ($SWW_{+30\%}$) minus CTRL. (c) T-S diagram showing AABW and NADW properties (squares and circles, respectively) in the wind-reduced case after 100 years (red), 2000 years (green) and at equilibrium (blue), respectively. Black square and circle symbols indicate values in the CTRL experiment at equilibrium. The values shown are averaged over grid cells with the twenty highest potential density values between 1000 m and 2000 m depth in the respective regions of water mass formation. Densities were calculated using the 2000-m isobath as a reference level; (d) same as (c) but for the wind-increased case.

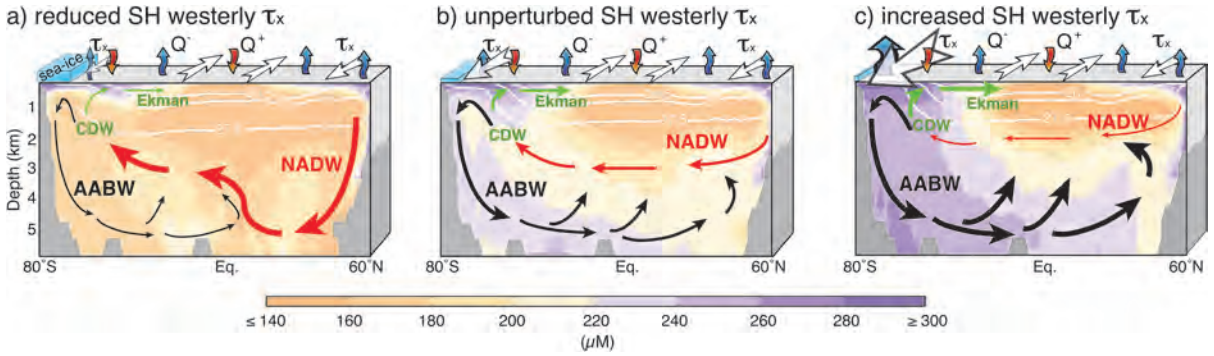

Figure III.3: Oxygen concentrations and schematic diagrams of the water-mass ventilation in the three experiments. (a) The reduced westerly wind stress case, (b) the control experiment, and (c) the increased westerly wind case. The schematic depicts both the Upper and Lower Cells as well as density surfaces and oxygen concentration (Marshall and Speer, 2012). Arrows within the ocean mark the pathways for the different water masses/transport processes. Red arrows represent North Atlantic Deep Water (NADW), black arrows mark Antarctic Bottom Water (AABW) and green arrows represent Circumpolar Deep Water (CDW) and upper-ocean northward Ekman transport. Arrow thickness indicates a change in water mass formation strength compared to the unperturbed control conditions, with thicker arrows for stronger water mass formation and vice versa for thinner arrows. White contours mark the depth of the $\sigma_{26.5}$, $\sigma_{27.0}$ and $\sigma_{27.5}$ isopycnals. Blue and red arrows at the sea surface indicate heat exchange with the atmosphere (blue represents heat loss to the atmosphere and red indicates ocean heat gain). White surface arrows indicate the direction of the zonal mean wind stress at specific latitudes. The blue rectangle at the sea surface in the Southern Ocean represents sea-ice cover. Colour shading indicates the annual and zonal mean oxygen concentration in each experiment (μM).

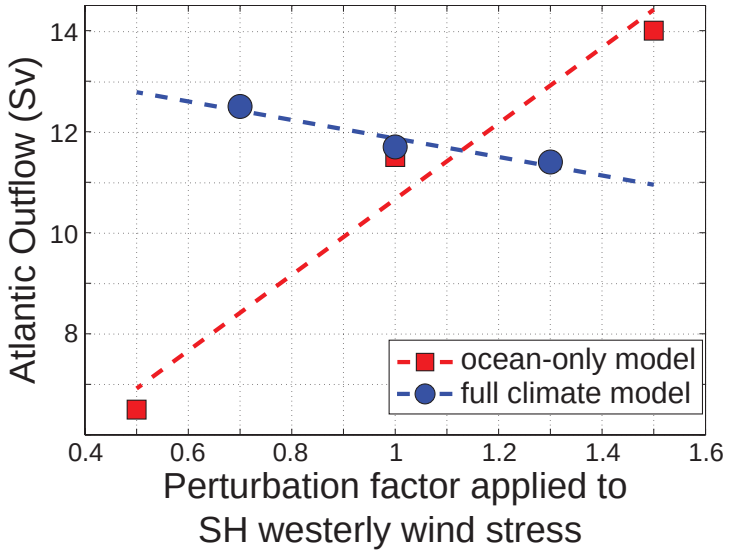

Figure III.4: Relationship between simulated North Atlantic Deep Water outflow and Southern Ocean wind stress. Results from a past ocean-only study (Toggweiler and Samuels, 1995) are compared to the coupled climate model results obtained here. The strength of the Atlantic outflow from the ocean-only model ignoring sea-ice feedbacks (black squares) suggests direct proportionality to Southern Hemisphere (SH) westerly wind stress. This correlation collapses, and is even slightly reversed, when sea-ice feedbacks are included (blue circles). Bold dashed lines indicate the best-fit linear relationship between NADW outflow and SH westerly wind stress in each case.

Part IV: Comparison of the response in ocean circulation to changes in low-latitude and mid-latitude wind stress

IV.1 Introduction

Variations in ocean overturning at high-latitudes, in particular in the Southern Ocean (SO), have been suggested to be one of the main drivers behind major global climate shifts (e.g. Sigman et al., 2010). However, it has been shown that changes at the low-latitudes could have a significant contribution to the oceanic control over atmospheric carbon dioxide (Part I). Both regions, low- and southern mid- to high-latitudes, have experienced changes in the local prevailing wind fields and thus the mechanical forcing at the ocean's surface throughout the history of the global climate, with future projections predicting further changes (e.g. Thompson and Solomon, 2002; Haywood et al., 2005; Ravelo et al., 2006; Shukla et al., 2009; Collins et al., 2010; Swart and Fyfe, 2012). At low-latitudes for instance, paleo-proxies, more recent observations and numerical model studies suggest that the strength of equatorial trade winds varies with global mean temperature (e.g. Collins et al., 2010; Tokinaga et al., 2012). Another example are the Southern Hemisphere (SH) westerly winds, which have been observed to undergo a poleward intensification in response to stratospheric ozone depletion over the past decades (e.g. Thompson and Solomon, 2002). In addition the prevailing wind forcing in both regions is expected to change further under future climate change (e.g. Vecchi and Soden, 2007; Swart and Fyfe, 2012).

This part of this thesis compares the impact of wind stress changes in both low- and southern mid-latitudes on oceanic parameters affecting important biogeochemical processes. Special attention is given to the circulation and overturning changes in both cases, as well as to the induced modifications in temperature, salinity and density. Further we will assess the impact on the nutrient return from the southern to the equatorial oceans by comparing changes in Subantarctic Mode Water (SAMW) formation and transport (Toggweiler et al., 1991; Sarmiento et al., 2004). The analysis will isolate the effect of wind-driven isopycnal heave to allow a more detailed assessment of all mechanisms involved in the modelled changes (Bindoff and McDougall, 1994). Thus this Part extends the results presented in Parts I, II and III by presenting a comparison of the different impacts of wind-driven circulation changes in both regions on a variety of important oceanic properties.

To allow a consistent comparison between the impact of low- and mid-latitude wind stress changes on ocean circulation and overturning, as well as on oceanic carbon and dissolved oxygen (as presented in Part I and II), this study focuses on variations in the strength of Southern Hemisphere westerlies and neglects the possibility of latitudinal wind shifts. This isolates the systems response to changes in wind stress strength, rather than adding the separate additional effect of a poleward shift. This maintains a clean comparison with the tropical wind shift experiments presented in Parts I and II. In addition, the wind shift component has been assessed in detail in previous studies (e.g. Sijp and England, 2009).

IV.2 Model and experimental setup

This study analyses results yielded by an Earth system model of intermediate complexity (UVic ESCM; Weaver et al., 2001, see also sections 2 in Parts I, II and III of this thesis) consisting of a three-dimensional ocean general circulation model (MOM2; Pacanowski, 1995), a two-dimensional energy-moisture balance atmospheric model, a dynamic-thermodynamic sea-ice model (Semtner, 1976; Hibler, 1979; Hunke and Dukowicz, 1997), a land surface scheme (TRIFFID; Meissner et al., 2003) and a sediment model (Archer, 1996). The UVic ESCM represents marine biogeochemistry using an NPZD model nested within the global ocean model and has been shown to represent important oceanic and biogeochemical tracers, e.g. temperature, salinity and oxygen concentrations, reasonably well (Schmittner et al., 2008; Oschlies et al., 2008; Cocco et al., 2013). The model was forced using four different wind stress fields. For this the unperturbed fixed monthly mean wind climatology based on NCAR reanalysis data (Kalnay et al., 1996) used in the UVic ESCM was altered to include zonal wind changes of ±30% in (i) the tropical easterly winds (TEW) stress at latitudes between 30°S and 30°N (hereafter $TEW_{-30\%}$ and $TEW_{+30\%}$) and (ii) the Southern Hemisphere westerly wind stress south of 60°S (hereafter $SWW_{-30\%}$ and $SWW_{-30\%}$). These perturbations induce differences in the integrated momentum flux at the ocean surface of (i) 4.4×10^{12} N for low-latitude perturbations ($TEW_{-30\%}$ minus $TEW_{+30\%}$) and (ii) 5.5×10^{12} N for perturbations in the SO ($SWW_{-30\%}$ minus $SWW_{-30\%}$). The low-latitude experiments are equivalent to the ±30% perturbation cases in Parts I and II of this thesis; the Southern Hemisphere west-

erly experiments are the same as in Part III, accordingly the model uses a constant Gent and McWilliams (1990) isopycnal thickness diffusion coefficient, which neglects the impact of adjusting eddy dynamics that might occur in response to wind stress changes. Ocean models using a constant GM scheme for parameterized eddies tend to overestimate Ekman fluxes without resolving eddy compensation. Thus in our study, a higher resolution allowing the inclusion of eddies and their response to wind changes would potentially compensate the increased northward Ekman transport by inducing a poleward mass flux. This could in turn impact the distribution of DIC and dissolved oxygen in the model.

For a more detailed analysis of the wind-driven variations in oceanic processes, the set of parameters accounted for in the UVic ESCM was extended to include two additional passive tracers (as per England, 1995). Both tracers, one dye and one age tracer, follow the model's transport equation for tracers. The dye tracer was used to track the formation and transport of SAMW as well as to identify changes in the pathways of nutrient resupply from high- to low-latitudes. For this dye tracer concentrations in the uppermost model layer of the geographical region representative for SAMW formation (Figure IV.1) are set to one during every time step. At depth and outside of the major formation region of SAMW the dye tracer evolves freely following the modelled oceanic transport.

The second tracer was introduced to track ocean ventilation using water age. Its concentration is fixed to zero everywhere in the uppermost model layer. Below that the tracer is increased by a constant value equal to the length of the model time step and obeys the model's transport equation for tracers. For more details on the model and the performed experiments also referred to Parts I - III of this thesis.

IV.3 Results

IV.3.1 Comparison of modifications in ocean overturning and circulation

Meridional overturning circulation (MOC)

The application of wind stress changes in the tropics affects almost exclusively the shallow equatorial overturning cells (Figure IV.2a). This response of the equatorial overturning

cells is caused by an alteration in the divergence of the surface transport at the equator due to the low-latitude wind stress perturbations. Intensified tropical winds increase the divergence at the equator. This strengthens the shallow equatorial overturning cells and thus increases equatorial upwelling (Figure IV.2a and Table IV.1). Weakened winds have the opposite effect of decreasing divergence at the equator and thus reducing equatorial upwelling. However, these changes mainly affect the upwelling of water masses within the upper 1000 m, i.e. intermediate and mode waters. The upwelling of deep water masses, which would affect the MOC on the global scale (as reviewed in Kuhlbrodt et al., 2007), remains unchanged between both low-latitude experiments (Figure IV.2a). The limitation of the upwelling to intermediate waters, in combination with the dissipation of the wind-induced energy in the upper layers of the ocean, restricts the impact of the applied tropical wind changes to shallow depths at the low-latitudes. The application of constant mixing coefficients within the UVic ESCM further contributes to this limitation of the affected region as it prevents wind-induced alterations in turbulent mixing processes, which have been identified to significantly contribute to the upwelling of deep water masses and are thus one of the main drivers of the global overturning circulation (as reviewed in Kuhlbrodt et al., 2007). Consequently, circulation differences between the two low-latitude perturbation experiments in regions outside the tropical surface ocean are limited to values below 2 Sv (Figure IV.2a; see also Part I) and are too small to significantly impact ocean temperature and salinity in the ocean's interior as discussed in detail below. The North Atlantic Deep Water (NADW) cell shows only small changes in overturning strength, which hints to a slightly shallower overturning cell under weaker wind conditions and a deeper cell under strengthened winds (Figure IV.2a). This is most likely caused by the alterations in the strength of the subduction at mid-latitudes due to the wind-driven variations in the strength of the shallow equatorial overturning cells. For stronger winds the increased subduction of light surface water changes the buoyancy forcing in this region (Figure IV.3b and IV.3c) and forces the denser NADW to sink slightly deeper into the basin, while weaker winds subduct less light surface water and allow NADW to remain at shallower depths. However, these changes in local overturning strength are small in comparison to the assumed 5 Sv inter-annual variability of AMOC (reviewed in Rhein et al., in press) and are thus overall negligible. The Antarctic Bottom Water (AABW) cell remains virtually unaffected by the applied perturbation in low-latitude surface wind stress. This finding of only small changes in the global MOC

in combination with the wind-driven changes in the Indonesian throughflow (ITF, Table IV.2) in the low-latitude experiments contradicts the theory of thermocline upwelling of NADW in the Pacific Ocean and its subsequent return to the North Atlantic through the ITF and the Agulhas Current (Gordon, 1986).

Southern Hemisphere (SH) wind perturbations induce significant modifications in the upwelling of deep water masses due to their impact on the Circumpolar Deep Water (CDW) cell (Figure IV.2b, see also Part III). The upwelling in the SO is driven by the wind-induced surface divergence south of the zonal westerly wind stress maximum and the subsequent removal of the upwelled water to the equator via northward Ekman transport. The wind-driven upwelling in the Southern Ocean circumpolar belt is not limited to the upper ocean. Instead the unique bathymetry of the SO, which prevents a net meridional geostrophic flow at latitudes of the Drake Passage between the surface and the shallowest point at each latitude (i.e. the Drake Passage Effect; Toggweiler and Samuels, 1993), allows surface winds to affect the flow in this region down to depths of the shallowest bathymetry feature due to the flow's ageostrophic nature. As a result the CDW cell, and with this the upwelling of deep water, as well as the northward Ekman transport in the SO are accelerated for stronger SH westerly wind stress and vice versa reduced for weaker winds (Figure IV.2b). At the same time, the perturbations in surface wind stress affect the advection of sea-ice around the Antarctic continent and lead to significant changes in sea-ice thickness and coverage (Figure IV.4 and Table IV.3; see also Part III). The resulting difference in the thermal forcing at the surface ocean at southern high-latitudes between the two perturbation experiments causes a significant change in the AABW density. Thus the buoyancy forcing within the ocean interior is modified, with an increasing density difference between AABW and NADW for stronger SH westerlies and vice versa a decreasing difference for weaker winds (Figure IV.5b). The shift in AABW density compared to unperturbed conditions finally affects NADW and thus the Atlantic Meridional Overturning Circulation (AMOC). For stronger SH westerlies the increased bottom water density restricts the sinking of NADW to the deep Atlantic and thus slightly decelerates the NADW cell (Figures IV.2b and IV.6). Weakened SH westerlies have the opposite effect of decreasing the density difference between AABW and NADW, enabling NADW to invade the deep Atlantic Ocean and thus increase the NADW cell (Figures IV.2b and IV.6). This reverses the link between SH westerly wind

strength and NADW formation as suggested by Toggweiler and Samuels (1995) and contradicts their view that NADW formation and the Atlantic outflow is merely the closing branch of the loop of upwelled CDW.

Horizontal streamfunction

As for the changes in MOC, low-latitude wind perturbations induce modifications in the streamfunction (ψ), which are located almost exclusively in the equatorial and subtropical regions, i.e. the geographical region that directly experiences the wind changes (Figure IV.7a to IV.7c). The main features of the difference field between the two experiments include changes in the subtropical gyres of all ocean basins (Figure IV.7c). Here the different wind perturbations cause variations in the wind-driven Ekman transport that in turn alter the horizontal gradients of sea surface height, piling additional water into the subtropical gyres for strengthened winds, and vice-versa for weakened winds. Strengthened trade winds thus accelerate the equatorial currents and subtropical gyres, while weakened winds have the opposite effect (Figure IV.7a - IV.7c). The circulation in high-latitudes remains unchanged in both low-latitude perturbation experiments reflecting the limitation of the wind-driven circulation changes to the shallow equatorial circulation and the subtropical gyres (Figure IV.7c).

Wind stress perturbations in the SH westerlies mainly change the Antarctic Circumpolar Current (ACC) and the Southern Hemispheric subtropical gyres (Figures IV.7d to IV.7f). The modelled variations in the ACC are, however, overestimated due to the non-eddy resolving nature of the applied ocean model, which omits the possibility of the wind energy being absorbed into eddy kinetic energy without affecting ocean transport in the ACC (the so called "eddy-saturation effect", e.g. Hallberg and Gnanadesikan, 2001; Meredith and Hogg, 2006; Hogg, 2010). Significant differences in the horizontal streamfunction can also be found in the depth-integrated circulation in the Atlantic basin. These changes are caused by the alterations in deep ocean density, which lead to modifications in the interaction of the ocean flow with bottom topography in the North Atlantic basin due to the joint effect of baroclinicity and relief (JEBAR, Figure IV.7f).

Water age and ventilation

Alterations in water age reflect the changes in ocean circulation with overall older, less ventilated water in perturbation cases using weaker wind stress in either region and younger, more rapidly ventilated water for stronger winds (Figure IV.8 and Table IV.4). For tropical wind perturbations the age changes highlight the decrease in equatorial upwelling for weakened winds compared to stronger winds with a maximum increase in water age in the upper 1000 m around the equator. This feature is mainly caused by changes in the equatorial upwelling in the equatorial Pacific and Indian Oceans where weaker winds cause a reduction in the overturning and thus older waters at mid-depths (upper 1000 m depth), while stronger winds increase their ventilation (Figures IV.9a and IV.9c). The response of the Atlantic Ocean differs from this pattern. The changes in ventilation due to wind-driven alterations in the shallow overturning cells is dominated by the depth changes of the NADW cell (Figure IV.2b). This increases the ventilation of intermediate waters in the North Atlantic basin for weaker low-latitude wind conditions while the water in the deep Atlantic (below 2500 m depth) becomes older (vice versa for stronger winds; Figure IV.9a). The Southern Ocean only shows small changes in water age, which are mainly related to the variations in the subduction of Antarctic Intermediate Water (AAIW) and Subantarctic Mode Water (SAMW) due to changes in the shallow overturning cells (Figure IV.9g). Overall the wind-driven changes in ocean overturning and water-mass formation lead to a global mean age of 374.9 years for a 30% reduction in the low-latitude easterly winds and 356.6 years for an equivalent increase. Unperturbed conditions lead to a global mean value of 366.1 years, highlighting the modest change in overall ocean ventilation due to equatorial wind anomalies (Table IV.4). The maximum age of water in the global ocean (located in the deep Pacific) slightly increases from 647.2 years under unperturbed conditions to 659.2 years for 30% weaker trade winds and decreases to 637.6 years for 30% stronger winds. This implies that the ocean's oldest deep water is not significantly influenced by changes in the equatorial winds.

The pattern of zonal mean age change caused by perturbations in southern mid-latitude westerly wind stress is dominated by the changes in AABW cell and deep water formation in the SO (Figure IV.8f). The decrease in AABW formation due to weakened SH westerly wind stress significantly increases the age of waters in the Southern and the deep ocean. Stronger SH westerlies in contrast lead to a more rapidly ventilated deep

and Southern Ocean (Figures IV.8d - IV.8f). The wind-driven alterations in the CDW cell contribute to the changes in ventilation set by the variations in AABW formation and mostly affect waters at roughly 500 m to 2000 m depth. Here strengthened winds increase the upwelling in the circumpolar belt, thus leading to younger waters at these depths, while weakened winds decrease the ventilation of these waters (Figure IV.2b). Except for the Atlantic Ocean this pattern of change is present in all ocean basins. The Atlantic Ocean is dominated by the changes in the formation of NADW and the AMOC leading to younger, more rapidly ventilated waters in the northern deep Atlantic under weakened wind conditions and vice versa older waters for stronger winds (Figure IV.9b). Overall, the changes in the strength of the AABW cell caused within the two perturbation cases leads to a significant variation in global mean age between the two southern mid-latitude experiments, reaching a difference of 136.7 years ($SWW_{-30\%}$ minus $SWW_{+30\%}$; refer also to Table IV.4). The oldest water age under increased mid-latitude winds is, however, virtually unchanged from unperturbed conditions due to the small changes in the strength of AMOC and AABW across these experiments (see Part III), and thus in the ventilation rate of the deep ocean in the North Pacific. Reduced SH westerlies in contrast show an increase in maximum water age despite a generally faster ventilation from the deep North Atlantic Ocean. This suggests that the increase in age of the old deep North Pacific water derives from changes in AABW, which is less ventilated under weaker wind conditions (Figure IV.9).

Northward heat transport

The wind-induced changes in oceanic transport also affects the northward heat transport (NHT) within the ocean. In experiments with low-latitude wind perturbations a weakening of the equatorial trade winds results in an overall lower poleward heat transport compared to stronger low-latitude winds as a result of the reduction in the equatorial overturn (Figure IV.10). While these changes are seemingly small, a recent study has suggested comparable observed low-latitude wind stress perturbations over the equatorial Pacific to be the main driver of the heat transport changes leading to the currently observed hiatus in global surface temperature change (England et al., 2014).

The NHT difference between weak and strong southern mid-latitude westerly wind experiments ($SWW_{-30\%}$ - $SWW_{+30\%}$) highlights the wind-driven alterations in northward

Ekman transport between the two experiments. Stronger SH wind stress increases the NHT between ~65°S and ~35°S reaching a maximum difference of 0.5 PW compared to weaker SH westerlies. The magnitude of NHT changes caused by low-latitude perturbations ($TEW_{-30\%}$ - $TEW_{+30\%}$) is lower and reaches an absolute maximum of 0.25 PW at around 30°N.

IV.3.2 Modifications of hydrographic properties

Temperature changes

The modest circulation changes in the equatorial wind perturbation experiments ($TEW_{-30\%}$ and $TEW_{+30\%}$) cause small changes in large-scale average ocean temperature. Overall ocean temperatures are colder under weaker tropical wind stress conditions, while stronger winds increase ocean temperatures slightly (Figure IV.11a - IV.11c). This is because of changes in the subduction of heat due to the wind-driven variations in the strength of the subtropical overturning cells (Figure IV.2a) and the ventilated thermocline (Luyten et al., 1983), with weaker cells reducing oceanic heat uptake and stronger overturning cells increasing the uptake of heat (as per England et al., 2014). As a result, maximum zonal mean temperature differences are located in the regions of the subducting branches of the equatorial overturning cells at around 1000 m depth (Figure IV.11c). Removing the impact of isopycnal heave shows that this pattern is predominantly caused by depth changes of isopycnal surfaces (Figures IV.12a and IV.13a). The remaining changes in temperature are caused by the variations in poleward heat transport (Figure IV.10) and heat exchange with the atmosphere, which lead to a warming of the surface ocean at low-latitudes and a cooling of the equatorward flowing intermediate waters, e.g. Antarctic Intermediate Water and Subantarctic Mode Water, for weakened compared to stronger winds (Figure IV.13a). The temperatures of NADW and AABW remain virtually unchanged between experiment $TEW_{-30\%}$ and $TEW_{+30\%}$ (Figures IV.5a and IV.13a).

In contrast, the difference in zonal mean temperature between the two southern mid-latitude perturbation cases shows a significantly warmer SO (south of 60°S) and a warmer deep ocean for weaker winds compared to stronger winds (Figures IV.11d - IV.11f). While the changes in the deep ocean are mainly due to alterations in isopycnal depths (Figure

IV.13b), the warming in the surface ocean south of ∼60°S is mainly caused by the wind-driven changes in Antarctic sea-ice thickness (Figure IV.4 and Table IV.3) and the thus resulting alterations in heat exchange with the atmosphere (see Part III). At latitudes of Antarctic Intermediate Water (AAIW) and SAMW formation, temperature changes are dominated by ocean transport changes and through this induced alterations in heat exchange with the atmosphere. As a result the decrease in northward Ekman transport under weaker SH westerly wind conditions leads to colder AAIW and SAMW and vice versa warmer intermediate waters for stronger SH wind conditions (Figure IV.4b). At depth below the intermediate waters ocean temperatures are increased for weaker winds compared to stronger winds (Figure IV.13b). This is the result of an increased contribution of NADW to this depth regime (Figure IV.6) in combination with the increased temperature of AABW under reduced SH westerly winds compared to stronger winds (Figure IV.5b).

Salinity changes

Similar to the differences in temperature, low-latitude wind stress changes only cause modest alterations in zonal mean salinity (Figures IV.14a - IV.14c). These changes are limited to the upper 1000 m and are mainly due to wind-driven modifications in isopycnal heave and in the fresh water flux at the ocean's surface, i.e. evaporation and precipitation (Figure IV.14c, IV.15a and IV.15c). Thus, temperature and salinity changes due to low-latitude wind stress perturbations are too small to significantly affect water mass density or the buoyancy forcing in the ocean interior (Figure IV.5a). They thus do not contribute to changes in the overturning circulation.

Perturbations in southern mid-latitude westerlies cause salinity changes that are more pronounced. They span the entire global ocean and reflect the impact of the SH westerly winds on the NADW circulation (Figures IV.14d - IV.14f and IV.6). In the upper 1000 m reduced Southern Hemisphere westerlies lead to a freshening of the water (Figure IV.14f), which south of 60°S is due to the heave in isopycnals (Figure IV.15b). Removing the effect of the wind-driven changes in isopycnal heave leaves this region in the surface of the SO saltier for weaker winds compared to stronger SH westerlies. The freshening north of 60°S for weaker SH westerlies, however, is mainly caused by the altered global

distribution of NADW between the southern mid-latitude experiments (Figures IV.15d and IV.6). The same mechanism, i.e. the deepening of AMOC for weakened winds and vice versa for stronger winds, leads to a saltier deep ocean due to the increased inflow of salty NADW under decreased SH winds compared to increased wind conditions (Figures IV.14f and IV.5b; Part III). The changes in ocean temperature and salinity caused by alterations in SH westerly winds are sufficiently strong to alter the stratification of the deep ocean (Figure IV.5b). They thus contribute to the wind-driven changes in the overturning circulation (see also Part III).

IV.3.3 Implications for biogeochemical tracers

Marine biological productivity is most pronounced in the photic layer in the surface ocean. Here phytoplankton transforms inorganic carbon into organic carbon using nutrients and energy provided by photons, i.e. photosynthesis. The organic carbon produced by photosynthesis eventually sinks to depth below the photic zone, mostly in the form of detritus, and is eventually remineralized to inorganic carbon in a chemical reaction using dissolved oxygen to produce nutrients (remineralization). This "surface production-deep remineralization loop" (Sarmiento and Gruber, 2006) removes vital nutrients from the surface ocean and increases their concentration at depth. Biological activity in the surface ocean is maintained through the constant upwelling of deep, nutrient-rich waters to the photic layer, which secures the photosynthetic production of dissolved oxygen. Consequently, the most active biological regions in the global ocean are located near important upwelling regions as for instance the equatorial region and eastern boundary upwelling systems. As most upwelling of deep water masses occurs in the Southern Ocean (see section on MOC changes above) it plays an important role in the re-supply of nutrients to the low-latitudes (e.g. Toggweiler et al., 1991; Sarmiento et al., 2004). The main pathway for the resupply of nutrients from the southern high-latitudes to the equatorial ocean is assumed to be SAMW originating in the Southern Ocean and flowing northward into all ocean basins (e.g. Sarmiento et al., 2004). Due to its characteristic temperature and salinity signature the position of SAMW within the ocean can be approximated using the depth of the $\sigma_{26.8}$-isopycnal surface (Sarmiento et al., 2004). Previous studies have placed the main source of the waters upwelled along the Equator and at the South Pacific eastern boundary upwelling system (EBUS) to be in the Pacific sector of

the Southern Ocean south of Australia and New Zealand (Tsuchiya, 1981; Toggweiler et al., 1991). From there the water is believed to travel across the western Pacific to the Equator where it joins the lower layers of the Equatorial Undercurrent before being transported across to the eastern boundary and finally upwelled in the EBUS off Peru and Chile (Toggweiler et al., 1991).

The analysis in the previous section of this Part has shown that the oceanic transport in the southern subtropical gyres as well as in the equatorial currents is sensitive to perturbations in the wind stress forcing in the tropics and at southern mid-latitudes (see Section IV.3.1). This section analyses the implications of this sensitivity on the tracer transport within SAMW. Special attention will be given to the supply pathway to the south Pacific EBUS off Peru and Chile due to its important role in global marine biogeochemistry as one of the biggest marine ecosystems. For this a dye tracer released at latitudes representative of the origin of SAMW is used (see Section IV.2) to track the tracer transport along the $\sigma_{26.8}$-isopycnal surface. Variations in the concentration of this passive tracer on $\sigma_{26.8}$ are caused by a combination of two mechanisms: (i) by depth changes of the $\sigma_{26.8}$-isopycnal itself, which therefore intersects with different parts of the tracer field (i.e. isopycnal heave; Bindoff and McDougall, 1994); and (ii) the direct change in the transport of dye due to advection and mixing changes. For instance, increased ocean circulation and mixing moves the dye faster from the region of release to the Equator and vice versa for decreased circulation, which slows its transport. This section will first investigate the wind-driven depth changes in all experiments and then focus on the concentration changes on the $\sigma_{26.8}$-isopycnal at different times after initial tracer release, and assess the change in oceanic transport. Finally this section will give a brief examination of the impact of the transport changes on a choice of oxygen and DIC concentration metrics.

Depth changes of the $\sigma_{26.8}$-isopycnal

Depth changes of the $\sigma_{26.8}$-isopycnal in all four experiments are mostly located in regions directly affected by the applied wind perturbation (Figure IV.12). In case of the low-latitude perturbation experiments, the alteration of the equatorial divergence at the ocean surface and the induced changes in ocean temperature (Figures IV.13) cause a

decrease in ocean stratification for stronger tropical wind stress conditions and vice versa for weakened winds. As a result the $\sigma_{26.8}$-isopycnal deepens for stronger tropical wind stress while weaker winds lead to a shallower $\sigma_{26.8}$-surface due to the increase in stratification (Figures IV.12a and IV.16a). At high-latitudes, in particular south of 40°S, the difference in depth of $\sigma_{26.8}$ between stronger and weaker equatorial winds decreases as the impact of the wind-stress changes on ocean temperature become smaller closer to the poles. The depth of the $\sigma_{26.8}$-isopycnal remains slightly shallower in the weaker winds case and could potentially compensate the wind-driven decrease in ocean upwelling in this experiment.

Experiments containing wind perturbations in the Southern Hemisphere westerlies affect the depth of $\sigma_{26.8}$ mainly south of 40°S (Figure IV.16b). The increased upwelling of cold circumpolar deep water caused by stronger winds (Figure IV.2b) leads to a shallower $\sigma_{26.8}$ surface and vice versa a deeper isopycnal for weaker winds. The equatorial depth of the $\sigma_{26.8}$-isopycnal remains almost unaffected by the SH mid-latitude wind changes (Figure IV.16b).

Change in passive tracer concentrations on the $\sigma_{26.8}$-isopycnal

Assuming a supply pathway of high-latitude SAMW to the south Pacific EBUS through the northward transport along the western Pacific boundary and the EUC (Toggweiler et al., 1991), a change in the strength of the South Pacific subtropical gyre and the EUC should lead to variations in the amount of water that is upwelled off the coast of Peru and Chile of the same sign. As a result the transport of the passive dye tracer in the experiments should decrease (i) off Peru and Chile and (ii) in the equatorial region of the EUC under weakened wind conditions due to the wind-induced weakening of the South Pacific subtropical gyre. Equivalently, strengthened wind stress conditions would be expected to increase the dye concentrations in these regions. However, the difference fields of the dye tracer concentrations on the $\sigma_{26.8}$-isopycnal show patterns contradicting this assumption (Figure IV.17). For tropical wind perturbations the concentration of the passive dye tracer injected at the surface of the SO increases in the upwelling region off Peru and Chile for weakened winds compared to stronger winds (Figures IV.16a and IV.16b) despite a decrease in the strength of the subtropical gyre (Figure IV.7c) and the EUC (Table IV.2) and the dye tracer concentration within the EUC (Figures IV.16a and

IV.16b). This suggests that the above-mentioned ventilation pathway of the south Pacific EBUS via the EUC as suggested by Toggweiler et al. (1991) is not operating in the model applied in this study (UVic ESCM). This is further supported by the results of the SH westerly experiments, which show a decrease in dye concentrations in the south Pacific EBUS despite increased dye concentrations in the equatorial region coinciding with the EUC (Figure IV.17d). The dye concentration difference between the different experiments suggests that the supply pathway of SAMW to the southeast Pacific in the UVic ESCM seems to follow pathways similar to the ones described by Sloyan and Rintoul (2001): i.e. from its origin in the SO, a major part of the SAMW is transport westward in the southern limb of the south Pacific gyre and in the ACC. In the southeast Pacific some of the SAMW is then entrained into the Peru Current, transported northward along the eastern boundary of the basin and thus directly ventilates the south Pacific EBUS off Peru and Chile. The part of the SAMW that flows northwards along the western boundary of the Pacific basin and joins the EUC seems to be mainly relevant for the ventilation of the upwelling region at the eastern boundary directly at the equator and in the North Pacific, as can be seen in the dye concentration difference in this region between weaker and stronger winds in all four experiments, i.e. dye changes occur with the same sign in the equatorial region of the EUC and the eastern boundaries of the North Pacific Ocean (Figure IV.17).

Another interesting feature in the difference fields is the increase in dye tracer concentrations under weaker wind conditions in either latitude band following the Agulhas Current along South Africa and the northward flowing western boundary current in the Atlantic Ocean. This suggests an increase in the transport of water for decreased wind stress conditions along this pathway, which had been suggested as the main return pathways of NADW to the North Atlantic (Gordon, 1986). While this pathway could provide an additional return flow for the increase in NADW formation under weakened southern mid-latitude westerlies, the lack of change in the AMOC following low-latitude wind stress perturbations (see Section IV.3.1) supports that this return pathway is of less importance for the strength of NADW formation as argued for example by Rintoul (1991).

Response in oceanic oxygen and carbon

The concentrations of oxygen (O_2) and dissolved inorganic carbon (DIC) on the $\sigma_{26.8}$-isopycnal are significantly impacted by wind stress changes in both latitude bands (Figure

IV.18). As biogeochemical tracers their concentrations are determined by a combination of ocean transport, mixing, isopycnal heave and biogeochemical processes, in contrast to the passive dye tracer, which is only affected by oceanic transport, mixing and isopycnal heave. The implications of this difference is particularly obvious for low-latitude wind stress perturbations when comparing the changes in DIC and O_2 concentrations to those in water age within the lower pycnocline, here represented by the $\sigma_{26.8}$-isopycnal (Figures IV.18a and IV.18c). At this depth most regions show O_2 and DIC concentration changes that are in good agreement with those in water age, i.e. younger waters containing more O_2 and less DIC and vice versa. However, not all regions follow this pattern set by the wind-driven ventilation changes, with some regions responding with the opposite sign, i.e. increased O_2 (decreased DIC) concentrations in older waters and vice versa. This is a strong indicator for the importance of modifications in biogeochemical processes for the determination of O_2 and DIC concentrations in the pycnocline under different low-latitude wind conditions. Relating the wind-driven alterations in global mean water age to the total O_2 and DIC content of the ocean suggests that on average the wind-driven changes in biological productivity and remineralization dominate the alterations in ocean oxygenation and carbon content (Tables IV.5 and IV.6). As a result, stronger than normal tropical easterly winds result in a decrease dissolved oxygen and DIC concentrations. The highest changes in O_2 are located in the deep ocean while the ocean's DIC content is mainly altered in the upper 1000 m. This suggests that remineralization changes at depth dominate the response of O_2 to the low-latitude wind stress changes, while solubility changes in the surface ocean are more important for DIC. Weaker winds have the opposite effect and lead to higher O_2 concentrations and only slightly change DIC concentrations (see also Part I). As for increased tropical easterlies, the major changes under weaker wind conditions are located in the deep ocean for O_2 and in the surface ocean for DIC (Tables IV.5 and IV.6) supporting the dominance of biological processes in the response of dissolved O_2. This important finding and its implications for dissolved O_2 concentrations in the global ocean is assessed in detail in Part II of this thesis.

Concentration changes in the lower pycnocline driven by perturbations in Southern Hemisphere westerlies show a higher correlation between O_2 and DIC changes to alterations in water age, which suggests that variations in ocean dynamics dominate the changes in O_2 and DIC concentrations in the lower pycnocline while alterations in marine biol-

ogy are of minor importance. The opposite is true in the abyssal ocean, where water is more ventilated by NADW due to the alterations in AABW density and thus the changed buoyancy forcing within the deep ocean (see Section IV.3.1). As a result weakened SH westerly wind stress leads to a decrease in abyssal DIC. Strengthened southern mid-latitude westerlies produce increased oxygen concentrations and decreased carbon concentrations throughout the ocean and at all depth, following the changes in ocean ventilation and highlighting the importance of transport changes over biogeochemical changes on oceanic carbon and oxygen.

IV.4 Summary and conclusions

The aim of this part of the thesis was to provide a catalogue of changes comparing the implications of wind stress perturbations at low- and southern mid-latitudes on ocean circulation and hydrographic as well as biogeochemical properties. The results suggest that the impact of tropical wind stress perturbations is limited to the upwelling of shallow equatorial waters from the upper 1000 m depth. Weakened low-latitude easterlies lead to a reduction in equatorial upwelling, while strengthened winds lead to an increase. Their impact on deep water mass formation is however minor. This suggests that the thermocline water upwelled in the equatorial Pacific and returned to the North Atlantic via the ITF, the Agulhas Leakage and finally the Gulf Stream as described in Gordon (1986) is unlikely to significantly influence the formation of NADW or the AMOC. Temperature and salinity changes induced by perturbations in tropical easterlies are small and not sufficient to alter the buoyancy forcing within the ocean interior. Thus, variations in the low-latitude easterly wind stress are unlikely to significantly affect the global overturning circulation outside of the shallow equatorial overturning cells, the equatorial surface currents and the subtropical gyres. However, they do have the potential to contribute to decadal climate variability by altering the subduction of heat within the subtropical overturning cells, a process that has been recently identified to drive the currently observed hiatus in global surface temperature (England et al., 2014). Furthermore, the results suggest a high sensitivity of biogeochemical processes controlling DIC and O_2 concentrations to changes in the low-latitude easterly wind stress due to ventilation changes of key biological regions, e.g. the South Pacific eastern boundary

upwelling system. This is discussed in more detail in Part II of this thesis. In contrast, perturbations in southern mid-latitude wind stress impose circulation changes on a global scale. In agreement with observed changes in the age of water masses derived from CFC measurements (Waugh et al., 2013), the results of this study suggest that increased SH westerlies may be presently contributing to observed large-scale ventilation changes, with younger SAMW and older polar CDW, which reflect significant changes in the upwelling of deep waters and water mass formation. However, in contrast to observed changes in ocean temperature, salinity and global mean oxygen concentrations (e.g. Gille, 2002; Joos et al., 2003; Böning et al., 2008; Stramma et al., 2008) an increased wind forcing in our model experiments results in colder and less saline conditions in the ACC and an increased global mean oxygen concentration. This indicates that factors other than Southern Hemisphere wind magnitude changes, for example latitudinal shifts in the atmospheric jet, and air-sea heat/freshwater flux changes, are dominating the evolution of current climate conditions in regards to temperature and salinity in the ACC and global ocean oxygenation.

The impact of perturbations in southern mid-latitude wind stress on biogeochemical processes is less significant, in comparison to the implied variations in temperature and salinity, which determine gas saturation concentrations in seawater, as well as ocean ventilation rates and water-mass age.

In summary, the results presented here support the notion that southern mid-latitude winds exert a greater control over the global ocean overturning circulation than tropical winds. Changes of wind conditions in the tropics and in the equatorial region are mainly restricted to the surface ocean but have the potential to significantly alter the cycling of important biogeochemical tracers.

IV.5 Figures

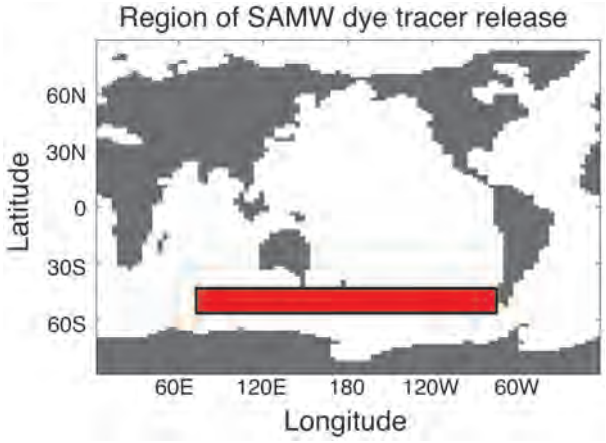

Figure IV.1: Region with constant dye tracer value of one in upper most model layer to represent Subantarctic Mode Water transport (red box).

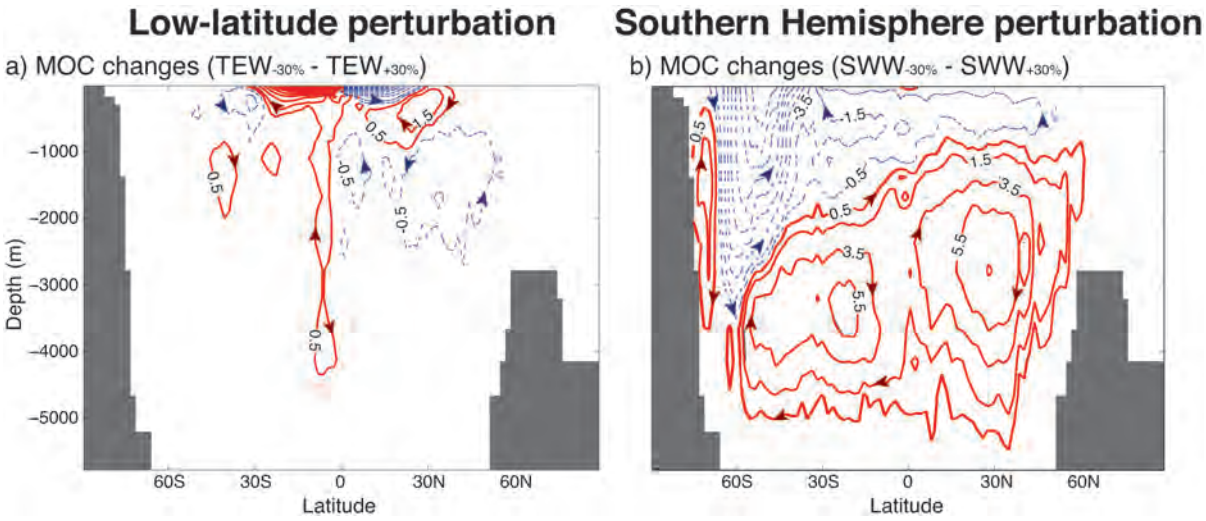

Figure IV.2: Changes in MOC (Sv) between experiments with perturbed surface wind stress at (a) low-latitudes ($TEW_{-30\%}$ minus $TEW_{+30\%}$) and (b) southern mid-latitudes ($SWW_{-30\%}$ minus $SWW_{+30\%}$). Contours start at $\pm$ 0.5 Sv with contour intervals of 1 Sv. Solid lines indicate circulation changes with positive sign; dashed lines represent negative changes.

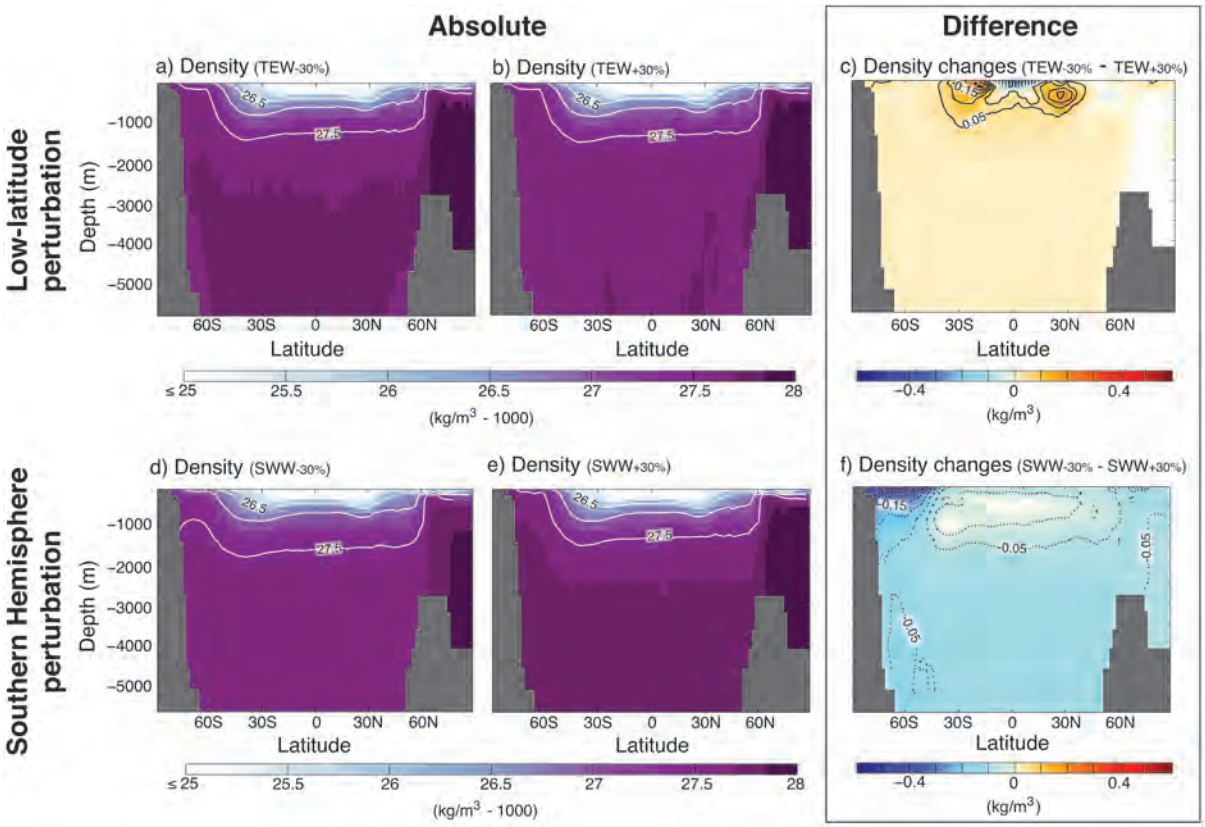

Figure IV.3: (a) Zonal mean density (kg m^{-3} minus 1000) in experiment $TEW_{-30\%}$. Contour intervals are 0.5 kg m^{-3}; (b) as (a) but for experiment $TEW_{+30\%}$, (c) Changes in the zonal mean density (kg m^{-3} minus 1000) between low-latitude perturbation experiments ($TEW_{-30\%}$ minus $TEW_{+30\%}$). Contour intervals are 0.05 kg m^{-3} starting at ± 0.05 kg m^{-3}. Solid lines indicate an increase in water density; dotted lines represent a decrease. (d, e, f) as (a, b, c) only for $SWW_{-30\%}$, $SWW_{+30\%}$ and $SWW_{-30\%}$ minus $SWW_{+30\%}$, respectively.

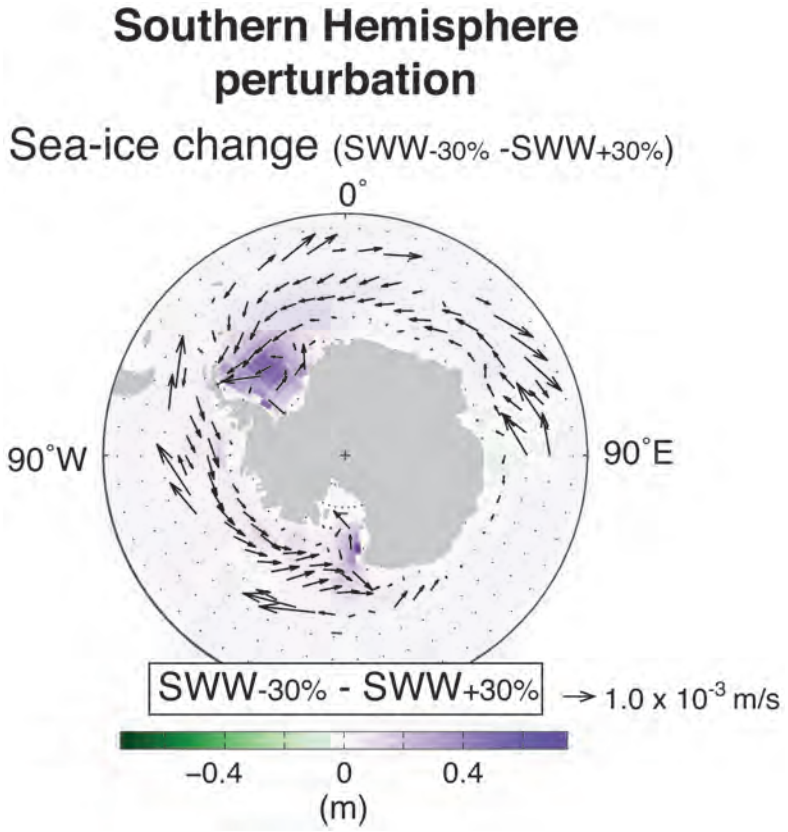

Figure IV.4: Changes in Antarctic sea-ice cover (m; shading) and sea-ice advection (m s^{-1}; vectors) driven by perturbations in zonal surface wind stress at southern mid-latitude ($SWW_{-30\%}$ minus $SWW_{+30\%}$).

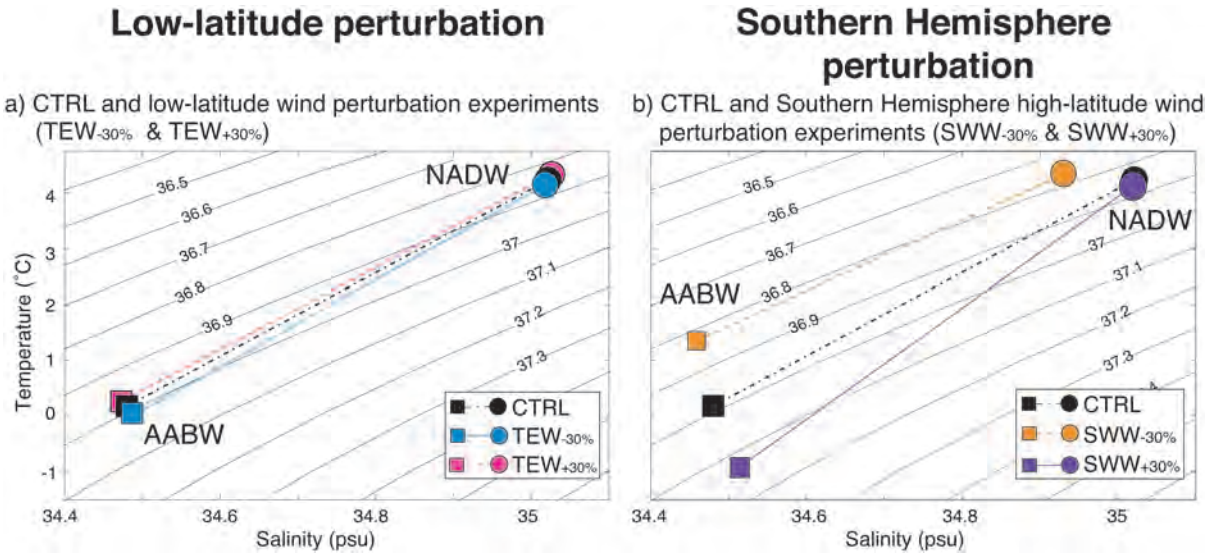

Figure IV.5: Temperature-Salinity diagram of AABW (squares) and NADW (circles) under unperturbed conditions (CTRL; black) compared to water masses in (a) low-latitude perturbation experiments ($TEW_{-30\%}$: blue; $TEW_{+30\%}$: pink) and (b) southern mid-latitude perturbation experiments ($SWW_{-30\%}$: orange; $SWW_{+30\%}$: purple). Contours mark water density to reference level of 2000 m (kg m^{-3} minus 1000).

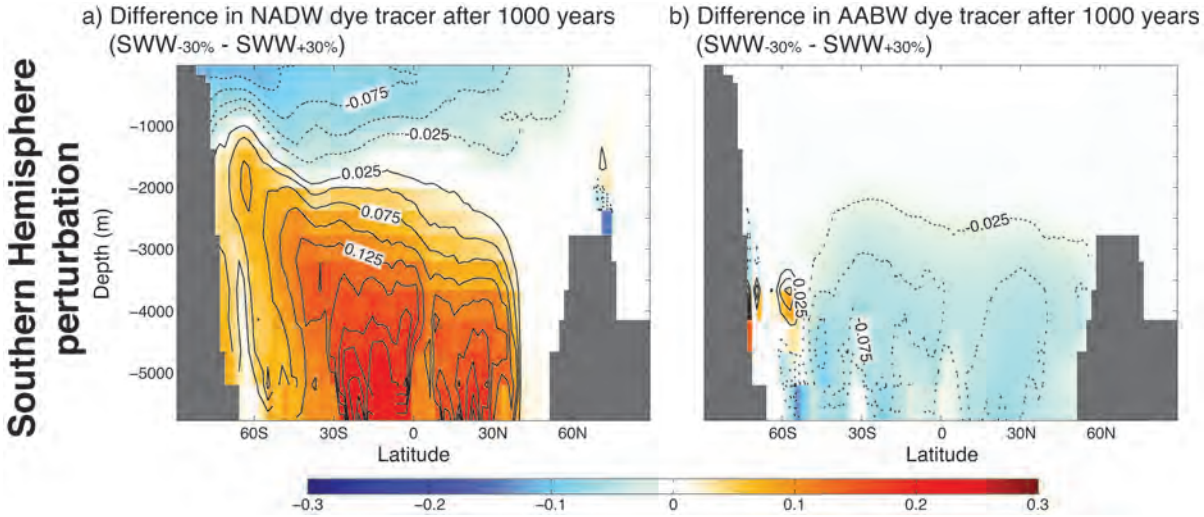

Figure IV.6: Difference in zonal mean dye concentration (dimensionless) between $SWW_{-30\%}$ and $SWW_{+30\%}$ for a dye release tracking (a) NADW and (b) AABW after 1000 years of dye release. Solid contours indicate higher dye concentrations under weaker SH wind stress ($SWW_{-30\%}$) than under stronger SH westerly conditions ($SWW_{+30\%}$) while dotted contours mark lower dye concentrations. Contour intervals are 0.025 starting at ± 0.025.

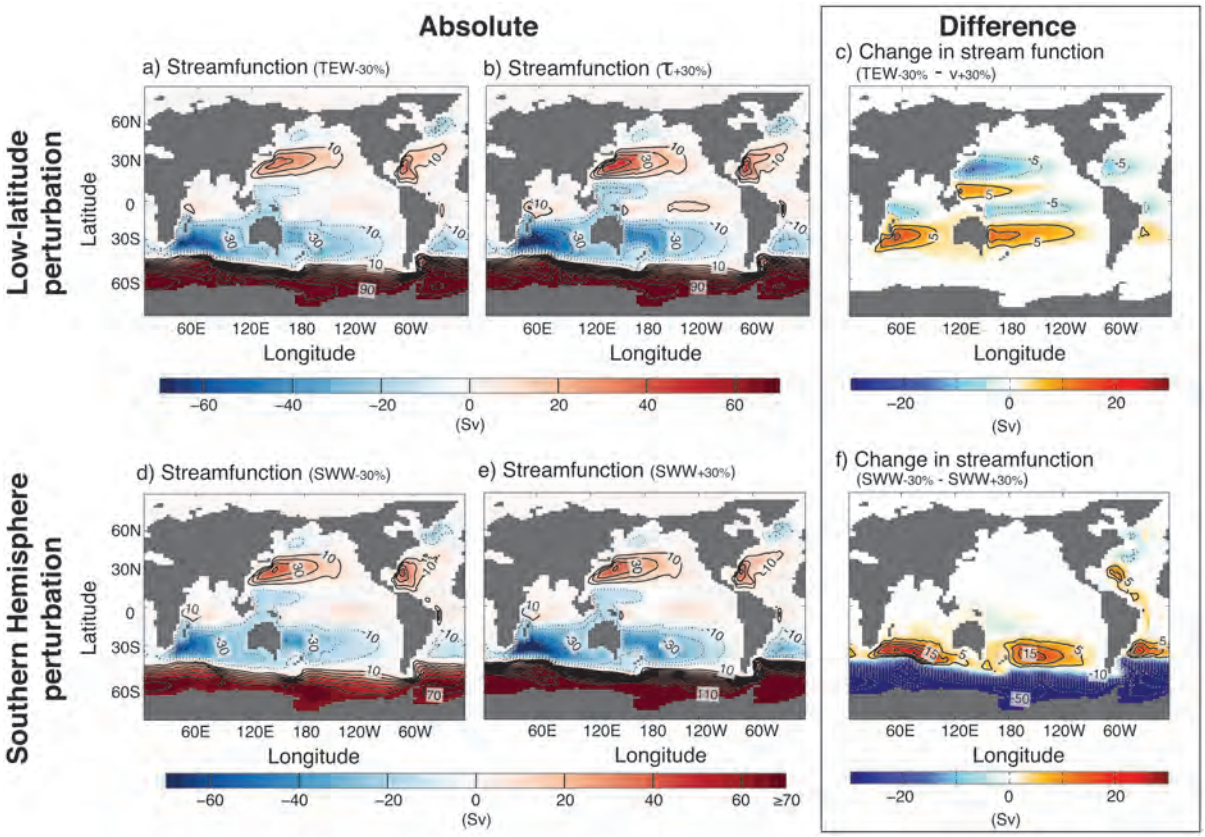

Figure IV.7: (a) Streamfunction (Sv) in experiment $\mathrm{TEW}_{-30\%}$. Contour intervals are 10 Sv starting at ±10 Sv; (b) as (a) but for experiment $\mathrm{TEW}_{+30\%}$. (c) Changes in the streamfunction (Sv) between low-latitude perturbation experiments ($\mathrm{TEW}_{-30\%}$ minus $\mathrm{TEW}_{+30\%}$). Contour intervals are 5 Sv starting at ±5 Sv. Solid lines indicate circulation changes with positive sign; dotted lines represent changes with negative sign. (d, e, f) as (a, b, c) only for $\mathrm{SWW}_{-30\%}$, $\mathrm{SWW}_{+30\%}$ and $\mathrm{SWW}_{-30\%}$ minus $\mathrm{SWW}_{+30\%}$, respectively.

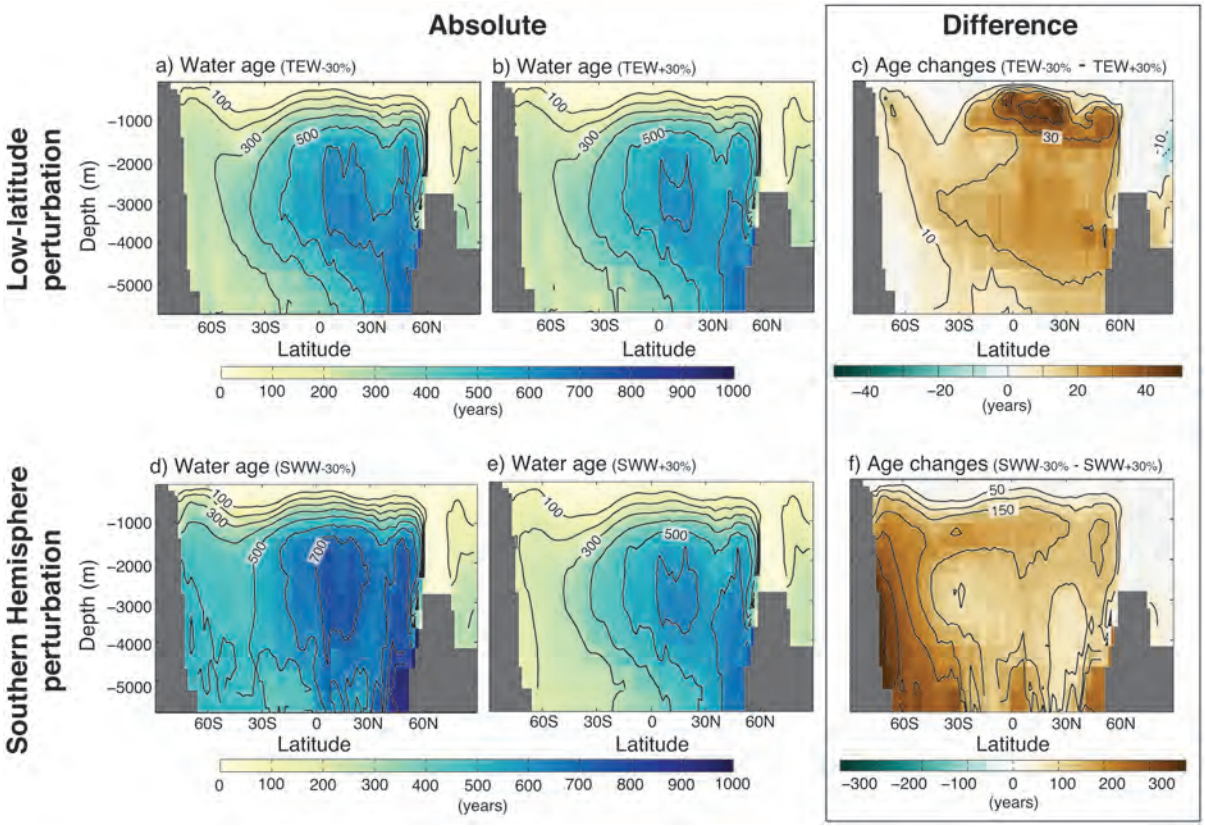

Figure IV.8: (a) Zonal mean water age (years) in experiment $\text{TEW}_{-30\%}$. Contour intervals are 100 years; (b) as (a) but for experiment $\text{TEW}_{+30\%}$. (c) Changes in zonal mean water age (years) between low-latitude perturbation experiments ($\text{TEW}_{-30\%}$ minus $\text{TEW}_{+30\%}$). Contour intervals are 10 years starting at ± 10 years. Solid lines indicate older waters in weaker wind case; dotted lines represent younger waters for weaker winds. (d, e) as (a, b) only for $\text{SWW}_{-30\%}$ and $\text{SWW}_{+30\%}$, respectively. (f) as (c) but for $\text{SWW}_{-30\%}$ minus $\text{SWW}_{+30\%}$ and contour intervals of 50 years starting at ± 50 years. Note the different colour axes between (c) and (f).

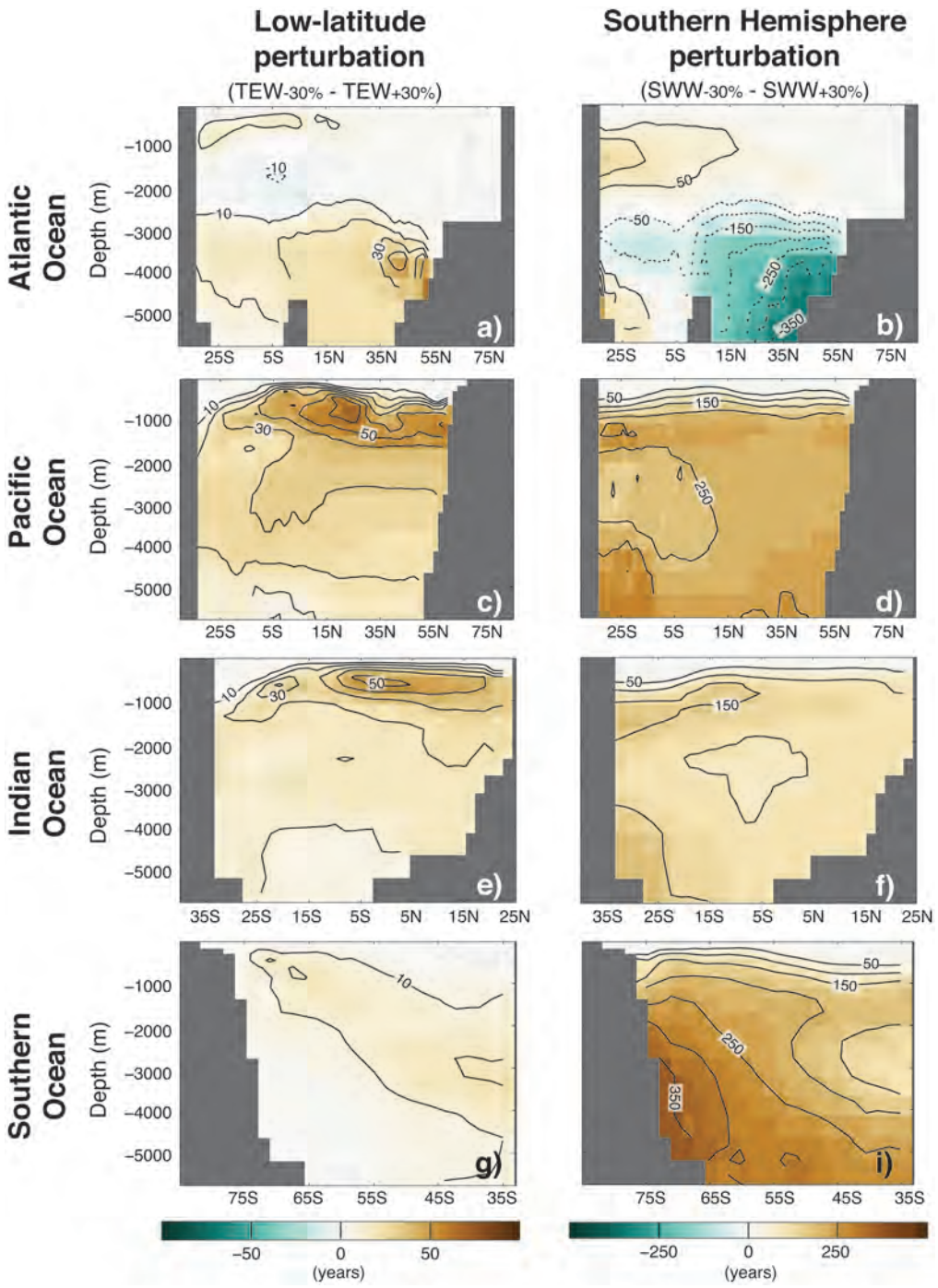

Figure IV.9: (a) Changes in Atlantic zonal mean water age between low-latitude experiments ($TEW_{-30\%}$ minus $TEW_{+30\%}$). Contour intervals are 10 years starting at ±10 years. Solid lines indicate older waters in weaker wind case, while dotted lines represent younger waters. (b) as (a) but for $SWW_{-30\%}$ minus $SWW_{+30\%}$. Contour intervals are 50 years starting at ±50 years. Note the different colour axes between both panels. (c, d), (e, f), (g, h) as (a,b) but for the Pacific, Indian and the Southern Ocean respectively.

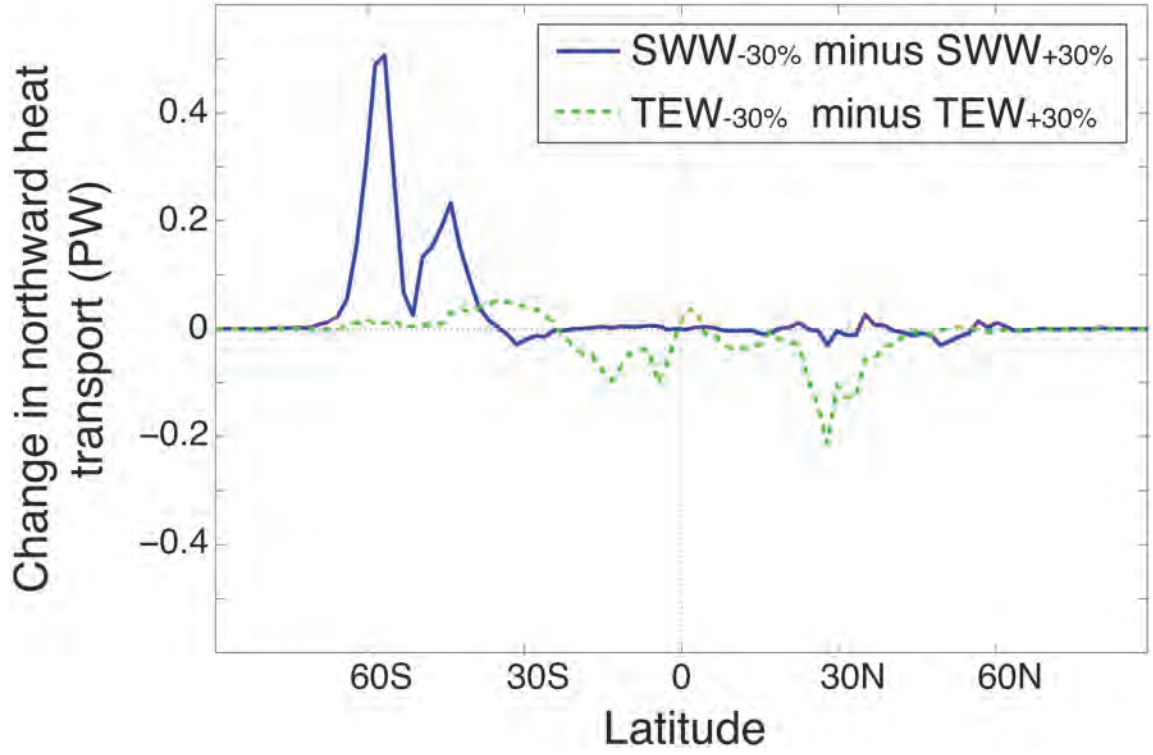

Figure IV.10: Difference in Northward Heat Transport (NHT) in PW between experiments with weak wind stress conditions compared to equivalent strong wind experiment ($SWW_{-30\%}$ minus $SWW_{+30\%}$: solid, purple line; $TEW_{-30\%}$ minus $TEW_{+30\%}$: dashed, green line).

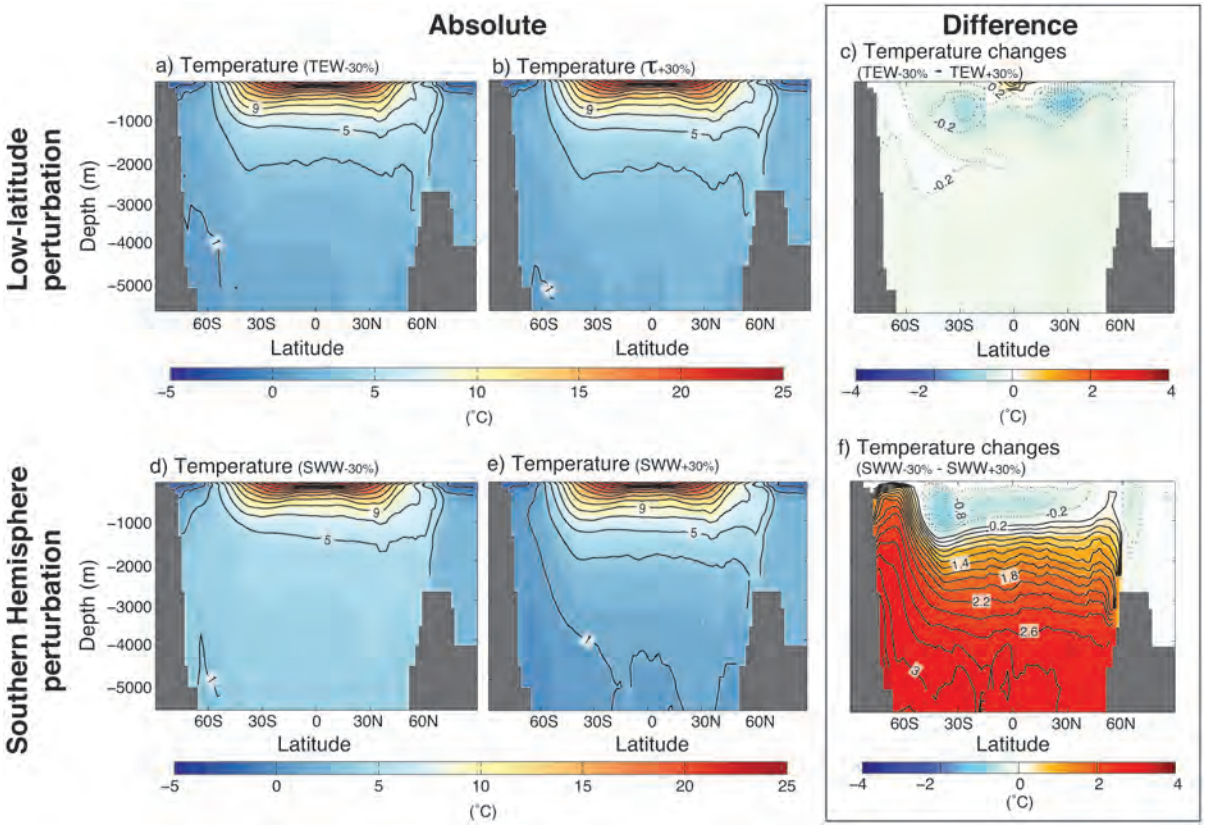

Figure IV.11: (a) Zonal mean temperature (°C) in experiment $\mathrm{TEW}_{-30\%}$. Contour intervals are 2°C; (b) as (a) but for experiment $\mathrm{TEW}_{+30\%}$. (c) Changes in zonal mean temperature (°C) between low-latitude perturbation experiments ($\mathrm{TEW}_{-30\%}$ minus $\mathrm{TEW}_{+30\%}$). Contour intervals are 0.2°C starting at ±0.2°C. Solid lines indicate a warming in the experiment with weaker wind conditions while dotted lines represent a cooling. (d, e, f) as (a, b, c) only for $\mathrm{SWW}_{-30\%}$, $\mathrm{SWW}_{+30\%}$ and $\mathrm{SWW}_{-30\%}$ minus $\mathrm{SWW}_{+30\%}$, respectively.

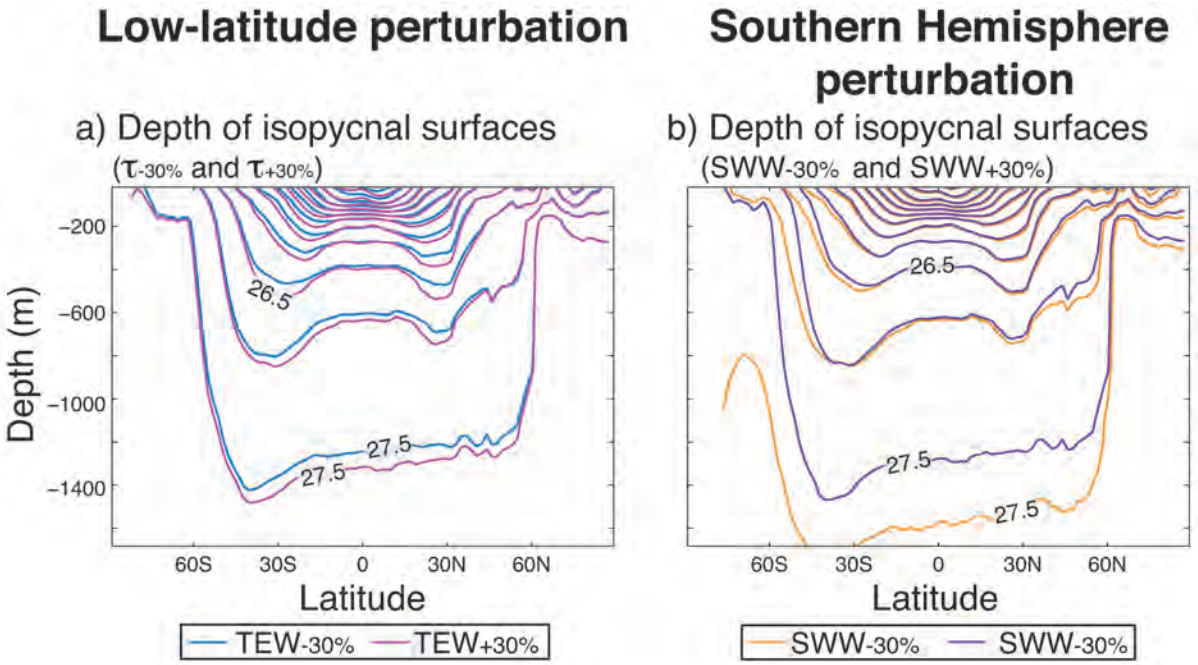

Figure IV.12: (a) Zonal mean depth of isopycnal surfaces in experiments with perturbed low-latitude wind stress ($TEW_{-30\%}$: blue; $TEW_{+30\%}$: pink). Contour intervals are 0.5 kg m^{-3}. (b) as (a) but for experiments $SWW_{-30\%}$ (orange) and $SWW_{+30\%}$ (purple).

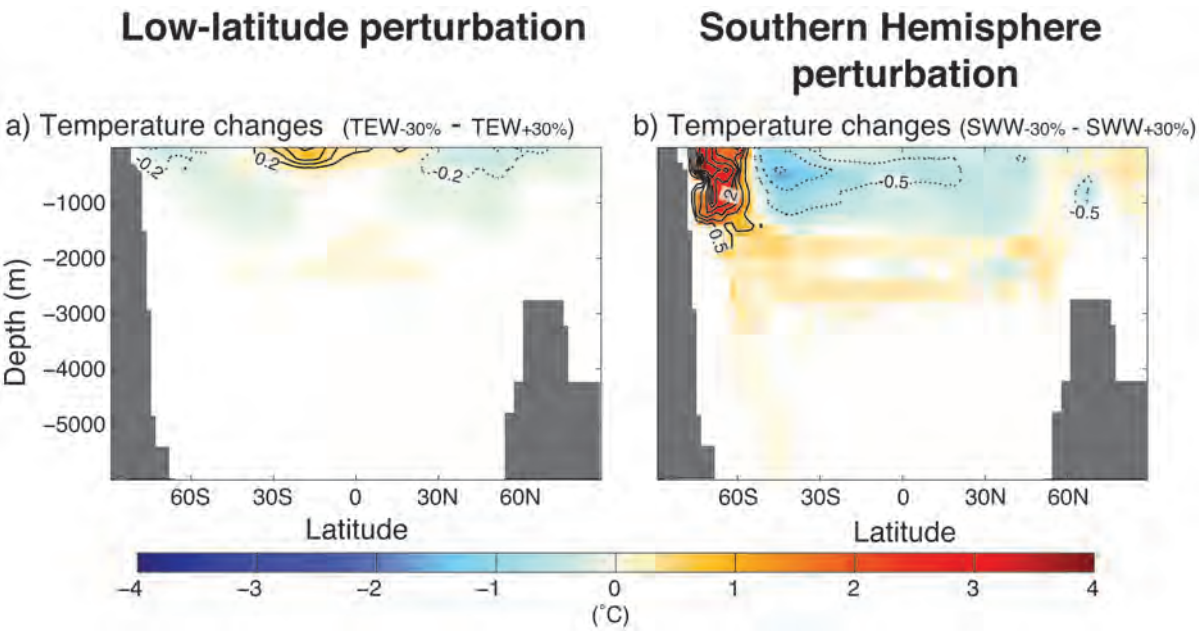

Figure IV.13: (a) Difference in zonal mean temperature (°C) between low-latitude perturbation experiments ($TEW_{-30\%}$ minus $TEW_{+30\%}$) with the effect of changes in isopycnal heave removed. Contour intervals are 0.2°C starting at ±0.2°C. (b) as (a) but for southern mid-latitude perturbation experiments ($SWW_{-30\%}$ minus $SWW_{+30\%}$). Contour intervals are 0.5°C starting at ±0.5°C.

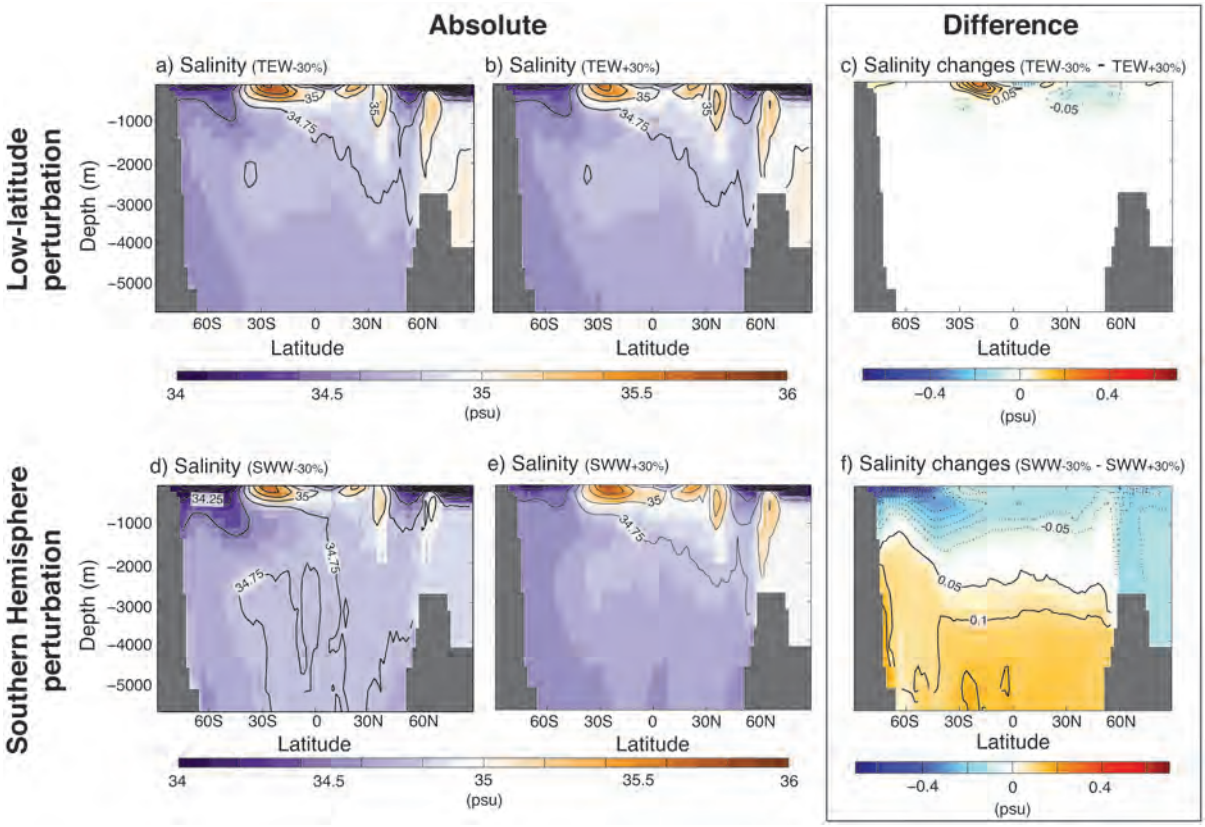

Figure IV.14: (a) Zonal mean salinity (psu) in experiment $\mathrm{TEW}_{-30\%}$. Contour intervals are 0.25 psu; (b) as (a) but for experiment $\mathrm{TEW}_{+30\%}$. (c) Changes in zonal mean salinity (psu) between low-latitude perturbation experiments ($\mathrm{TEW}_{-30\%}$ minus $\mathrm{TEW}_{+30\%}$). Contour intervals are 0.05 psu starting at ± 0.05 psu. Solid lines indicate increased salinity in the experiment with weaker wind conditions while dotted lines represent a decrease. (d, e, f) as (a, b, c) only for $\mathrm{SWW}_{-30\%}$, $\mathrm{SWW}_{+30\%}$ and $\mathrm{SWW}_{-30\%}$ minus $\mathrm{SWW}_{+30\%}$, respectively.

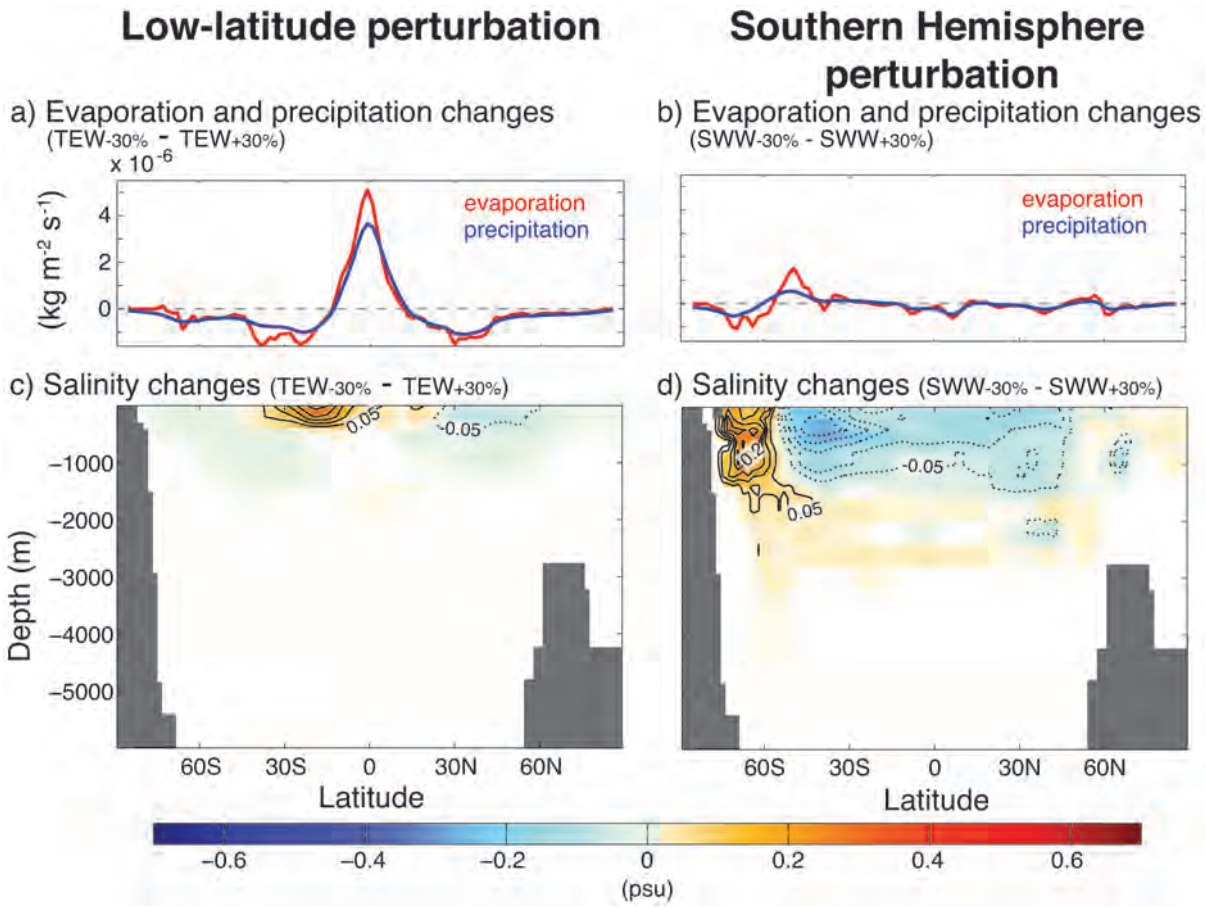

Figure IV.15: (a) Zonal mean change in evaopartion (kg m^{-2} s^{-1}; red) and precipitation (kg m^{-2} s^{-1}; blue) between low-latitude perturbation experiments ($TEW_{-30\%}$ and $TEW_{+30\%}$). (b) as (a) but for southern mid-latitude experiments ($SWW_{-30\%}$ minus $SWW_{+30\%}$). (c) Difference in zonal mean salinity (psu) between low-latitude perturbation experiments ($TEW_{-30\%}$ and $TEW_{+30\%}$) with the impact of changes in the isopycnal heave removed. Contour intervals are 0.05 psu starting at ±0.05 psu; (d) as (c) but for southern mid-latitude experiments ($SWW_{-30\%}$ minus $SWW_{+30\%}$).

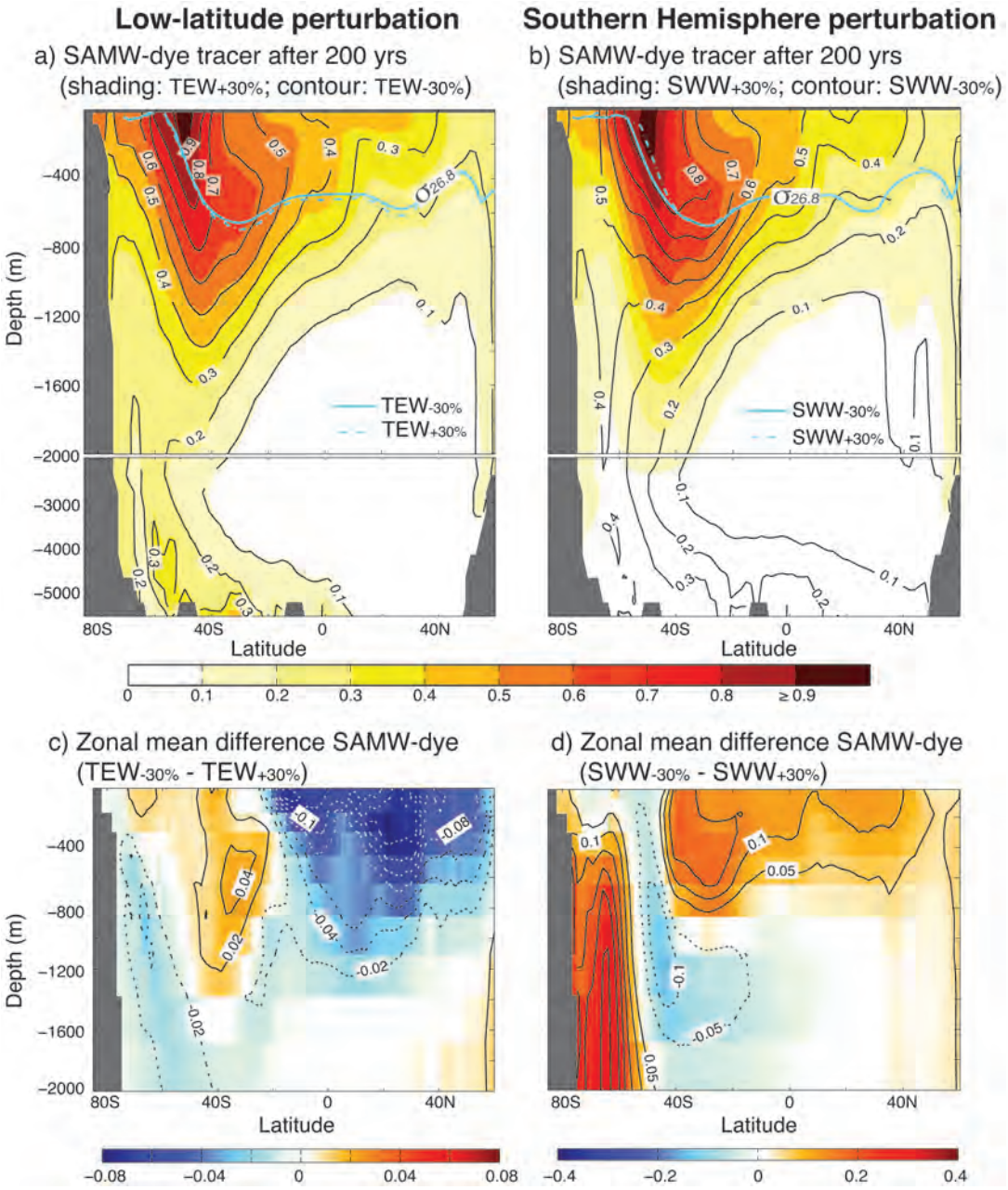

Figure IV.16: (a) Zonal mean dye tracer concentration (dimensionless) 200 years after the onset of the release at latitudes of SAMW formation under strengthened ($TEW_{+30\%}$; colour shading) and weakened low-latitude winds ($TEW_{-30\%}$; contours). Bold, cyan coloured contours indicate the zonal mean depth of the $\sigma_{26.8}$-isopycnal surface in both experiments, $TEW_{+30\%}$ (dash-dotted) and $TEW_{-30\%}$ (solid). (b) as (a) but for perturbed Southern Hemisphere westerly winds ($SWW_{+30\%}$: shading and dash-dotted contour; $SWW_{-30\%}$: solid black and blue contours). (c) Difference in zonal mean dye tracer concentration (dimensionless) in the upper 2000 m between low-latitude experiments ($TEW_{-30\%}$ minus $TEW_{+30\%}$). Contour intervals are 0.02 starting at ±0.02. Dotted contours indicate lower dye concentrations under weaker wind conditions, solid lines mark higher concentrations. (d) as (c) but for $SWW_{-30\%}$ minus $SWW_{+30\%}$ and contour intervals of 0.05 starting at ±0.05.

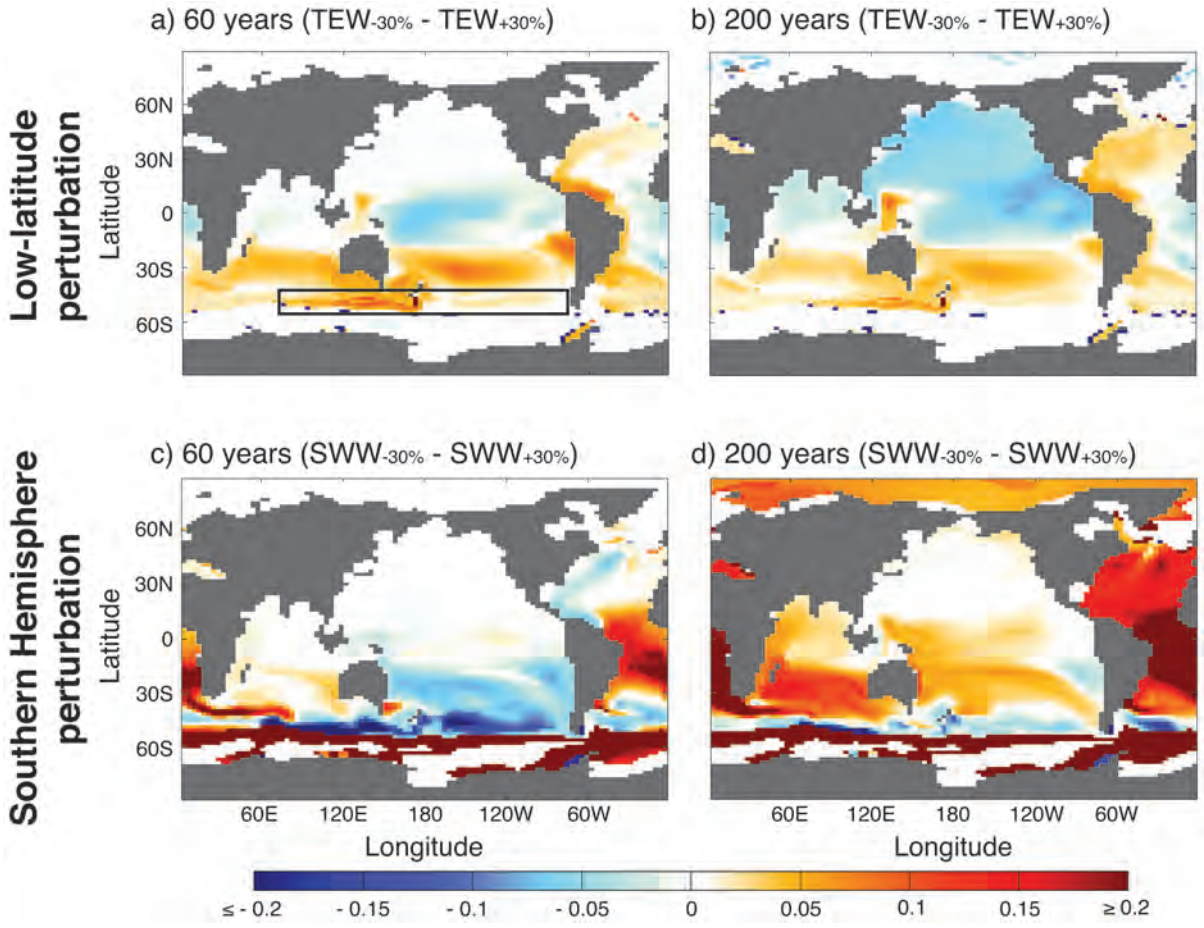

Figure IV.17: (a) Difference in dye tracer concentration (dimensionless) on $\sigma_{26.8}$-isopycnal between low-latitude wind stress perturbation experiments ($\mathrm{TEW}_{-30\%}$ minus $\mathrm{TEW}_{+30\%}$) after 60 years of dye release in the formation region of Subantarctic Mode Water (black box). (b) as (a) but after 200 years of dye release. (c, d) as (a, b) but for perturbations in Southern Hemisphere westerly winds ($\mathrm{SWW}_{-30\%}$ minus $\mathrm{SWW}_{+30\%}$).

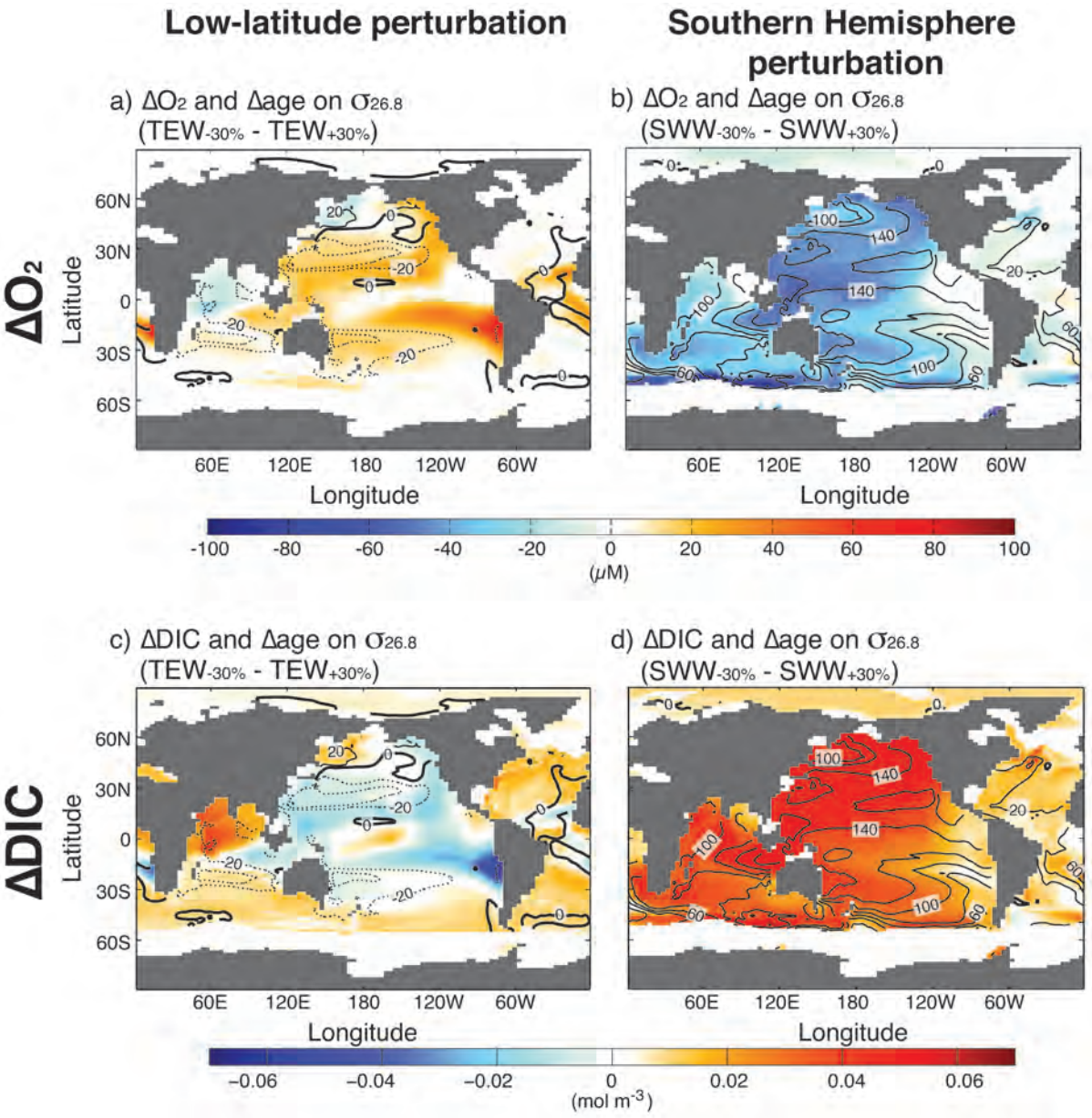

Figure IV.18: (a) Difference in O_2 concentration (μM; colour shading) on $\sigma_{26.8}$-isopycnal between experiments with weakened and strengthened wind stress at low-latitudes compared to age changes (years, contours) on the same isopycnal ($TEW_{-30\%}$ minus $TEW_{+30\%}$). Bold contour marks zero change in age. Solid contours indicate older waters in weaker wind case while dotted lines represent younger waters. Contour intervals are 20 years. (b) as (a) but for southern mid-latitude wind stress perturbations ($SWW_{-30\%}$ minus $SWW_{+30\%}$). (c, d) as (a, b) but for DIC concentration changes (mol m^{-3}, colour shading) versus age changes (years, contours).

Table IV.1: Total upwelling through 1000 m depth surface under unperturbed conditions (CTRL) as well as in experiments with wind perturbations in the tropical easterly ($TEW_{-30\%}$ and $TEW_{+30\%}$) and the southern mid-latitude westerly wind stress ($SWW_{-30\%}$ and $SWW_{+30\%}$).

	Upwelling through 1000m-surface		
	global	north of 30°S	between 10°S/N
CTRL	0.764	11.56	4.73
$TEW_{-30\%}$	0.759	11.55	4.65
$TEW_{+30\%}$	0.769	11.66	4.84
$SWW_{-30\%}$	0.690	5.71	5.11
$SWW_{+30\%}$	0.866	10.79	3.74

Table IV.2: Average surface air temperature south of 60°S (SH SAT; °C), ocean temperature in upper 1000 m south of 60°S (SH UOT; °C), strength of the Indonesian Throughflow (ITF; Sv) as well as of the Equatorial Undercurrent (EUC; integral of all easterly velocities at 170°W between 15°S-15°N and 50 - 600 m depth; Sv) in experiments with unperturbed conditions (CTRL), perturbed tropical easterly winds ($TEW_{-30\%}$ and $TEW_{+30\%}$) and pertubed southern mid-latitude westerlies ($SWW_{-30\%}$ and $SWW_{+30\%}$).

	SH SAT (°C)	SH UOT (°C)	ITF (Sv)	EUC (Sv)
CTRL	-15.0	1.44	16.3	16.5
$TEW_{-30\%}$	-15.1	1.36	15.1	9.1
$TEW_{+30\%}$	-14.8	1.51	17.5	23.6
$SWW_{-30\%}$	-15.3	2.25	15.0	16.2
$SWW_{+30\%}$	-15.0	0.77	16.7	16.5

Table IV.3: Volume and surface area of Southern Hemisphere (SH) sea-ice cover (10^6 km^3 and 10^6 km^2, respectively) in experiments with unperturbed conditions (CTRL), perturbed tropical easterly winds ($TEW_{-30\%}$ and $TEW_{+30\%}$) and pertubed southern mid-latitude westerlies ($SWW_{-30\%}$ and $SWW_{+30\%}$).

	SH ice volume (10^6 km^3)	sea-ice area (10^6 km^2)
CTRL	16.0	19.1
$TEW_{-30\%}$	16.6	19.3
$TEW_{+30\%}$	15.7	18.9
$SWW_{-30\%}$	19.8	20.5
$SWW_{+30\%}$	14.6	19.3

Table IV.4: Values for global maximum and global mean age (years) under unperturbed wind conditions (CTRL) and in model experiments with changed wind conditions in the tropics ($TEW_{-30\%}$ and $TEW_{+30\%}$) and at southern mid-latitudes ($SWW_{-30\%}$ and $SWW_{+30\%}$).

	age	
	maximum (years)	global mean (years)
CTRL	647.2	366.1
$TEW_{-30\%}$	659.2	374.9
$TEW_{+30\%}$	637.6	356.6
$SWW_{-30\%}$	856.0	483.9
$SWW_{+30\%}$	647.5	347.2

Table IV.5: Total content of oxygen (PgO_2) in the global, deep (below 1000 m) and abyssal (between 85°S and 55°N, below 3000 m) ocean under unperturbed wind conditions (CTRL) and in model experiments with changed wind conditions in the tropics ($TEW_{-30\%}$ and $TEW_{+30\%}$) and at southern mid-latitudes ($SWW_{-30\%}$ and $SWW_{+30\%}$).

	total ΔO_2		
	global (PgO_2)	deep (PgO_2)	abyssal (PgO_2)
CTRL	-	-	-
$TEW_{-30\%}$	191.4	153.41	34.9
$TEW_{+30\%}$	-155.8	-124.0	-32.3
$SWW_{-30\%}$	-1377.9	-1187.5	-492.2
$SWW_{+30\%}$	651.2	562.88	256.5

Table IV.6: As Table IV.5 but for DIC (PgC).

	total ΔDIC		
	global (PgC)	deep (PgC)	abyssal (PgC)
CTRL	-	-	-
$TEW_{-30\%}$	-0.6	-19.7	-3.4
$TEW_{+30\%}$	-26.2	-0.4	-3.6
$SWW_{-30\%}$	74.7	17.5	-47.0
$SWW_{+30\%}$	-110.4	-87.2	-26.4

Part V: Sensitivity of ocean oxygenation to diapycnal mixing in an ocean circulation model

Abstract

This study examines the sensitivity of ocean oxygenation to a suite of diapycnal background diffusivity (κ_v) parameterizations in a numerical ocean model. For this a series of model experiments is performed, in which the vertical diffusivity of the upper 1000 m of the ocean is represented by three different parameterization schemes, one of them across a variety of global mean strengths. The results of the different experiments suggest that those experiments with the lowest global mean vertical diffusivities lead to the highest global mean oxygen concentrations, despite showing an increase in ocean stratification and thus a decrease in ocean ventilation; vice versa experiments with high global mean vertical diffusivities show decreasing ocean stratification and reduced global mean oxygen concentrations. The cause of this counterintuitive behaviour lies in the dominance of the impact of changes in (i) thermocline thickness, which lead to alterations in temperature and thus oxygen solubility, and (ii) marine biology caused by an alteration in the nutrient supply to low-latitudes, and thus ultimately variations in the depletion of oxygen through respiration. These biological processes dominate over ocean ventilation changes in determining the ocean oxygen response to altered vertical diffusivity. In experiments with high global mean vertical diffusivities, a low equatorial value of vertical diffusivity dampens the effect of increased mixing strength and thus the higher supply of nutrients to the equatorial region from high-latitudes through a reduction in equatorial upwelling. The best agreement with observational values of oxygen and chlorophyll concentrations is yielded by the experiment with the lowest global mean diffusivity and reduced equatorial mixing.

V.1 Introduction

Ocean oxygenation plays a crucial role in the Earth system. Its influence on biogeochemical processes has a significant impact on marine ecosystems and the cycling of important oceanic tracers such as carbon and nitrogen. The distribution of oxygen (O_2) within the ocean is known to reflect the complex interplay of physics and marine biology. Considerable effort has been invested into the accurate description of this interplay within numerical ocean models and their biogeochemical counterparts. To allow reliable predictions for the future evolution of ocean oxygenation many numerical model studies

have assessed the sensitivity of dissolved oxygen concentrations to a variety of changing conditions, focusing especially on low oxygen regions and the biological control within those zones (e.g. Matear and Hirst, 2003; Frölicher et al., 2009a; Duteil and Oschlies, 2011; Ridder and England, under review). Here we focus on the sensitivity of ocean oxygenation to a choice of diapycnal diffusivity parameterizations, which differ in their global mean mixing strengths and zonal mean profile, in the upper 1000 m of an ocean general circulation model.

The transport of tracers across neutral density surfaces, i.e. diapycnal diffusivity, in the ocean's interior is partly due to nonlinear interactions within the background internal wave field (Gargett, 1984; Henyey et al., 1986). These processes are unresolved by ocean climate models and their effect is parameterized in the form of a background diffusivity, (κ_v), which is typically assumed to range from 10^{-5} to 10^{-4} m^2 s^{-1}. In ocean climate model applications, the background diffusivity is often chosen to have a globally uniform value, or to vary with depth with larger values in the deeper ocean where stratification is generally weaker. The efficiency of internal wave dissipation in generating dianeutral mixing has also been assumed to vary inversely with the vertical stability, as measured by the buoyancy frequency, N (Gargett, 1984; Dunne et al., 2013). Harrison and Hallberg (2008, hereafter HH) examined the sensitivity of a potential density coordinate ocean model to extremely weak levels of background mixing near the equator. This was suggested by observations and predictions (Henyey et al., 1986; Gregg et al., 2003) that for a statistically uniform background wave field, nonlinear wave-wave interactions are weakened intense near the equator. As a result less wave breaking occurs and leads to smaller diffusivities for smaller values of the Coriolis parameter reaching a minimum in the order of 10^{-6} m^2 s^{-1} comparable to molecular levels for heat at the equator. HH found in their model that applying this limit leads to a stronger equatorial pycnocline and overall cooling in low latitudes associated with the upward displacement of the thermocline compared to a globally uniform vertical diffusivity background of κ_v=2×10^{-5} m^2 s^{-1}. Further, upwelling temperatures were significantly colder along the Peruvian and Central American coasts, and warmer to the west of the Galapagos in their model, with changed equatorial κ_v=10^{-6} m^2 s^{-1} and mid-latitude κ_v=2×10^{-5} m^2 s^{-1}.

While the vertical transport through mixing processes is generally orders of magnitude smaller than the horizontal transport, i.e. lateral diffusivity which has been shown to significantly impact ocean oxygenation and the extent of low-oxygen zones (e.g. Gnanadesikan, 1999; Gnanadesikan et al., 2004, 2013), diapycnal diffusivity plays an important role in ocean dynamics and biogeochemical cycling. The impact of vertical diffusive transport on ocean oxygenation occurs via both its influence on ocean tracer transport and global nutrient fluxes. In particular its effect on ocean temperature and salinity, which determine (i) oxygen solubility and (ii) indirectly, through their influence on ocean circulation, the horizontal and vertical transport within the ocean, i.e. ocean ventilation and the distribution of high-oxygen waters. Vertical transport further affects the nutrient supply to the photic zone and thus biological activity. The distribution of Subantarctic Mode Water (SAMW) for instance, which has been identified as the major pathway for the resupply of high-latitude nutrients to the equatorial ocean (Toggweiler et al., 1991; Sarmiento et al., 2004), could be affected in various ways, including through an increase in stratification and thus modifications in gyre circulation distributing SAMW within the different ocean basins (Rodgers et al., 2003).

A first insights into the sensitivity of ocean oxygenation to global mean vertical mixing strength was provided by a previous model study based on the results of a model of intermediate complexity of relatively coarse resolution and representing marine biology using a simple NPZD-model (Duteil and Oschlies, 2011). With the applied model configuration, which is limited to globally uniform background diffusivities and omits potentially important small-scale processes due to the model's coarse resolution, Duteil and Oschlies (2011) found that increasing diffusivities lead to increased global ocean oxygenation due to increased ocean ventilation and vice versa, thus confirming the hypothesised impact of ocean stratification on ocean oxygenation.

This study builds on the approach of Duteil and Oschlies (2011) to assess the sensitivity of ocean oxygenation to vertical diffusivity changes. In contrast to previous studies the model configuration chosen here offers the critical scales to resolve important physical aspects of the global ocean. It further offers the exploration of different vertical diffusivity schemes additionally to the global mean diffusivity used by Duteil and Oschlies (2011).

Here we use vertical diffusivity schemes comparable to HH, adding a set of experiments to allow an assessment of the impact of variations in the amplitude of the vertical upper ocean background diffusivity. The additional experiments facilitate a comparison of the influence of high-latitude to low-latitude diffusivities on the modelled results. As an extension of the work of Harrison and Hallberg (2008), this paper additionally includes results from a marine biogeochemical model of intermediate complexity, which allows an assessment of the response of the biogeochemical component within the ocean to changed vertical background diffusivities. This delivers a more thorough analysis of the implications for the main processes determining dissolved oxygen concentrations.

Overall the findings of this study agree with those of HH in that they show overall reduced ocean temperatures for diffusivity schemes following the latitudinal dependence by Henyey et al. (1986). They further agree with the results in Duteil and Oschlies (2011) and show a decreased extent of low-oxygen waters for low vertical diffusivities. However, the results of the present study suggest that ocean oxygen concentrations increase for lowered background diffusivities despite an increase in ocean stratification in these experiments and vice versa for higher background diffusivities. This contradicts the findings of previous studies such as Matear and Hirst (2003) or Duteil and Oschlies (2011), who find higher O_2 for higher mixing and vice versa for lower mixing in their equilibrium experiments. We find that biological changes and temperature variations due to alterations in thermocline thickness dominate the impact of varying ocean stratification on ocean oxygenation and also that latitudinal variability of vertical diffusivity can have an important effect on these changes.

V.2 Method and experimental design

This study uses the Modular Ocean Model (MOM4p1) developed at the Geophysical Fluid Dynamics Laboratory (GFDL) as described in Griffies et al. (2009) and forces it with seven different vertical background diffusivity schemes for the top 1000 m of the model ocean (Figure V.1). The configuration used here is a Boussinesq z-coordinate model with a tripolar grid. It has a horizontal resolution of 1° with a meridional refinement to 1/3° around the equator. Depth levels are unevenly distributed with a higher

resolution in the upper 200 m (10 m). The model accounts for changes in oceanic tracer concentration through advection, horizontal and vertical mixing and a tracer specific source/sink term. The model assumes the vertical diffusive transport of ocean tracers is a function of density, thickness of the respective depth layer and a time constant vertical diffusivity coefficient (κ_v; Griffies et al., 2009).

The CTRL experiment in this study uses a setup similar to the ocean component in Dunne et al. (2012, 2013) and includes a diffusivity scheme with only a small equatorial reduction in surface background diffusivity (Figure V.1). The transition between a constant high-latitude value of κ_v= 1.5×10^{-5} m^2 s^{-1} to the slightly reduced low-latitude value of 10^{-5} m^2 s^{-1} takes place between latitudes of ∼40° and 30° in both hemispheres (Table V.1). The lateral transport of passive tracers via eddies is realised by introducing an isoneutral diffusion parameterization (Griffies et al., 1998) with a diffusion coefficient A_{redi} = 600 m^2 s^{-1}. Tidal mixing is represented using a vertical profile following Simmons et al. (2004).

The suite of additional experiments includes three background diffusivity schemes with lower global mean mixing (Figures V.1a, V.1b and V.1c; hereafter LLv, SL0.5v and SLv, respectively), one scheme with similar global mean mixing (Figure V.1d; hereafter SSv) and two experiments with higher global mean background mixing (Figures V.1e and V.1f; hereafter HLv and HH-, respectively). Experiment names are derived from the comparison of the diffusivity coefficients in the respective experiment to those in CTRL with the first letter referring to mid-latitude values and the second to equatorial diffusivities. "L" marks lower, "S" similar and "H" higher diffusivity coefficients than CTRL. The first five experiments (all labeled with "v" to represent their shape with reduced mixing towards the equator) follow the parameterization of background diffusivity developed in Henyey et al. (1986). They derive κ_v as a function of latitude with a prescribed equatorial value and a fixed value at 30°S/N (Table V.1). The diffusivity coefficient at other latitudes is then calculated as a function of latitude. Overall the transition between high-latitude and equatorial values in these experiments is more gradual than in CTRL. The last experiment, HH- (Figure V.1f), uses a globally constant upper ocean vertical background diffusivity of 2.5×10^{-5} m^2 s^{-1} and resembles parameterization schemes used in a variety of global ocean models.

All experiments start from the same initial conditions (with nutrient distributions from Levitus et al., 1993), and evolve over 100 years of integration. Oxygen concentration differences in an equilibrated state are extrapolated from the evolution of O_2 differences in the first 100 years assuming a constant curvature of the convergence towards equilibrium. Apart from the different vertical background diffusivities all experiments are identical and use CORE normal year forcing (Large and Yeager, 2009).

The ocean model is coupled to a biogeochemistry model of intermediate complexity (Tracers of Ocean Phytoplankton with Allometric Zooplankton version 2; TOPAZ2, Dunne et al., 2013), which represents 30 tracers including three classes of phytoplankton (Dunne et al., 2005; Dunne et al., 2013). The biology model includes a variety of tracers and processes, such as the cycling of carbon and oxygen, as well as N_2 fixation, gas exchange and denitrification in the water column and sediments. It further uses co-limitation for phytoplankton by light, nitrogen, phosphorus and iron and accounts for runoff of O_2, C, N, Fe, alkalinity and lithogenic material and burial of calcium carbonate ($CaCO_3$) in sediments. In a model configuration following Dunne et al. (2012, 2013) modelled oxygen concentrations slightly underestimate observed global mean oxygen values of 174.2 μM to 177.9 μM (Bianchi et al., 2012) by roughly 10 μM and overestimates the volume of suboxic regions within the ocean (Table V.2). Nevertheless, the model configuration has been shown to reproduce observed ocean tracer fields as well as ocean circulation reasonably well and are considered a reliable tool for the assessment of oceanic processes (Dunne et al., 2013).

V.3 Results

V.3.1 Changes in ocean circulation

The density changes induced by the mixing-driven modifications in temperature and salinity alter ocean stratification in the upper ocean and thus the density-driven circulation. A decrease in the global mean diffusivity coefficient increases the density gradient in the upper ocean (Figure V.2a) and leads to an overall reduction in ocean ventilation (Figure V.2c). Increasing global mean background diffusivity has the opposite effect of decreasing ocean stratification (Figure V.2a) and enhancing ocean ventilation (Figure

V.2c). The response in ocean stratification in experiment HLv, which is less stratified than the ocean in experiment HH- but has a lower global mean vertical mixing than HH- (Figures V.1e and V.1f), suggests that high-latitude mixing coefficients are of higher importance for the determination of upper ocean stratification than the overall global mean value (compare Figures V.2a and V.2c).

The changes in equatorial ocean stratification in the different model experiments changes the amount of energy that is needed to vertically displace a water parcel against the density background within the upper ocean of the respective experiment. As a result, increased stratification due to decreased equatorial vertical diffusivity requires more energy to upwell dense intermediate water at the equator and subduct light surface water at mid- to low-latitudes. Decreased stratification requires less energy. Since the prevailing equatorial easterlies between all experiments remain unchanged the energy provided by the momentum exchange between atmosphere and ocean is equal in all experiments. Thus the shallow equatorial overturning cells weaken for decreased low-latitude vertical diffusivities and increased surface stratification (Figure V.3). Experiment HH-, where a higher equatorial diapycnal diffusivity coefficient reduces low-latitude stratification compared to CTRL, shows the opposite response of strengthened shallow overturning in the equatorial ocean since less energy is needed to displace water parcels in a more weakly stratified density field (Figures V.2, V.3 and Table V.3).

At high latitudes, the reduction in ocean stratification due to increased vertical mixing in this region has important implications for the formation of North Atlantic Deep Water (NADW). Here stronger mixing decreases the density gradient between the surface ocean and layers below by increasing the vertical exchange of salinity between these layers. As a result, high-latitude surface waters are lighter than in CTRL causing a reduction in the formation of NADW and therefore in the strength of the Atlantic Meridional Overturning Circulation (AMOC) in experiments with increased vertical diffusivity coefficients at high latitudes (Figures V.3 and V.4a). Reduced high-latitude mixing, which is only realised in experiment LLv, increase the salinity of the surface ocean through the reduction in the vertical diffusive transport of salt. This strengthens and, in combination with its stronger pycnocline caused by increased equatorial stratification, deepens the

NADW cell (Figures V.3a and V.4a). Low equatorial vertical diffusivity thus increases the ventilation of the deep Atlantic Ocean (Figure V.5c) and counteracts the effect on water age set by the reduction in ocean overturning and in the formation of intermediate and mode waters, in particular Pacific intermediate water (PIW), Antarctic Intermediate water (AAIW) and Subantarctic Mode Water (SAMW; Figures V.5 and V.6). Thus the deep Atlantic Ocean in experiment LLv contains slightly younger waters than CTRL and the other experiments, while the reduction of AAIW, SAMW and PIW formation increases water age at high latitudes in all experiments with lower global mean vertical background diffusivities than CTRL (Figure V.5d). The abyssal cell shows a similar response as the NADW cell, i.e. the abyssal overturning decreases for a weaker NADW cell and vice versa increases for a stronger NADW cell (Figure V.4b), due to equivalent processes at southern high-latitudes.

The response of SAMW to changes in the diapycnal background diffusivity is of particular interest for the analysis of the sensitivity of ocean oxygenation to the applied vertical mixing parameterization schemes as it has been identified as a major supply pathway of nutrients and oxygen to the equatorial oceans (Toggweiler et al., 1991; Sarmiento et al., 2004). SAMW originates in the Southern Ocean, where deep, nutrient-rich waters are upwelled to the surface ocean and low sea surface temperatures in combination with shallow isopycnal depths facilitate the uptake of oxygen from the atmosphere. The mean depth of SAMW can be approximated by the depth of the $\sigma_{26.85}$-isopycnal and lies within the lower pycnocline. The transport within the SAMW is affected by the response of (i) the mixed layer depth (MLD) in the formation region of the water mass (Figure V.7 and Table V.4) and (ii) isopycnal heave, which alters the volume of SAMW, to the changed diapycnal background diffusivity schemes (Figure V.8). Stratification changes in the south-east Indian and south-east Pacific sectors of the Southern Ocean, driven by the applied variations in vertical mixing, alter the extent of regions with MLDs sufficient to ventilate SAMW and thus impact the amount of oxygen transported within the SAMW layer (500 m - 1000 m depth). For lower global mean diffusivities this region shrinks thus leading to lower oxygen concentrations in SAMW for an unchanged air-sea oxygen flux (vice versa for higher global mean mixing; Figure V.7). Furthermore, the isopycnal squeeze caused by the increase in ocean stratification due to weaker global vertical mixing

reduces the depth and thickness of the $\sigma_{26.85}$-isopycnal (Figure V.7) and thus decreases the volume that is transported within this water mass (Figure V.8). As a result the amount of oxygen that is transported into the Pacific Ocean across 50°S between 110°W-75°W within the pycnocline, is reduced by roughly 34% from approximately 1.12×10^8 Tg O_2 yr^{-1} in CTRL to 0.74×10^8 Tg O_2 yr^{-1} in the experiment with the lowest global mean κ_v (LLv). The same mechanisms but of the opposite sign increase the transport by 7% and 38% from 1.12×10^8 Tg O_2 yr^{-1} in CTRL to 1.20×10^8 Tg O_2 yr^{-1} and 1.54×10^8 Tg O_2 yr^{-1} in the two experiments with the highest global mean background diffusivities (HLv and HH-), respectively.

V.3.2 Changes in interbasin transport

The infusion of SAMW into the ocean interior, its distribution over the ocean basins, and with this the distribution of nutrient- and oxygen-rich water, is impacted by changes in the horizontal interbasin current systems in addition to changes in the global overturning circulation. Of particular interest is the gyre circulation, which has been shown to impact the path of SAMW (Rodgers et al., 2003) and thus contributes to the determination of the supply of oxygen- and nutrient-rich waters to the equatorial ocean. While the subtropical gyres are mainly driven by surface wind stress at the atmosphere-ocean interface, they respond to changes in the density gradient between high- and low-latitudes as well as between eastern and western boundaries caused by the different vertical mixing backgrounds (Figure V.9). Modest changes can be found in the strength of the North and the South Pacific subtropical gyres and lead to variations in the ventilation of the eastern boundary of the Pacific Ocean leaving the equatorial and eastern Pacific in both hemispheres with older waters for decreased global mean vertical mixing and more rapidly ventilated waters for stronger global mean mixing (Figure V.10).

The transport from the equatorial western to eastern boundary in the Pacific Ocean, which is mainly realised through the Equatorial Undercurrent (EUC), is likewise affected by the mixing-driven density changes. For decreased equatorial vertical diffusivity the west-east gradient of ocean density within the upper 500 m increases. Since the energy input to the surface ocean does not compensate for the change in the east-west density gradient, the EUC, which is one of the supply pathways to the oxygen minimum zones

(OMZs) in the East Pacific (Stramma et al., 2010), weakens. As a result the integrated transport through the 170°W zonal surface between 3°S - 3°N and 50 m - 350 m depth is reduced in experiments with weaker global mean diapycnal mixing and increases for stronger vertical mixing (Table V.3). This change in lateral transport contributes to the variations in ocean ventilation and water age (Figure V.2c) set by the aforementioned changes in equatorial upwelling due to variations in the shallow overturning cells spanning the equatorial thermocline (Figure V.3), and in the formation rate of intermediate and mode waters.

V.3.3 Response of global oxygen concentrations

Starting from the same initial conditions the global mean oxygen concentrations in all experiments diverge linearly from the CTRL state (Figure V.11). They generally show a negative relationship to global mean vertical background diffusivity, i.e. global mean O_2 increases for low global mean vertical mixing despite a reduction in ocean ventilation and vice versa O_2 decreases for higher mixing and more rapid ventilation (Figure V.11). Therefore, experiments with lower global mean diffusivities than CTRL, i.e. LLv, SL0.5v and SLv, show global mean oxygen concentrations of up to 2.5 μM (LLv) closer to the observed range of 174.2 to 177.9 μM (Bianchi et al., 2012) than CTRL with a bias of roughly 10μM. The same relation is generally true for the three- and two-dimensional representation of oxygen concentrations with experiment LLv showing the lowest standard deviation and bias in all data sets (Table V.5). Experiment HH- shows the highest bias and lowest correlation to observations.

To determine the main drivers of the response of oxygen concentrations to changes in the vertical mixing background, the influence of variations in oxygen saturation concentration (O_2^{sat}) on global ocean oxygenation has to be separated from the influence of changes in ocean transport and marine biology, i.e. the apparent oxygen utilization (AOU; Figure V.12). In the surface ocean, down to roughly 100 m, O_2^{sat} and AOU variations contribute equally to alterations in O_2, with the exception of experiment HLv where saturation changes dominate the response (Figures V.12c and V.12d). At this depth oxygen saturation is mainly affected by temperature changes caused by (i) the different exchange of heat and salinity between neighbouring ocean layers and (ii) modifications in the depth

and thus thickness of the thermocline driven by the stratification changes in the different experiments (Table V.3). At depths below ∼100 m down to intermediate depths (∼1000 m) the circulation changes described above dominate the response in AOU to the different vertical mixing parameterizations and lead to decreased oxygen concentrations for low global mean diapycnal mixing and increased O_2 for stronger vertical mixing (Figures V.10 and V.12d). At shallower depths and below this region, the response of ocean ventilation in the different experiments, which mostly lead to oxygen and age changes of the same sign, indicates that alterations in marine biology contribute significantly to variations of AOU and are thus discussed in detail below.

V.3.4 Changes in biology

The changes in ocean circulation resulting from mixing-driven temperature and salinity changes described above ultimately lead to changes in the supply of nutrients to the photic zone and thus biological activity. This is especially obvious in regions of strong upwelling, such as the equatorial ocean and the eastern boundary upwelling regions and is mainly driven by the impact of local diffusivities (i.e. the diffusivity in the respective latitude band) on regional stratification and isopycnal slope rather than by the global mean value (Figure V.12c; compare Figures V.13b to V.13c). As discussed in Sections V.3.1 and V.3.2, experiments using low equatorial diapycnal diffusivities show increased ocean stratification in the surface ocean at low latitudes. These stratification changes reduce the isopycnal slope towards the eastern boundary and thus weaken the upwelling of nutrient-rich water around the Equator. This contributes to the equatorial upwelling changes caused by variations in the shallow overturning cells (vice versa for higher vertical mixing in experiment HH-, Figures V.3, V.14a, V.14c and V.14e). The reduction in the nutrient supply due to variations in ocean upwelling is amplified by the lower nutrient content of the upwelled water caused by changes in the resupply of nutrients from southern high-latitudes via SAMW. Consequently biological productivity in the equatorial oceans decreases for reduced equatorial vertical mixing and vice versa increases for stronger vertical mixing. This is reflected in the response of the chlorophyll concentrations at the surface of these regions in the different experiments, with lower chlorophyll concentrations for reduced equatorial diapycnal diffusivities and vice versa higher concentrations for stronger equatorial vertical mixing (Figure V.13). These variations in

biological activity alter the production of organic matter, which is exported to greater depths and thus impacts the rate of remineralization, i.e. the dissipation of oxygen, leading to higher O_2 and reduced dissolved inorganic carbon (DIC) concentrations in shallow model layers and at depths for lower vertical mixing and vice versa to reduced O_2 and higher DIC in experiment HH- with stronger equatorial vertical mixing (Figure V.15). In experiment HLv the increase in SAMW transport completely offsets the effect of the applied reduction in the equatorial vertical background diffusivity. In this experiment SAMW supplies more nutrients and oxygen to the equatorial region compensating for the reduced nutrient supply via equatorial upwelling. As a result biological activity remains virtually unchanged compared to CTRL and DIC and O_2 concentrations at 75 m and 2500 m depth experience only small to insignificant changes in the equatorial Pacific (Figures V.13b and V.15b).

Along the eastern boundary upwelling zones at mid- to high latitudes (outside of 20°S to 20°N) decreased local vertical diffusivity has the opposite effect. Here lower equatorial diapycnal diffusivity steepens isopycnals allowing more nutrient-rich waters to reach the surface (Figure V.14b and V.14d). As a result biological activity at the surface and the dissipation of oxygen through remineralization at depths below ∼2000 experience a modest increase (Figure V.13a and V.15a). The same mechanisms but of the opposite sign are at play for increased low-latitude vertical diffusivity coefficients, leading to a decrease in O_2 concentrations in the surface and at depths (Figures V.14c and V.14f).

The impact of changed ocean transport and marine biology on ocean oxygen concentrations is also visible on isopycnal surfaces within the pycnocline. While upper pycnocline levels in the range from $\sigma_{25.5}$ to $\sigma_{26.25}$ reflect the changes in ocean biology, i.e. reduced NPP and thus remineralization, with increasing oxygen concentrations in regions with lower surface chlorophyll concentrations for decreased vertical diffusivities, deeper layers ($\sigma_{26.5}$ - $\sigma_{27.0}$) highlight the changes in the supply of oxygen through the inflow of SAMW with a decrease in O_2 off the southern tip of South America (Figure V.16; vice versa for increased κ_v, Figure V.17).

In summary, the influence of variations in vertical background diffusivity strength on

biological activity tends to counteract the impact of ventilation changes in the surface and the deep ocean. Changes in O_2 at depth between 100 m to 1000 m are dominated by variations in ocean circulation reversing changes in oxygen concentrations set by changes in oxygen utilization. In the surface ocean and at depth below 2000 m at low-latitudes, especially at the eastern boundary of the Pacific and the Atlantic Ocean, the effect of changed biological consumption of oxygen outweighs the influence of altered ventilation, with increased O_2 concentrations in experiments with reduced global mean vertical diffusivity and vice versa decreased O_2 for higher global mean diapycnal mixing coefficients. Overall this generally leads to a better agreement between experiments applying low equatorial mixing and observations in regards to zonal mean oxygen concentrations and surface chlorophyll concentrations (Figure V.18).

V.3.5 Response of the suboxic volume

The described impact of changed lateral transport and marine biology on dissolved O_2 concentrations discussed above also affect low-oxygen regions within the ocean model. While the modelled low-oxygen volumes remain overestimated under all parameterization schemes (Figures V.19 and Table V.2) the model bias is slightly reduced for experiments with reduced equatorial vertical mixing compared to CTRL. The main drivers behind this response in the low-oxygen volume are (i) changes in the O_2 concentrations in the waters of the EUC leading to variations in the integrated rate of oxygen transported through 170°W between 3°S - 3°N and 50 m - 350 m depth from 8.11×10^7 Tg O_2 yr^{-1} in the experiment with the highest global mean vertical diffusivity (HH-) to 8.47×10^7 Tg O_2 yr^{-1} in the lowest κ_v experiment (LLv; 8.32×10^7 Tg O_2 yr^{-1} in CTRL), and (ii) changes in biological activity due to variations in the equatorial upwelling of nutrient-rich waters (higher for stronger vertical mixing and vice versa weaker for lower vertical diffusivity coefficients).

V.3.6 Influence of changes in equatorial vertical diffusivity compared to changes in the global mean value

While the main response in modelled global mean O_2 concentrations is set by the global mean value of diapycnal diffusivity, weak vertical mixing at low latitudes acts to dampen

this response (compare Figures V.20a and V.20b). For example, experiment HLv shows little variation in global mean O_2 compared to CTRL despite having a largely increased global mean background diffusivity (Figure V.20b). This counterintuitive behaviour is caused by the two competing effects of: (i) the increased supply of nutrients and O_2 through SAMW due to strong high-latitude mixing and (ii) the weakened equatorial upwelling of nutrients caused by weak low-latitude mixing and its impact on ocean stratification. Thus the changes in low-latitude vertical diffusivities dampen the increase in biological activity, which the model would experience if the nutrient supply were controlled by changes at high-latitudes alone, i.e. SAMW formation, ocean ventilation and transport (compare Figures V.10b with V.10c, V.13b with V.13c, and V.15b with V.15c).

The impact of low-latitude vertical mixing strengths on low-oxygen volumes is similar to its impact on global mean oxygen concentrations. While the modelled hypoxic and suboxic volumes shrink for lower global mean κ_v and vice versa expand for higher mixing, the equatorial strength of vertical mixing dampens this effect due to its impact on respirational oxygen depletion (Figures V.20c and V.20d) and EUC transport of O_2.

V.4 Summary and Conclusions

This study shows an inverse relationship between oxygen concentration and the strength of the background vertical diffusivity in the upper 1000 m of a global ocean model, with higher oxygen concentrations for low global mean diffusivities and vice versa for high diffusivities. This is contrary to the notion that ocean oxygenation would increase for higher ocean stratification, and vice versa decrease for reduced stratification. We identify temperature-driven changes in oxygen solubility within the model's thermocline, due to thermocline thickness changes, and variations in marine biology as the driving mechanisms behind this counterintuitive response, which act to offset the impact of ocean stratification and ventilation changes. The direct impact of vertical diffusivity on ocean oxygenation through temperature and salinity changes alters modelled oxygen saturation concentrations due to modifications in ocean stratification and thus variations in thermocline thickness. The changes in biology are driven by variations in the nutrient supply to the equatorial ocean, which result mainly form the impact of high-latitude diffusivity changes on SAMW formation and transport and the effect of low latitude diffusivities on

equatorial and eastern boundary upwelling. These variations in nutrient supply influence biological activity in the model and thus determine the consumption of oxygen through respiration at depths.

This work extends on a previous study of the influence of spatially varying vertical diffusivity by Harrison and Hallberg (2008) from modelled ocean temperature and salinity to include biogeochemical processes. The assessment of the response of OMZs to the different diffusivity scenarios confirms the finding in Duteil and Oschlies (2011) of decreased low-oxygen volumes for lower global mean diffusivities. However, with their comparably coarse resolution model configuration, Duteil and Oschlies (2011) show that on the global scale the increased oxygen consumption due to a higher biological activity in experiments with higher vertical diffusivity is completely compensated for by the increase in ocean vertical mixing. The present study does not agree with this result. Instead our model suggests that biology and thermocline thickness changes dominate the response of the modelled oxygen concentration to different vertical mixing values.

Furthermore, the presented results indicate that the performance of the coupled ocean-biogeochemistry model used in this study, which already performs reasonably well for global mean values of dissolved oxygen, could be further improved by the application of reduced equatorial background diffusivities with values of the order of 10^{-6} m^2 s^{-1}. Model performance in regards to low-oxygen regions, as well as the spatial distribution of dissolved oxygen, only show modest improvements in response to the different diapycnal diffusivity schemes. To overcome the model biases in this regard, the higher sensitivity of ocean oxygenation to lateral diffusivity schemes as described in, e.g. Gnanadesikan et al. (2013), could be used to determine the optimal parameterization of horizontal and vertical diffusivity parameterization schemes with regard to the representation of dissolved oxygen. Such a sensitivity assessment is left to future studies.

In conclusion, the present study shows that different surface background diffusivity parameterizations in the upper ocean have a significant impact on ocean oxygenation in a numerical 1-degree ocean model. They thus have the potential to influence predictions of the modelled climate state in regards to ocean oxygenation and the extent of low-oxygen

volumes. Furthermore, our results suggest that increased stratification due to changed background vertical mixing in isolation of other perturbations does not decrease ocean oxygenation, as has been widely assumed. Instead, lower background mixing, and with this stronger ocean stratification, increases oxygen concentrations despite a significant decrease in ocean ventilation (and vice versa for higher background mixing). This suggests that temperature-driven changes in oxygen saturation due to variations in thermocline thickness and biogeochemical processes balance the lower rate of ocean ventilation and might play an important role in the future evolution of oceanic oxygen concentrations. We further argue for the implementation of a variation of the low equatorial-diffusivity following the parameterization of reduced equatorial mixing suggested by Henyey et al. (1986) and used in Harrison and Hallberg (2008) with lower diffusivities than those currently used in global ocean biogeochemical models.

V.5 Figures

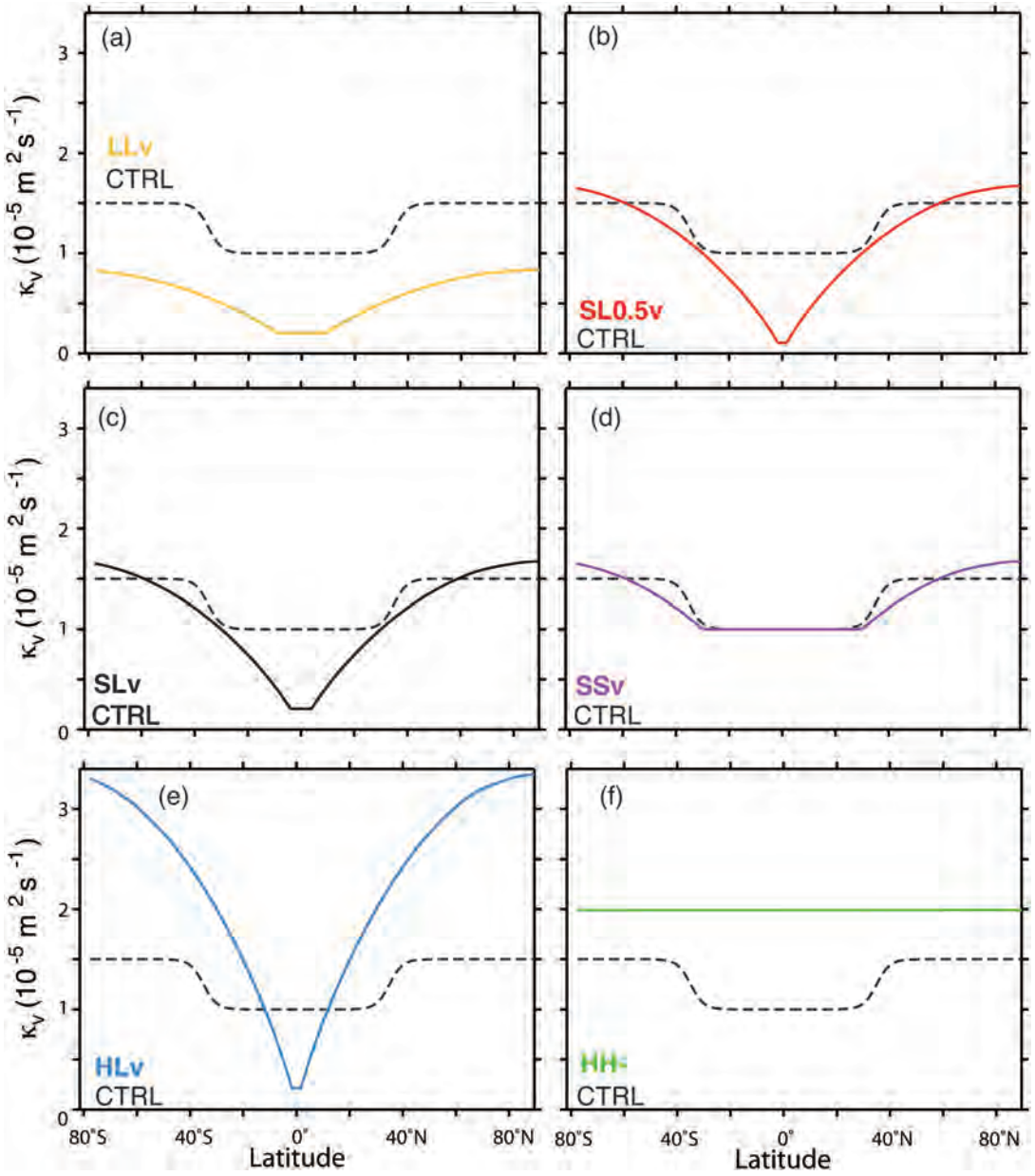

Figure V.1: Zonal mean vertical background diffusivity in the upper 1000 m of the ocean (10^{-5} m^2 s^{-1}) applied in the different model experiments. (a) LLv, (b) SL0.5v, (c) SLv, (d) SSv, (e) HLv and (f) HH-. Dashed black profile represents zonal mean vertical background diffusivity used in CTRL.

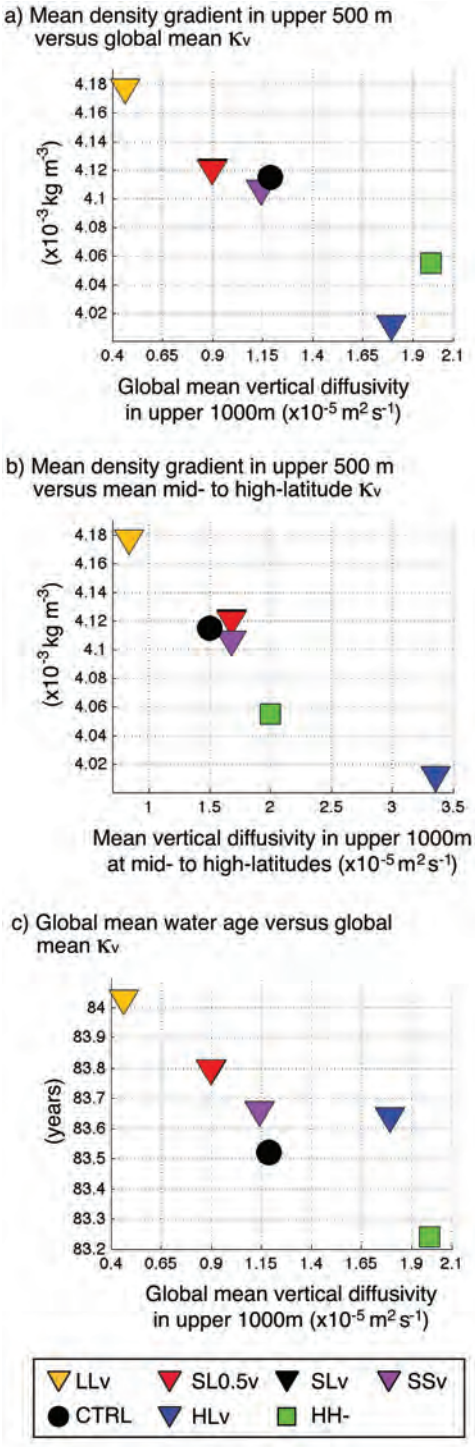

Figure V.2: (a) Mean density gradient in the upper 500 m as a function of global mean vertical background diffusivity (10^{-5} m^2 s^{-1}) in the different experiments applying parameterization schemes based on Henyey et al. (1986, triangles), globally constant diffusivity (green square) and the CTRL experiment (black circle). (b) as (a) but for high-latitude diffusivities (average of mid- to high-latitude coefficients south of 40°S and north of 40°N; 10^{-5} m^2 s^{-1}). (c) Global mean age (years) as a function of global mean diffusivity (10^{-5} m^2 s^{-1}) in all experiments as for (a).

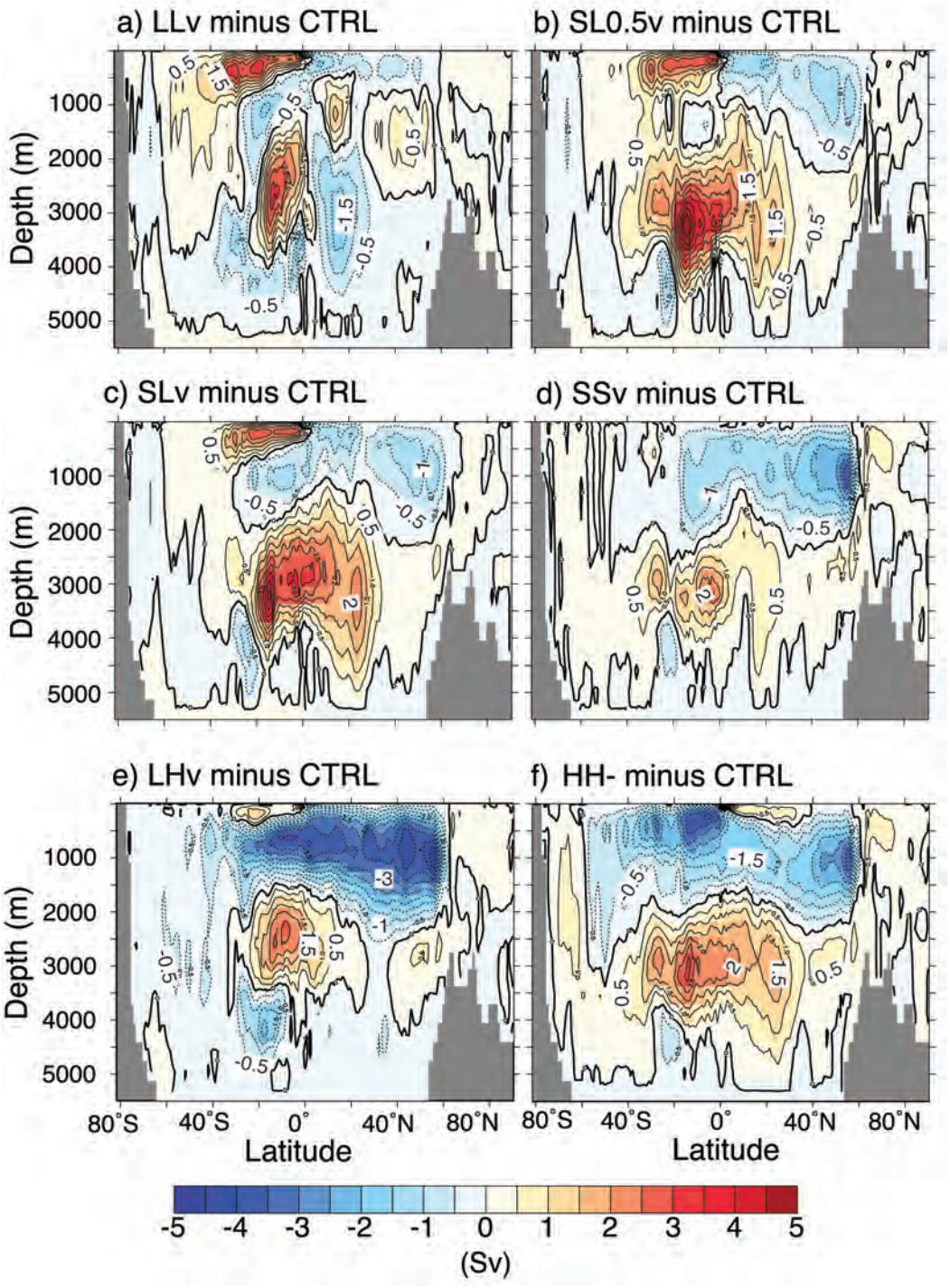

Figure V.3: Changes in the meridional overturning circulation (Sv) between (a) SLv minus CTRL, (b) SL0.5v minus CTRL, (c) HLv minus CTRL, (d) LLv minus CTRL, (e) HH- minus CTRL and (f) SSv minus CTRL. Contour intervals are 0.5 Sv.

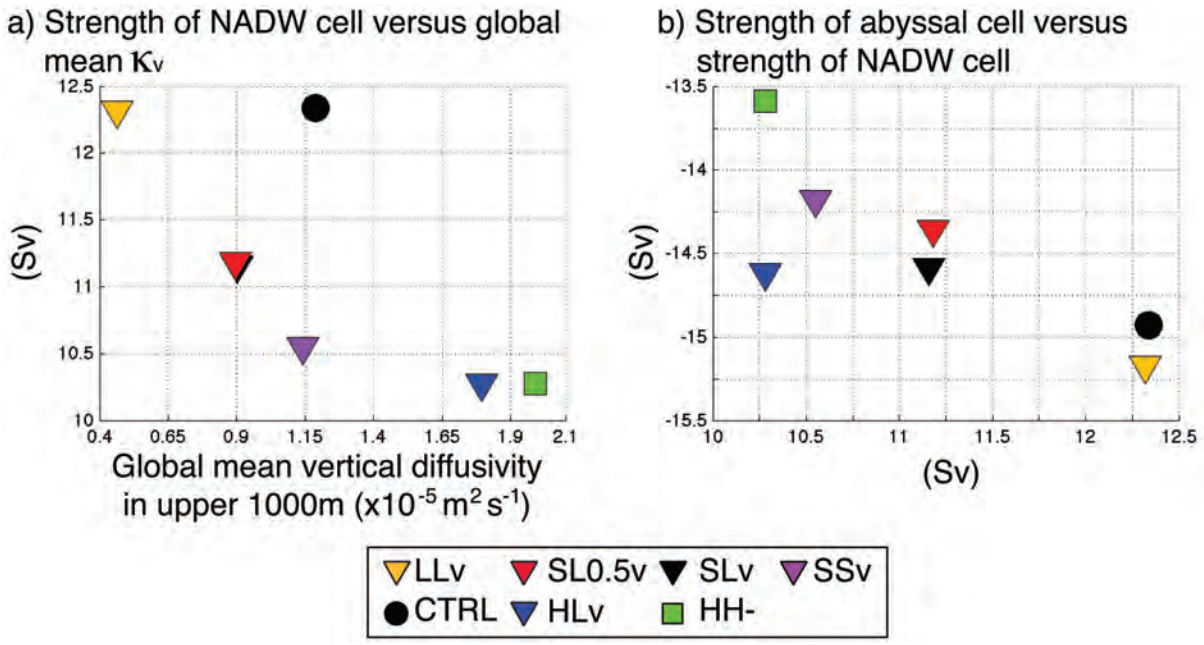

Figure V.4: (a) Maximum strength of the NADW cell (AMOC) in Sv as a function of global mean vertical background diffusivity (10^{-5} m^2 s^{-1}) in all experiments. (b) Maximum strength of the abyssal cell versus maximum strength in the NADW cell in all experiments.

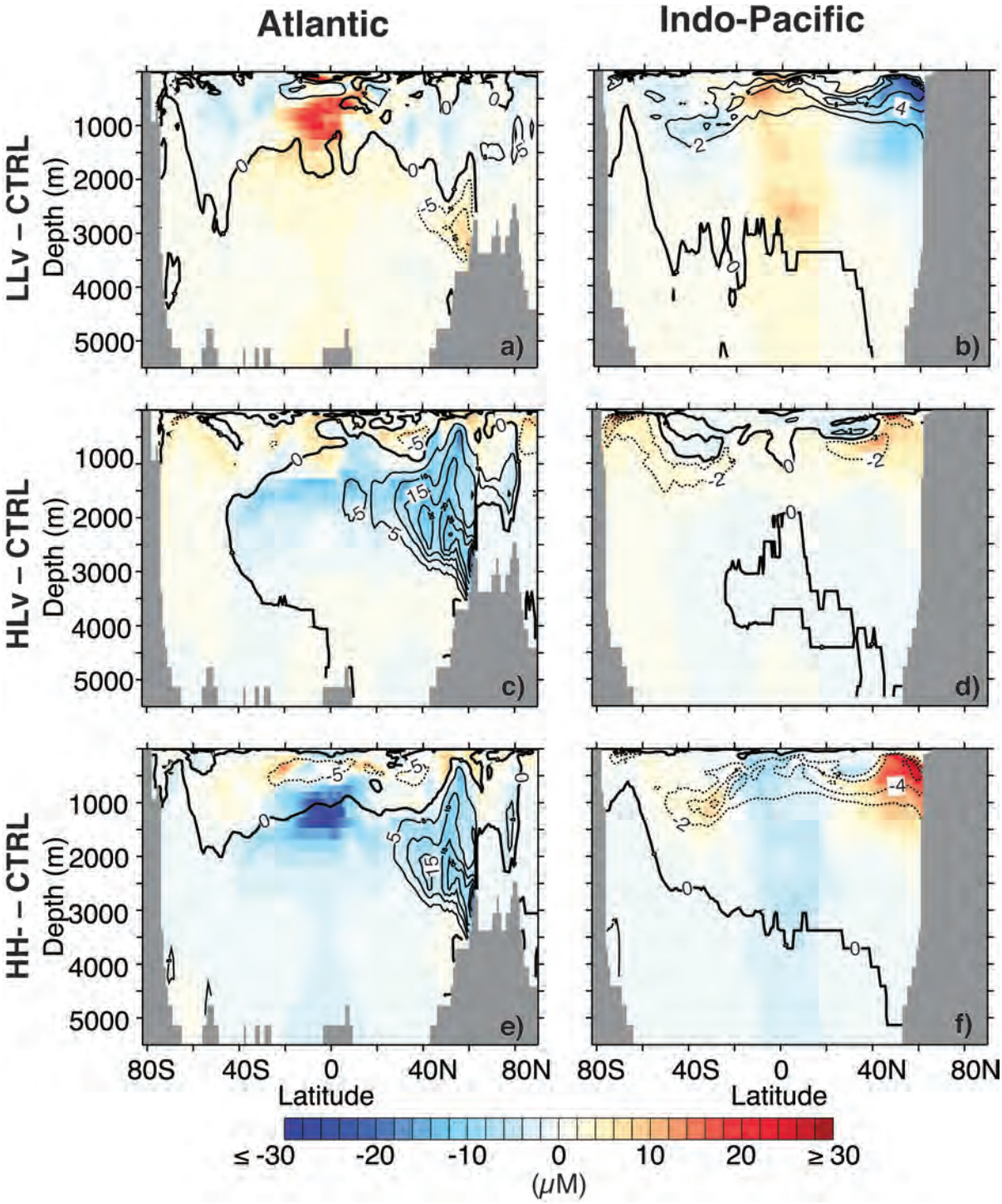

Figure V.5: Difference in zonal mean oxygen concentrations (μM) in the (left) Atlantic and (right) Indo-Pacific oceans between (a, b) LLv and CTRL, (c, d) HLv and CTRL and (e, f) HH- and CTRL, after 100 years of integration. Contours indicate changes in age between each experiment and CTRL. Contour intervals are (a, c, e) 5 years in the Atlantic Ocean and (b, d, f) 2 years in the Indo-Pacific Ocean. Solid contours indicate older waters in the respective experiment compared to CTRL, dotted contours mark younger waters.

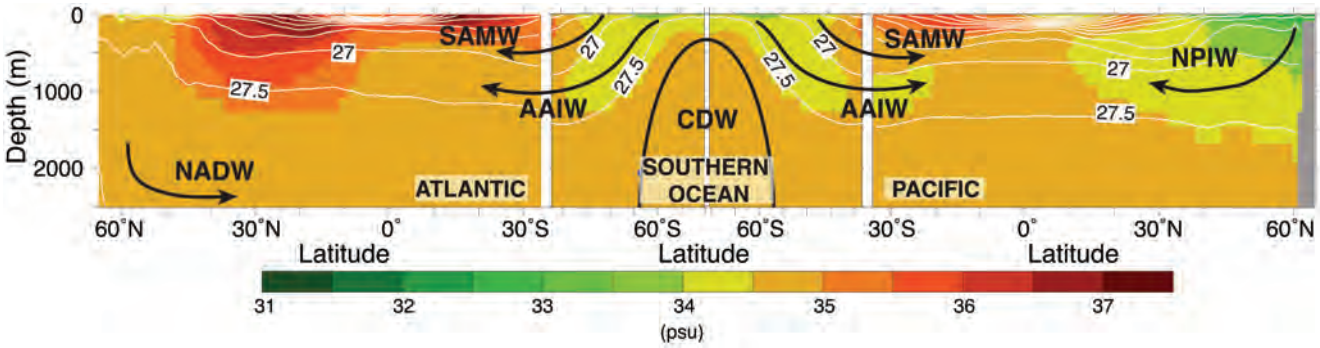

Figure V.6: Position of important water masses (black arrows) in the surface and intermediate ocean in experiment CTRL. Shown are North Atlantic Deep Water (NADW), Circumpolar Deep Water (CDW), Subantarctic Model Water (SAMW), Antarctic Intermediate Water (AAIW) and North Pacific Intermediate Water (NPIW). White contours mark isopycnal surfaces with contour intervals of 0.5 kg m^{-3}. Colour shading indicates annual zonal mean salinity (psu) in the Atlantic (left), the Southern Ocean (middle) and the Pacific Ocean (right) in experiment CTRL. Note the different scales and limits of the x-axis between the panels.

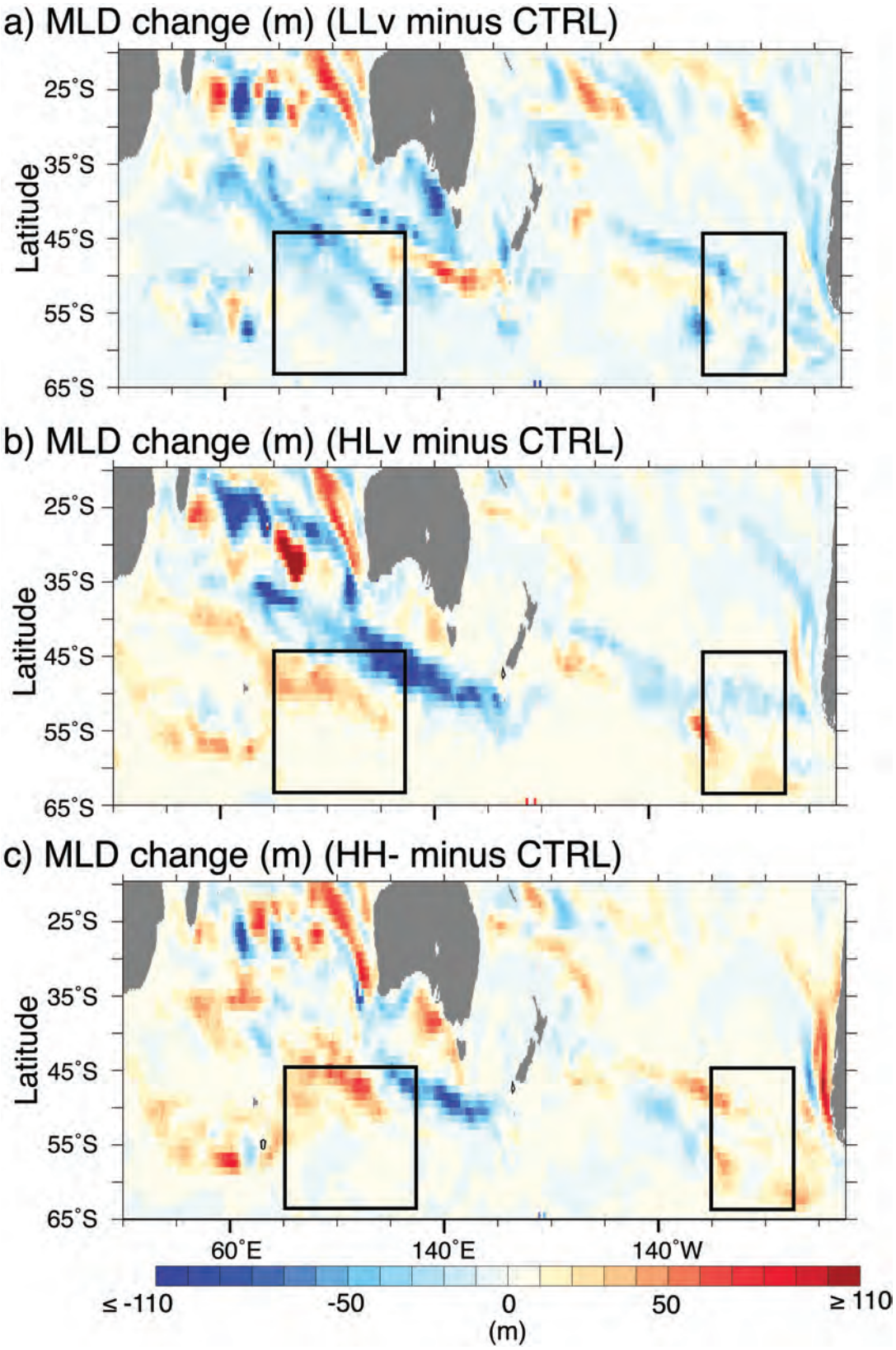

Figure V.7: Changes in maximum mixed layer depth (m) between (a) LLv minus CTRL, (b) HLv minus CTRL and (c) HH- minus CTRL. Black boxes mark approximate Subantarctic Mode Water formation regions in the Southern Ocean as in Sloyan et al. (2010).

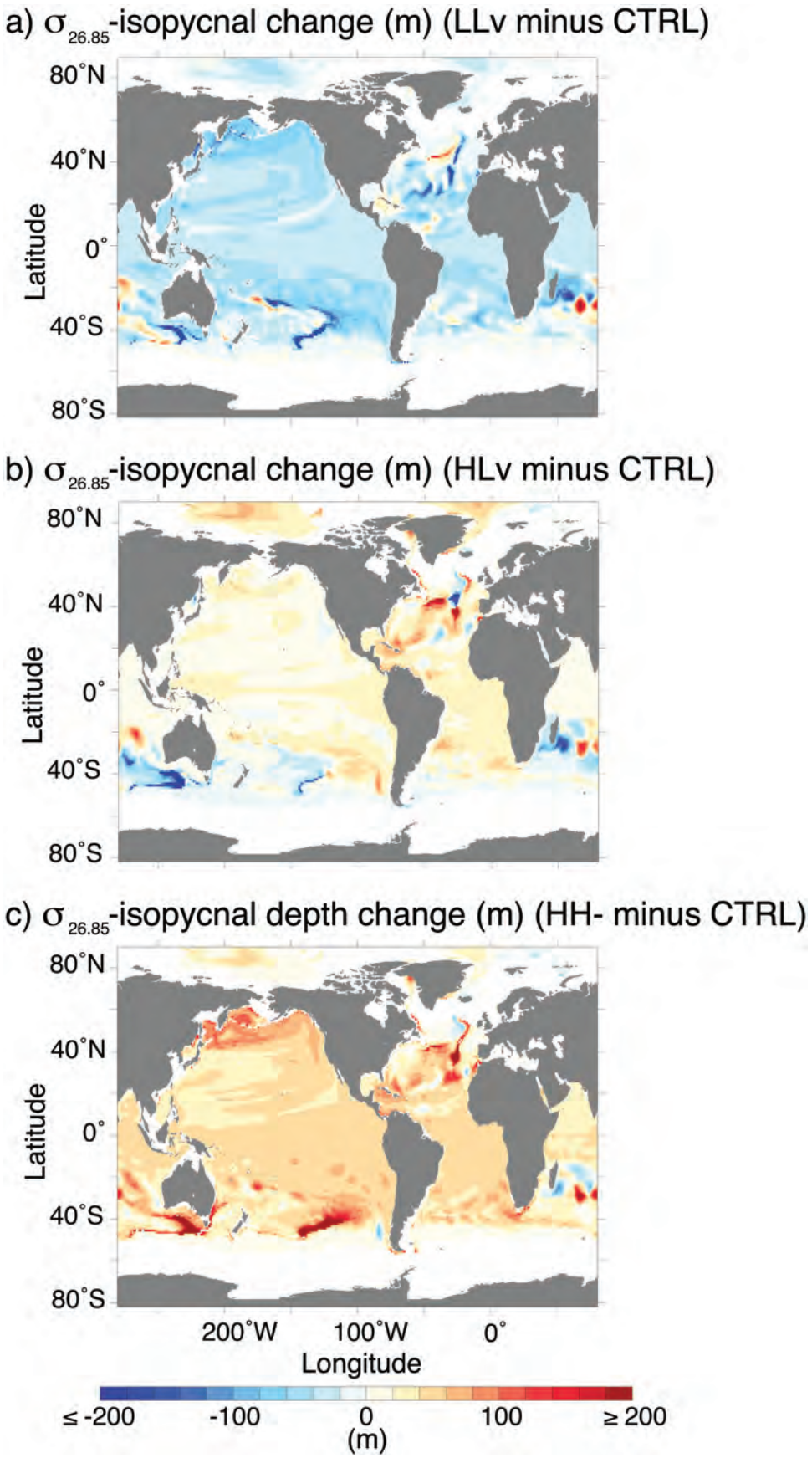

Figure V.8: Changes in $\sigma_{26.85}$-isopycnal depth (m) between (a) LLv minus CTRL, (b) HLv minus CTRL and (c) HH- minus CTRL.

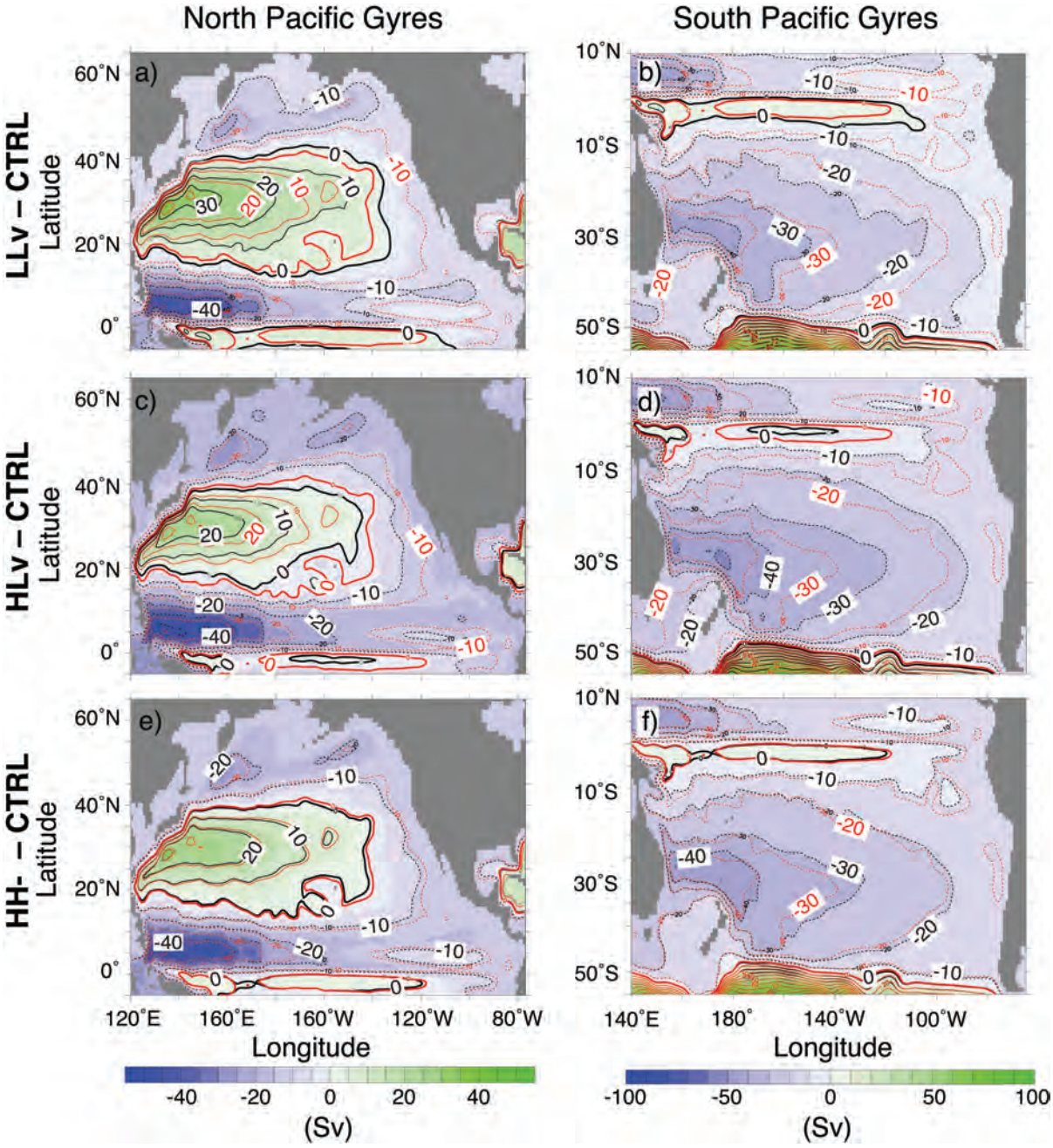

Figure V.9: (a) Annual mean horizontal streamfunction (Sv) in the North Pacific Ocean of experiment LLv (shading and black contours) and in CTRL (red contours). Contour intervals are ±10 Sv with solid contours marking positive values and dotted contours indicating negative values. (b) as (a) but for the South Pacific Ocean; (c, d) and (e, f) as (a) but for HLv and HH-, respectively.

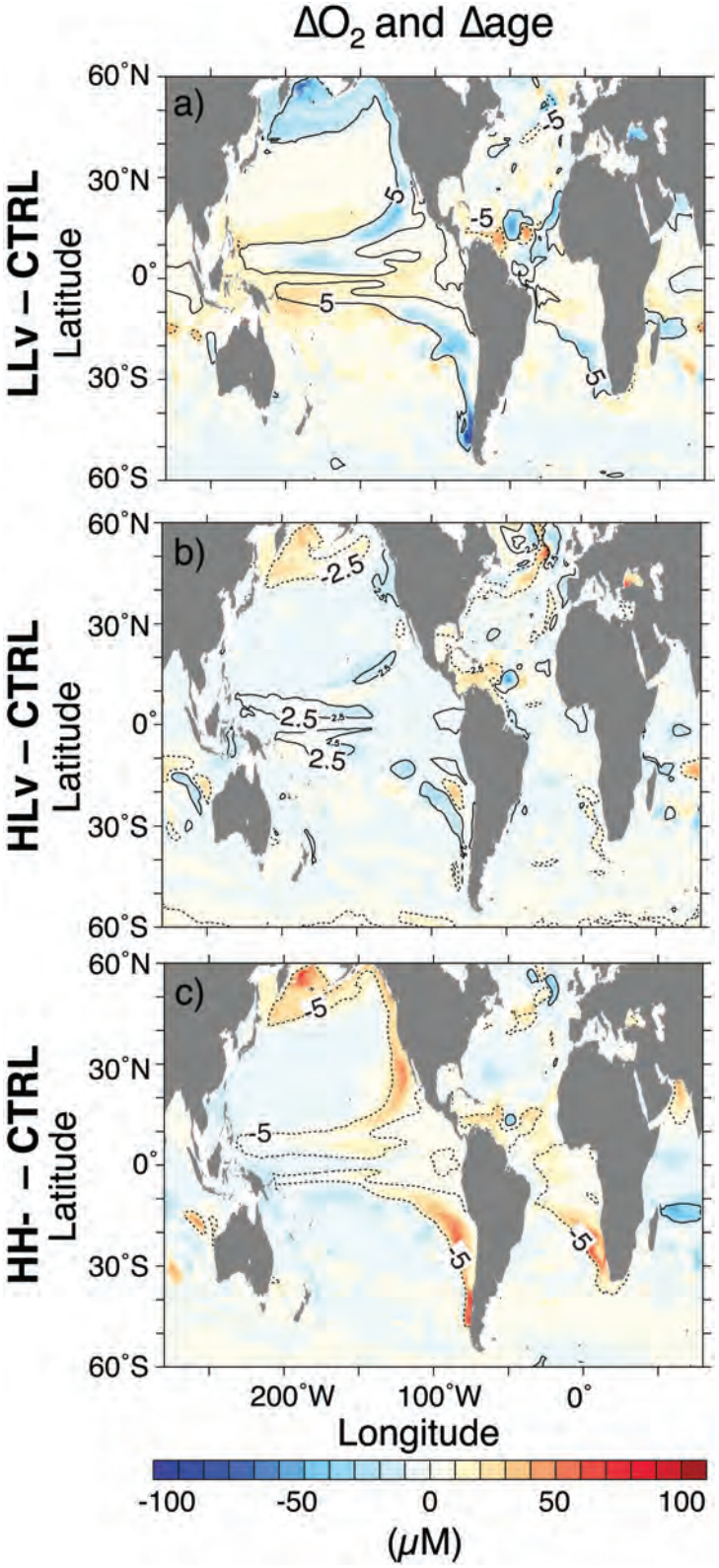

Figure V.10: (a) Annual mean O_2 changes (μM; saturation effect removed; colour shading) and changes in age (years; contours) at 250 m depth between LLv minus CTRL. Solid contours mark older water in LLv compared to CTRL; dashed contours show younger water. Only +5 year- (solid) and -5 year-contour lines (dashed) are shown to highlight the sign of change. (b) as (a) but with ± 2.5 years -contour line and for HLv minus CTRL. (c) as (a) but for HH- minus CTRL.

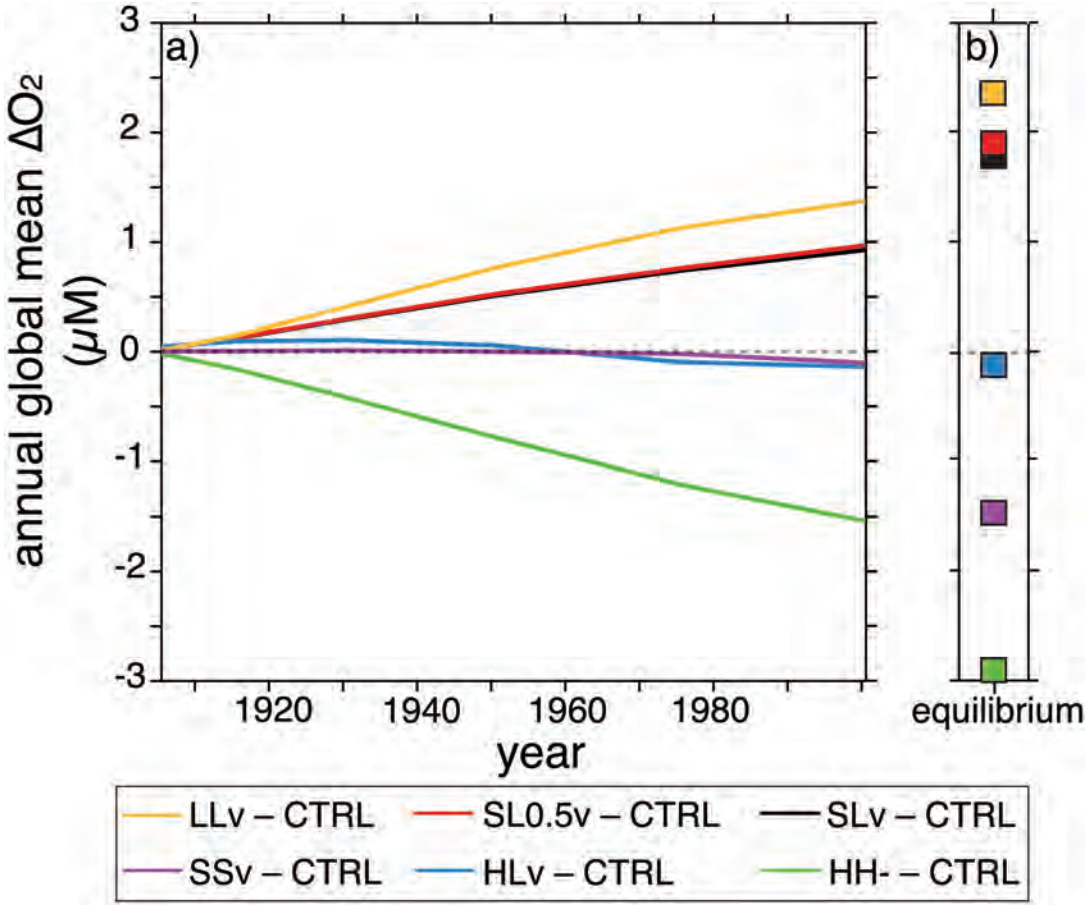

Figure V.11: Annual global mean oxygen concentrations (μM) in all experiments (a) within the first century of integration and (b) extrapolated to equilibrium.

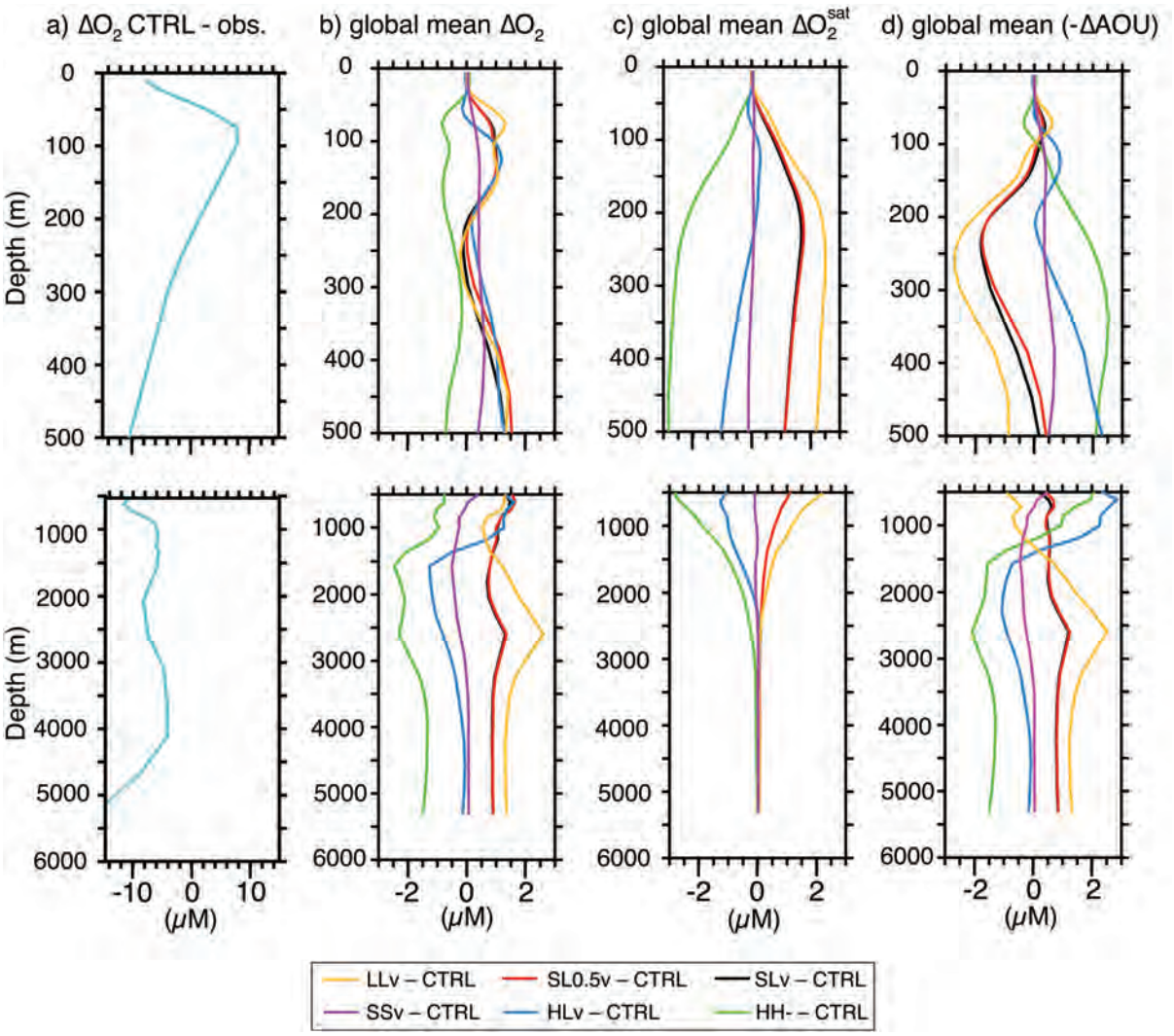

Figure V.12: (a) Annual global mean oxygen concentration difference (μM) between CTRL and observations (equivalent to "gamma2"-corrected value in Bianchi et al. (2012)) (b) Annual mean oxygen concentration profile changes (μM) between SLv minus CTRL (black), SL0.5v minus CTRL (red), HLv minus CTRL (blue), LLv minus CTRL (yellow), HH- minus CTRL (green) and SSv minus CTRL (purple); (c, d) as (b) but for oxygen saturation concentration (μM) and inverse apparent oxygen utilization profile changes (-1×AOU; μM), respectively.

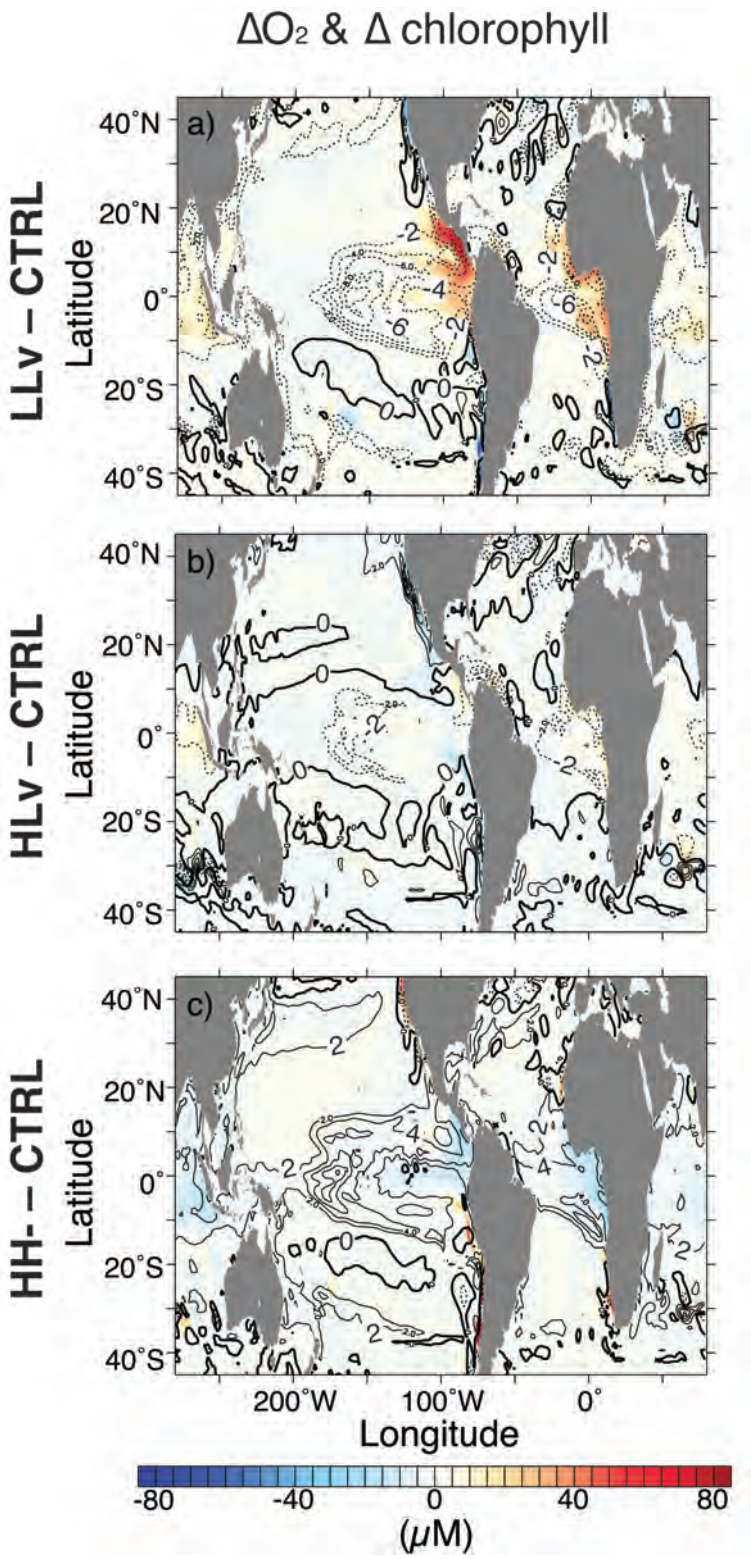

Figure V.13: (a) Annual mean O_2 changes (μM; saturation effect removed; colour shading) at 75 m depth and total chlorophyll content between surface and 50 m depth (mg m^{-3}; contours) between LLv minus CTRL. Solid lines indicate an increase, dotted line a decrease in chlorophyll in experiment LLv compared to CTRL. Contour intervals are 2 mg m^{-3}. (b, c) as (a) but for HLv minus CTRL and HH- minus CTRL, respectively.

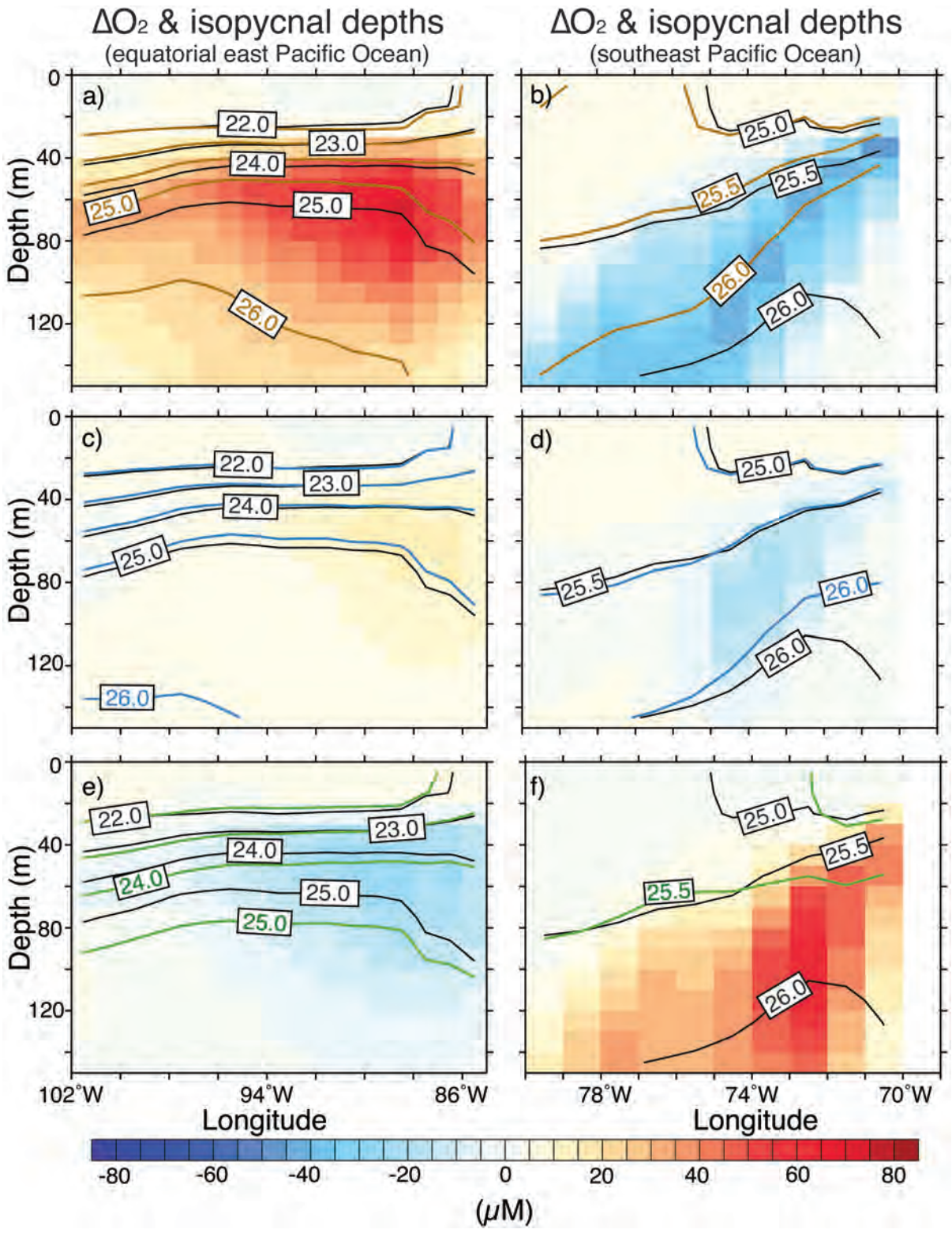

Figure V.14: (a) Annual mean O_2 concentration changes (μM; colour shading) in equatorial east Pacific Ocean (averaged between 8°N and 17°N) between LLv minus CTRL. Contours mark position of isopycnal surfaces (averaged over the same region) in CTRL (black) and in LLv (orange). (b) as (a) but for the south east Pacific Ocean (average over 36°S-20°S). (c, e) as (a) and (d, f) as (b) but for HLv minus CTRL and HH- minus CTRL, respectively.

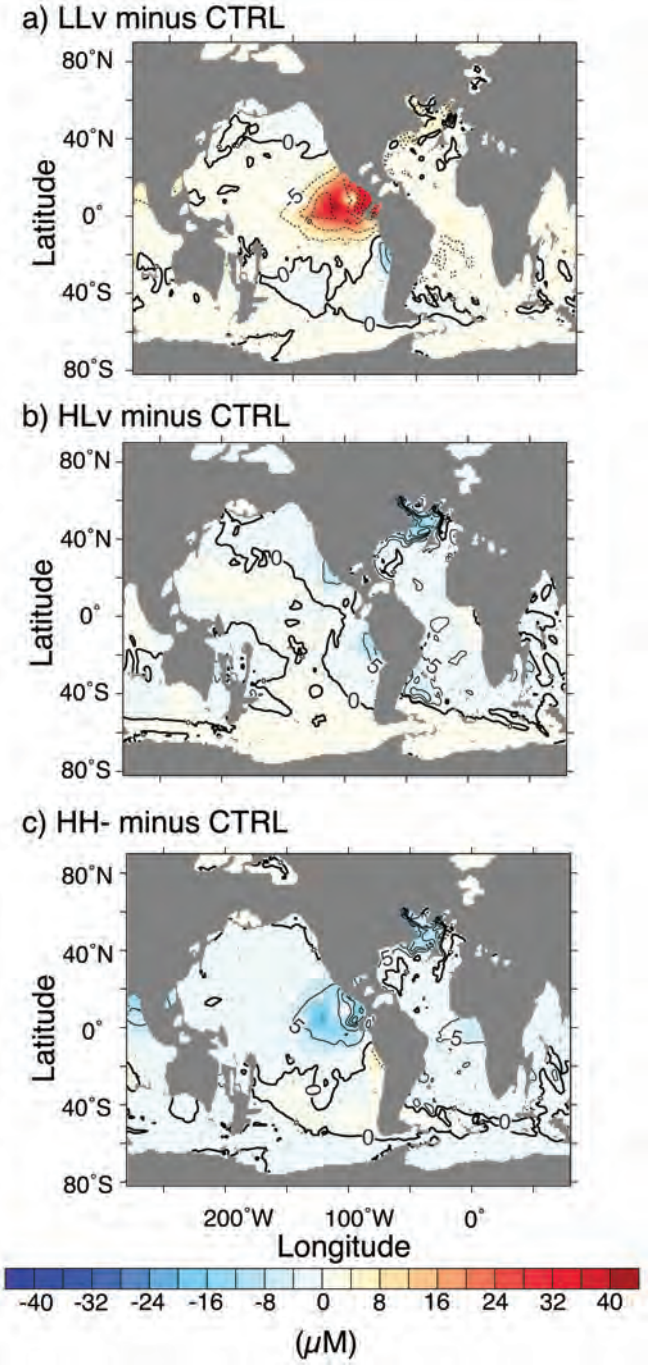

Figure V.15: Annual mean O_2 concentration changes (μM; saturation effect removed; colour shading) and changes in annual mean DIC (mmol m^{-3}; contours) at 2500 m depth between (a) SLv minus CTRL, (b) HH- minus CTRL, (c) HLv minus CTRL and (d) LLv minus CTRL. Contour intervals are in 5 mmol m^{-3} with solid contours marking an increase in DIC concentrations in the respective experiment compared to CTRL and dotted lines indicating a decrease.

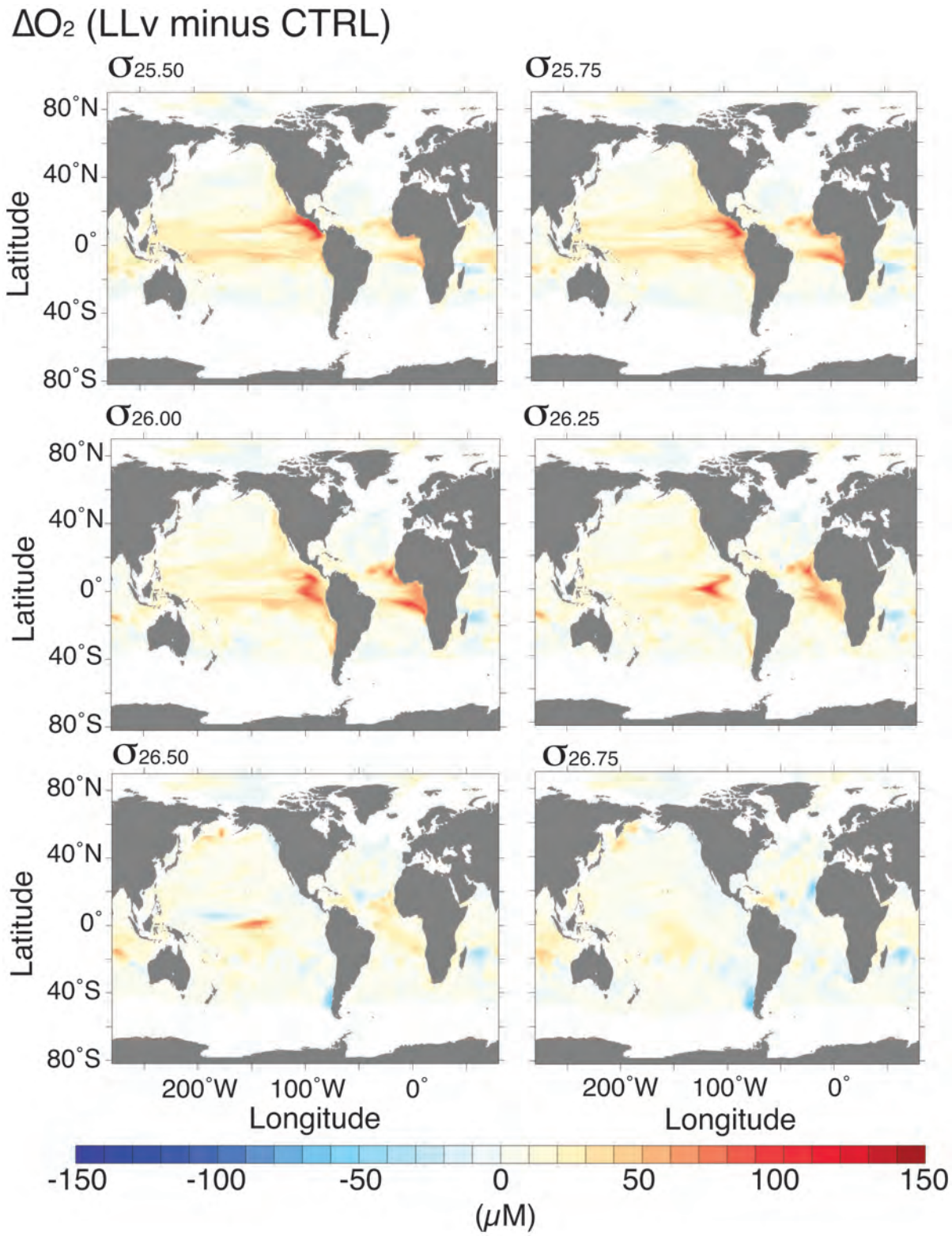

Figure V.16: Annual global mean oxygen concentration changes (ΔO_2; μM) on isopycnal surfaces throughout the pycnocline (LLv minus CTRL).

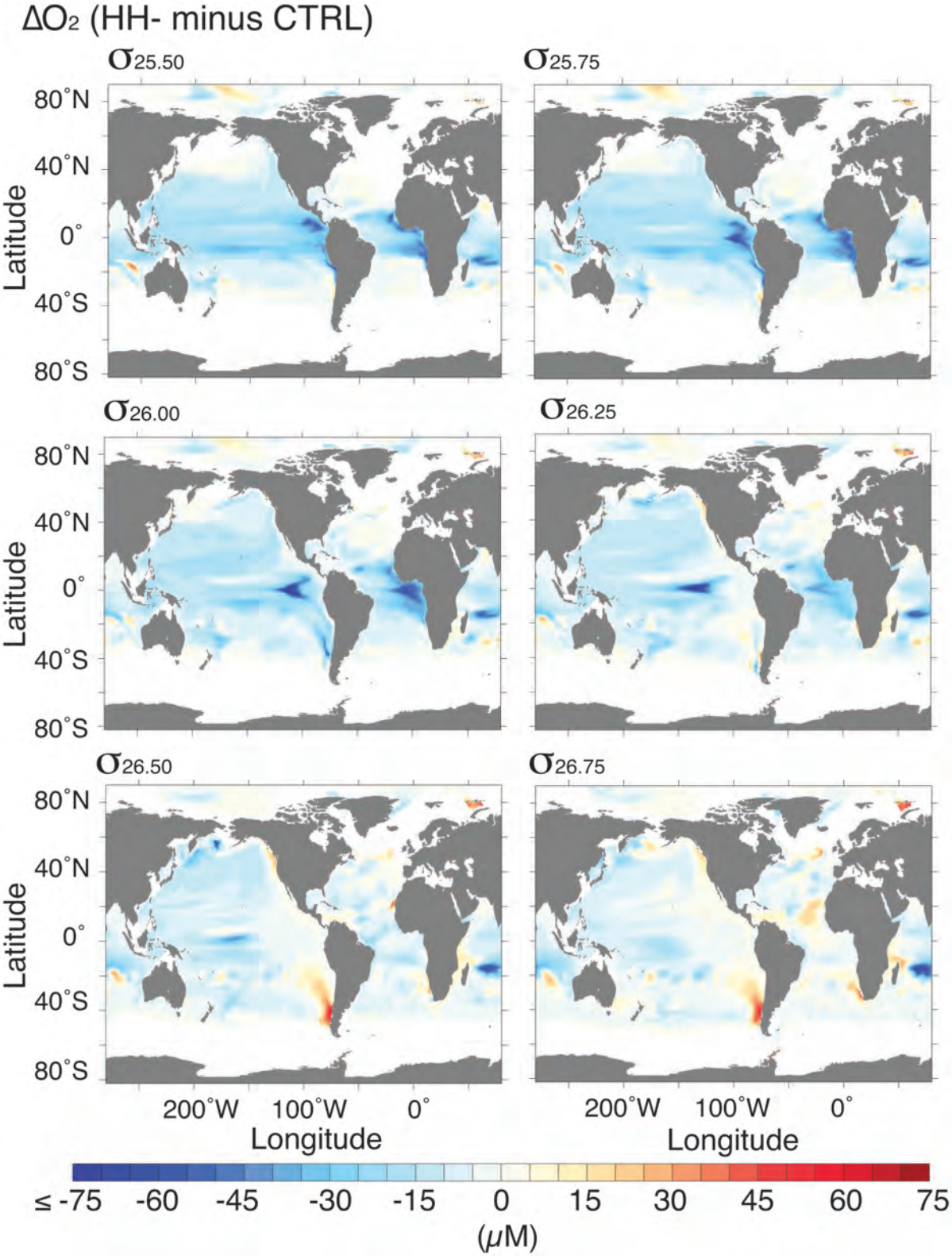

Figure V.17: Annual global mean oxygen concentration changes (ΔO_2; μM) on isopycnal surfaces throughout the pycnocline (HH- minus CTRL).

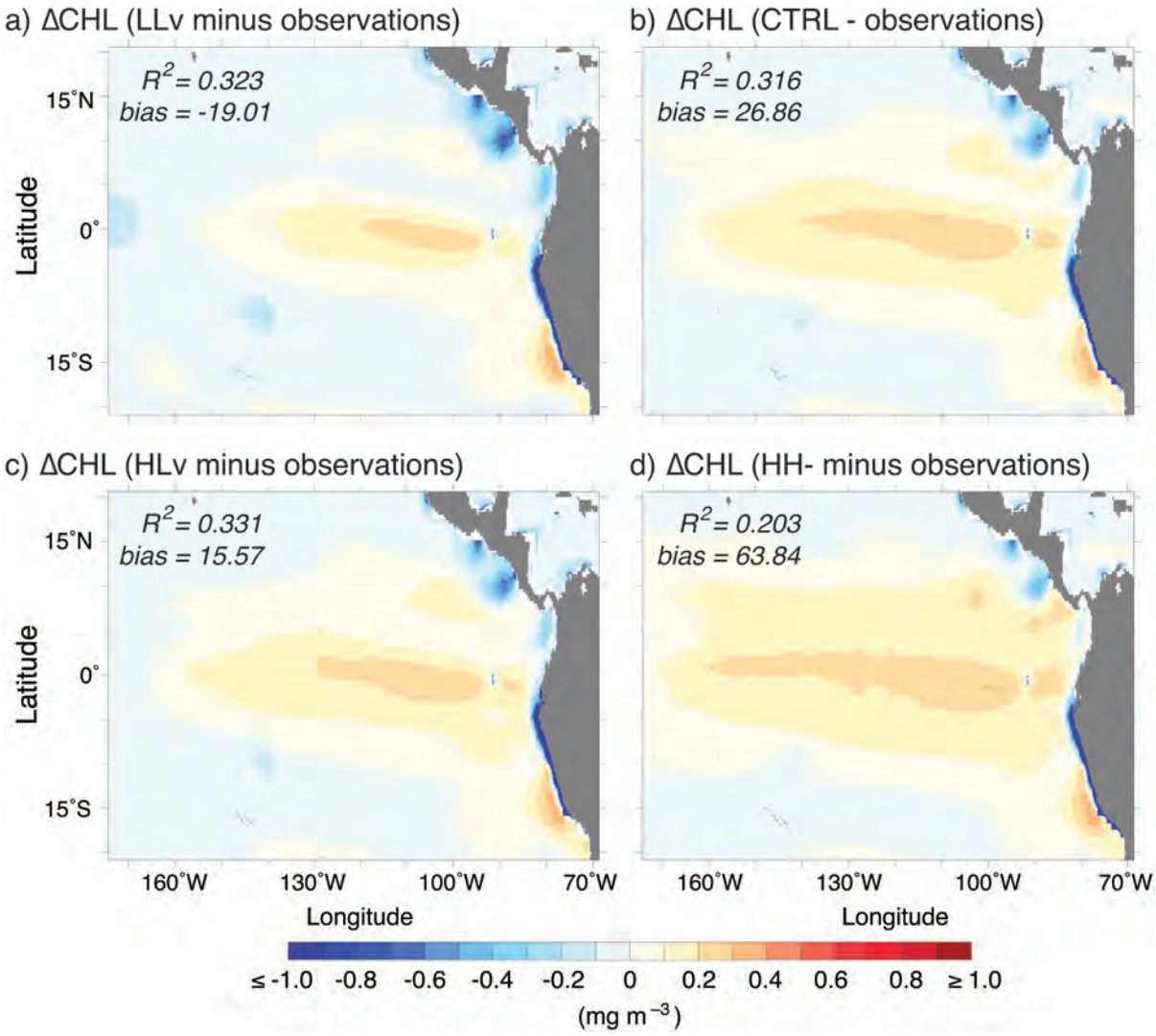

Figure V.18: Difference in annual global mean chlorophyll concentrations (ΔCHL; mg m^{-3}) in the uppermost model layer compared to ten-year (1997-2007) annual mean remote sensing data derived from SeaWiFs satellite (Giovanni project NASA). (a) LLv minus observations, (b) CTRL minus observation, (c) HLv minus observations and (d) HH- minus observations. Also shown is the correlation (R^2) between the respective experiment and observations and the model bias for the respective parameterization scheme.

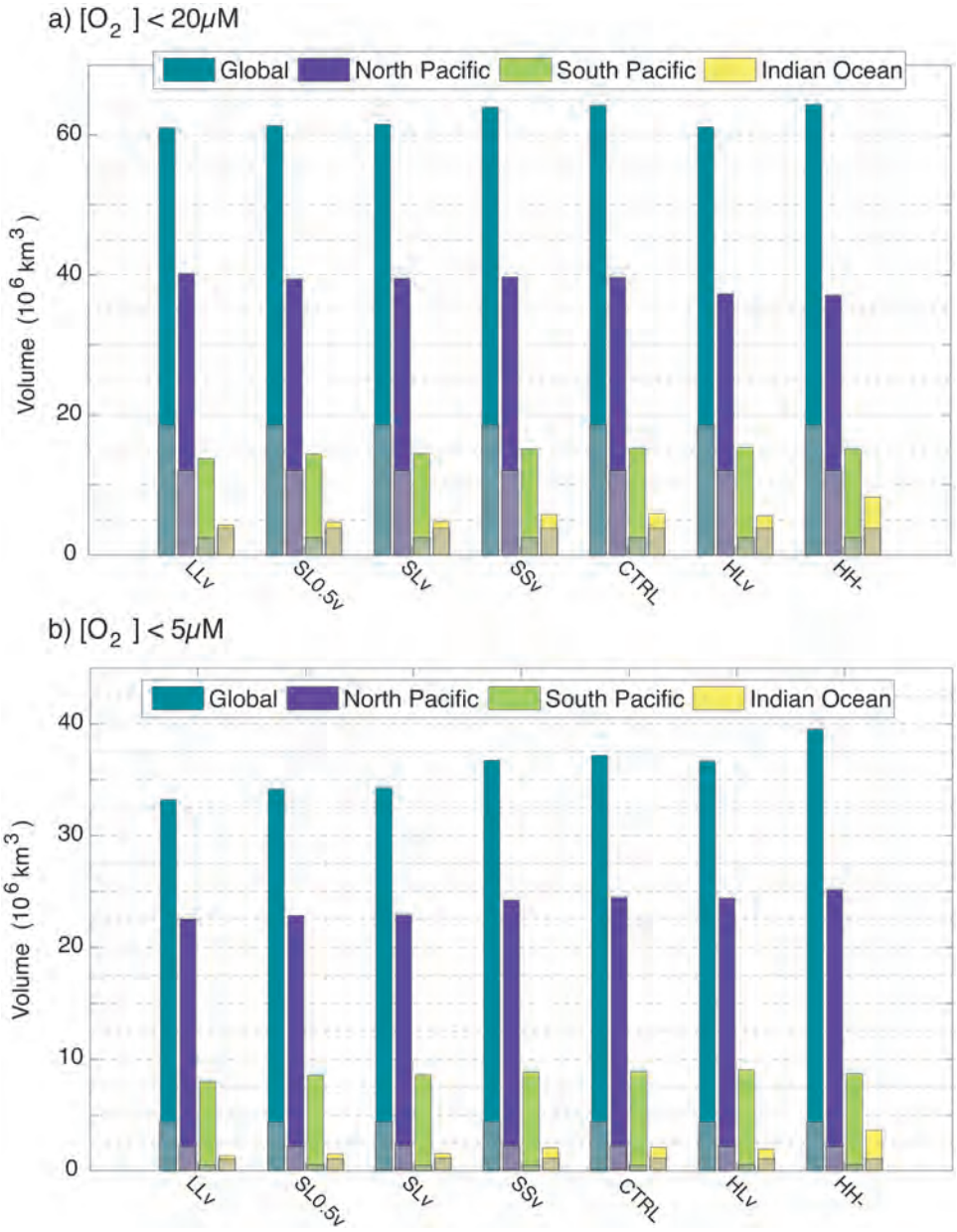

Figure V.19: (a) Volume of waters (10^6 km^3) with oxygen concentrations below 20 μM in the global ocean (blue), the North Pacific (purple), the South Pacific (green) and the Indian Ocean (yellow) in all experiments. Grey shading indicate observational values (equivalent to "gamma2"-corrected value in Bianchi et al. (2012)). (b) as (a) but for waters with oxygen concentrations below 5 μM. Note the different y-axis between the two panels.

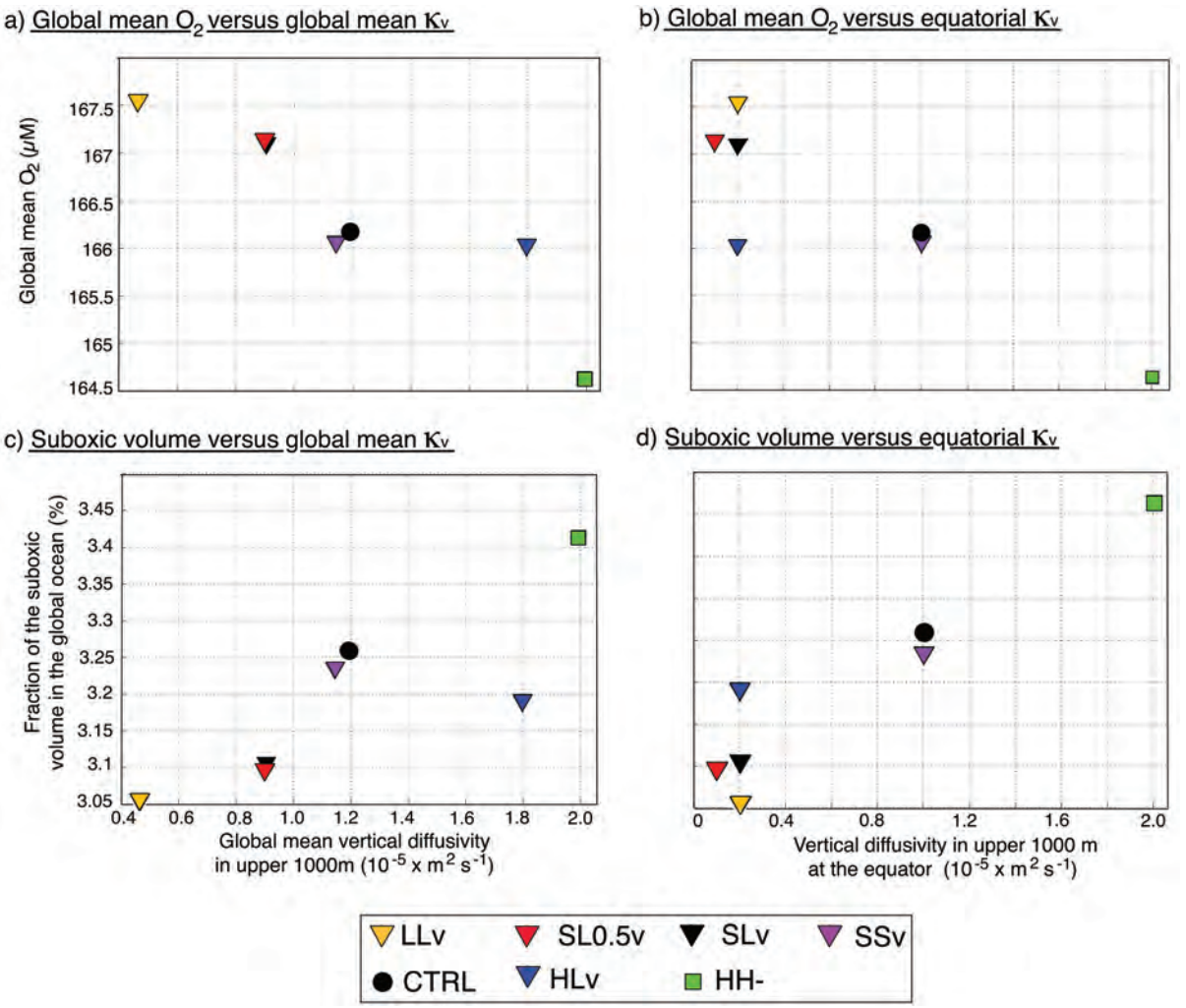

Figure V.20: (a) Annual global mean oxygen concentrations (μM) as a function of global mean vertical background diffusivity ($\times 10^{-5}$ m^2 s^{-1}; averaged over upper 1000 m) in all experiments after the first century of integration. (b) Annual global mean oxygen concentrations (μM) as a function of the equatorial vertical diffusivity coefficients in all experiments after the first century of integration. (c) Annual mean fraction of the global ocean with suboxic conditions versus global mean vertical background diffusivity (averaged over upper 1000 m) in all experiments after the first century of integration. (d) Annual mean fraction of the global ocean with suboxic conditions as a function of the equatorial vertical diffusivity coefficients in all experiments after the first century of integration.

Table V.1: Global mean, equatorial and mid-latitude diffusivity coefficients in all model experiments. Experiment names are derived from the comparison of the diffusivities in the respective experiment to CTRL with the first letter referring to mid-latitude values and the second to equatorial diffusivities. "L" marks lower, "S" similar and "H" higher diffusivity coefficients than CTRL. All experiments, which follow the diffusivity parameterization by Henyey et al. (1986), are marked with "v" to represent the shape of their zonal profile with reduced mixing at the equator. The dash in "HH-" highlights the globally uniform vertical diffusivity used in this experiment.

	global mean diffusivity ($\times 10^{-5}$ m^2 s^{-1})	equatorial diffusivity ($\times 10^{-5}$ m^2 s^{-1})	mid-latitude diffusivity ($\times 10^{-5}$ m^2 s^{-1})
LLv	0.46	0.20	0.50
SL0.5v	0.90	0.10	1.00
SLv	0.90	0.20	1.00
SSv	1.14	1.00	1.00
CTRL	1.19	1.05	1.00
HLv	1.79	2.00	0.20
HH-	2.00	2.00	2.00

Table V.2: Volume (10^6 km^3) of suboxic waters in the Pacific and the Indian Oceans in the different model experiments, in comparison to observations (equivalent to "gamma2"-corrected value in Bianchi et al. (2012)

		North Pacific	South Pacific	Indian Ocean	Global
Observations	$[O_2] < 20$ μM	12.0	2.5	3.6	18.1
CTRL		39.7	15.2	5.9	64.2
LLv		40.2	13.8	4.3	61.0
SL0.5v		39.4	14.4	4.7	61.3
SLv		39.5	14.5	4.8	61.3
SSv		39.7	15.1	5.8	64.0
HLv		37.3	15.3	5.6	61.2
HH-		37.1	15.1	8.2	64.4
Observations	$[O_2] < 5$ μM	2.41	0.61	1.11	4.13
CTRL		24.47	8.86	2.08	37.16
LLv		22.53	7.95	1.31	33.19
SL0.5v		22.83	8.51	1.48	34.15
SLv		22.90	8.53	1.51	34.27
SSv		24.22	8.79	2.03	36.72
HLv		24.40	9.00	1.92	36.64
HH-		25.17	8.66	3.60	39.51

Table V.3: Deep equatorial upwelling (Sv) through 1000 m depth surface between 30°S and 30°N, Southern Ocean upwelling (Sv) through 1000 m depth surface south of 60°S, volume transport of EUC (Sv) through the 170°W zonal surface between 3°S and 3°N and the global volume (10^6 km^3) of water masses above and including 20°C-isotherm (D_{20}) used as a measure for thermocline thickness in all model experiments.

	equatorial upwelling (Sv)	SO upwelling (Sv)	EUC (Sv)	V_{D20}-isothermal ($\times 10^6$ km^3)
LLv	2.89	12.58	34.41	27.0
SL0.5v	2.21	12.56	33.86	27.3
SLv	2.88	12.56	34.35	27.3
SSv	1.94	12.53	34.92	28.4
CTRL	3.50	12.54	34.89	28.4
HLv	1.38	12.57	34.00	28.0
HH-	3.37	12.55	36.01	30.1

Table V.4: Mean maximum mixed layer depth (m) in the two formation regions of SAMW in all experiments. The Indian sector of the Southern Ocean is located between 80°E - 130°E and 64°S - 45°S; the "Pacific sector" refers to the region between 120°W - 70°W and 64°S - 45°S.

	Indian sector (m)	Pacific sector (m)
LLv	231.7	258.4
SL0.5v	237.8	266.4
SLv	238.7	263.6
SSv	242.5	495.5
CTRL	241.2	264.7
HLv	244.3	266.7
HH-	248.6	275.3

Table V.5: Standard deviation (STD) and bias of all experiments compared to observations (equivalent to "gamma2"-corrected value in Bianchi et al., 2012) for (a) global values (3D) and (b) zonal mean (2D) values. Experiment with lowest STD and bias for both dimensions is marked in bold.

	STD	bias
(a) 3D		
CTRL	23.46	-4.70
LLv	**22.44**	**-3.36**
SL0.5v	22.73	-3.74
SLv	22.71	-3.78
SSv	23.40	-4.80
HLv	23.39	-4.81
HH-	24.53	-6.21
(b) 2D		
CTRL	13.01	-5.34
LLv	**12.16**	**-4.59**
SL0.5v	12.43	-4.80
SLv	12.44	-4.82
SSv	12.89	-5.49
HLv	12.92	-5.46
HH-	14.07	-6.41

Concluding remarks

The sensitivity of ocean circulation and biogeochemical tracers, namely DIC and O_2, to variations in two physical mechanisms, one acting at the air/sea interface, the other within the upper 1000 m of the global ocean, has been investigated using a climate model of intermediate complexity and a one degree-resolution ocean model. Ocean oxygenation and the cycling of carbon between atmosphere and ocean are key components in the control of the global climate. It is thus crucial to understand the response of oceanic carbon and oxygen concentrations as well as ocean circulation to alterations in the physical forcing to be able to accurately represent and describe past, present as well as future changes in the global climate system. The central goal of this project was to examine the impact of variations in surface wind stress and vertical background diffusivity in the upper ocean on oceanic properties, circulation and their influence on physical and biogeochemical processes determining ocean oxygenation and ocean carbon sequestration. This thesis thus addressed crucial questions about the control of physical mechanisms over processes determining the concentration of two of the most important biogeochemical tracers in the ocean. Amongst other things, the results of this thesis highlight the potential contribution of oceanic low-latitude processes to the ocean's control over the global climate and illustrate the importance of marine biology in the equatorial region for oceanic carbon sequestration (Part I). In addition, the findings of this thesis challenge the dominance of two widely accepted oceanic mechanisms, namely (i) the control of NADW formation by SH westerly wind strength through wind-driven alterations in northward Ekman transport at latitudes of the Drake Passage (Part III) and (ii) the dominant impact of ocean stratification on ocean oxygenation (Parts II and V).

Observational data of dissolved oxygen concentrations in the global ocean and its evolution over the past century are sparse. However, the sampling density of oxygen measure-

ments has improved significantly over the past decade. New measurement techniques, such as the equipping of ARGO floats with oxygen sensors, will ensure a growth of available oxygen measurements that will contribute to a more reliable representation of global biogeochemical processes. Additional observational data will allow further assessment of the driving mechanisms presented in this thesis. Furthermore, the additional observational data will allow a better understanding of the possible future development of oxygen minimum zones and facilitate more reliable predictions of the cycling of important geochemical tracers between the atmosphere and ocean.

While a comparison between the results of our model experiments and current observations have to be made with caution due to the transient nature of current climate change along with a variety of simultaneously changing boundary conditions, the results presented in Part IV in response to mid-latitude wind stress changes suggest analogous conditions to the changes observed in current measurements. For instance, while strengthened westerly wind stress leads to an overall decrease in global mean temperature in our model experiment, the inter-hemispheric comparison suggests that the Southern Hemisphere is cooling more than the Northern Hemisphere. This response of the modelled SH temperature field could account for a component of the slower Southern Hemisphere warming of the current climate, with the wind-induced cooling partly counteracting the changes in radiative forcing due to increased greenhouse gases in the atmosphere. The different response between the two hemispheres in our model results stems mainly from changes in the northward Ekman transport, ventilation depth and Antarctic sea-ice thickness as discussed in Part IV. Whether or not this mechanism can account for the discrepancies between northern and southern hemisphere warming remains to be investigated, ideally using a model resolving eddy-scale circulation.

To extend the here presented study to further gain insight into the impact of the chosen physical mechanisms on oceanic carbon and oxygen concentrations, the following list presents four examples of possible future studies. These are five of the most pressing and interesting extensions to this project in the light of recent observations, as well as in regards to past and possible future climate conditions.

1. *Addition of atmospheric and terrestrial feedbacks*

   The aim of Part I, which was to identify the impact of wind-driven ocean circulation changes on the oceanic carbon content, was undertaken purposefully excluding possible feedbacks from variations in atmospheric CO_2 and terrestrial carbon. The sensitivity study presented in Part I could be extended to include these carbon cycle feedback responses. This would allow a full assessment of all components of the global carbon cycle and enable more precise predictions about possible past and future climate conditions in regards to tropical trade wind variations.

2. *Implications of circulation changes driven by variations in SH westerly winds on the oceanic carbon content*

   Part III identified significant alterations in the global overturning circulation in response to variations in Southern Hemisphere westerly winds, while Part IV presented how these could potentially alter physical parameters that control ocean oxygenation and carbon sequestration. Future work should analyse the implications of the presented changes in oceanic properties, e.g. water mass formation, carbon/oxygen solubility as well as biological activity, on oceanic carbon and O_2, in high resolution. It could then identify the dominant mechanisms acting on the marine carbon cycle in response to Southern mid-latitude wind perturbations, which previous studies have already identified to have a significant influence on oceanic carbon sequestration (e.g. Le Quéré et al., 2007; Zickfeld et al., 2007; Lovenduski et al., 2007, 2008; Zickfeld et al., 2008).

3. *Application of more realistic wind stress perturbations*

   As highlighted in Part II, the chosen approach to include wind stress perturbations by applying the same wind stress factor everywhere in the affected latitude region is an idealisation of the observed and predicted changes. While this approach is appropriate in the framework of this thesis given that its aim is the assessment of ocean sensitivity to wind stress changes, a future study could apply more realistic wind stress fields derived from past observations and/or from ensembles of model predictions of the future. Such a study, which addresses the complex interplay of

regionally opposing variations in wind stress, would allow more realistic predictions of possible past and future states of the global ocean and marine biogeochemistry, building on the findings of this project (Parts I - IV).

4. *Vertical mixing and ocean biogeochemistry*

   The findings in Part V present an assessment of the impact of diapycnal diffusivity parameterizations on modelled ocean oxygenation. A future study could include an analysis of the resulting conditions under transient climate conditions representing continuous changes in ocean stratification. The results of such a study could contribute to the improvement of the representation of biogeochemical processes within numerical models by performing an in-depth model assessment comparing model results to paleo-proxy data as well as to observations of recent climate conditions.

5. *Changes in the oceanic uptake of anthropogenic carbon*

   The results of this thesis support the paradigm that current changes in surface wind fields are likely to impact the oceanic uptake of anthropogenic carbon. The poleward intensification for instance has been suggested to have caused an anomalous uptake of anthropogenic carbon in the Southern Ocean despite an overall weakening of the Southern Ocean carbon sink (Lovenduski et al., 2007). To determine the impact of wind stress changes on the oceanic uptake of anthropogenic carbon, the model experiments performed for this thesis could be repeated using pre-industrial and historic values for atmospheric CO2 to investigate the changes in anthropogenic carbon uptake when wind perturbations are applied.

Bibliography

Archer, D.: A data-driven model of the global calcite lysocline, *Global Biogeochem. Cycles*, **10**, 511–526, 1996.

Bianchi, D., Dunne, J. P., Sarmiento, J. L., and Galbraith, E. D.: Data-based estimates of suboxia, denitrification, and N_2O production in the ocean and their sensitivities to dissolved O_2, *Global Biogeochem. Cycles*, **26**, GB2009, 2012.

Bindoff, N. L. and McDougall, T. J.: Diagnosing climate change and ocean ventilation using hydrographic data, *J. Phys. Oceanogr.*, **24**, 1137–1152, 1994.

Böning, C. W., Dispert, A., Visbeck, M., Rintoul, S. R., and Schwarzkopf, F. U.: The response of the Antarctic Circumpolar Current to recent climate change, *Nature Geoscience*, **1**, 864–869, 2008.

Bopp, L., Le Quéré, C., Heimann, M., Manning, A. C., and Monfray, P.: Climate-induced oceanic oxygen fluxes: Implications for the contemporary carbon budget, *Global Biogeochem. Cycles*, **16**, 1022, 2002.

Brix, H. and Gerdes, R.: North Atlantic Deep Water and Antarctic Bottom Water: Their interaction and influence on the variability of the global ocean circulation, *J. Geophys. Res.*, **108**, 3022, 2003.

Broecker, W. S.: Glacial to interglacial changes in ocean chemistry, *Progress in Oceanography*, **11**, 151–197, 1982.

Broecker, W. S.: Paleocean circulation during the last deglaciation: a bipolar seesaw?, *Paleoceanography*, **13**, 119–121, 1998.

Bryden, H. L., Longworth, H. R., and Cunningham, S. A.: Slowing of the Atlantic meridional overturning circulation at 25°N, *Nature*, **438**, 655–657, 2005.

Cai, W. and Baines, P. G.: Interactions between thermohaline- and wind-driven circulations and their relevance to the dynamics of the Antarctic Circumpolar Current, in a coarse-resolution global ocean general circulation model, *J. Geophys. Res.*: Oceans (1978–2012), **101**, 14 073–14 093, 1996.

Cane, M. A.: A role for the tropical Pacific, *Science*, **282**, 59–61, 1998.

Clarke, A. J. and Lebedev, A.: Long-Term Changes in the Equatorial Pacific Trade Winds., *J. Climate*, **9**, 1020–1029, 1996.

Cline, J. D. and Richards, F. A.: Oxygen deficient conditions and nitrate reduction in the eastern tropical North Pacific Ocean, *Limnol. Oceanogr.*, 885–900, 1972.

Cocco, V., Joos, F., Steinacher, M., Frölicher, T. L., Bopp, L., Dunne, J., Gehlen, M., Heinze, C., Orr, J., Oschlies, A., et al.: Oxygen and indicators of stress for marine life in multi-model global warming projections, *Biogeosciences Discussions*, **9**, 10 785–10 845, 2013.

Codispoti, L., Brandes, J. A., Christensen, J., Devol, A., Naqvi, S., Paerl, H. W., and Yoshinari, T.: The oceanic fixed nitrogen and nitrous oxide budgets: Moving targets as we enter the anthropocene?, *Scientia Marina*, **65**, 85–105, 2001.

Collins, M., An, S., Cai, W., Ganachaud, A., Guilyardi, E., Jin, F., Jochum, M., Lengaigne, M., Power, S., Timmermann, A., Vecchi, G., and Wittenberg, A.: The impact of global warming on the tropical Pacific Ocean and El Niño, *Nature Geoscience*, **3**, 391–397, 2010.

Crowley, T. J.: North Atlantic deep water cools the southern hemisphere, *Paleoceanography*, **7**, 489–497, 1992.

Dunne, J. P., Armstrong, R. A., Gnanadesikan, A., and Sarmiento, J. L.: Empirical and mechanistic models for the particle export ratio, *Global Biogeochem. Cycles*, **19**, GB4026, 2005.

Dunne, J. P., John, J. G., Adcroft, A. J., Griffies, S. M., Hallberg, R. W., Shevliakova, E., Stouffer, R. J., Cooke, W., Dunne, K. A., Harrison, M. J., et al.: GFDL's ESM2 Global Coupled Climate-Carbon Earth System Models. Part I: Physical Formulation and Baseline Simulation Characteristics, *J. Climate*, **25**, 6646–6665, 2012.

Dunne, J. P., John, J. G., Shevliakova, E., Stouffer, R. J., Krasting, J. P., Malyshev, S. L., Milly, P., Sentman, L. T., Adcroft, A. J., Cooke, W., et al.: GFDL's ESM2 Global Coupled Climate-Carbon Earth System Models. Part II: Carbon System Formulation and Baseline Simulation Characteristics, *J. Climate*, **26**, 2247–2267, 2013.

Duteil, O. and Oschlies, A.: Sensitivity of simulated extent and future evolution of marine suboxia to mixing intensity, *Geophys. Res. Lett.*, **38**, L06 607, 2011.

England, E. H., McGregor, S., Meehl, G. A., Timmermann, A., Wenju Cai, Sen Gupta, A., and McPhaden, M. J.: Recently intensified Pacific Ocean wind–driven circulation and the ongoing warming hiatus, *Nature Climate Change*, doi:10.1038/nclimate2106, 2014.

England, M. H.: The age of water and ventilation timescales in a global ocean model, *J. Phys. Oceanogr.*, **25**, 2756–2777, 1995.

Ewen, T. L., Weaver, A. J., and Eby, M.: Sensitivity of the inorganic ocean carbon cycle to future climate warming in the UVic coupled model, *Atmosphere-Ocean*, **42**, 23–42, 2004.

Eyring, V., Cionni, I., Arblaster, J., Sedlácek, J., Perlwitz, J., Young, P., Bekki, S., Bergmann, D., Cameron-Smith, P., Collins, W. J., et al.: Long-term changes in tropospheric and stratospheric ozone and associated climate impacts in CMIP5 simulations, *J. Geophys. Res.*, 5029–5060, 2013.

Farneti, R. and Gent, P. R.: The effects of the eddy-induced advection coefficient in a coarse-resolution coupled climate model, *Ocean Modelling*, **39**, 135–145, 2011.

Farneti, R., Delworth, T. L., Rosati, A. J., Griffies, S. M., and Zeng, F.: The role of mesoscale eddies in the rectification of the Southern Ocean response to climate change, *J. Phys. Oceanogr.*, **40**, 1539–1557, 2010.

Frölicher, T., Joos, F., Plattner, G.-K., Steinacher, M., and Doney, S. C.: Natural variability and anthropogenic trends in oceanic oxygen in a coupled carbon cycle–climate model ensemble, *Global Biogeochem. Cycles*, **23**, GB1003, 2009a.

Frölicher, T. L., Joos, F., Plattner, G.-K., Steinacher, M., and Doney, S. C.: Natural variability and anthropogenic trends in oceanic oxygen in a coupled carbon cycle–climate model ensemble, *Global Biogeochemical Cycles*, **23**, 2009b.

Gargett, A. E.: Vertical eddy diffusivity in the ocean interior, *J. Mar. Res.*, **42**, 359–393, 1984.

Gent, P. R. and McWilliams, J. C.: Isopycnal mixing in ocean circulation models, *J. Phys. Oceanogr.*, **20**, 150–155, 1990.

Gille, S. T.: Warming of the Southern Ocean since the 1950s, *Science*, **295**, 1275–1277, 2002.

Gnanadesikan, A.: A simple predictive model for the structure of the oceanic pycnocline, *Science*, **283**, 2077–2079, 1999.

Gnanadesikan, A. and Hallberg, R. W.: On the relationship of the Circumpolar Current to Southern Hemisphere winds in coarse-resolution ocean models, *J. Phys. Oceanogr.*, **30**, 2013–2034, 2000.

Gnanadesikan, A., Dunne, J. P., Key, R. M., Matsumoto, K., Sarmiento, J. L., Slater, R. D., and Swathi, P. S.: Oceanic ventilation and biogeochemical cycling: Understanding the physical mechanisms that produce realistic distributions of tracers and productivity, *Global Biogeochem. Cycles*, **18**, 2004.

Gnanadesikan, A., Dunne, J., and John, J.: Understanding why the volume of suboxic waters does not increase over centuries of global warming in an Earth System Model, *Biogeosciences*, **9**, 1159–1172, 2012.

Gnanadesikan, A., Bianchi, D., and Pradal, M.-A.: Critical role for mesoscale eddy diffusion in supplying oxygen to hypoxic ocean waters, *Geophys. Res. Lett.*, **40**, 5194–5198, 2013.

Gordon, A. L.: Interocean exchange of thermocline water, *J. Geophys. Res.*: Oceans (1978–2012), **91**, 5037–5046, 1986.

Gregg, M. C., Sanford, T. B., and Winkel, D. P.: Reduced mixing from the breaking of internal waves in equatorial waters, *Nature*, **422**, 513–515, 2003.

Griffies, S. M., Gnanadesikan, A., Pacanowski, R. C., Larichev, V. D., Dukowicz, J. K., and Smith, R. D.: Isoneutral diffusion in az-coordinate ocean model, *J. Phys. Oceanogr.*, **28**, 805–830, 1998.

Griffies, S. M., Schmidt, M., and Herzfeld, M.: Elements of MOM4p1, *GFDL Ocean Group Tech. Rep*, **6**, 444, 2009.

Hall, A. and Visbeck, M.: Synchronous Variability in the Southern Hemisphere Atmosphere, Sea Ice, and Ocean Resulting from the Annular Mode, *J. Climate*, **15**, 3043–3057, 2002.

Hallberg, R. and Gnanadesikan, A.: An exploration of the role of transient eddies in determining the transport of a zonally reentrant current, *J. Phys. Oceanogr.*, **31**, 3312–3330, 2001.

Harrison, D.: Post World War II Trends in Tropical Pacific Surface Trades, *J. Climate*, **2**, 1561–1562, 1989.

Harrison, M. and Hallberg, R.: Pacific subtropical cell response to reduced equatorial dissipation, *J. Phys. Oceanogr.*, **38**, 1894–1912, 2008.

Haywood, A. M., Dekens, P., Ravelo, A. C., and Williams, M.: Warmer tropics during the mid-Pliocene? Evidence from alkenone paleothermometry and a fully coupled ocean-atmosphere GCM, *Geochemistry, Geophysics, Geosystems*, **6**, Q03010, 2005.

Helly, J. J. and Levin, L. A.: Global distribution of naturally occurring marine hypoxia on continental margins, *Deep Sea Res., Part I*, **51**, 1159–1168, 2004.

Henyey, F. S., Wright, J., and Flatté, S. M.: Energy and action flow through the internal wave field: An eikonal approach, *J. Geophys. Res.*: Oceans (1978–2012), **91**, 8487–8495, 1986.

Hibler, III, W. D.: A Dynamic Thermodynamic Sea Ice Model, *J. Phys. Oceanogr.*, **9**, 815–846, 1979.

Hogg, A. M.: An Antarctic Circumpolar Current driven by surface buoyancy forcing, *Geophys. Res. Lett.*, **37**, L23 601, 2010.

Houghton, J. T., Ding, Y., Griggs, D. J., Noguer, M., van der Linden, P. J., Dai, X., Maskell, K., and Johnson, C. A., eds.: Climate Change 2001: The Scientific Basis. Contribution of Working Group I to the Third Assessment Report of the Intergovernmental Panel on Climate Change, Cambridge University Press, 2001.

Hunke, E. C. and Dukowicz, J. K.: An Elastic Viscous Plastic Model for Sea Ice Dynamics, *J. Phys. Oceanogr.*, **27**, 1849–1867, 1997.

Joos, F., Plattner, G.-K., Stocker, T. F., Körtzinger, A., and Wallace, D. W. R.: Trends in marine dissolved oxygen: Implications for ocean circulation changes and the carbon budget, *Eos, Transactions American Geophysical Union*, **84**, 197–201, 2003.

Kalnay, E., Kanamitsu, M., Kistler, R., Collins, W., Deaven, D., Gandin, L., Iredell, M., Saha, S., White, G., Woollen, J., Zhu, Y., Leetmaa, A., Reynolds, B., Chelliah, M., Ebisuzaki, W., Higgins, W., Janowiak, J., Mo, K. C., Ropelewski, C., Wang, J., Jenne, R., and Joseph, D.: The NCEP/NCAR 40-Year Reanalysis Project, *Bulletin of the American Meteorological Society*, **77**, 437–472, 1996.

Kamenkovich, I. and Radko, T.: Role of the Southern Ocean in setting the Atlantic stratification and meridional overturning circulation, *J. Mar. Res.*, **69**, 2–3, 2011.

Knorr, G. and Lohmann, G.: Southern Ocean origin for the resumption of Atlantic thermohaline circulation during deglaciation, *Nature*, **424**, 532–536, 2003.

Kuhlbrodt, T., Griesel, A., Montoya, M., Levermann, A., Hofmann, M., and Rahmstorf, S.: On the driving processes of the Atlantic meridional overturning circulation, *Rev. Geophys.*, **45**, RG2001, 2007.

Large, W. G. and Yeager, S. G.: The global climatology of an interannually varying air–sea flux data set, *Clim. Dynam.*, **33**, 341–364, 2009.

Le Quéré, C., Rödenbeck, C., Buitenhuis, E. T., Conway, T. J., Langenfelds, R., Gomez, A., Labuschagne, C., Ramonet, M., Nakazawa, T., Metzl, N., et al.: Saturation of the Southern Ocean CO_2 sink due to recent climate change, *Science*, **316**, 1735–1738, 2007.

Levitus, S., Conkright, M. E., Reid, J. L., Najjar, R. G., and Mantyla, A.: Distribution of nitrate, phosphate and silicate in the world oceans, *Progress in Oceanography*, **31**, 245 – 273, 1993.

L'Heureux, M. L., Lee, S., and Lyon, B.: Recent multidecadal strengthening of the Walker circulation across the tropical Pacific, Nature Climate Change, **3**, 571–576, 2013.

Lovenduski, N. S., Gruber, N., Doney, S. C., and Lima, I. D.: Enhanced CO_2 outgassing in the Southern Ocean from a positive phase of the Southern Annular Mode, *Global Biogeochem. Cycles*, **21**, B2026, 2007.

Lovenduski, N. S., Gruber, N., and Doney, S. C.: Toward a mechanistic understanding of the decadal trends in the Southern Ocean carbon sink, *Global Biogeochem. Cycles*, **22**, B3016, 2008.

Luyten, J., Pedlosky, J., and Stommel, H.: The ventilated thermocline, *J. Phys. Oceanogr.*, **13**, 292–309, 1983.

Marshall, J. and Radko, T.: Residual-mean solutions for the Antarctic Circumpolar Current and its associated overturning circulation, *J. Phys. Oceanogr.*, **33**, 2341–2354, 2003.

Marshall, J. and Speer, K.: Closure of the meridional overturning circulation through Southern Ocean upwelling, *Nature Geoscience*, 171–180, 2012.

Matear, R. and Hirst, A.: Long-term changes in dissolved oxygen concentrations in the ocean caused by protracted global warming, *Global Biogeochem. Cycles*, **17**, 1125–1142, 2003.

Matear, R., Hirst, A., and McNeil, B.: Changes in dissolved oxygen in the Southern Ocean with climate change, *Geochemistry, Geophysics, Geosystems*, **1**, 1050, 2000.

McDermott, D. A.: The regulation of northern overturning by Southern Hemisphere winds, *J. Phys. Oceanogr.*, **26**, 1234–1255, 1996.

McPhaden, M. J.: TOGA-TAO and the 1991- 93 El Niño-Southern Oscillation Event, *Oceanography*, **6**, 36–44, 1993.

Meissner, K., Schmittner, A., Weaver, A., and Adkins, J.: Ventilation of the North Atlantic Ocean during the Last Glacial Maximum: A comparison between simulated and observed radiocarbon ages, *Paleoceanography*, **18**, 1023, 2003.

Meissner, K. J., Weaver, A. J., Matthews, H. D., and Cox, P. M.: The role of land surface dynamics in glacial inception: a study with the UVic Earth System Model, *Clim. Dynam.*, **21**, 515–537, 2003.

Meissner, K. J., McNeil, B. I., Eby, M., and Wiebe, E. C.: The importance of the terrestrial weathering feedback for multimillennial coral reef habitat recovery, *Global Biogeochem. Cycles*, **26**, GB3017, 2012.

Meredith, M. P. and Hogg, A. M.: Circumpolar response of Southern Ocean eddy activity to a change in the Southern Annular Mode, *Geophys. Res. Lett.*, **33**, L16 608, 2006.

Morrison, A. K. and McC. Hogg, A.: On the relationship between Southern Ocean overturning and ACC transport, *J. Phys. Oceanogr.*, **43**, 140–148, 2013.

Oguz, T., Ducklow, H. W., and Malanotte-Rizzoli, P.: Modeling distinct vertical biogeochemical structure of the Black Sea: Dynamical coupling of the oxic, suboxic, and anoxic layers, *Global Biogeochem. Cycles*, **14**, 1331–1352, 2000.

Oke, P. R. and England, M. H.: Oceanic response to changes in the latitude of the Southern Hemisphere subpolar westerly winds, *J. Climate*, **17**, 1040–1054, 2004.

Orsi, A. H., Johnson, G. C., and Bullister, J. L.: Circulation, mixing, and production of Antarctic Bottom Water, *Progress in Oceanography*, **43**, 55–109, 1999.

Oschlies, A., Schulz, K. G., Riebesell, U., and Schmittner, A.: Simulated 21st century's increase in oceanic suboxia by CO2-enhanced biotic carbon export, *Global Biogeochem. Cycles*, **22**, GB4008, 2008.

Pacanowski, R. C.: MOM 2 documentation: User's guide and reference manual, version 1.0, *GFDL Ocean Group Tech. Rep. 3*, 1995.

Paulmier, A. and Ruiz-Pino, D.: Oxygen minimum zones (OMZs) in the modern ocean, *Progress in Oceanography*, **80**, 113–128, 2009.

Pérez, F. F., Mercier, H., Vázquez-Rodríguez, M., Lherminier, P., Velo, A., Pardo, P. C., Rosón, G., and Ríos, A. F.: Atlantic Ocean CO_2 uptake reduced by weakening of the meridional overturning circulation, *Nature Geoscience*, **6**, 146–152, 2013.

Petit, J.-R., Jouzel, J., Raynaud, D., Barkov, N. I., Barnola, J.-M., Basile, I., Bender, M., Chappellaz, J., Davis, M., Delaygue, G., et al.: Climate and atmospheric history of the past 420,000 years from the Vostok ice core, Antarctica, *Nature*, **399**, 429–436, 1999.

Philander, S. G. H.: The Response of Equatorial Oceans to a Relaxation of the Trade Winds, *J. Phys. Oceanogr.*, **11**, 176–189, 1981.

Rahmstorf, S. and England, M. H.: Influence of Southern Hemisphere winds on North Atlantic deep water flow, *J. Phys. Oceanogr.*, **27**, 2040–2054, 1997.

Ravelo, A., Dekens, P., and McCarthy, M.: Evidence for El Niño-like conditions during the Pliocene, *GSA TODAY*, **16**, 4–11, 2006.

Reid Jr, J. L.: Intermediate waters of the Pacific Ocean, Tech. rep., DTIC Document, 1965.

Rhein, M., Rintoul, S. R., Aoki, S., Campos, E., Chambers, D., Feely, R. A., Gulev, S., Johnson, G. C., Josey, S. A., Kostianoy, A., Mauritzen, C., Roemmich, D., Talley, L. D., and Wang, F.: Climate Change 2013: The Physical Science Basis. Contribution of Working Group I to the Fifth Assessment Report of the Intergovernmental Panel on Climate Change, chap. Observations: Ocean, Cambridge University Press, Cambridge, United Kingdom and New York, NY, USA, in press.

Ridder, N., Meissner, K., and England, M.: Sensitivity of the oceanic carbon reservoir to tropical surface wind stress variations, *Geophys. Res. Lett.*, doi:doi:10.1002/grl.50498., 2013.

Ridder, N. N. and England, M. H.: Sensitivity of marine dissolved oxygen concentrations to permanently changed low-latitude zonal surface wind stress, *Global Biogeochem. Cycles*, under review.

Rintoul, S., Hughes, C., and Olbers, D.: The Antarctic Circumpolar Current system. Ocean Circulation and Climate: Observing and Modelling the Global Ocean, *International Geophysics*, **77**, 271–302, 2001.

Rintoul, S. R.: South Atlantic interbasin exchange, *J. Geophys.Res.: Oceans*, **96**, 2675–2692, 1991.

Rintoul, S. R.: On the origin and influence of Adélie Land Bottom Water, *Ocean, Ice, and Atmosphere: Interactions at the Antarctic Continental Margin*, 151–171, 1998.

Rodgers, K. B., Blanke, B., Madec, G., Aumont, O., Ciais, P., and Dutay, J.-C.: Extratropical sources of equatorial Pacific upwelling in an OGCM, *Geophys. Res. Lett.*, **30**, 1084, 2003.

Rodgers, K. B., Aumont, O., Menkes, C., and Gorgues, T.: Decadal variations in equatorial Pacific ecosystems and ferrocline/pycnocline decoupling, *Global Biogeochem. Cycles*, **22**, GB2019, 2008.

Russell, J. L., Dixon, K. W., Gnanadesikan, A., Stouffer, R. J., and Toggweiler, J. R.: The Southern Hemisphere Westerlies in a Warming World: Propping Open the Door to the Deep Ocean, *J. Climate*, **19**, 6382, 2006.

Sabine, C. L., Feely, R. A., Gruber, N., Key, R. M., Lee, K., Bullister, J. L., Wanninkhof, R., Wong, C. S., Wallace, D. W. R., Tilbrook, B., Millero, F. J., Peng, T., Kozyr, A., Ono, T., and Rios, A. F.: The Oceanic Sink for Anthropogenic CO_2, *Science*, **305**, 367–371, 2004.

Saenko, O. A.: Projected strengthening of the Southern Ocean winds: Some implications for the deep ocean circulation, *Geophysical Monograph Series*, **173**, 365–382, 2007.

Saenko, O. A., Gupta, A. S., and Spence, P.: On challenges in predicting bottom water transport in the Southern Ocean, *J. Climate*, **25**, 1349–1356, 2012.

Sarmiento, J., Gruber, N., Brzezinski, M., and Dunne, J.: High-latitude controls of thermocline nutrients and low latitude biological productivity, *Nature*, **427**, 56–60, 2004.

Sarmiento, J. L. and Gruber, N.: Ocean biogeochemical dynamics, vol. **1015**, Princeton University Press Princeton, 2006.

Schmittner, A., Oschlies, A., Matthews, H. D., and Galbraith, E. D.: Future changes in climate, ocean circulation, ecosystems, and biogeochemical cycling simulated for a business-as-usual CO_2 emission scenario until year 4000 AD, *Global Biogeochem. Cycles*, 22, GB1013, 2008.

Semtner, Jr., A. J.: A Model for the Thermodynamic Growth of Sea Ice in Numerical Investigations of Climate, *J. Phys. Oceanogr.*, **6**, 379–389, 1976.

Shaffer, G., Olsen, S. M., and Pedersen, J. O. P.: Long-term ocean oxygen depletion in response to carbon dioxide emissions from fossil fuels, *Nature Geoscience*, **2**, 105–109, 2009.

Shukla, S. P., Chandler, M. A., Jonas, J., Sohl, L. E., Mankoff, K., and Dowsett, H.: Impact of a permanent El Niño (El Padre) and Indian Ocean Dipole in warm Pliocene climates, *Paleoceanography*, **24**, A262 221, 2009.

Siegenthaler, U. and Sarmiento, J. L.: Atmospheric carbon dioxide and the ocean, *Nature*, **365**, 119–125, 1993.

Sigman, D. M., Hain, M. P., and Haug, G. H.: The polar ocean and glacial cycles in atmospheric CO2 concentration, *Nature*, **466**, 47–55, 2010.

Sijp, W. P. and England, M. H.: Southern Hemisphere westerly wind control over the ocean's thermohaline circulation, *J. Climate*, **22**, 1277–1286, 2009.

Simmons, H. L., Jayne, S. R., Laurent, L. C. S., and Weaver, A. J.: Tidally driven mixing in a numerical model of the ocean general circulation, *Ocean Modelling*, **6**, 245–263, 2004.

Simpkins, G. R., Ciasto, L. M., and England, M. H.: Observed variations in multidecadal Antarctic sea ice trends during 1979–2012, *Geophys. Res. Lett.*, **40**, 3643–3648, 2013.

Sloyan, B. M. and Rintoul, S. R.: Circulation, Renewal, and Modification of Antarctic Mode and Intermediate Water, *J. of Phys. Oceanogr.*, **31**, 1005–1030, 2001.

Sloyan, B. M., Talley, L. D., Chereskin, T. K., Fine, R., and Holte, J.: Antarctic Intermediate Water and Subantarctic Mode Water formation in the southeast Pacific: The role of turbulent mixing, *J. Phys. Oceanogr.*, **40**, 1558–1574, 2010.

Solomon, S., Qin, D., Manning, M., Chen, Z., Marquis, M., Averyt, K. B., Tignor, M., and Miller, H. L., eds.: Contribution of Working Group I to the Fourth Assessment Report of the Intergovernmental Panel on Climate Change, Cambridge University Press, 2007.

Sowers, T. and Bender, M.: Climate records covering the last deglaciation, *Science*, **269**, 210–214, 1995.

Spence, P., van Sebille, E., Saenko, O. A., and England, M. H.: Using Eulerian and Lagrangian approaches to investigate wind-driven changes in the Southern Ocean abyssal circulation, *J. Phys. Oceanogr.*, doi:http://dx.doi.org/10.1175/JPO-D-13-0108.1, 2013.

Stramma, L., Johnson, G. C., Sprintall, J., and Mohrholz, V.: Expanding oxygen-minimum zones in the tropical oceans, *Science*, **320**, 655–658, 2008.

Stramma, L., Johnson, G. C., Firing, E., and Schmidtko, S.: Eastern Pacific oxygen minimum zones: Supply paths and multidecadal changes, *J. Geophys. Res.*: Oceans (1978–2012), **115**, C09 011, 2010.

Stramma, L., Oschlies, A., and Schmidtko, S.: Mismatch between observed and modeled trends in dissolved upper-ocean oxygen over the last 50 yr, *Biogeosciences*, **9**, 4045–4057, 2012.

Swart, N. C. and Fyfe, J. C.: Observed and simulated changes in the Southern Hemisphere surface westerly wind-stress, *Geophys. Res. Lett.*, **39**, L16 711, 2012.

Thompson, D. W. and Solomon, S.: Interpretation of recent Southern Hemisphere climate change, *Science*, **296**, 895–899, 2002.

Thompson, D. W. J., Solomon, S., Kushner, P. J., England, M. H., Grise, K. M., and Karoly, D. J.: Signatures of the Antarctic ozone hole in Southern Hemisphere surface climate change, *Nature Geoscience*, **4**, 741–749, 2011.

Toggweiler, J., Dixon, K., and Broecker, W.: The Peru upwelling and the ventilation of the South Pacific thermocline, *J. Geophys. Res.*: Oceans (1978–2012), **96**, 20 467–20 497, 1991.

Toggweiler, J. R. and Samuels, B.: Is the magnitude of the deep outflow from the Atlantic Ocean actually governed by Southern Hemisphere winds, *The Global Carbon Cycle*, **1**, 303–331, 1993.

Toggweiler, J. R. and Samuels, B.: Effect of Drake Passage on the global thermohaline circulation, *Deep Sea Res., Part I*, **42**, 477–500, 1995.

Toggweiler, J. R. and Samuels, B.: On the ocean's large-scale circulation near the limit of no vertical mixing, *J. Phys. Oceanogr.*, **28**, 1832–1852, 1998.

Tokinaga, H. and Xie, S.-P.: Weakening of the equatorial Atlantic cold tongue over the past six decades, *Nature Geoscience*, 222–226, 2011.

Tokinaga, H., Xie, S.-P., Timmermann, A., McGregor, S., Ogata, T., Kubota, H., and Okumura, Y. M.: Regional Patterns of Tropical Indo-Pacific Climate Change: Evidence of the Walker Circulation Weakening, *J. Climate*, **25**, 1689–1710, 2012.

Trenberth, K. E. and Hurrell, J. W.: Decadal atmosphere-ocean variations in the Pacific, *Clim. Dynam.*, **9**, 303–319, 1994.

Tsuchiya, M.: The origin of the Pacific Equatorial 13°C Water, *J. Phys. Oceanogr.*, **11**, 794–812, 1981.

Vecchi, G. A. and Soden, B. J.: Global Warming and the Weakening of the Tropical Circulation, *J. Climate*, **20**, 4316–4340, 2007.

Vecchi, G. A., Soden, B. J., Wittenberg, A. T., Held, I. M., Leetmaa, A., and Harrison, M. J.: Weakening of tropical Pacific atmospheric circulation due to anthropogenic forcing, *Nature*, **441**, 73–76, 2006.

Wara, M. W., Ravelo, A. C., and Delaney, M. L.: Permanent El Niño-like conditions during the Pliocene warm period, *Science*, **309**, 758–761, 2005.

Watson, A., Nightingale, P., Cooper, D., Leach, H., Follows, M., Watson, A., Nightingale, P., Cooper, D., Leach, H., and Follows, M.: Modelling Atmosphere-Ocean CO_2 Transfer [and Discussion], *Philosophical Transactions of the Royal Society of London. Series B: Biological Sciences*, **348**, 125–132, 1995.

Waugh, D. W., Primeau, F., DeVries, T., and Holzer, M.: Recent changes in the ventilation of the southern oceans, *Science*, **339**, 568–570, 2013.

Weaver, A., Eby, M., Wiebe, E. C., Bitz, C. M., Duffy, P. B., Ewen, T. L., Fanning, A. F., Holland, M. M., MacFadyen, A., Matthews, H. D., Meissner, K. J., Saenko, O., Schmittner, A., Wang, H., and Yoshimori, M.: The UVic Earth System Climate Model: Model description, climatology and application to past, present and future climates, *Atmosphere-Ocean*, **39**, 361–428, 2001.

Weiss, R. F.: The solubility of nitrogen, oxygen and argon in water and seawater, in: *Deep Sea Research and Oceanographic Abstracts*, vol. **17**, 721–735, Elsevier, 1970.

Williams, R. and Follows, M.: Ocean Dynamics and the Carbon Cycle: Principles and Mechanisms, Ocean Dynamics and the Carbon Cycle: Principles and Mechanisms, Cambridge University Press, 2011.

Zickfeld, K., Fyfe, J. C., Saenko, O. A., Eby, M., and Weaver, A. J.: Response of the global carbon cycle to human-induced changes in Southern Hemisphere winds, *Geophys. Res. Lett.*, **34**, 2007.

Zickfeld, K., Fyfe, J. C., Eby, M., and Weaver, A. J.: Comment on: Saturation of the Southern Ocean CO_2 Sink Due to Recent Climate Change, *Science*, **319**, 2008.

List of acronyms

AABW	Antarctic Bottom Water
AAIW	Antarctic Intermediate Water
ACC	Antarctic Cirumpolar Current
AMOC	Atlantic meridional overturning circulation
AOU	aparent oxygen utilization
C^{hard}	hard tissue carbon
C^{sat}	saturation carbon
C^{soft}	soft tissue carbon
CDW	Circumpolar Deep Water
D_{20}	20-degree isotherm
ΔC	disequilibrium carbon
DIC	dissolved inorganic carbon
EBUS	eastern boundary upwelling system
ENSO	El Niño Southern Oscillation
ESCM	Earth system climate model
EUC	Equatorial Undercurrent
GFDL	Geophysical Fluid Dynamics Laboratory
ITF	Indonesian Throughflow
κ_{v}	vertical mixing/diapycnal diffusivity
MLD	mixed layer depth
MOC	meridional overturning circulation
MOM	Modular Ocean Model
NADW	North Atlantic DeepWater
NCEP	National Centers for Environmental Prediction
NHT	northward heat transport

NPP	net primary productivity
NPZD	Nutrient Phytoplankton Zooplankton Detritus
O_2^{sat}	oxgen saturation concentration
OCMIP	Ocean Carbon-Cycle Model Intercomparison Project
OGCM	ocean general circulation model
OMZ	oxygen minimum zone
psu	practical salinity units
R	remineralization rate
SAMW	Subantractic Mode Water
SAT	surface air temperature
SEC	South Equatorial Current
SG	subtropical gyre
SH	Southern Hemisphere
SO	Southern Ocean
SRES	Special Report Emission Scenarios
SSS	sea surface salinity
SST	sea surface tempreature
Sv	Sverdrup ($1\ \text{Sv} \equiv 1 \times 10^6\ \text{m}^3\ \text{s}^{-1}$)
τ_x	zonal surface wind stress
TOPAZ2	Tracers of Ocean Phytoplankton with Allometric Zooplankton version 2
UVic ESCM	University of Victoria Earth system climate model